Medical Room Design for a Fission Converter-Based Boron Neutron Capture Therapy Facility

by

Michelle N. Ledesma

B.S, Nuclear Engineering
Massachusetts Institute of Technology (1998)

Submitted to the Department of Nuclear Engineering
in partial fulfillment of the requirements for the degree of

MASTER OF SCIENCE IN NUCLEAR ENGINEERING

at the

MASSACHUSSETTS INSTITUTE OF TECHNOLOGY

August 1998

Signature of Author: _____
Department of Nuclear Engineering
August 23, 1998

Certified by: _____
Prof. Otto K. Harling
Thesis Supervisor

_____
Dr. Gordon Kohse
Thesis Reader

_____
Prof. Tarcisio Campos
Thesis Reader

Accepted by: _____
Prof. Lawrence M. Lidsky
Chairman, Department Committee on Graduate Students

Medical Room Design for a Fission Converter Based Boron Neutron Capture Therapy Facility

by

Michelle N. Ledesma

Submitted to the Department of Nuclear Engineering

on August 24, 1998 in Partial Fulfillment of the requirements for the

Degree of Master of Science in Nuclear Engineeing

ABSTRACT

A design of a shielded medical room to be used in Boron Neutron Capture Therapy was developed. The design included analytical shielding calculations, computational methods using the Monte Carlo N-particle transport code, and experimental measurements using the current medical room.

The design included the shielded wall of the medical room, a shielding door for entrance into the room, a viewing window, and patient positioning system. From the shielding analysis the amount of high density concrete needed to reduce the dose rate outside the walls of the room to 1 mrem/hr was calculated. The side walls and ceiling need 73 cm of Ilmenite I-2a concrete and the back wall needs 100 cm. Several options were proposed for the shielding material needed to fabricate the door. The most desirable option is 45 cm all steel door. A shielded window composed of 30 cm of mineral oil, 40 cm of lead glass with density of 3.95, and 28 cm of plain glass will provide sufficient shielding. The final medical room design incorporates existing concrete blocks for the majority of the shielding.

Thesis Supervisor: Otto K. Harling

Title: Professor of Nuclear Engineering

ACKNOWLEDGMENTS

I would like to thank my thesis advisor, Professor Harling, for all his guidance and advice throughout his project. I would also like to acknowledge Professor Tarcisio Campos and Dr. Gordon Kohse for their insightful assistance.

In addition, I want to thank all the students and staff that have been tremendously helpful and have given me lots of support. In particular, I would like to express my sincere gratitude to C. Chuang, T. Goorley, S. Kiger, K. Riley, B. Sutharshan, J. White, F. McWilliams, and T. Newton.

Finally, I would like to thank my parents for their encouragement, love, and support. To my best friend, Mikey Folkert, I never could have done it without you.

TABLE OF CONTENTS

LIST OF FIGURES

LIST OF TABLES

CHAPTER 1

INTRODUCTION

1.1 OBJECTIVE

The objective is to design a shielded medical room for the fission converter-based boron neutron capture therapy facility. The design includes: Analytical shielding calculations for the medical room walls,

1. Computational and experimental calculations to verify analytical methods,
2. Design of a shielding door and shielded viewing window,
3. Suggestions for a patient positioning system,
4. Design of the medical room shielding.

1.2 BORON NEUTRON CAPTURE THERAPY

Boron neutron capture therapy (BNCT) is a binary cancer therapy modality that employs a tumor selective B-10 containing compound and a source of low energy neutrons. The tumorcidal effect is brought about by the $B^{10}(n,\alpha)Li^7$ reaction, where the absorption of a thermal neutron (0.025 eV) by a B^{10} nucleus results in a fission of the compound nucleus and the subsequent emission of an α particle and a Li^7 ion.

$$ {}^{10}_{5}B + {}^{1}_{0}n\,(3838b) \rightarrow {}^{11}B^{*} \rightarrow {}^{7}_{3}Li + {}^{4}_{2}\alpha $$

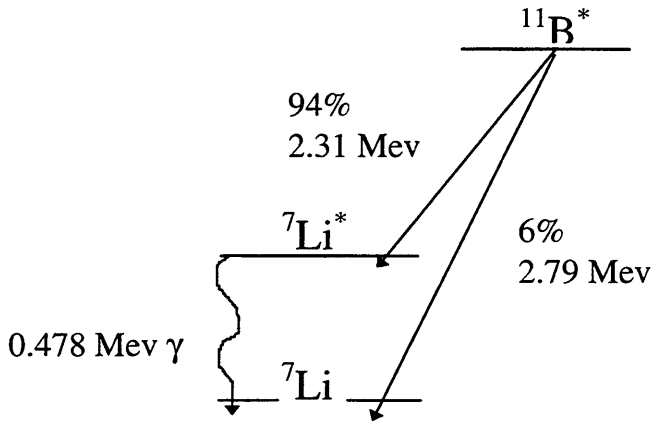

Figure 1.1 Boron neutron capture reaction.

These two high LET particles deposit all of their energy in a confined volume, as the ranges of the α particle and Li^7 ion in tissue are 8.8μm and 4.8μm, respectively. As both of these ranges are less than the diameter of a normal mammalian cell (for example, mammalian erythrocytes have a diameter of 10μm) the dose is restricted to the tumor cell in which the boron was located, leaving nearby healthy tissues intact.

In order to expose the bed of the tumor to thermal neutrons, the use of a beam of epithermal neutrons, with energies ranging from 1 keV to 10 keV, has been proposed and implemented. These epithermal thermal have sufficient energy to penetrate the skull and reach the tumor. During the course of this penetration they lose energy through scattering reactions with the tissue. By the time they reach the B^{10} in the tumor cells, their energy has been reduced to thermal levels, allowing them to be captured by the B^{10} nucleus and forcing the $B^{10}(n,\alpha)Li^{7}$ reaction described above.

1.3 FISSION CONVERTER BEAM

BNCT trials are currently being conducted at MIT using the current medical facility. The current beam has an epithermal neutron flux of $2x10^{8}$ n/cm^{2}sec. With this flux level irradiations take about three hours to deliver a healthy tissue dose of ~1000 RBE cGY. The length of the irradiation is difficult on the patient and will become a hinderance for routine therapy once advanced clinical trials begin.

A way of shortening the irradiation time and delivering a better quality beam of epithermal neutrons by the use of a fission converter plate is currently under construction. Neutrons from the reactor core hit a plate of fuel elements causing a fission reaction. These fission neutrons are then moderated down to the desired lower energy epithermal neutrons while fast neutrons and gammas are filtered. The result is a high quality epithermal neutron beam with a flux two orders of magnitude higher than the current facility. Irradiation times with the fission converter beam will be on order of a few minutes. The following figure is an isometric view of the fission converter beam.

With the construction of this high intensity beam comes the need for a medical room that will adequately shield radiation levels outside the room to a safe level for medical and reactor personnel.

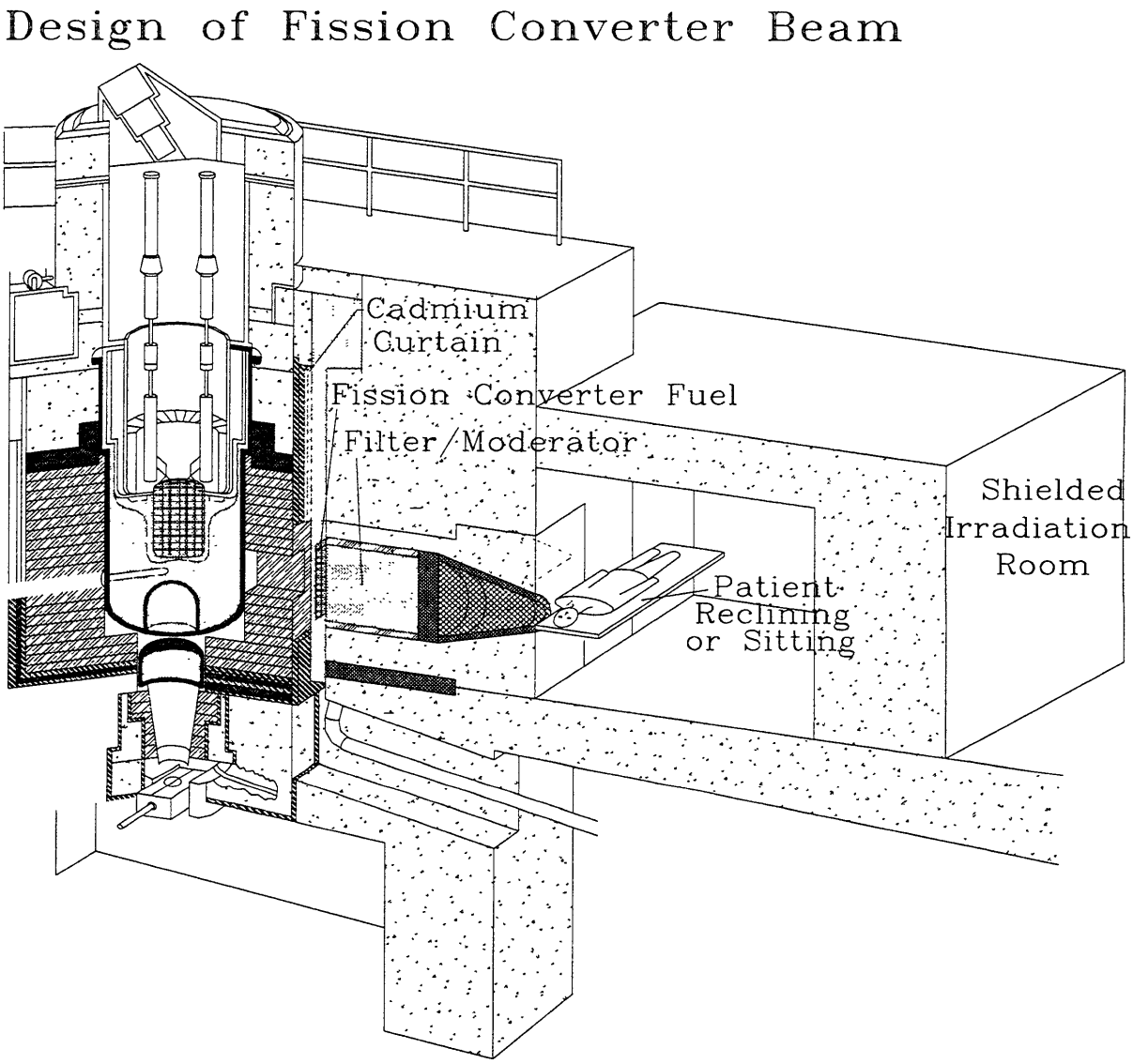

Figure 1.2 Isometric view of Fission Converter BNCT facility. (courtesy of W.S. Kiger).

1.4 REFERENCES

Barth, R.F., Solloway,A.H., Fairchild, R.G., "Boron Neutron Capture Therapy for Cancer", *Scientific American*, Oct. 1990.

Bernard, J, Hu, L.W., *Safety Evaluation Report for Fission Converter Facility*, MIT, 1997.

Hatanaka, H., "Clinical Results of Boron Neutron Capture Therapy", *Proceedings of an International Workshop on Neutron Beam Design, Development and Performance for Neutron Capture Therapy*, Massachusetts Institute of Technology, 1989.

Kiger, W.S, *Neutronic Design of a Fission Converter-Based Epithermal Beam for Neutron Capture Therapy,* Nucl. E. Thesis, Massachusetts Institute of Technology, 1996.

Locher, G.L., "Biological Effects and Therapeutic Possibilities of Neutrons", *Am. J. Roentgenol. Radium Ther.,* 36:1-13, 1936.

CHAPTER 2

MEDICAL ROOM DESIGN

2.1 INTRODUCTION

The fission converter BNCT irradiation facility will have a total flux two orders of magnitude higher than the current facility. Radiation in the beam consists of thermal, epithermal, and fast neutrons plus gamma rays. Fast neutron and gamma ray contamination, as well as epithermal and thermal neutrons, in the beam will contribute to significant amount of radiation to the medical area, requiring a shielded medical room for patient irradiations. The medical room will accommodate patients for BNCT treatments ranging on the order of minutes. Additionally, the medical room will shield the medical and reactor personnel from fast neutron and gamma radiation. This medical room will be located on the reactor floor in the area currently occupied by the Hohlraum. Several components make up the medical room. These are: the shielded walls of the room, a shielding door for entrance into the room, a shielded viewing window, a patient support and positioning system, and necessary electrical and ventilation ducts. Explanations for the design of these components are organized as follows:

- Section 2.4 describes the methods of determining the dose levels at the side walls, ceiling, floor, window, and backwall.
- Section 2.5 explains the shielding calculations for the side walls, ceiling, floor, and backwall.

- Chapter 3 provides the details of door shielding design, including experimental measurements of neutron reflection off concrete to aid in dose determination at the door location.
- Chapter 4 presents the information on the materials considered along with the shielding design for the viewing window.
- Chapters 5 and 6 describe the methods used for verification of the medical room shielding design. These sections include an explanation of the Monte Carlo computer simulation of the medical room as well as experimental measurements in the current medical room.
- Chapter 7 provides a description of the patient positioning system considerations and suggestions.
- Chapter 8 covers the actual design of the shielding for the medical room, using existing material and specifications for new shield blocks. An overall design is given as suggestion for the new medical room.

2.2 SPECIFICATIONS AND LIMITATIONS

The medical room must meet the following specifications[1]:

- high reliability and control,
- licenseable design,
- radiation exposure must meet 10 CFR part 20 standards,
- must have an emergency plan of exit.

[1] Beam Shutter and Medical Room Design for BNCT, Anne Le Gal and Marc Ledieu.

The radiation guidelines outlined in sections 21.1201 and 20.1301 of the United States Nuclear Regulatory Commission's Title 10, Chapter 1, Code of Federal Regulations part 20 state that the annual limit to radiation workers must not exceed the total effective dose equivalent of 5 rems or that the sum of the deep dose and committed dose equivalents to any organ (excluding the lens of the eye) must not exceed 50 rems. Additionally, radiation dose limits for members of the public must not exceed the total effective dose equivalent of 0.1 rem/year. Dose in any unrestricted area must not exceed 2 mrem per hour. Radioactive areas where members of the public are permitted must meet the regulation standards for non radiation workers. The medical room is located in a restricted area and therefore the dose rates should be "As Low As Reasonably Achievable". For the purpose of this shielding study, the "reasonably achievable" dose rate used is 1 mrem/hr, to provide a working environment to medical staff comparable to unrestricted areas, with a safety factor of 2.

The layout of the medical room is subject to several limitations imposed by the limited space on the reactor floor. Several important structures surround the location of the future medical room. The following drawing shows the top view of the reactor floor and the location of the future fission converter BNCT facility. The drawing also illustrates many of the limitations in the medical room design. A floor plug, which allows access into the equipment room, is located 32cm on the left side of the medical room wall. To the right of the medical room are several piping systems and a make-up

water system tank. Furthermore, the limited space between the front wall of the facility and the reactor containment building is shown in the drawing.

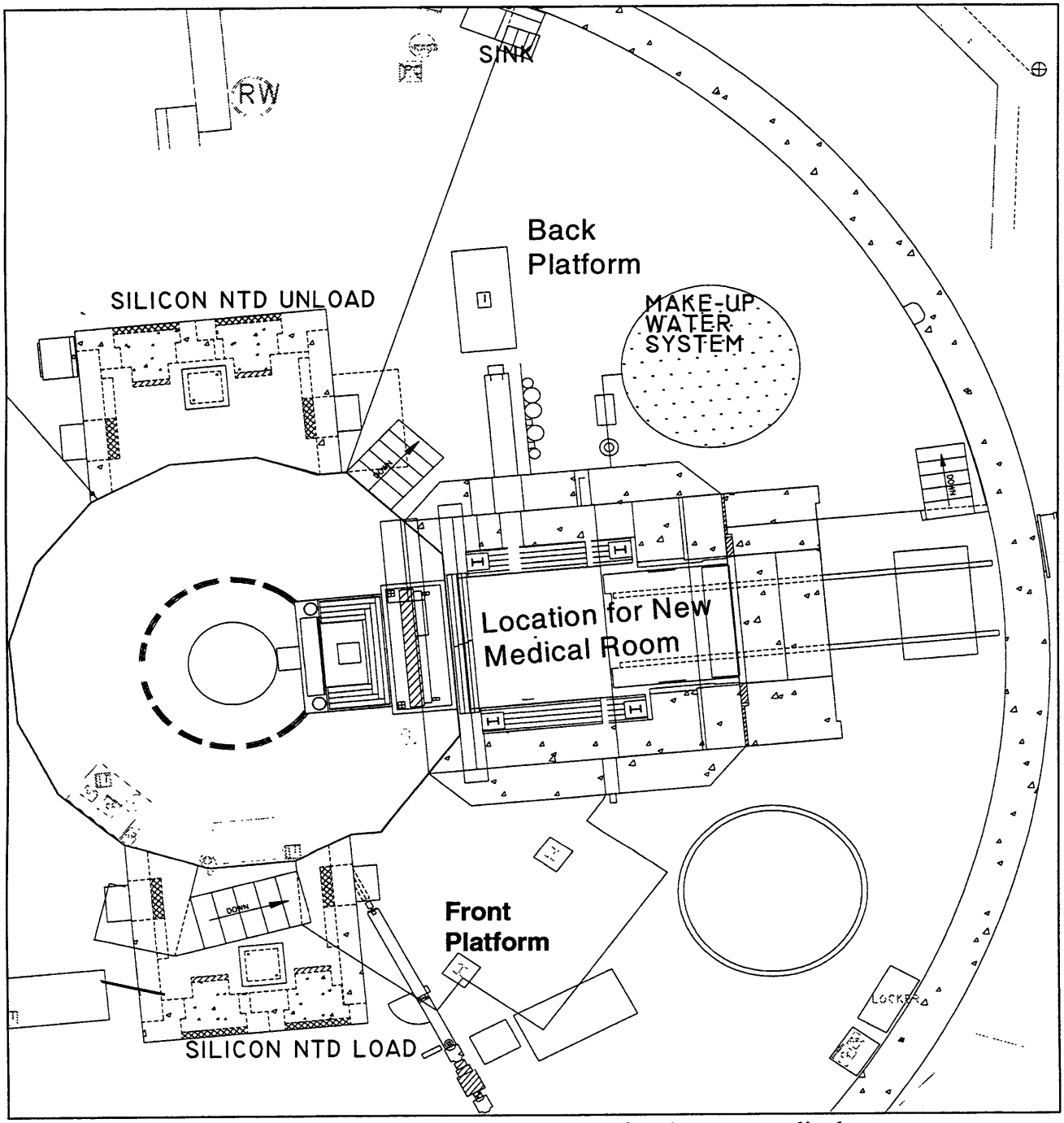

Figure2.1 Drawing of reactor floor showing location for the new medical room, top view.

2.3 PREVIOUS WORK

Previous work by Anne LeGal[2] and Balendra Sutharshan[3] resulted in two preliminary medical room designs, shown below. The first design was based on hand calculation methods. For the second design, MCNP was used to determine the amount of shielding needed at the back wall in direct line of the beam. Both of these designs have some observable disadvantages. The first design, which utilizes a double wall to minimize radiation to the back and doorway, leaves limited space inside the room. The second expands the inner dimensions of the room by using one single wall. However, this increases the amount of radiation incident on the door. Also, both designs block the access plug to the equipment room. Additionally, in both designs the allotted space inside the room is too small to treat some patients. Considering these items, the previous work was used as a reference point for the design of the room presented in the following sections.

[2] Beam Shutter Design and Medical Room Design, Anne LeGal and Marc Ledieu, MIT Sept. 1995.
[3] Engineering Design of a Fission Converter-Based Epithermal Beam for Neutron Capture Therapy, Balendra Sutharshan, MIT PhD thesis, February 1998.

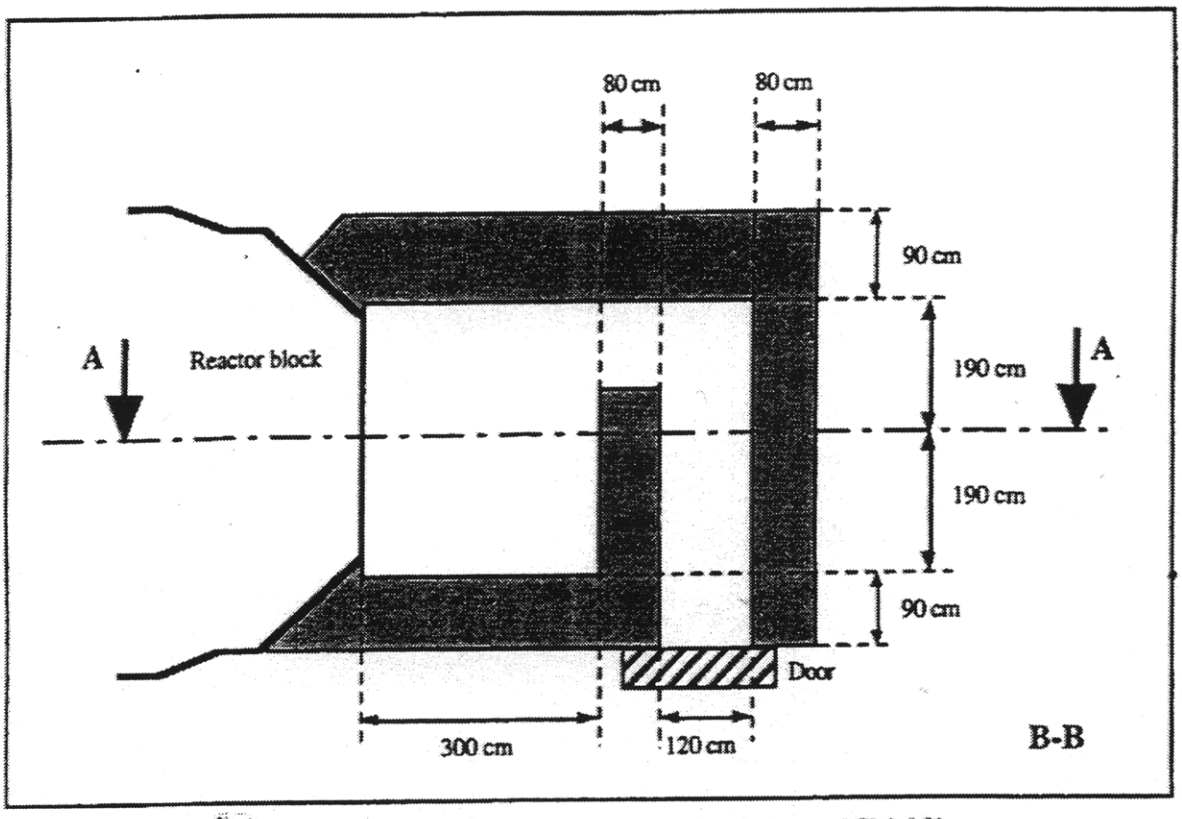

Figure2.2 Medical Room Design by Anne LeGal.

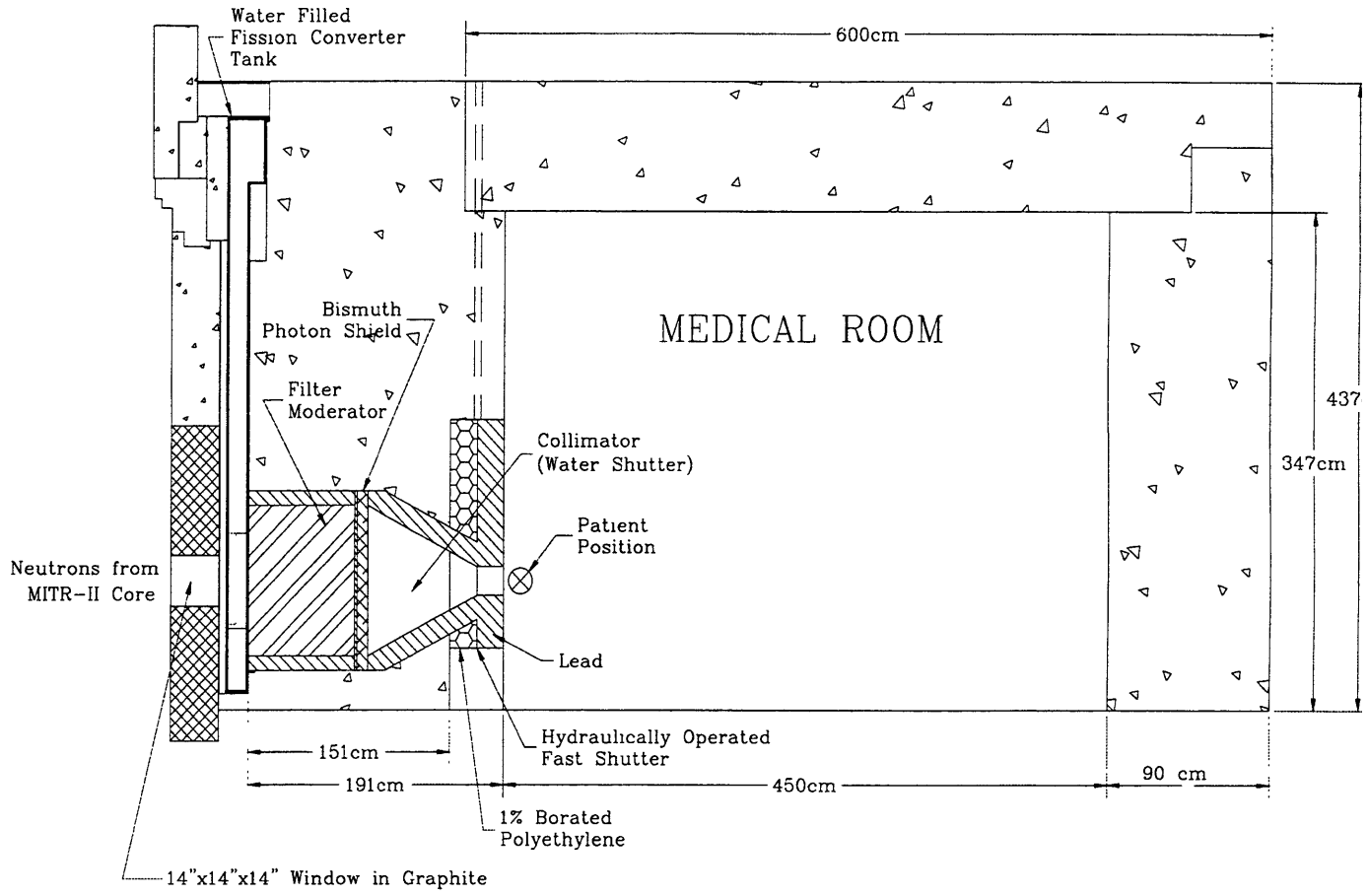

Figure 2.3 Medical room design by Balendra Sutharshan.

2.4 DOSE CALCULATIONS

2.4.1 Introduction

In addition to the desired epithermal neutrons used in BNCT therapy, the fission converter BNCT beam produces a considerable amount of fast neutrons and gamma rays. These types of radiation, which are essentially beam contaminants for this therapy, contribute undesirable dose rates outside the medical room. In compliance with the specifications outlined in section 2.2, the total dose rate outside the medical room should be less than 1 mrem/hr. This limit was chosen because it complies with federal regulations while providing a safety factor. The amount of shielding required to achieve the optimal dose level outside the medical room was determined for the various walls of the room. Shielded walls include the side walls, ceiling, floor, back wall and door. The shielded walls were then placed into an optimal layout for the overall medical room design.

The methods used for shielding determination in this work consisted of hand calculations, experimental measurements, and Monte Carlo computer simulations. Simple analytical methods based on hand calculations were used to find the optimal shielding for the walls and door. These analytical methods were then compared with experimentally measured values in the current medical room in order to verify their suitability. Also, reflection data from the experimental measurements in the current medical room provided an empirical approach for determining the shielding required for the door in the new medical room. Additionally, Monte Carlo computer simulations were utilized as another shielding design approach.

Before evaluating the amount of shielding required for adequate radiation attenuation, dose rates at the inside surface of the walls were determined. The dose calculations are divided into three categories: radiation scattered off a human head target, a direct beam of radiation, and radiation from multiple scattering surfaces. Dose calculations for the side wall, window, floor, and ceiling assume a beam of radiation incident upon a human head or phantom. The radiation then scatters off the head. Conversely, the dose rate at the back wall was determined beginning with a direct beam of radiation that has a 30 degree spread. These scenarios give the maximum dose rates. Methods used to estimate the amount of radiation transported to the door assume multiple paths that require greater detail and will be discussed in Chapter 3.

2.4.2 Dose Calculations for Side Wall and Window

Calculating the dose incident on the side walls of the medical room was necessary to find the amount of shielding required for the side walls. This dose calculation assumes a direct radiation beam consisting of gamma and fast neutron radiation. This beam penetrates a human head with an 8 cm radius, scatters, and finally travels a distance of 300 cm to the outside of the adjacent medical room wall (see Figure 2.4).

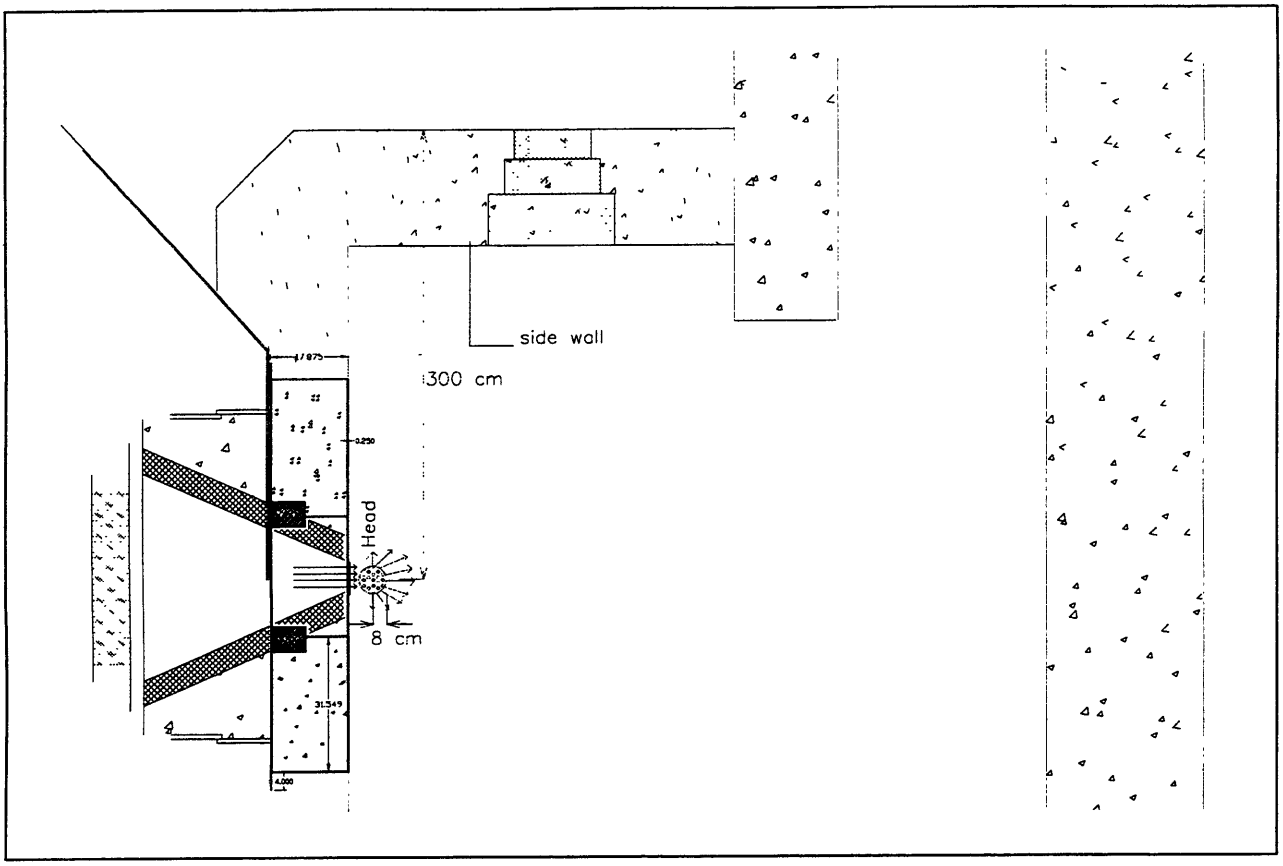

Figure 2.4 Schematic of radiation transport assumptions for dose calculations.

Dose coming out of beam

The fluxes for maximum output of the fission converter were used in designing the medical room shielding. These maximum rates assume a 10 MW reactor power and all fresh fuel elements[4].

ϕepithermal = 1.7×10^{10} n/cm^2.sec

ϕthermal = 9.6×10^{8} n/cm^2.sec

ϕfastneutron = 1.1×10^{8} n/cm^2.sec

ϕgamma = 1.2×10^{8} n/cm^2.sec

[4] Neutron fluxes were obtained from W.S Kiger's thesis, Neutronic Design of a Fission-Convertered Based Epithermal Beam for Neutron Capture Therapy, Table 5.21.

For shielding purposes, fast neutrons and gamma rays were considered. The contribution of epithermal and thermal neutrons to shielding requirements consists mostly of the production of capture gamma radiation in the walls. Aside from this, epithermal and thermal neutrons did not significantly affect the dose levels requiring shielding. This point will be further discussed in Chapter 5. For the hand calculations, average energies of 1 Mev and 3 Mev were used for fast neutrons and gamma rays, respectively. Dose rates at the beam opening are obtained from the fluxes by the following relationship,

$$Dfn = \frac{\phi fastneutron}{K(E)} \qquad \textbf{(2.1)}$$

where $\phi fastneutron$ is the flux (n/cm^{2}sec) of fast neutrons entering the medical room from the fission converter beam. K(E) is the kerma conversion factor for fluence to dose equivalent for specific energy neutrons. The following Kerma factors for converting fluence to dose equivalent were used throughout the shielding design to convert neutron flux to dose rates.

Neutron Energy (Mev)	Quality Factor	Fluence/dose equivalent (n/cm2rem)
2.50E-08	2	9.80E+08
1.00E-07	2	9.80E+08
1.00E-06	2	8.10E+08
1.00E-05	2	8.10E+08
1.00E-04	2	8.40E+08
1.00E-03	2	9.80E+08
1.00E-02	2.5	1.01E+09
1.00E-01	7.5	1.70E+08
5.00E-01	11	3.90E+07
1	11	2.70E+07
2.5	9	2.90E+07
5	8	2.30E+07
7	7	2.40E+07
10	6.5	2.40E+07
14	7.5	1.70E+07
20	8	1.60E+07

Table 2.1 Neutron Dose Conversion and Quality Factors.[5]

Gamma dose rates entering the medical room from the beam opening are obtained by the following,

$$D\gamma = \frac{\phi gamma \cdot E \cdot 1.6\times10^{-6}\,\mathrm{erg}\cdot\mu/\rho^{air}\cdot Q}{100\,\mathrm{erg/g}} \qquad \textbf{(2.2)}$$

where Φ_γ = gamma flux coming out of beam,

μ/ρ^{air} = energy absorption coefficient for air at specific energies, and

Q = quality factor for gamma rays = 1.

The value of μ/ρ_{air} for 3 Mev gamma rays is 0.035768 cm^2/g.

[5] From NRC's 10 CFR part 20.

Dose rates in the direct beam at the end of the collimator:

$Dfn = 1.47x10^4$ rem/hr

$D\gamma = 1.2x10^3$ rem/hr

Dose rates scattered from the patients head- or phantom

The major radiation source responsible for dose rates at the side wall is the result of fast neutrons and gammas scattered off a phantom or human brain, located at the patient position, and gamma rays from (n,γ) reactions with hydrogen in the target. This assumption provides the largest, most conservative, estimate of the dose at the side wall, 90 degrees from the beam direction. An additional source of radiation reaches the side walls by reflection off of the lead collimator. This dose component will be discussed in greater detail in Chapter 5.The assumed radius of a brain target is 8 cm. Listed in the following table is the elemental composition[6] of brain tissue, which has a density of 1.040 g/cm^3.

Table 2.2 Composition of Brain Tissue and Removal Cross Sections for Fast Neutrons.

Element	weight fraction	Σ_r (cm^{-1})[7]	fraction x Σ_r
H	0.1017	0.158[8]	0.01607
C	0.1450	0.0838	0.01215
N	0.0220	0.0560	0.00123
O	0.7120	0.0579	0.04122
Na	0.0020	0.0313	6.26e-5
P	0.0040	0.0493	1.972e-4
S	0.0020	0.0540	1.08e-4
Cl	0.0030	0.0799	2.397e-4
K	0.0030	0.1533	4.599e-4

[6] From http://physics.nist.gov/PhysRefData/XrayMassCoef/tab2.html.
(7) From Reactor Shielding for Nuclear Engineers, Schaeffer, Table 4.3, p. 182-183.
(8) From Neutron Cross Sections, D. Hughes and R. Schwartz, United States Atomic Energy Commission.

The sum of Σ_r fractions provides the total fast neutron macroscopic removal cross section, Σ_r, 0.0717 cm^{-1}. The total gamma attenuation coefficient for the brain, μ, is 0.041 cm^{-1}[6].

To calculate the dose scattered from the brain several assumptions were made. First, fast neutrons and gamma rays travel, on average, the distance of the brain's radius before scattering. Furthermore, it is assumed that the buildup factor for gamma rays in the brain is equal to that of water. From the Berger approximation method of gamma ray buildup factors, the buildup factor is 1.0. Also, the removal cross section for fast neutrons was used instead of the total cross section to correct for the uncollided flux density for scattered neutrons in the brain, rather than using buildup factors. These removal cross sections are experimentally determined values for a fission neutron spectrum and are therefore very conservative considering the fast neutron spectrum present in the fission converter beam. Based on these assumptions the dose at the center of the brain was computed by the following equation:

$$Dbrain = D_o B(\mu, E) e^{-\mu R} \qquad \textbf{(2.3)}$$

where B(μ,E) is approximated to be 1.0 for gamma rays, neutron removal cross section, Σ_r, is 0.0717 cm^{-1} for fast neutrons, and gamma rays are attenuated exponentially with a coefficient, μ, of 0.041 cm^{-1} [2]. From equation 2.3, the fast neutron dose and gamma dose at the brain were obtained as follows:

$D_{fn,brain} = 8.28 \times 10^3$ rem/hr

$D_{\gamma,brain} = 864$ rem/hr + $D_{capture_\gamma}$

In addition to these dose rates, hydrogen neutron capture in the brain contributes a significant amount of dose to the brain and is the largest component of the gamma source that reaches the medical room walls. The method was used to quantify the capture gamma dose rate is as follows:

$$\phi capt\gamma = vN\sigma\phi\, th_{avg} \qquad \textbf{(2.4)}$$

The term v represents the brain volume (cm^3), N is the number density ($atoms/cm^3$) of hydrogen in the brain. The cross section for thermal neutron capture by hydrogen is represented by σ in the units of cm^2, and the average thermal neutron flux in the brain, ϕth_{avg}, is approximated as one half of the maximum thermal neutron flux in the brain, which was obtained from W.S. Kiger's MCNP calculations[2]. The capture gamma flux was then converted to a dose rate by,

$$Dcapt\gamma = \frac{\phi capt\gamma \cdot E\,\mu/\rho^{air} \cdot 1.6\times10^{-6} \cdot Q}{100} \cdot \exp^{-\mu R} \qquad \textbf{(2.5)}$$

Hydrogen neutron capture results in gamma rays with energy of 2.2 Mev, represented as E in the above equation. The value for μ/ρ^{air} at this energy is 0.042241 cm^2/g. The value for gamma attenuation in the brain, μ, mentioned earlier, is 0.041 cm^{-1}, and the radius of the brain, R, is also assumed to be 8 cm here. This results in a capture gamma dose of $3.3x10^3$ rem/hr at the surface of the brain.

Dose directly outside of medical room side wall

The total dose rates used for the shielding calculations are the dose rates at the location directly outside the medical room wall, assuming no attenuation by shielding structures. Assumptions made to obtain these dose rates are as follows. First, the distance between the brain and outside the medical room wall was approximated to be 300 cm. This distance may slightly underestimate the dose if the side wall is thinner than anticipated. Also, the radiation at the brain is assumed to be uniformly distributed over the entire brain. Therefore, the dose outside the medical room is proportional to the ratio of the area of the brain and the area of the radiation seen immediately outside the medical room wall. Finally, the radiation intensity incident upon the wall is dependent upon the angle at which it scatters off the brain. This excludes the capture gamma dose component which scatters isotropically. As a result, the dose rate outside the medical room wall, prior to shielding, is represented by the point source assumption:

$$Doutsidewall = \frac{Dscatter \cdot 4\pi r^2}{4\pi X^2} \qquad \textbf{(2.6)}$$

where r represents the radius of brain, 8 cm, and distance to outside of the wall, X, is 300 cm. $D_{scatter}$ describes the dose after loss of energy from a 90 degree scatter.

The dose as a function of the scattering angle, $D_{scatter}$, was calculated for both scattered neutrons and gamma rays. The hydrogen capture gamma component is assumed isotropic, see above. Figure2.5 illustrates the scatter of neutrons off a head target.

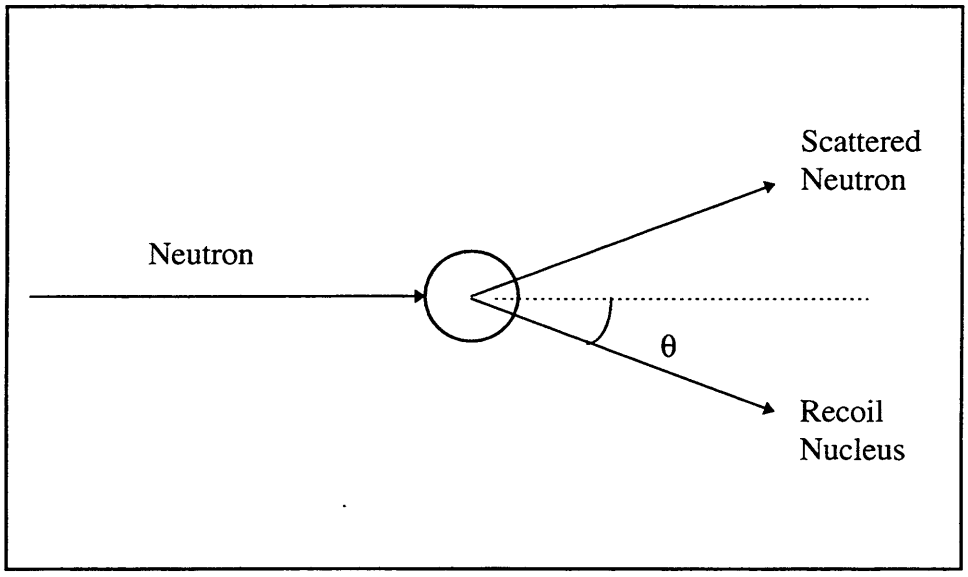

Figure2.5 Neutron Scattering off a head target.

The energy of the recoil nucleus depends on the angle at which it is scattered.

$$E_R = \frac{4A}{(1+A)^2} \cdot \cos^2\theta \cdot En \qquad \textbf{(2.7)}$$

The energy of recoil nucleus, ER, is a function of the energy of the incident neutron, En, the atomic mass, A, of the target nucleus, and the angle of recoil, θ. Due to energy conservation, the energy of the scattered neutron is related to E_R by:

$$En' = En - E_R . \qquad \textbf{(2.8)}$$

Four different nuclei in the brain tissue contribute to the neutron scattering. These are ^{1}H, ^{12}C, ^{14}N and ^{16}O. 16 % of the interactions occur from collisions with ^{1}H, 21% from ^{12}C, 1.8% from ^{14}N and 61 % from ^{16}O. 90 degrees was chosen as the angle of scatter towards the side wall.

Table 2.3 Scattering Properties of Elements in Brain Tissue for 1 Mev neutrons.

Element	Σscattering (cm^{-1})	% of total $\Sigma scattering_i$ in brain	Energy at 90° scatter (mev)
H	0.158	16.06	0
C	0.143	20.68	0.716
N	0.081	1.79	0.751
O	0.0863	61.47	0.778

The energy of the 1 Mev neutron scattered at 90 degrees is 0 Mev from interactions with ^{1}H, 0.716 Mev from ^{12}C, 0.751 Mev from ^{14}N, and 0.778 Mev from ^{16}O interactions. The contribution of each element to the total neutron dose rate scattering towards the side wall at 90 degrees is 1085 rem/hr from ^{12}C, 95 rem/hr from ^{14}N, and 3360 rem/hr from ^{16}O. Thus, a total neutron dose, $D_{n,scatter}$, of $4.54x10^3$ rem/hr is incident on the the side wall at 90° to the incoming beam direction.

The energy of the scattered gamma radiation was computed using similar methods. The energy of the scattered photon was found by:

$$h\nu' = \frac{h\nu}{1+(h\nu/mc^2)(1-\cos\theta)} \qquad \textbf{(2.9)}$$

where hν represents the initial photon energy of 3 Mev, mc^2 is equal to 0.511 Mev, the electron rest mass, and θ of 90 degrees denotes the angle of the scattered photon with energy hν'.

The energy of the photons scattering off of the brain at 90 degrees is 0.437 Mev, which corresponds to a dose rate, $D_{\gamma,scatter}$, of 70.9 rem/hr at the surface of the brain.

However, this dose does not include the $3.0x10^3$ rem/hr, at the surface of the brain, from capture gamma rays produced in the in the brain by hydrogen. The capture gamma dose was assumed to be uniformly distributed over the surface of the brain and to scatter isotropically. The dose rate from capture gamma rays created in the head was found assuming a point source in the center of the brain,

$$Dcapt\gamma outsidewall = \frac{Dcapt\gamma \cdot e^{-\mu R}}{4\pi X^2} \qquad \textbf{(2.10)}$$

The values for X, the distance between the brain and outside of the wall, R, the brain radius, and μ, the gamma attenuation coefficient in the brain are :

X = 300 cm, R = 8 cm, $\mu = 0.041$ g/cm^3.

This gives $3.0x10^3$ rem/hr for the hydrogen capture gamma dose rate at the distance corresponding to the outside surface of the side wall, 300 cm. Using equation 2.6, the dose rates outside the medical room side wall, prior to shielding are:

Dfn,outsidewall = 3.23 rem/hr

Dγ, outsidewall = Dγ + Dcaptγ =2.45 rem/hr

The shielding materials in the wall create additional gammas from (n,γ) reactions. MCNP was used to obtain this added capture gamma dose, described in Chapter 5. An approximation of the capture gamma dose was found by tallying the thermal neutron flux as a function of depth in the concrete of the side wall. The neutron capture reactions in

the concrete create gamma rays with energy equal to 1.05 Mev.[9] The number of gammas created by neutron capture in the concrete, as a function of depth in concrete, was found by multiplying the thermal neutron flux at depth in concrete, x, by the neutron capture cross section, Σ_c and by the number of gammas produced per neutron capture, f, as shown below.

$$S_\gamma(x,E) = \phi th(x) \cdot \Sigma c(E) \cdot f \qquad \textbf{(2.11)}$$

The values used for the constants in equation 2.11 are listed below:

$\Sigma c = 0.0975\ cm^{-1}$

$f = 1.25\ \gamma$'s per n capture.

This source of gammas, $S\gamma$, was then converted into a dose rate by:

$$D\gamma = \frac{S\gamma \cdot B(\mu, t-x) e^{(-\mu(t-x))} \cdot E \cdot 1.6\times10^{-6} erg \cdot \mu/\rho^{air} \times Q}{4\pi(t-x)^2 \cdot 100 erg/g} \qquad \textbf{(2.12)}$$

where t = total shield thickness, 60 cm

x = depth in shield

μ = photon attenuation coefficient for concrete, 0.1361 cm^{-1}

B = photon buildup factor in concrete

E = average energy of photon created =1.05 Mev (from MCNP)

$\mu/\rho^{air} = 0.035768\ cm^2/g$.

[9] Average energy obtained from MCNP simulations. This energy is consistent with values listed in Engineering Compendium on Radiation Shielding, v.I, p.87, Jaeger.

Using this method, the dose from gammas created by neutron capture in concrete is $5x10^{-8}$ rem/hr at the outside of the side wall. The graph below displays the capture gamma flux as a function of depth in concrete. It also shows the effect each flux point has on the capture gamma dose after 60 cm of concrete. Obviously, this dose is small in comparison to the total gamma dose outside the medical room prior to shielding. Therefore, the total gamma dose outside the medical room is not significantly affected by capture gammas created in concrete.

Figure 2.6 Results of capture gamma calculations at different depths through side

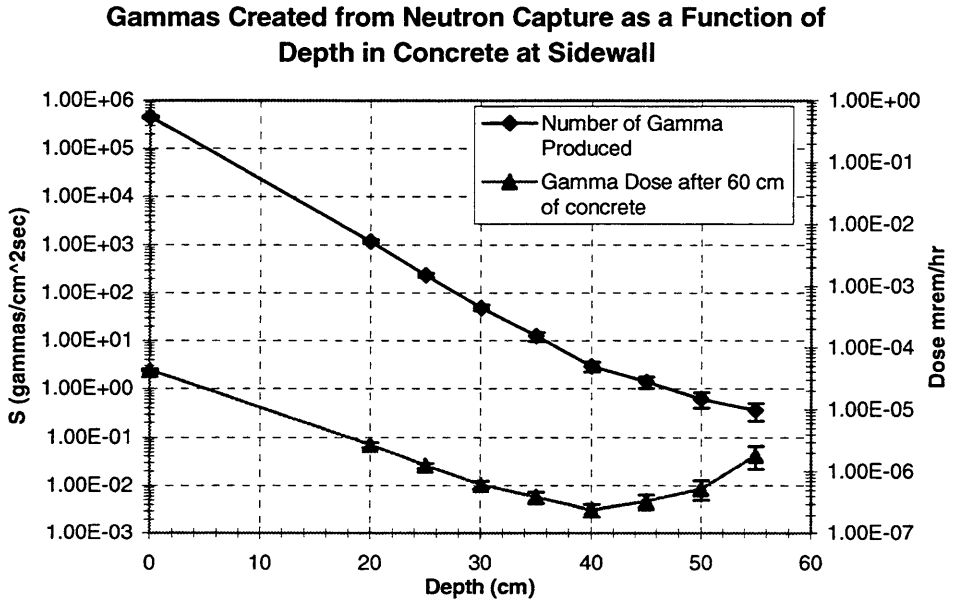

wall.

*Dose only graphed to depth of 55 cm because the MCNP simulation did not detect any thermal neutrons at depths greater than 55 cm.

2.4.3 Dose Calculations at Ceiling

When the radiation coming out of the beam is scattered by the patient's head, or a phantom, it can scatter in all directions. This means that some radiation will scatter up towards the ceiling. The distance to the outside of the ceiling is approximately equal

to the distance outside of the side walls. Therefore, dose rates directly outside the ceiling are the same as the dose rates outside the side wall.

2.4.4 Dose Calculations at Floor

As in the case of the ceiling, the floor also receives radiation from scatter off a head or phantom. The floor, however, is about 90 cm closer to the head than the ceiling and side walls. As shown in section 2.4.2, the dose rate below the floor is inversely proportional to the squared distance between the head and the outside of the wall. Adjusting for this shorter distance, X of 107 cm, the neutron and gamma doses were calculated using the same method as the side wall dose calculations.

Neutron dose outside floor = 5.58 rem/hr

Gamma dose outside floor = 4.90 rem/hr

The area underneath the medical room is occupied by the equipment room. Three feet of ordinary concrete separate the two rooms. The equipment room is a high radiation area with minimal occupancy. Entrance into the equipment room is only allowed when the reactor is shut down. This is useful in considering the floor shielding of the medical room. Because no one will enter the equipment room while a patient, or phantom, is being irradiated in the fission converter beam, additional analysis of the shielding for the floor is unnecessary.

2.4.5 Dose Calculations at Back Wall

Estimates of the dose rates at the back wall utilize a direct beam of radiation that has a 30 degree spread. A schematic displaying the radiation incident upon the back wall is shown in the figure below. Throughout this section, the relationship between the dose rate at the beam opening and the back wall is assumed to be inversely proportional to the squared radius of the radiation area. These radiation illuminated areas are related to the degree to which the beam spreads. To obtain the maximum dose rate at the back wall of the medical room it was assumed that there is no target blocking the beam.

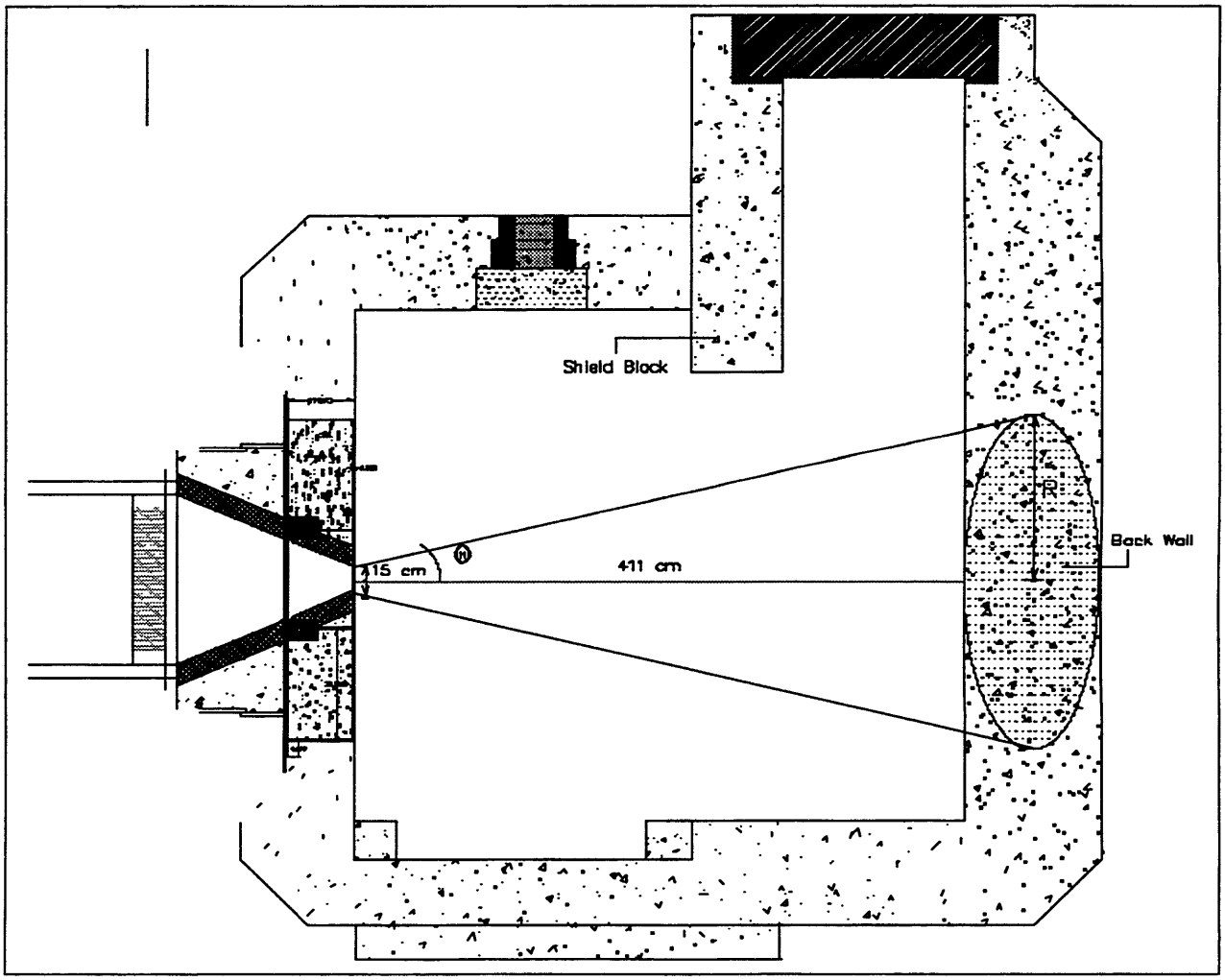

Figure 2.7 Schematic of radiation transport to back wall.

The degree of spread in the beam was obtained by fitting data presented in Figure 5.31 from W.S. Kiger's thesis[2]. The figure shows the neutron flux as a function of distance from the core. This data was fit to $1/r^2$ attenuation to obtain the degree of spread in the beam.

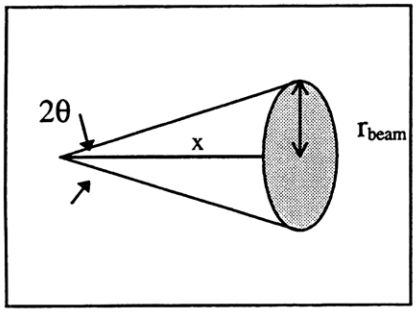

$$\theta = \tan^{-1} \cdot \frac{r_{beam}}{x} \qquad \textbf{(2.13)}$$

From the graph a point was chosen to represent the zero point of the beam spreading cone. The arctan of the ratio of the beam width to the distance between the zero point to the beam opening gave a beam spread of 25°. Additional beam spread angles were found using the values given for fast neutron flux at 10, 20, 30, and 50 cm away from the beam opening. Taking the average of the different values for beam spreading, 30° was chosen for the beam spreading angle.

In addition to a 30 degree spread, the beam is also assumed to have a 15 cm diameter. Moreover, the beam displays a $1/r^2$ geometric attenuation as it expands to a radius of 110 cm at back wall. From this, the dose at the inside of the backwall of the medical room, at the surface of the shielding, is calculated by the following equation,

$$Dbackwall = Dfn \frac{\cdot R^2_{beamopening}}{R^2_{backwall}} \qquad \textbf{(2.14)}$$

$$Rbackwall = x \tan\theta \qquad \textbf{(2.15)}$$

where $R_{beam\ opening}$ is the radius of the beam opening , 7.5 cm. The backwall is located a distance, x, of 411 cm away from the beam opening. The backwall radius, $R_{backwall}$, is 110 cm as a result of a 15 degree θ, which represents one half of the total beam spread.

Dose Rates at Beam Opening, Reactor at 10 MW power with fresh fuel

Dfn = 1.47×10^4 rem/hr

Dγ = 1200 rem/hr

Dose Rates at Surface of Back Wall 411 cm from Beam Aperature

Dfn,backwall = 68.15 rem/hr

Dγ,backwall = 5.564 rem/hr

2.5 SHIELDING CALCULATIONS

2.5.1 Shielding Calculations for Side Wall and Ceiling

The shielding calculations were performed using Swedish I-2a concrete. This type of concrete was used for the shielding analysis because it is the type of concrete currently used to the shield the BTF area. Further use of the existing blocks of I-2a concrete is discussed in Chapter 8 along with a more detailed analysis of the shielding properties of I-2a concrete.

Table 2.4 Concrete Properties[10]

Type	Density (g/cm^3)	Gamma Attenuation Coefficient (1/cm)	Fast Neutron Macroscopic Removal Cross Section (1/cm)
I-2a Swedish Ore	3.76	0.1361	0.111

In accordance with the design specifications set forth in section 2.2, the dose rate outside the medical room must be reduced to 1 mrem/hr. The amount of concrete required achieve this dose rate is represented by the following equations:

$$\frac{D\gamma'}{D\gamma} = Be^{-\mu x} \qquad \textbf{(2.16)}$$

where $D\gamma'$ is the desired gamma dose rate. The initial dose rate, $D\gamma$, is attenuated exponentially as a function of the gamma attenuation coefficient of the material and by x, the amount of material in the shield. B represents the buildup factor in the material.

[10] From Engineering Compendium on Radiation Shielding VII, Jaeger, Tables 9.1.12-85, 86.,pp.179-180

Similarly, the amount of material to reduce the neutron dose rate to a desired level is found by:

$$\frac{Dfn'}{Dfn} = e^{-\Sigma_r x} \qquad \textbf{(2.17)}$$

where Dfn' is the desired neutron dose rate. Dfn in the neutron dose rate prior to shielding which can be reduced by a shield of x thickness. The removal cross section for fast neutrons in the material is expressed as Σr. The buildup factors for gamma rays in concrete were calculated using the exponential fit equation:

$$B(\mu, x) = Ae^{-\alpha\mu \cdot x} + (1 - A)e^{-\alpha_2 \mu \cdot x}. \qquad \textbf{(2.18)}$$

The buildup factor is function of the shield thickness, x, the attenuation coefficient of the material, μ and the energy of the gamma rays. The symbols in the equation above, A, α, and α2 are constants particular to a certain shield. These too are function of energy, shield thickness, and the gamma attenuation coefficient in the certain material of interest.

The removal cross section was used for the fast neutron attenuation calculations to account for the uncollided flux density of scattered neutrons in the material, rather than applying buildup factors. Neutron buildup factors, unlike those for photons, need to be experimentally determined for each particular problem because the buildup of fast neutrons depends on a complex set of dependent factors including, the initial energy of the neutrons, the energy dependence of the cross sections for the material, and on the

angular distribution of the neutrons.[11] The use of the removal cross section is a method for accounting for the buildup of neutrons in a material.

Table 2.5 Side Wall Shielding Results

$D\gamma = 2.45$ rem/hr , $Dn = 3.23$

Material	Thickness needed to shield gamma rays to 1 mrem/hr (cm)	Buildup Factor for gamma rays	Thickness needed to shield fast neutrons to1 mrem/hr (cm)
I-2a concrete	73	8.41	73

2.5.2 Back Wall Shielding Calculations

Using the attenuation properties given in table 2.4 for I-2a concrete and inserting them into equations 2.14 and 2.15, the amount of concrete required to sufficiently attenuate the dose rate at the back wall was calculated.

Table 2.6 Back Wall Shielding Results

$D\gamma = 5.564$ rem/hr , $Dn = 68.2$

Material	Thickness needed to shield gamma rays to 1 mrem/hr (cm)	Buildup Factor for gamma rays	Thickness needed to shield fast neutrons to1 mrem/hr (cm)
I-2a concrete	79	9.07	100

[11] Principles of Radiation Shielding. Chilton. Prentice Hall, 1984. Pp 218-241.

2.6 REFERENCES

Campos, T., Personal communication.

Cember, H., *Introduction to Health Physics*, 3rd edition, McGraw-Hill, 1996.

Chilton, A., Shultis, J.K, Faw, R., *Principles of Radiation Shielding,* Prentice Hall, Inc., NJ, 1984.

Harling, O.K., Personal communication.

Hughes, D., Schwartz, R., *Neutron Cross Sections*, United States Atomic Energy Commision.

Jaeger, R.G, "Shielding Materials", *Engineering Compendium on Radiation Shielding*, Vol.II, Springer-Verlag, New York Inc, 1975.

Jaeger, R.G, "Shield Fundamentals and Methods", *Engineering Compendium on Radiation Shielding*, Vol.III, Springer-Verlag, New York Inc, 1968.

Kiger, W.S, *Neutronic Design of a Fission Converter-Based Epithermal Beam for Neutron Capture Therapy,* Nucl. E. Thesis, Massachusetts Institute of Technology, 1996.

LeGal, A., Ledieu, M., *Beam Shutter Design and Medical Room Design,* MIT, Sept. 1995.

Masse, F., Personal communication.

NRC, "Title 10, Chapter 1, Part 20" *Code of Federal Regulations-Energy*, United States Nuclear Regulatory Commission, 1995.

NIST, http://physics.nist.gov/PhysRefData/XrayMassCoef.

Rockwell, T. , *Reactor Shielding Design Manual,* D. Van Nostrand Company, Inc., 1956.

Schaeffer, N.M., *Reactor Shielding for Nuclear Engineers,* U.S. Atomic Energy Commission, 1973.

Shultis, J.K., Faw, R., *Radiation Shielding*, Prentice Hall, Inc., NJ, 1996.

Sutharshan, B, *Engineering Design of a Fission Converter-Based Epithermal Beam for Neutron Capture Therapy,* Ph.D. thesis, Massachusetts Institute of Technology, 1998.

CHAPTER 3

SHIELDING DOOR

3.1 INTRODUCTION AND SPECIFICATIONS

The door is an important component of the medical room. It allows access into the room and minimizes the outside dose to reactor and medical staff during treatment. In order to be most efficient, the following specifications must be used in designing the door:

- The door needs an opening and closing mechanism that can be operated quickly.
- The material of the door needs to be of a high density to shield gamma rays, high in hydrogen content to moderate neutrons, or high in other materials which can attenuate fast neutrons, and contain heavy elements to absorb secondary gammas.
- The size of the door must be optimized to provide for adequate shielding while meeting the weight requirements of the crane and occupying a minimal amount of floor space.
- The door must have safety mechanisms to allow manual operation and quick removal of patient in an emergency.

A large part of the shielded door analysis relied on determining the best location for the medical room door. Important factors considered in deciding upon the door location were radiation levels, space limitations both inside the room and on the reactor floor, ease of design, and dimensions. Ideally, the door should be located in an area with little or no direct radiation. This would reduce the overall bulk of the door, and therefore improve space limitations in the room and on the reactor floor. The best location for the door was found to be on the front corner of the right wall, adjacent to the beam, shown in Figure 3.1. One advantage of this location is that it minimizes the amount of radiation directly hitting the door. This location also eliminates blocking the equipment room access plug and does not require the use of two doors to meet the weight specifications. Additionally, putting the door on the back corner of the right wall stills allows for plenty of space outside of the room to place the necessary control panels and dosimetry computers.

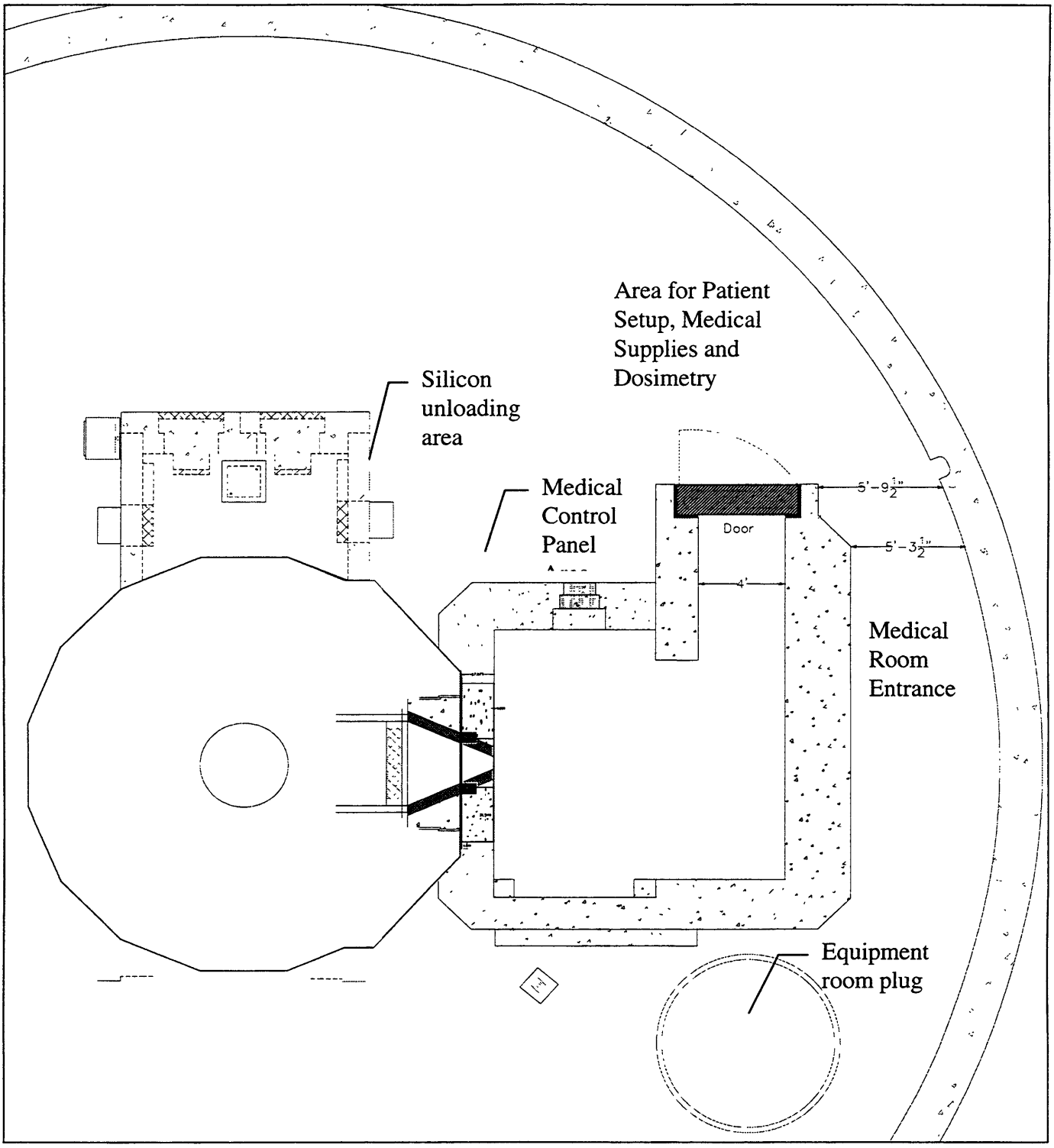

Figure 3.1 Layout of room showing the location for the shielded door in the reactor building.

3.2 DOSE CALCULATIONS

Dose levels on the inner door surface arise from three radiation components. These are direct radiation, leakage radiation, and scattered radiation. The direct radiation component is eliminated by the use of a shield block located at the start of the doorway, in the path of the direct beam, see figure3.1. The beam diverges a total of ~30 degrees from the forward direction, as mentioned in chapter 2. Direct radiation from this degree of spread should not reach the door. However, radiation reflection off the lead collimator results in a beam of radiation incident on the doorway area, which will be discussed further in chapter 5. Because of this radiation component, a shield block, 45 cm long x 60 cm wide, was placed at the start of the doorway. The radiation penetrating through the shield block comprises the leakage component of the dose rate at the door. The scattering component of the dose rate at the door consists of radiation scattering off the back wall, floor and shield block. The radiation reflected from these surfaces and transported to the door is calculated to be the most significant source of radiation at the door. These radiation components were quantified prior to determining the shielding for the door.

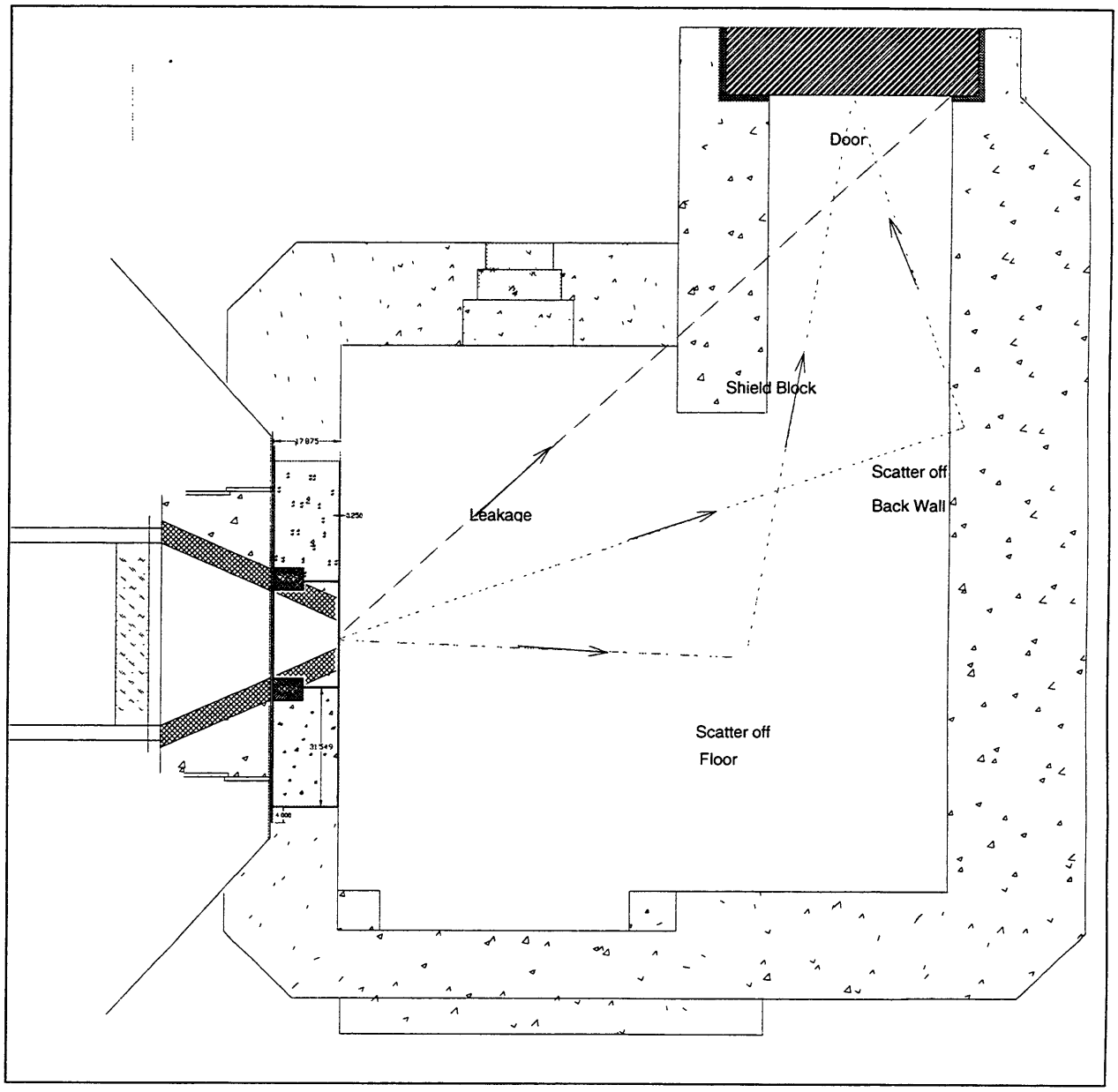

Figure 3.2 Schematic of Radiation Components at Door.

3.2.1 Leakage Component

As mentioned above, direct radiation does not hit the door. The shield block shading the entire hall eliminates any direct radiation that might otherwise reach the door. Even though a small amount of radiation penetrates through the shield block and eventually reaches the door, this dose alone is negligible. However, in this process gammas are produced from neutron capture in the shield block and wall of the doorway. This additional gamma dose component is calculated to be the major contributor of gamma dose at the door. Furthermore, thermal and epithermal neutron doses that were considered negligible, prior to now, contribute a significant amount of dose due to gamma production from neutron capture reactions in the concrete, particularly the shield block.

To prove its insignificance to the total dose at the door, the dose rate from radiation penetrating through the concrete shield block was determined by the following equations for incident neutrons and gamma rays. The dose rates in the following equations represent a single dose point. To get the total dose rate, these were integrated over the entire shield block area.

$$D_1 = \frac{Do \cdot r_{beam}{}^2}{(x \tan\theta)^2} \qquad (3.1)$$

$$D_2 = \frac{D_1 \cdot B(\mu,d)}{4\pi d^2} \qquad (3.2)$$

$$D_3 = \frac{D_2}{4\pi r^2} \qquad (3.3)$$

D_1,D_2, and D_3 are defined in figure 3.3.

D_1 represents the dose rate at the beginning of the shield block located 230 cm, x, from the beam opening. The beam is assumed to have a beam spread, θ, of 35 degrees, and beam opening radius, rbeam, of 7.5 cm. Note that this degree of beam spreading is much larger than the value reported earlier.

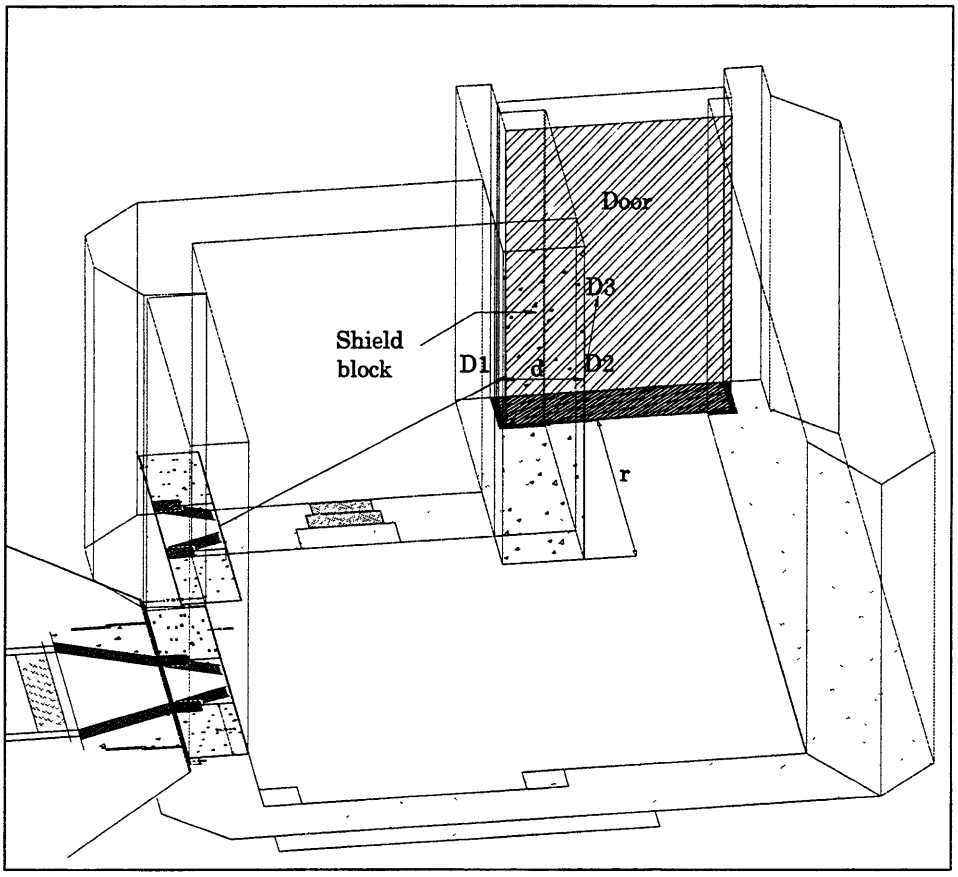

Figure 3.3 Diagram of leakage radiation through shield block.

The discrepancy arises from the fact that radiation scatter off the lead collimator results in a greater than 30 degree total spread along the perimeter of the room. The $1/r^2$ attenuation is assumed for radiation reflecting off the collimator. The angle of 35 degrees is the angle that radiation would have to depart from the straight, 0 degree, path, as it bounced off the lead collimator in order to touch the shield block. The amount of radiation that penetrates through the shield block is defined by the dose rate, D_2. D_2 is a function of the attenuation coefficient for concrete, μ, and the thickness of the shield block, d. The amount of radiation that eventually reaches the door from the shield block is expressed as D_3.

The dose rates at the inside surface of the door from leakage through the shield block are 5.4×10^{-5} mrem/hr for fast neutrons and 2.4×10^{-6} mrem/hr for gammas. These dose rates are small and, for the purpose of shielding calculations may be neglected. However, the dose rates from thermal neutron capture gamma rays must still be considered. This gamma dose was obtained in a manner similar to that outlined in section 2.4.2. The thermal neutron flux within the concrete shield block was obtained using MCNP. A detailed description of this MCNP study is discussed in Chapter 5.

Using MCNP, the thermal neutron flux at the hallway face of the shield block was found to be 5.62×10^{5} n/cm^{2}sec with an error of 5.7 percent. The dose rate at the door from capture gammas was calculated to be 1.6 ± 0.091 rem/hr.

3.2.2 Neutron Scattering Component

The scattering component of the total dose rate seen at the door consists of two parts: scatter off the back wall, and scatter off the floor. These dose rates were obtained using albedo methods. The neutron albedo is the ratio of the amount of radiation incident upon one surface that is scattered to another surface at a particular angle. The albedo for concrete was determined using the energy-dependent, four-parameter formula, equation 3.5. This equation is a linear combination of the single-scattering and multi-scattering albedo expressions. Energy loss within the medium is taken into account by the use of this albedo equation. Also, the albedo from concrete was determined experimentally using the current medical room beam and measuring the albedo. The following equations show how the dose at the door was obtained with the albedo methods[12,13].

$$D = \int \frac{Do\,\alpha(Eo,\theta o,\theta,\psi)\cos\theta o}{r^2} dA \qquad (3.4)$$

$$\alpha(Eo,\theta o,\theta,\psi) = M\cos\theta + \frac{B + C\cos\theta_s}{1 + Y(\cos\theta o/\cos\theta)} \qquad (3.5)$$

[12] Reactor Shielding for Nuclear Engineers, N.M. Schaeffer, p. 356, 7.6-3.
[13] Principles of Radiation Shielding, Chilton, Shultis, Faw, p.278, 9.29.

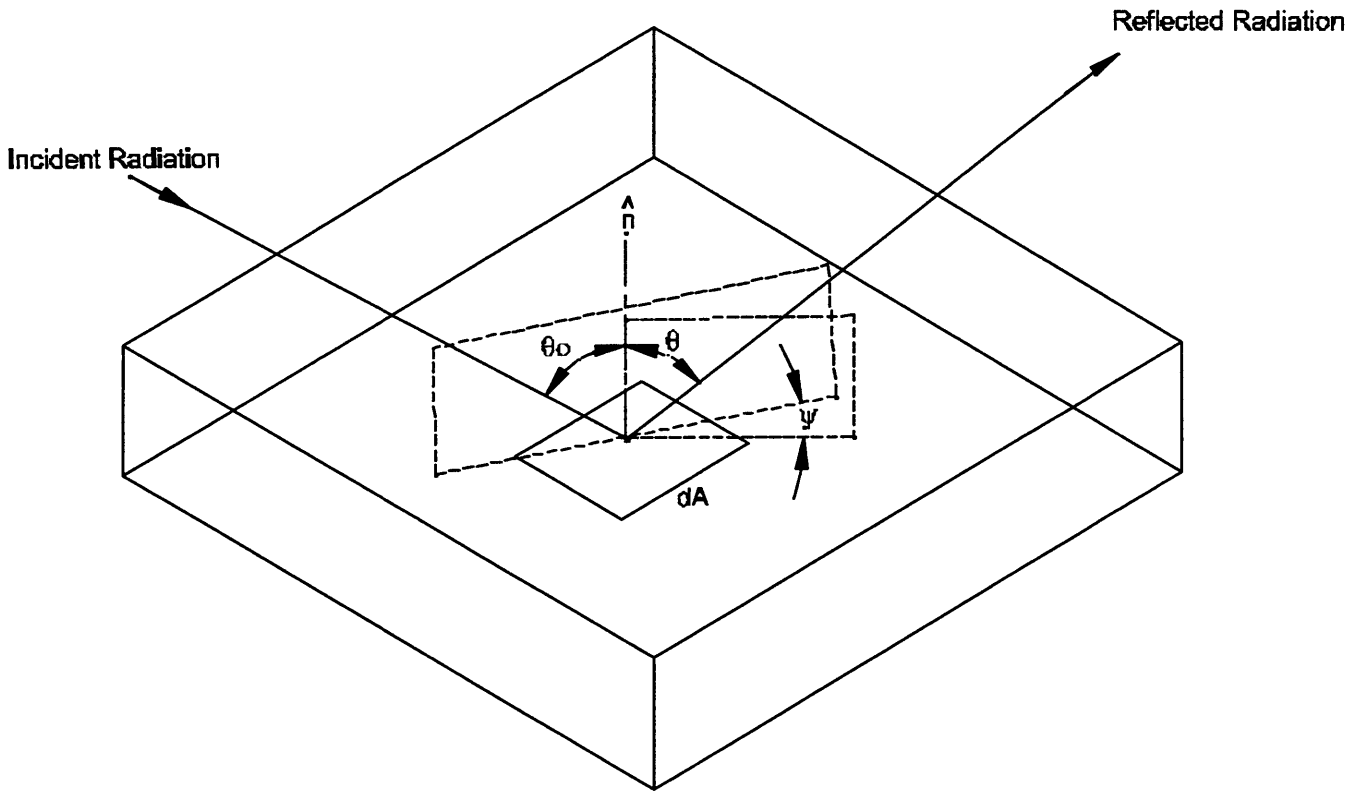

Figure 3.4 Diagram specifying angle notation.

The reflection coefficient, α, depends on the initial neutron energy, the incident angle, θo, the angle of reflection, θ, and on azimuthal angle, ψ. The incident and reflection angles are defined in reference to the normal, **n**, to the reflecting surface, dA, as shown in the figure above. The angle, θs, is found by the law of cosines:

$$\cos\theta s = \sin\theta o \sin\theta \cos\psi - \cos\theta o \cos\theta \qquad (3.6)$$

The parameters M, B, C, and Y assume an incident neutron energy of 1 Mev with concrete as the reflection surface.[14] The following graph shows the albedo for concrete

[14] Principles of Radiation Shielding, Chilton, Shultis, Faw. Table 9.4, p. 280.

with an incident angle of 15 degrees, and azimuthal angle of 90 degrees. This incident angle was used because of the 30 degree beam spread discussed in section 2.4.5.

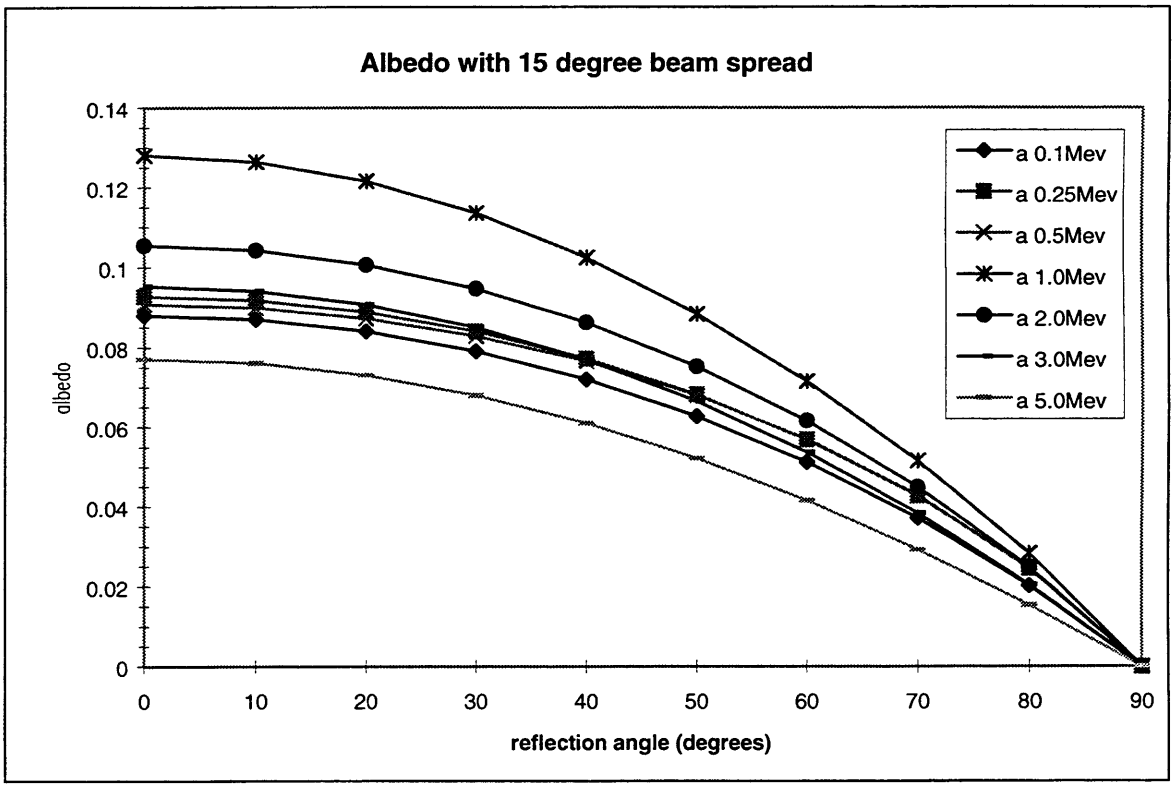

Figure 3.5 Reflection coefficients for a beam with 15 degree spread incident on concrete at an angle of incidence of 15 degrees(θo), $\psi = 90^{o}$.

These values for amount of radiation that reflects off the concrete of the back wall and floor were applied to equation 3.4 to determine the neutron dose rate at the door. Do, represents the dose rate at the reflecting medium assuming monoenergetic point sources distributed over the differential area, dA. The distance between the reflecting surface and the door is represented by r.

3.2.2.1 Neutron Scatter off the Back wall

The dose scattering off the back wall to the center of the door was calculated using albedo methods mentioned above. Values used for θo, θ, and r are displayed in the picture below. The differential area of the reflection surface, dA, is defined as $2\pi x$, where x is the radius of irradiated portion of the back wall. This radius is equal to the tangent of angle of incident radiation, θo, times the distance between the beam opening and back wall, as described in section 2.4.5.

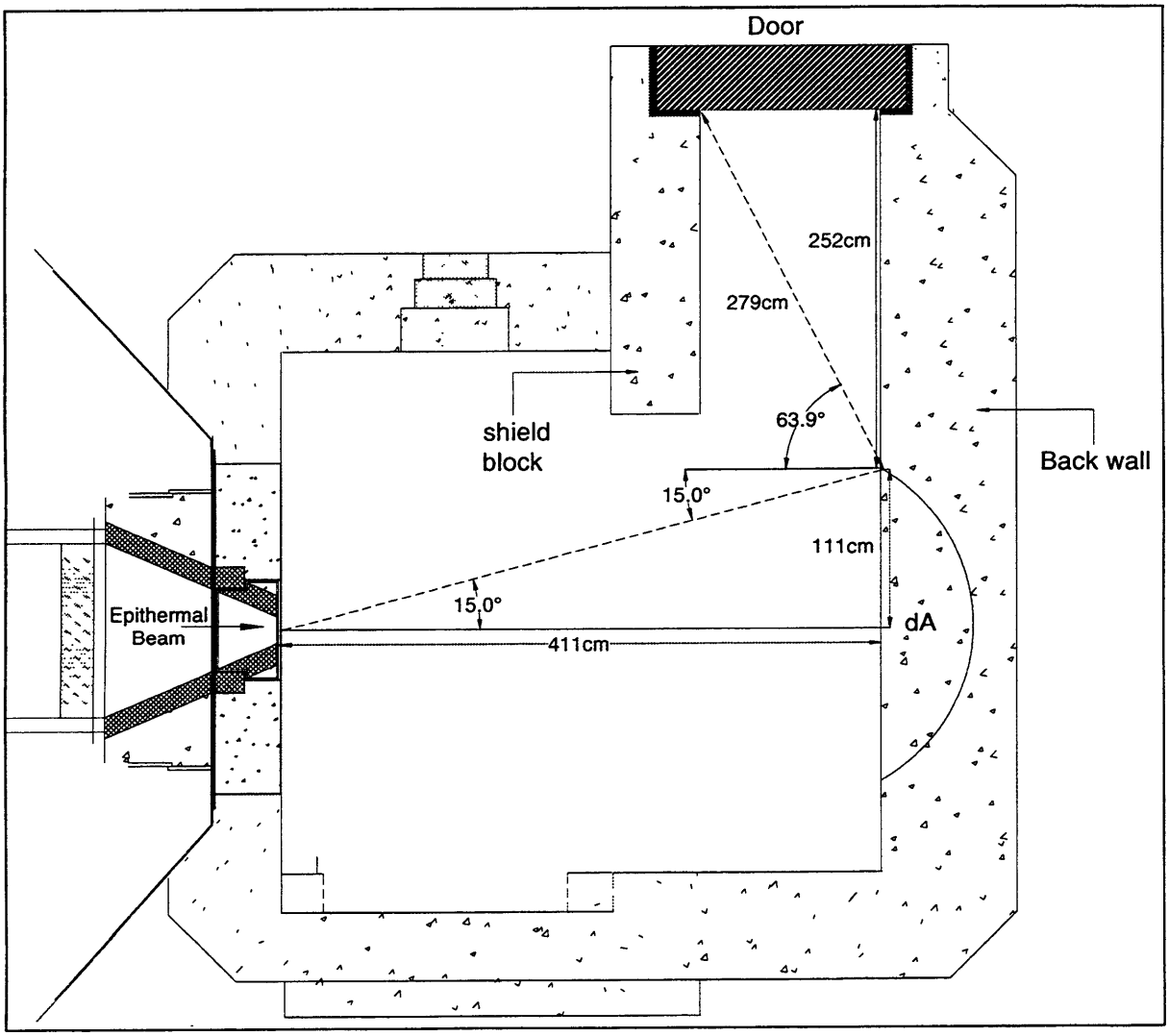

Figure 3.6 Neutron radiation at the door from reflection off the back wall.

To get the dose rate at the door from radiation reflecting off the back wall, equation 3.4 was integrated over the different variables outlined above.

$$D = \iiint \frac{2\pi Do(Eo,\theta o)\alpha(Eo,\theta o,\theta,\psi)x(\theta o)}{r^2(\theta)} dEo\, d\theta o\, d\theta\, d\psi \qquad (3.7)$$

To simplify this integration process some assumptions were made. First the neutrons were assumed monoenergetic with incident energy of 1 Mev. Second, the reflection coefficient, α, remained constant with respect to the incident angle, θo. Varying the incident angle from 0 degrees to 15 degrees changes the albedo by only 3.5 %, as seen in

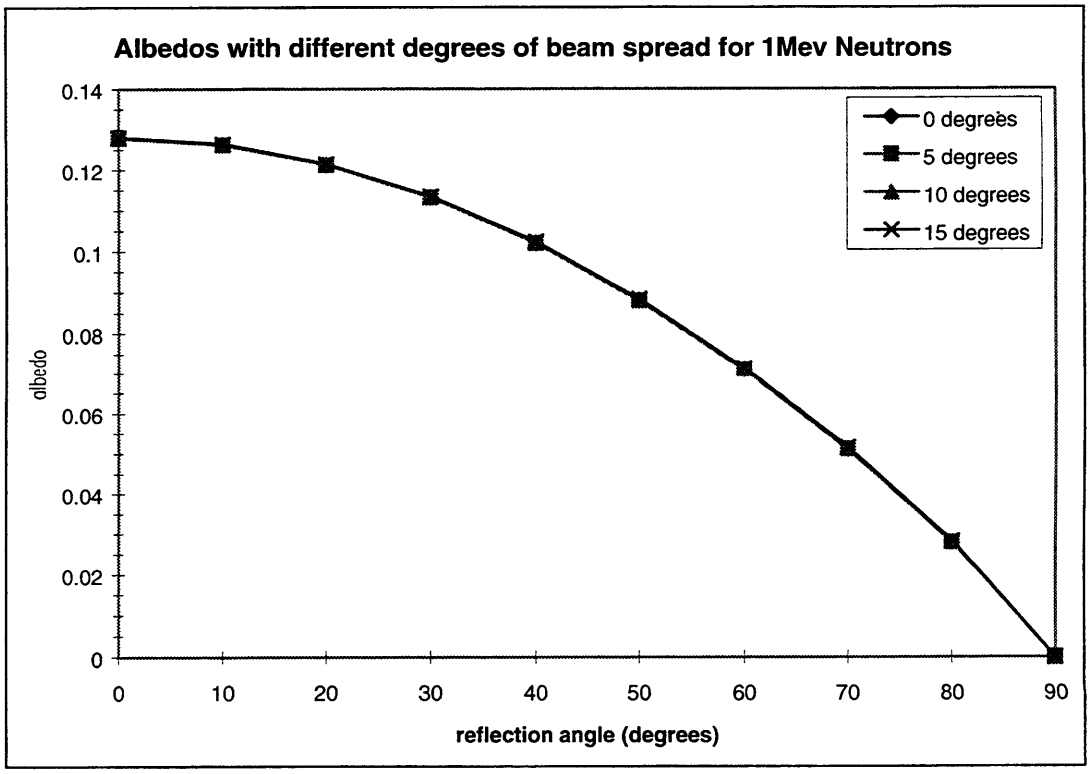

Figure 3.7 Reflection coefficients for 1 Mev neutrons incident on concrete with various angles of incidence.

the following graph. Additionally, the azimuthal angle, ψ, was kept constant at 90 degrees. Finally, the distance, r, between the reflected area and the door used for evaluating equation 3.4 was 252 cm. This value was chosen because it is the shortest distance between the reflecting area and the door. It therefore gives the most conservative estimate of the dose rate at the door.

Applying these assumptions to equation 3.4, the neutron dose rate at the door arising from reflection off the back wall was determined to be:

$$Dn,_{backwallscatter} = 1.2 \text{ rem/hr.}$$

This is the dose rate with a 90 degree reflection angle. The dose rates at the door at angles less than 90 degrees were slightly higher. However, when considering the extra shielding material these particles will travel because of their penetration angle, the 90 degree case is the most conservative in determining the shielding required for the location.

3.2.2.2 Neutron Scatter off the Floor

The direct beam of radiation scatters vertically as well as horizontally. This means a significant amount of radiation is incident upon the floor of the room. Some of this radiation is then scattered in the direction of the medical room door. Figure 3.5, below, shows the portion of radiation that reaches the floor with a 15 degree beam spread.

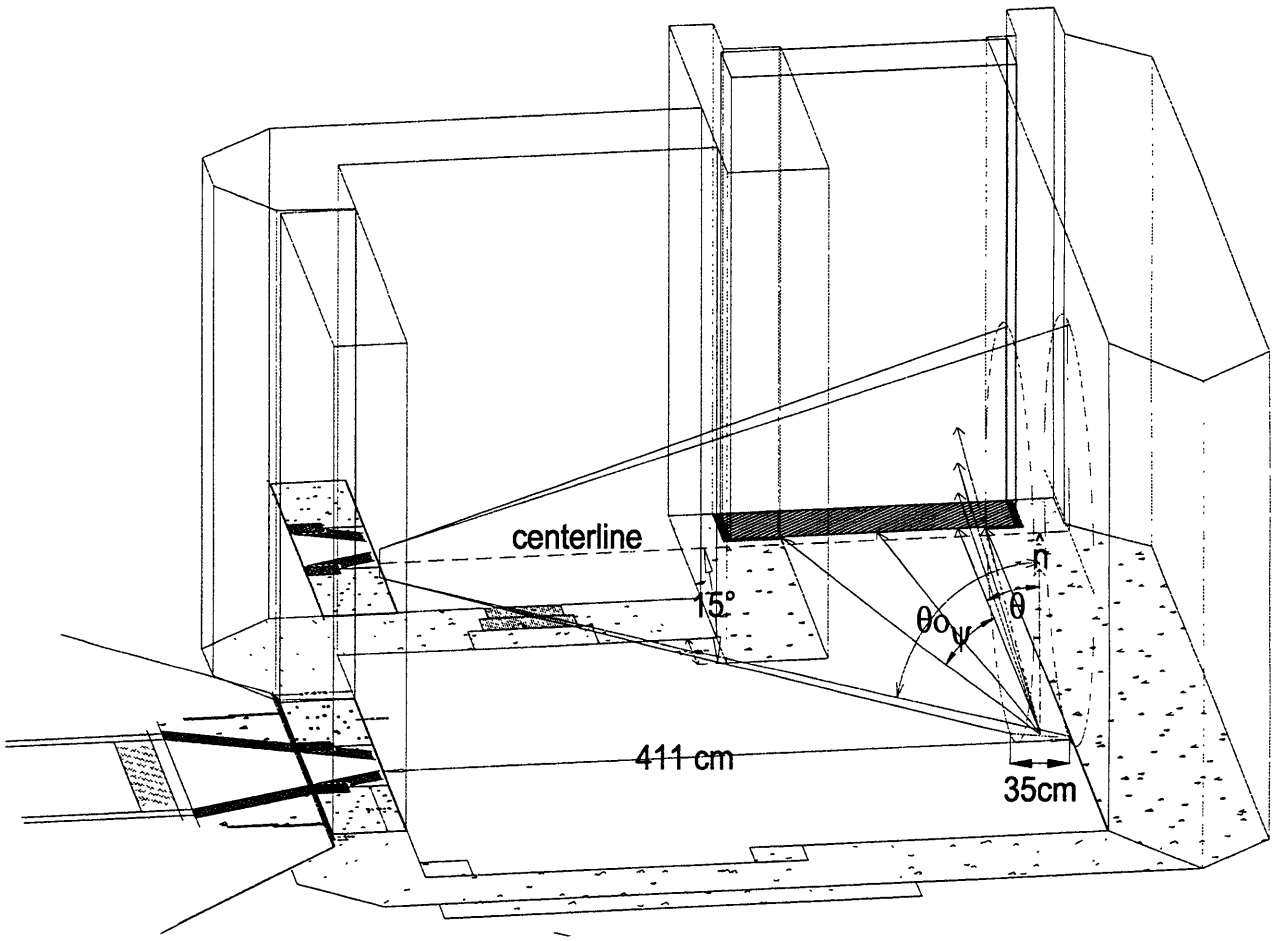

Figure 3.8 Schematic of radiation reaching the floor and reflected to the door.

The portion of the floor illuminated by the neutron radiation from the beam opening intercepts a small area in the center of the room, near the back wall. This area was assumed to be one half of a cone. The reasoning behind this assumption can be explained by the following diagram.

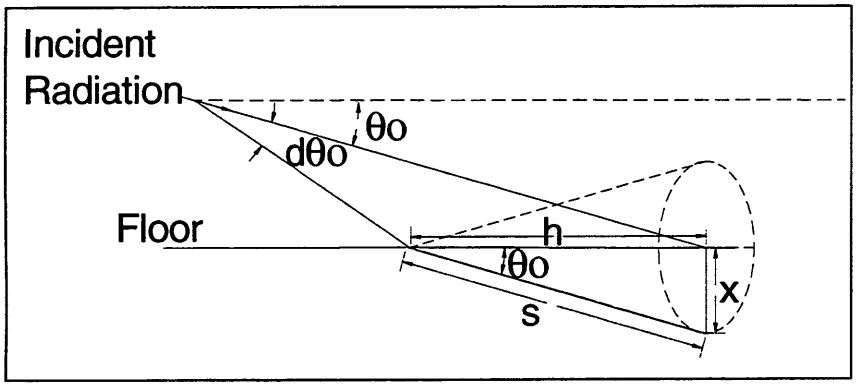

Figure 3.9 Radiation hitting the medical room floor.

To determine the neutron dose rate at the door from this source, equation 3.4 becomes:

$$D = \int \frac{Do \cdot \alpha(Eo, \theta o, \theta, \psi) \cdot \pi h^2 \sec^2 \theta o \sin \theta o \cos \theta o}{2r^2} d\theta o \qquad (3.8)$$

Here, the area of reflection is represented by $(\pi/2)h^2 \tan\theta o \cos\theta o$. The surface spans a distance, h, from the point where the radiation first hits the floor to the back wall. The distance r represents the perpendicular distance between the reflection surface at the floor and the door. This distance is 365 cm. In determining the neutron dose rate at the door from reflection off the floor the same assumptions were used as the back wall case. The incident angle was kept constant at 75 degrees, and the azimuthal angle was kept at 90

degrees. Again, the neutrons were assumed to be monoenergetic with incident energy of 1 Mev. Do, the dose rate at the floor, was determined using a similar method as that used for the dose at the back wall. Radiation hits the floor with an beam spread of 14 degrees. The total beam spread is 30 degrees, or a 75 degree maximum incident angle. So, only 1 degree of the total spread radiation reaches the floor. Using this information, the dose rate at the floor was determined.

$$Do, floor = \frac{1}{15} Dopening \cdot \frac{rbeam^2}{(x \tan \theta o)^2} \qquad (3.9)$$

A dose rate at the floor of 4.54 rem/hr was calculated using equation 3.9. Applying this dose rate and the assumptions mentioned above to equation 3.4, the dose rate at the door from reflection off the floor was determined to be:

$Dn,_{floorscatter} = 0.017$ rem/hr.

Like the dose rate at the door arising from reflection off the back wall, the dose rate from floor reflection uses a 90 degree angle of reflection for the shielding determination reasons mentioned earlier.

3.2.2.3 Total Neutron Dose at Door from Scattering

Table 3.1 Summary of neutron dose at door from scattering.

Scattering Surface	Neutron Dose at Surface (rem/hr)	Distance to Door (cm)	Neutron Dose at Door (rem/hr)
Back Wall	68.2	252	1.2
Floor	4.54	365	0.017

Total neutron dose rate at door from scattering = 1.22 rem/hr

3.3 EXPERIMENTAL MEASUREMENTS OF THE NEUTRON ALBEDO FOR CONCRETE

3.3.1 Introduction

It is obvious from the analytical methods outlined above that the greatest source of neutrons at the door comes from scattering off multiple surfaces. An accurate assessment of the albedo at the reflection surfaces is important for determining the shielding required for the door. Unfortunately, calculating this scattering component analytically can be extremely difficult due to its multi-angular dependence, so in section 3.2 many assumptions were made to simplify the analytical process. An albedo for fast neutrons was measured experimentally using the existing medical room to provide an independent and more accurate estimate of the scattered component.

3.3.2 Method

Measurements were performed in the current medical room to determine the albedo of concrete. Concrete blocks (8 ½ inch thick) were placed on the floor of the medical room to cover the hole in the floor where the hydraulic system sits. These blocks were used to provide a reflection surface for the neutrons. The reactor power was lowered to 10 kW and measurements of the radiation levels at various locations in the medical room were made using a Europium-doped LiI detector with a 10" bonner sphere. To determine the intensity of the radiation scattered off concrete at 90 degrees, a detector was placed to the side of the concrete. Shielding was put on top of the detector to stop any radiation from directly entering the detector before scattering off the concrete blocks. The

shielding consisted of 4" thick masonite blocks placed on a sheet of boral. The following drawing depicts the experimental setup and the various measurement locations.

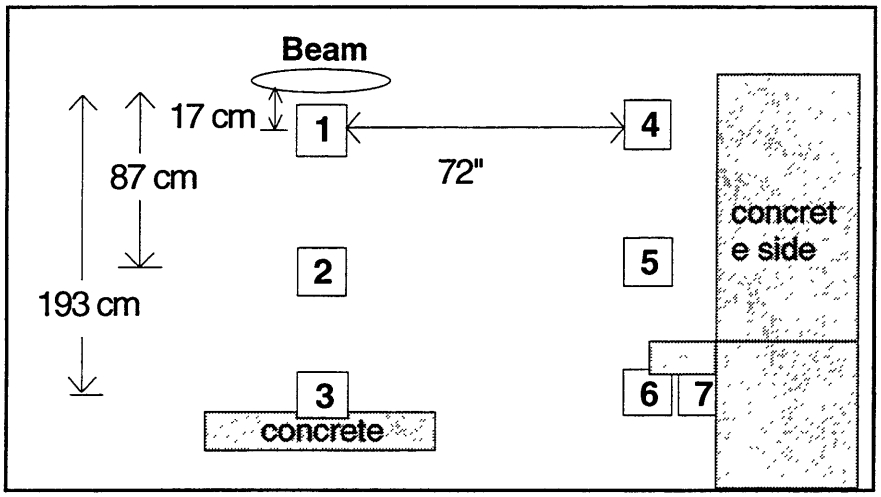

Figure 3.10 Experimental setup of albedo determination. Side view.

3.3.3 Results of Experiment

Previous sections of the shielding analysis use a $1/r^2$ geometric attenuation for determining the dose rate at different surfaces. The radius r, is dependent on the beam's spreading angle, θo. The angle of spread in the current beam was determined by fitting the count measurements from locations 1, 2 and 3 to a $1/r^2$ fit. This was calculated using the following equations.

$$D_i = \frac{rbeam^2 \cdot Do}{r^2} \qquad \textbf{(3.10)}$$

$$r = x \cdot \tan \theta o \qquad \textbf{(3.11)}$$

$$x = x_o + d \qquad \textbf{(3.12)}$$

Do, the dose rate at the beam opening[15], used here was 900 rem/hr. The dose rates measured along the beam centerline, D_i, were adjusted so they could be compared to the beam opening dose rate at 4.5 MW. A radius of 7.5 cm , r_{beam}, at the beam opening was used. The symbol d in equation 3.12 represents the distance from the beam opening to the location of the dose rate measurement. These distances are listed in Figure 3.10. The effective beginning of the beam spreading is located a distance, x_o, from the beam opening, as shown in the diagram below.

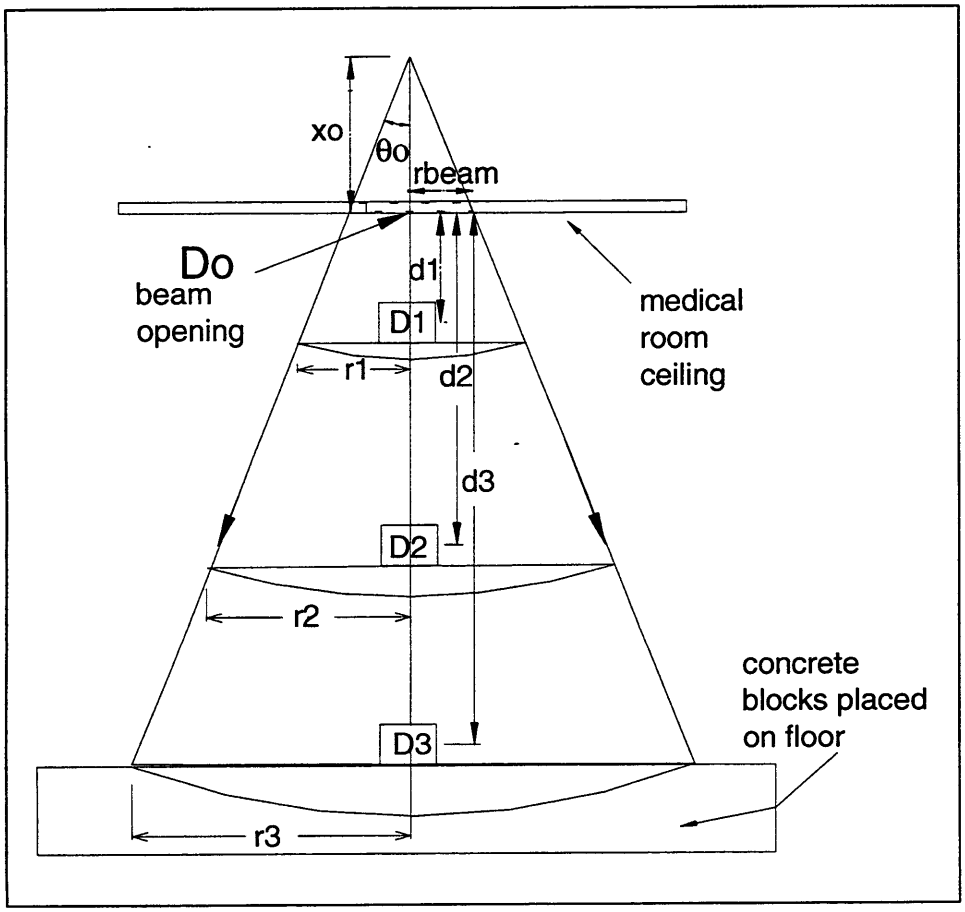

Figure 3.11 Diagram showing parameters in beam centerline dose rate measurements.

[15] Measured by Kent Riley during Spring 98 beam characterization.

Using the results from the measurements and manipulating equations 3.10-3.12, the beam spreading angle was determined. Results from the measurement are listed in the following table. The values listed have been corrected to account for the low reactor power at the time of the measurements. With the beginning of the cone located 32 cm above the beam opening, the beam spread was calculated as 19 degrees. This gives a total beam spread of 38 degrees.

Table 3.2 Results of Experimental Measurements in Current Medical Room adjusted to reactor power of 4.5 MW

Measurement Location	Average Counts per minute	Deviation from mean	Average Dose Rate (rem/hr)
1	1.09×10^{6}	5.44×10^{4}	180
2	1.53×10^{5}	4.71×10^{3}	31
3	9.24×10^{4}	2.46×10^{3}	11
4	8.76×10^{3}	9.39×10^{2}	NA
5	1.36×10^{4}	1.9×10^{3}	NA
6	1.63×10^{4}	1.44×10^{3}	NA
7	1.23×10^{4}	2.22×10^{3}	NA

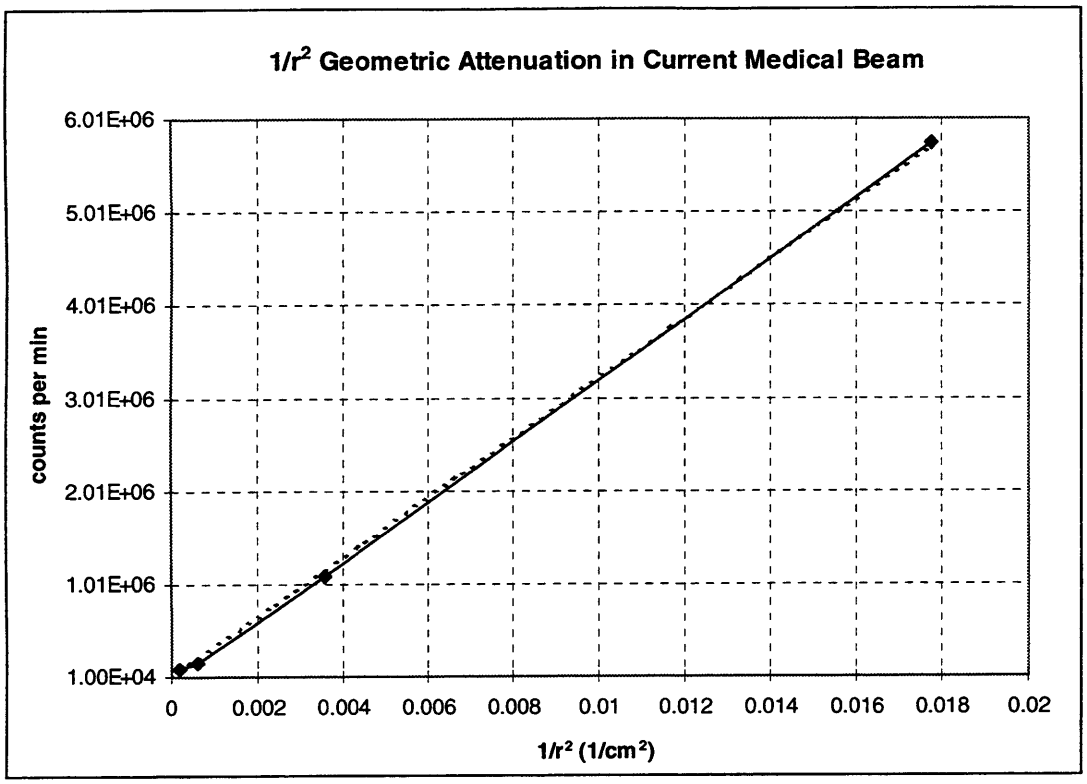

Figure 3.12 Graph showing the $1/r^2$ attenuation in the current beam.

Using the calculated beam spreading angle and the count rates listed in table 3.2, the albedo scattering coefficient was computed. Count rates used in this calculation were those measured at location 4, 5, and 7 that correspond to reflection angles of 45, 60 and 90 degrees, respectively. These values were applied to the following equation to determine the albedo at the three different reflection angles with a 90 degree azimuthal angle. The distance R_i refers to the distance between the detector at the reflection location and the detector at the incident location. The area of the reflection medium is πr_3^2. The radius r_3 was determined by equation 3.11.

$$\alpha(Eo,\theta o,\theta,\psi) = \frac{C_i \cdot R_i^{\,2}}{C_3 \cdot \cos\theta o \cdot \pi r_3^{\,2}} \qquad \textbf{(3.13)}$$

To make use of the values calculated by equation 3.13, the incident angle of 19 degrees was adjusted to the 15 degree incident angle in the fission converter beam. Table 3.3 Lists the albedos calculated from the experimental measurements. It is important to note that the incident energy of fast neutrons in the current beam may not be identical to the energy of the fast neutrons in the fission converter beam. For this study, the energy of the fast neutrons was assumed to be 1 Mev.

Table 3.3.3 Experimentally determined albedos for concrete.

Reflection Angle θ (degrees)	Albedo α
45	0.05
60	0.056
90	0.038

3.3.4 Application of the Experimentally Determined Albedo Results

The experimentally determined albedo coefficients for concrete were applied to the dose rate calculations mentioned in section 3.2.2. To reiterate, the dose rates at the door from neutron scattering off the back wall and floor assume a direct beam of radiation without a target in the beam. All parameters specified in that section were kept constant except for $\alpha(Eo,\theta o,\theta,\psi)$.

Table 3.4 Dose rates at door using experimentally determined albedos for concrete.

Scattering surface	Angle of Reflection θ degrees	Albedo α	Neutron Dose Rate at Scattering Surface rem/hr	Neutron Dose Rate at Door rem/hr
Back Wall	45	0.05	68.2	2.14
	60	0.056		2.4
	90	0.038		1.63
Floor	45	0.05	4.54	0.17
	60	0.056		0.19
	90	0.038		0.13

Total neutron dose rate at door from neutron scattering at a 90 degree reflection angle is 1.76 rem/hr by adding the contribution from both back wall and floor scattering.

3.3.5 Comparison of Measured and Calculated Neutron Dose Rates at Door

The following table compares the measured albedos for concrete to the calculated values and shows the resultant dose rates. The results are very close, especially considering all the assumptions required to calculate the albedo analytically from equation 3.5.

Table 3.5 Comparison of measured and calculated dose rates incident on door.

Reflection Angle θ (degrees)	Measured Albedo α	Calculated Albedo α	Neutron dose rate at door Measured α (rem/hr)	Neutron dose rate at door Calculated α (rem/hr)
45	0.05	0.096	1.27	2.45
60	0.056	0.062	1.84	2.09
90	0.038	0.028	1.76	1.22

3.4 GAMMA SCATTERING COMPONENT

Like neutrons, a significant amount of the gammas incident on the back wall and floor will scatter towards the door. The fraction of gammas that scatter in the direction of the door was found using albedo methods for photons. The albedo for gamma rays scattering off concrete was found using the expression[16]:

$$\alpha(Eo,\theta o,\theta,\psi) = F(Eo,\theta o,\theta,\psi)\frac{C(Eo)_e\sigma_{Ce}(Eo,\theta s)10^{26} + C'(Eo)}{1+(\cos\theta o/\cos\theta)(1+2\cdot Eo\cdot vers\theta s)^{1/2}} \quad \textbf{(3.14)}$$

$$F(Eo,\theta o,\theta,\psi) = A_1(Eo) + A_2(Eo)vers^2\theta o + A_3(Eo)vers^2\theta + A_4(Eo)vers^2\theta o\cdot vers^2\theta + A_5(Eo)vers\theta o\cdot vers\theta\cdot\cdot vers\psi \quad \textbf{(3.15)}$$

The above expression assumes gammas scatter a few times before emerging from the concrete. Listed in the table below are the values used for parameters in equation 3.14 and 3.15. Due to the limited available data, these values are for 2 Mev gamma rays incident on concrete. This incident energy is different from the 3 Mev incident gamma energy previously used. However, this only results in a slightly larger (<10%) albedo value.[17]

Table3.6 Parameters for Gamma Albedo Formula for Concrete.

Parameter	Eo = 2 Mev
C	0.2485217
C'	0.0213318
A_1	0.8340043
A_2	0.3813632
A_3	0.5819863
A_4	0.2871745
A_5	0.1442294

[16] Radiation Shielding , Shultis & Faw, p.243.
[17] NCRP Report No. 51, Appendix E.15 Reflection Coefficients for Monoenergetic X Rays in Concrete, Iron and Lead, p.110.

Assumptions used for determining the neutron albedo for concrete were kept the same for the gamma albedo calculation. The energy used for incident gammas was assumed monoenergetic, 3 Mev specifically. Also, the incident and azimuthal angles were kept constant at 15 degrees and 90 degrees, respectively. The values for the albedos at different reflection angles are presented in the graph below.

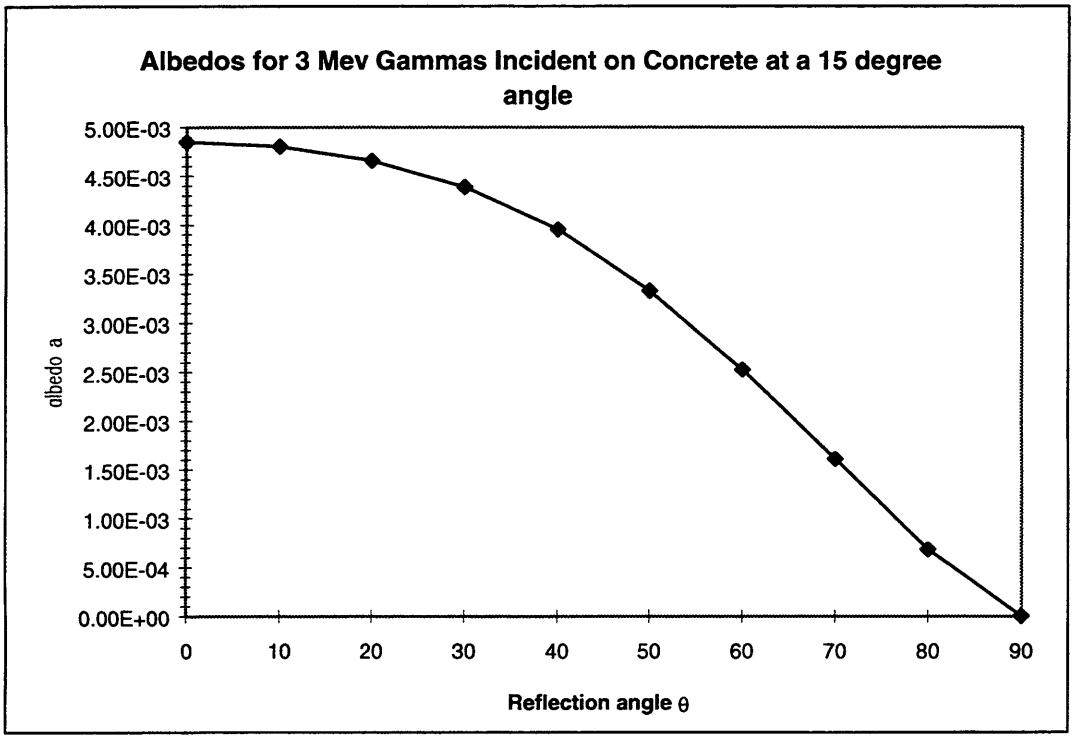

Figure 3.13 Gamma Albedo for 3 Mev gammas incident on concrete at a 15 degree angle and reflecting at different angles.

3.4.1 Gamma Reflection off Back Wall

The gamma radiation coming out of the beam, without a target in the beam, hits the back wall with a 30 degree total spread, as mentioned in Chapter 2. Similar to neutron scattering mentioned earlier, a portion of this gamma radiation is scattered towards the

door instead of penetrating deeper into the concrete. The dose rate at the door from this reflection is proportional to the area of the concrete illuminated by radiation, the dose at the back wall, the incident angle of radiation at the back wall, and the albedo for concrete. It is also inversely proportional to the squared distance between the back wall and the door. In other words, equation 3.4 was used to find the gamma dose rate at the door from reflection off the back wall using the same simplification outlined in section 3.2.2.1 except for incident energy. Here, 3 Mev was used as the monoenergetic incident gamma energy. As a result, the gamma dose rate at the back from reflection off back wall was determined to be

$$D_{\gamma,\ backwallscatter} = 0.008 \text{ rem/hr.}$$

3.4.2 Gamma Reflection off the Floor

Once again, the 30 degree total spread in the beam causes a small percentage of the gamma radiation to penetrate the floor. The dose rate at the location on the floor that receives radiation is 0.371 rem/hr. A fraction of this radiation is reflected off the floor and scattered towards the door. The dose rate at the door from gamma reflection off the floor was determined in the same manner as the neutron reflection off the floor. This calculation used the gamma albedos for concrete with incident energy of 3 Mev. Consequently, the dose rate at the door from this source is

$$D_{\gamma,floorscatter} = 0.05 \text{ mrem/hr}.$$

3.4.3 Summary of Gamma Dose Rates at the Door

Table 3.7. Photon dose to door determined by albedo methods.

Scattering Surface	Gamma Dose Rate at Surface (rem/hr)	Distance to Door (cm)	Gamma Dose Rate at Door (rem/hr)
Back Wall	5.564	252	0.008
Floor	0.371	365	5.35×10^{-4}

Total photon dose at door from scatter = 8.55 mrem/hr

3.5 DOSE RATE CALCULATIONS FOR CAPTURE GAMMAS CREATED IN THE DOOR

In addition the sources of gamma radiation described previously, gammas are created from (n,γ) reactions occurring with the elements in the door itself. The dose rate from these capture gamma rays was computed with use of MCNP. The thermal neutron flux as a function of depth in the door was used to compute the number of gamma rays created throughout the concrete door. This thermal neutron flux was multiplied by the neutron capture cross section in concrete and by the average number of gammas produced per capture. This gives a gamma flux that can then be converted to a dose rate as a function of depth in the concrete. Section 2.4.2 gives a more in depth description of calculating capture gamma dose rates. The dose rate outside the door from capture gammas created in the door was calculated as 1.88×10^{-5} mrem/hr. Dose rates at each point in the concrete, prior to attenuation by travel through the material, are shown in the graph below. One curve shows what the dose rates at each point in the concrete are assuming no attenuation

through the remaining concrete. For example, at 5 cm the top curve shows the dose rate of 10 mrem/hr from capture gammas created at that location. The bottom curve shows what the final dose rate from that point would be after it was attenuated 40 cm to the outside of the door. From the graph, it is obvious that the most of the capture gamma radiation originates from the beginning of the door and is therefore attenuated thoroughly before it reaches the outside of the door. Therefore, the dose rate from capture gammas is negligible.

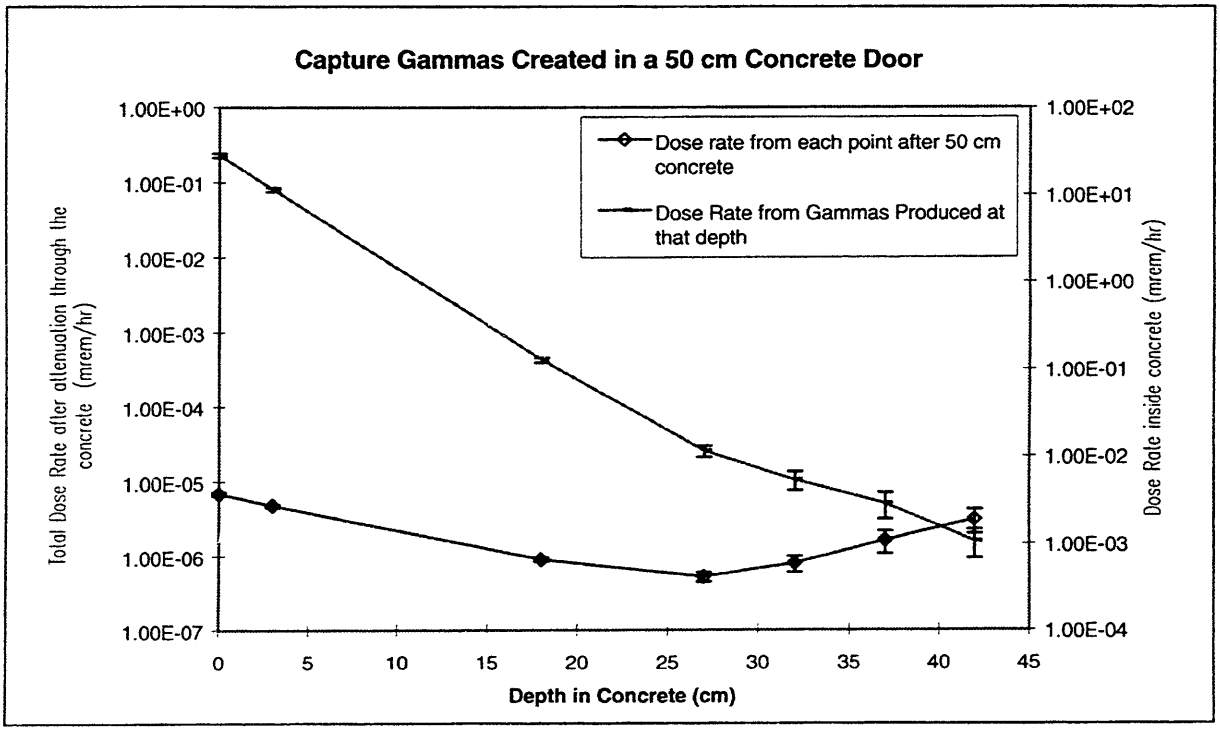

Figure 3.14 Dose rates from capture gamma rays created in a concrete door, ρ=3.76 g/cm^3 .

A significant point is that this dose rate is for a concrete door only. The thermal neutron flux in a door of different material will vary as well as the neutron capture cross section and the number of gammas produced per interaction. When analyzing other door materials, in the following section, the capture gamma dose outside the door is assumed to be that of a concrete door. It is felt that this a valid assumption because the type of concrete used to obtain the capture gamma dose incorporates a mixture of heavy elements and hydrogen. Therefore, capture gammas from both types of material have been considered. Additionally, the capture gamma dose from this type of concrete is negligible through thick shields, as obvious from Figure 3.12.

3.6 SUMMARY OF TOTAL DOSE RATES AT INSIDE OF DOOR

The following table lists the total fast neutron and gamma dose rates incident on the door. These are the dose rates used to determine the amount of material needed for shielding the door. The dose rates listed are the most conservative dose rates from the experimentally determined and analytically calculated values.

Table 3.8 Dose Rates Incident on Inner Surface of Door

Type of Radiation	Dose Rate Incident on Door (rem/hr)
Fast Neutron	1.76
Gamma	1.69

3.7 SHIELDING CALCULATIONS FOR MEDICAL ROOM DOOR

Several different materials were considered for the shielding door. The shielding material for the door must adequately attenuate both fast neutrons and gamma rays. The following table lists the materials considered for the door shielding, and it also shows each material's fast neutron and gamma ray attenuation properties.

Table3.9 Materials Considered for Door Shielding [18].

Material	Density (g/cm^3)	Gamma attenuation coefficient (1/cm)	Fast Neutron Macroscopic Removal Cross Section (1/cm)
Steel	7.8	0.271	0.168
I-2a concrete	3.76	0.1361	0.111
Polyethylene	0.93	0.0376	0.11
Masonite	1.1-1.4	~0.03	0.10
Lead	11.34	0.466	0.116

The amount of material needed to reduce the total dose rate from both neutron and gamma doses to 1 mrem/hr was determined using the method described in section 2.5. The results of those calculations are summarized in the following table.

Table 3.10 Summary of shielding needed to reduce dose rates at door to 1 mrem/hr.

Material	Amount of material needed to reduce gamma dose rate to 1 mrem/hr (cm)	Buildup Factor for Gamma Rays	Amount of Material needed to reduce neutron dose rate to 1 mrem/hr (cm)	Amount of Material needed to reduce Total Dose Rate to 1 mrem/hr (cm)
I-2a concrete	70	8.08	67	75
lead	19	4.79	64	64
polyethylene	258	9.7	68	258
steel	34	5.77	44	45
masonite	320	9.3	74	320

[18] From Engineering Compendium on Radiation Shielding, Vol. II, R.G. Jaeger.

3.8 OVERALL DESIGN OF DOOR

Combining the results of the analytical and experimental calculations, an optimal design of the door was produced. The design of the door is dependent upon many factors, including: 1) total weight of the door, 2) the total dimensions of the door, and 3) which materials to use for radiation attenuation. The total weight of the door must be less than 20 tons. This is the maximum weight capacity of the crane, which will be used to install and remove the door if necessary. Additionally, the overall dimensions of the door are restrictive due to the limited space available on the reactor floor, as previously mentioned. Also, the size of the door must allow for a reasonable and effective opening and closing mechanism. The combination of materials used must provide an adequate degree of radiation attenuation while minimizing the total weight and dimensions of the door. In the following table are different combinations of materials that will adequately reduce the dose rates at the door to 1 mrem/hr.

Table 3.11 Combinations of Materials that reduce the dose rates outside door to 1 mrem/hr.

Combination	Gamma Dose Rate (mrem/hr)	Neutron Dose Rate (mrem/hr)	Total Dose Rate (mrem/hr)	Thickness of material 1 (cm)	Thickness of material 2 (cm)	Total Shield thickness (cm)
concrete/lead	0.157	0.791	0.948	61	8	69
polyethylene/lead	0.269	0.779	1.05	50	19	69
concrete/steel	0.310	0.633	0.943	33	25.4	58.4
polyethylene/steel	0.701	0.337	1.04	30.48	31	61.48
masonite/steel	0.746	0.343	1.09	33	33	66

The total weight of the door combinations is an important item when considering the

mechanical difficulties in operating the door. In table 3.11 and 3.12, each option for the door is listed with the dose rates, shield thickness, density, volume, and weight. The first table lists the doors composed of single materials; the second lists those made of a combination of materials.

Table 3.12 Properties of single composition door options.

Single materials	Gamma Dose (mrem/hr)	Neutron Dose (mrem/hr)	Amount of material needed to reduce gamma dose to 1 mrem/hr (cm)	Amount of material needed to reduce neutron dose to 1 mrem/hr (cm)	volume (cm^3)	Density (g/cm^3)	Total Weight (tons) assuming door 4.5 ft wide x 8 ft tall
s1. Concrete	9.94E-01	1.04E+00	70	67	2.34E+06	3.94	10.16
s2. Lead	9.38E-01	9.85E-01	19	64	2.14E+06	11.34	26.74
s3. Steel	9.73E-01	9.17E-01	34	44	1.50E+06	7.8	12.93
s4. Polyethylene	1.00E+00	9.93E-01	258	68	8.62E+06	0.93	8.84
s5. Masonite	1.07E+00	1.08E+00	321	74	1.07E+07	1.4	16.56

Table 3.13 Properties of door options—combination of shielding materials.

Combination	Thickness of material 1 (cm)	Thickness of material 2 (cm)	Total thickness (cm)	Density of material 1 (g/cm^3)	Density of material 2 (g/cm^3)	Weight of material 1 assuming door 4.5 ft wide x 8 ft tall (tons)	Weight of material 2 assuming door 4.5 ft wide x 8 ft tall (tons)	Total Weight assuming door 4.5 ft wide x 8 ft tall (tons)
c1. concrete/lead	61	8	69	3.94	11.34	8.86	3.34	12.20
c2. poly/lead	50	19	69	0.93	11.34	1.71	7.94	9.65
c3. concrete/steel	33	25.4	58.4	3.94	7.8	4.79	7.30	12.09
c4. poly/steel	30.48	31.75	62.23	0.93	7.8	1.04	9.13	10.17
c5. masonite/steel	33	30.48	63.48	1.4	7.8	1.70	8.76	10.46

Further analysis of these door options leads to an engineering design of the door, which can be found in chapter 8. This design will incorporate the shielding properties of

the door options listed above with the overall size, weight, ease of fabrication, mechanical considerations and cost to construct the best door for the medical facility.

3.9 REFERENCES

Campos, T., Personal communication.

Chilton, A., Shultis, J.K, Faw, R., *Principles of Radiation Shielding,* Prentice Hall, Inc., NJ, 1984.

Harling, O.K., Personal Communication.

Jaeger, R.G, "Shielding Materials", *Engineering Compendium on Radiation Shielding*, Vol.II, Springer-Verlag, New York Inc, 1975.

Jaeger, R.G, "Shield Design and Engineering", *Engineering Compendium on Radiation Shielding*, Vol.III, Springer-Verlag, New York Inc, 1970.

McGinley, P., *Shielding Techniques for Radiation Oncology Facilities,* Medical Physics Publishing, WI, 1998.

McWilliams, F., Personal communication.

NCRP, "Radiation Protection Design Guidelines for 0.1-100 Mev Particle Accelerator Facilities", *NCRP Report No. 51*, National Council on Radiation Protection and Measurements, 1977.

Rockwell, T. , *Reactor Shielding Design Manual,* D. Van Nostrand Company, Inc., 1956.

Schaeffer, N.M., *Reactor Shielding for Nuclear Engineers,* U.S. Atomic Energy Commission, 1973.

Shultis, J.K., Faw, R., *Radiation Shielding*, Prentice Hall, Inc., NJ, 1996.

CHAPTER 4

SHIELDED VIEWING WINDOW

4.1 INTRODUCTION AND SPECIFICATIONS

A method of monitoring the patient during irradiation is essential in a treatment facility. This is important in assessing the patient's condition throughout the treatment and becomes crucial in the event of an emergency. The proposed monitoring system for the new BNCT facility will combine a shielded viewing window, mirrors, a video camera, and an intercom system to meet this requirement.

A window used in the treatment facility must provide adequate shielding from gamma rays and fast neutrons, while allowing for patient monitoring. The window should also be placed in a location that is not in the direct path of the beam to minimize possible radiation damage to the window materials. Ideal dose rates outside the window should be less than 1 mrem/hr. A stepped window is advantageous for this facility because it will allow a wider viewing range and prevent radiation streaming.

The proposed location of the window is the right wall adjacent to the reactor face. Placing the window at about 90 degrees from the patient position will help to minimize the radiation levels incident on the window. This is important for preserving the quality of the window. At high radiation exposures some window materials begin to darken, obstructing view, while others are chemically broken down due to free radical

production. The window will be composed of several panes of material, stepped with outer dimensions of 61 cm in width and 41 cm in length. The following picture shows the location of the window on the side wall.

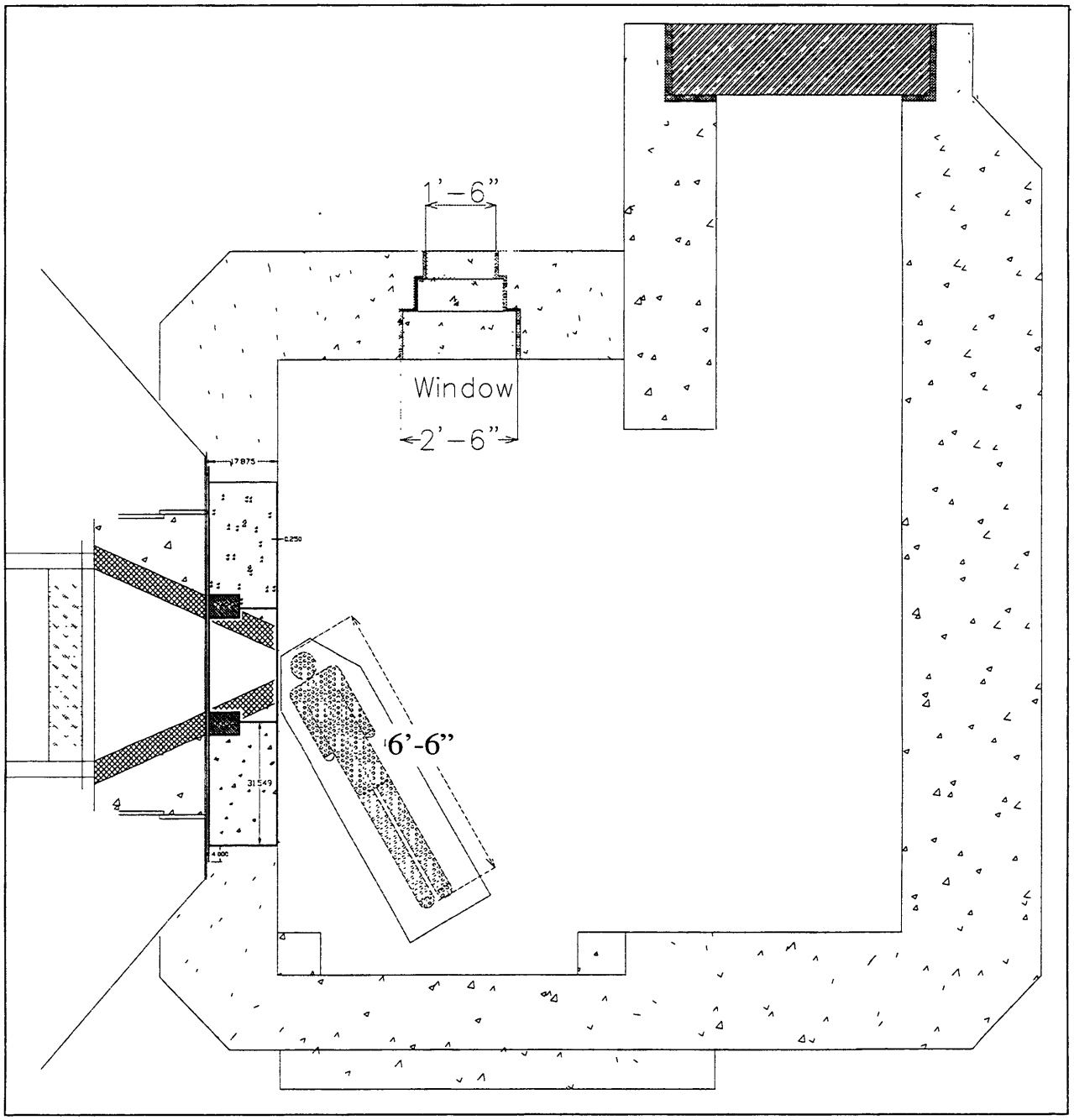

Figure 4.1 Medical room with window located 2.5 feet from beam opening. Top view.

4.2 WINDOW MATERIALS

A combination of materials, with varying attenuation properties, is required to provide adequate shielding from both gamma rays and fast neutrons. A transparent material high in density is needed to attenuate gamma rays, and a material with a high hydrogen content, or other low atomic number element, is needed to attenuate the fast neutrons at the window location. The following table shows some of the materials considered for the window and their optic properties.

Table 4.1 Typical gamma ray window shielding materials and their properties.[19]

Material	Density (g/cm^3)	Index of Refraction	% Tungsten Light Transmitance	% Sodium Light Transmitance
zinc bromide	2.52	1.56	98.5	99
lime glass	2.52	1.52	94.5	94.2
silicate glass	2.68	1.53	96.5	96.7
lead glass	3.27	1.59	97.5	98.1
lead glass	4.2	1.69	NA	NA
lead glass	6.2	1.95	NA	NA

The order of the materials used for the shielding window is a neutron shielding material first, then lead glass. The location of the lead glass was chosen because its primary purpose is to shield gamma rays. The material preceding the lead glass will be composed of a hydrogenous material that will produce a large amount of gamma rays from neutron capture. Placing the lead glass after this material will shield these secondary gamma rays as well as the incident primary gamma rays. Lead glass also darkens with exposure to high gamma fluxes, so placing it after another shielding

[19] Nuclear Engineering Handbook, Section 7-4, Table 1, 7-122.

material will help to prevent this darkening.[20] The neutron shield will consist of a material that is high in hydrogen content. Zinc bromide and mineral oil are the neutron shielding materials considered. The following table lists the elements used in the different materials considered for the window.

Table 4.2 Elements used in materials for shielding windows.

Material	Density (g/cm^3) [21]	Gamma Attenuation Coefficient, μ/ρ (cm^2/g)[5]	Fast Neutron Macroscopic Removal Cross Section, Σr (1/cm)[22]
silicon	2.33	0.0368	0.0681
lead	11.34	0.04234	0.1176
oxygen	1.43	0.03597	0.0579
potassium	0.862	0.03666	0.1533
calcium	1.55	0.0378	0.0354
sodium	0.971	0.03487	0.0313
carbon	1.7	0.03562	0.0838
bromide	3.12	0.03552	0.0523
zinc	7.14	0.03634	0.1306
hydrogen	0.0899	0.06921	0.157
mineral oil	0.627	0.02343	0.194

The information contained in Table 4.2 was used to determine the total gamma attenuation coefficient and macroscopic removal cross section for the various window compositions. Plain glass is composed of 20% sodium carbonate, 75% silica, and 5% calcium oxide. Lead glass is composed of 27% silica, 71% lead oxide, and 2% potassium

[20] Reactor Shielding Design Manual, 188.
(21) From website http://physics.nist.gov/PhysRefData/XrayMassCoef/tab2.html/.
(22) From Reactor Shielding for Nuclear Engineering, table 4.3, 182.

oxide. Zinc bromide solution is 80% $ZnBr_2$ in H_2O with 0.1 % hydroxylamine. The attenuation and removal cross sections were calculated using the following formulas[23]:

$$\Sigma_r = \Sigma_i N_i \sigma_i \qquad \textbf{(4.1)}$$

$$N_i = \frac{N_A \rho_i}{A} \qquad \textbf{(4.2)}$$

$$\rho_i = \frac{\%x \cdot \rho_x}{\Sigma \rho_i} \qquad \textbf{(4.3)}$$

Table 4.3 Plain Glass Composition and Fast Neutron Removal Cross Sections

element	weight fraction	Σ_r (cm^{-1})[24]	fraction x Σ_r
Na_2CO_3	0.20	0.057	0.0114
SiO_2	0.75	0.0625	0.0469
CaO_2	0.05	0.05	2.5e-3

Total macroscopic removal cross section $\Sigma r = 0.0608\ cm^{-1}$.

Table 4.4 Lead Glass Composition and Fast Neutron Removal Cross Sections

element	weight fraction	Σ_r (cm^{-1})[6]	fraction x Σ_r
Pb_2CO_3	0.71	0.108	0.0767
SiO_2	0.27	0.0625	0.0169
KO_2	0.02	0.0799	1.6e-3

Total macroscopic removal cross section $\Sigma r = 0.095\ cm^{-1}$.

(23) Equation 3.1-2 from Reactor Shielding for Nuclear Engineers, p.66, N.M Schaeffer, 1973.
(24) From Reactor Shielding for Nuclear Engineers, Schaeffer, Table 4.3, p. 182-183.

Table 4.5 Zinc Bromide Solution Composition and Fast Neutron Removal Cross Sections

element	weight fraction	Σ_r (cm^{-1})	fraction x Σ_r
$ZnBr_2$	0.80	0.094 [6]	0.0752
H_2O	0.20	0.10 [25]	0.02

Total macroscopic removal cross section $\Sigma r = 0.0952\ cm^{-1}$.

Table 4.6 Shielding Properties for Various Window Materials.

Material	Density (g/cm^3)	Gamma Attenuation Coefficient (1/cm)	Fast Neutron Macroscopic Removal Cross Section (1/cm)
plain glass	2.68	0.101[26]	0.0608
lead glass	6.2	0.25[6]	0.095
lead glass	4.2	0.163	0.095
lead glass	3.6	0.139	0.095
zinc bromide	2.52	0.162	0.0952
mineral oil	0.627	0.0544	0.194[7]

4.3 DOSE CALCULATIONS

The dose rate incident upon the window is equivalent to the dose rate incident upon the side wall, as outlined in section 2.4. The dose calculations, assuming a direct beam of radiation scattered off a human head or phantom, were used to determine the amount of window material needed to attenuate the dose outside the window to less than 1 mrem/hr. The dose rates seen at the other side of the window prior to shielding are 3.23 rem/hr and 2.45 rem/hr for fast neutrons and gamma rays, respectively.

---

[25] From Engineering Compendium on Radiation Shielding V II, Jaeger, Table 9.2-27, p.295.
[26] From Engineering Compendium on Radiation Shielding,V.II , Jaeger, Table 9.1-55, p.56.

4.4 SHIELDING CALCULATIONS FOR WINDOW

The amount of window material needed to reduce the dose rates outside the window to less than 1 mrem/hr were calculated using equations 2.16 and 2.17. Buildup factors for gamma rays in lead glass and plain glass were obtained from the following graphs.[27]

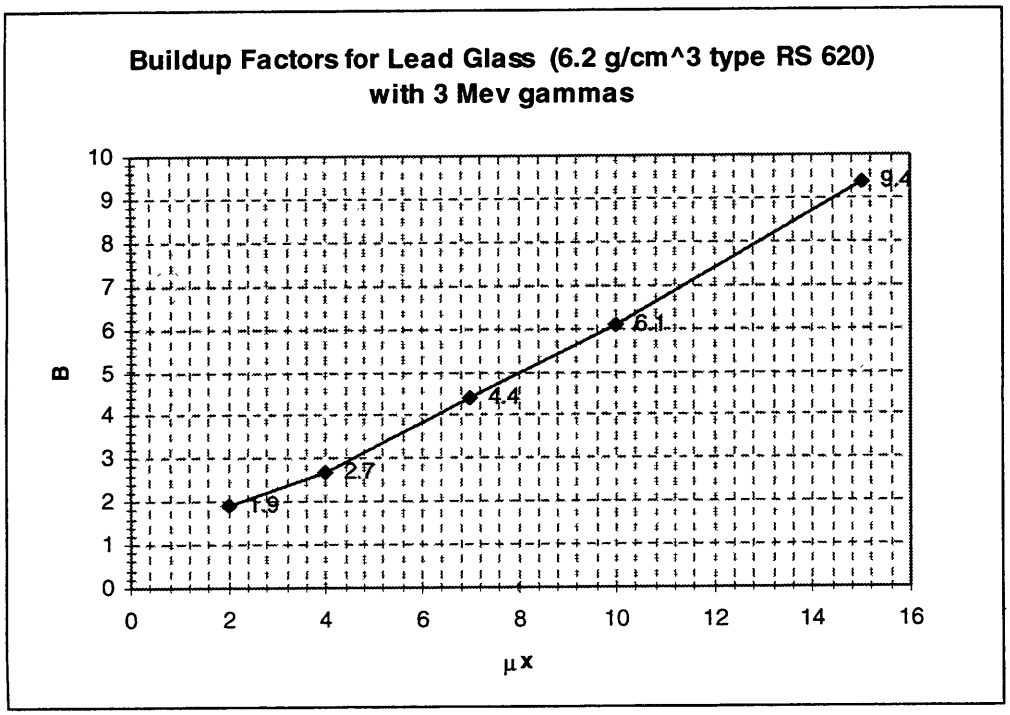

Figure 4.2 Buildup factors for lead glass with density 6.2 g/cm^3.

[27] From Engineering Compendium on Radiation Shielding,V.II , Jaeger, Table 9.1-60, p. 59.

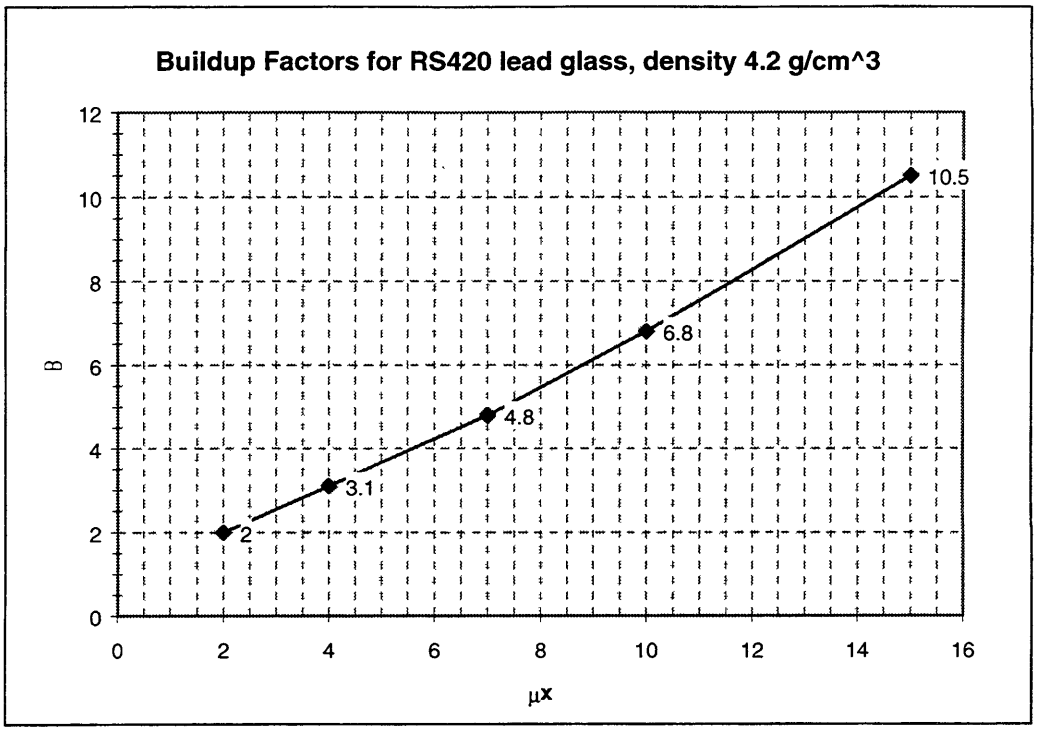

Figure 4.3 Buildup Factors for lead glass with density 4.2 g/cm^3.

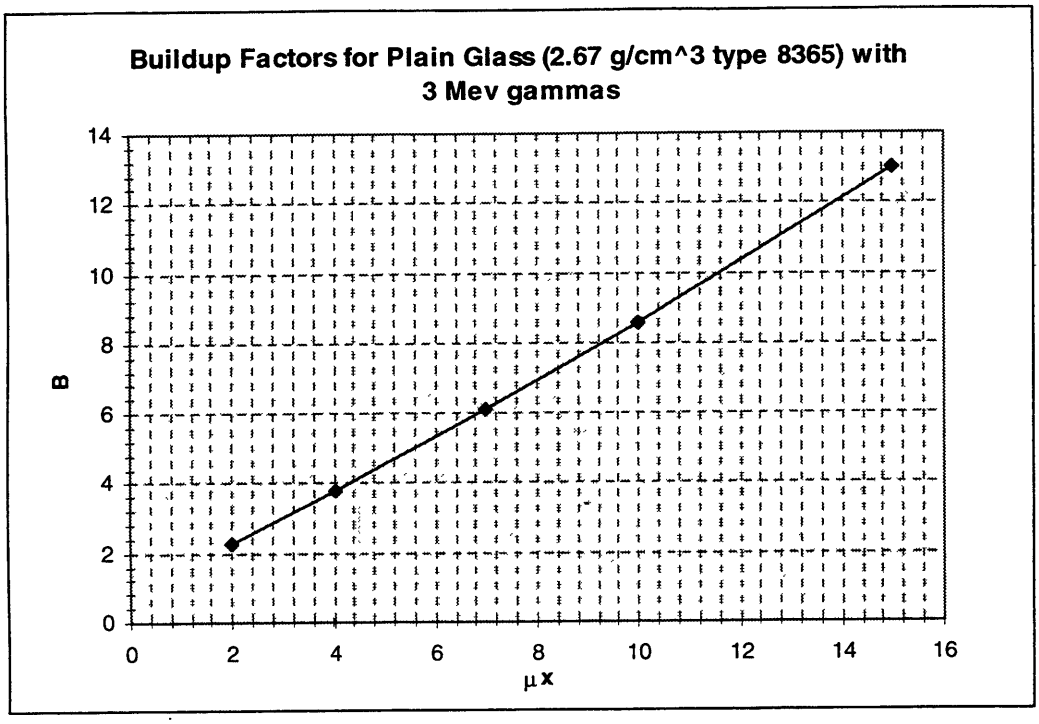

Figure 4.4 Buildup factors for plain glass.

Using the information in Table 4.6 for the attenuation coefficients of these different materials, the thickness of each material required to shield the window was determined. Listed in following table are the thicknesses of each material required to reduce the dose rate outside the medical room to 1 mrem/hr.

Table 4.7 Results of shielding calculations using single materials.

Dγ = 2.45 rem/hr , Dfn = 3.23 rem/hr

Single Materials	Density (g/cm^3)	Thickness needed to reduce gamma dose rate to 1 mrem/hr (cm)	Buildup Factor for Gamma Rays	Thickness needed to reduce neutron dose rate to1 mrem/hr (cm)
plain glass	2.68	98	8.6	133
lead glass	6.2	38	6.1	85
lead glass	4.2	65	6.6	85
zinc bromide	2.52	62	10.04	85
mineral oil	0.627	186	10.12	42

*Thickness have been rounded up to nearest whole cm.

Using these results, it was possible to compare several combinations of materials for consideration in the window shielding design. Table 4.8 shows the results of various combinations of materials for the window.

Table 4.8 Combination of Materials for Window Design.

Combination	Gamma Dose Rate (mrem/hr)	Neutron Dose Rate (mrem/hr)	Total Dose Rate (mrem/hr)	Thickness of material 1 (cm)	Thickness of material 2 (cm)	Total thickness (cm)
ZnBr + Lead glass (ρ 6.2 g/cm^3)	0.005	0.994	0.999	55	30	85
mineral oil + Lead glass (ρ 6.2 g/cm^3)	0.602	0.379	0.982	30.48	33	63.48
mineral oil + plain glass	0.937	0.036	0.972	30	92	122

4.5 OVERALL WINDOW DESIGN

The overall design of the window requires that the specific materials chosen above be incorporated into a window that can easily fit into the wall of the medical room without radiation streaming through the cracks. Based on the information presented Table 4.8, the best combination of materials for the window is one of mineral oil and lead glass. Several panes of lead glass were obtained through outside sources. Among those arriving in one piece, two 8" thick lead glass windows appear suitable for use. The two lead glass windows have a density of 3.95 g/cm^3. Actual composition of the windows is unknown, therefore the attenuation properties of the two glasses were assumed to be similar to the following types of lead glass: lead glass with a density of 3.6 g/cm^3 (RS 360) and non browning lead glass with a density of 4.2 g/cm^3 (RS 420), see table 4.6. The fast

neutron removal cross section was assumed to be the same for all lead glasses. However, the gamma attenuation coefficient varies with the density of the lead glass. Therefore, an estimate of the gamma attenuation coefficient for lead glass with a density of 3.95 g/cm^3 was found by linear extrapolation from the available attenuation coefficients. The result was a gamma attenuation coefficient of 0.155 cm^{-1} for the two 8" (20.32 cm) lead glass windows. Table 4.9, below, lists the different window combinations incorporating the two lead glass windows.

Table 4.9 Window options using the two available 20.32 cm thick lead glass windows.

Combination	Gamma Dose Rate (mrem/hr)	Neutron Dose Rate (mrem/hr)	Total Dose Rate (mrem/hr)	Thickness of material 1 (cm)	Thickness of material 2 (cm)	Thickness of material 3 (cm)	Total thickness (cm)
1. ZnBr + lead glass (ρ 3.95 g/cm^3)	0.111	0.904	1.015	55	31	NA	86
2. mineral oil + lead glass (ρ 3.95 g/cm^3)	0.967	0.047	1.014	30	56	NA	86
3. mineral oil + lead glass (ρ 3.95 g/cm^3) + lead glass (ρ 6.2g/cm^3)	0.807	0.065	0.872	30	40.64	12	82.64
4. mineral oil + lead glass (ρ 3.95 g/cm^3) + plain glass	1.005	0.037	1.042	30	40.64	28	98.64

From table 4.9, options #3 and #4 were chosen as the material combinations for the final window design. The availability and cost of the two different options will be considered and will determine which window is finally constructed. The physical design of the window will be done Tom Newton[28] and Bill Fecyth[29]. Below are pictures showing the two window design options.

[28] Assistant Reactor Superintendent, MITR-II.
[29] Consultant.

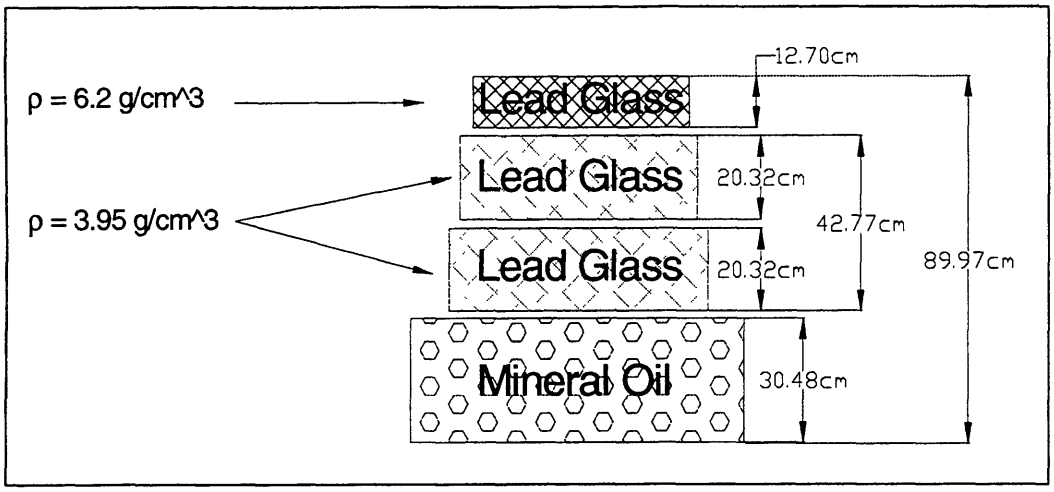

Figure 4.5 Window combination #3, incorporating the two medium density lead glass windows with mineral oil and high density lead glass.

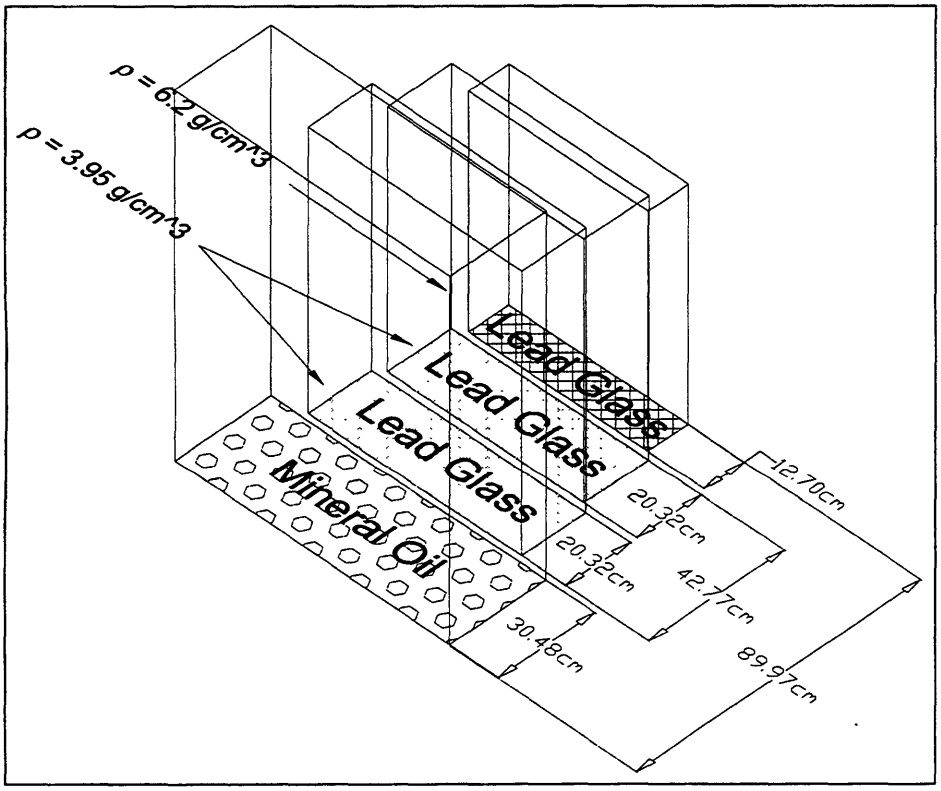

Figure 4.6 Side view of window combination # 3.

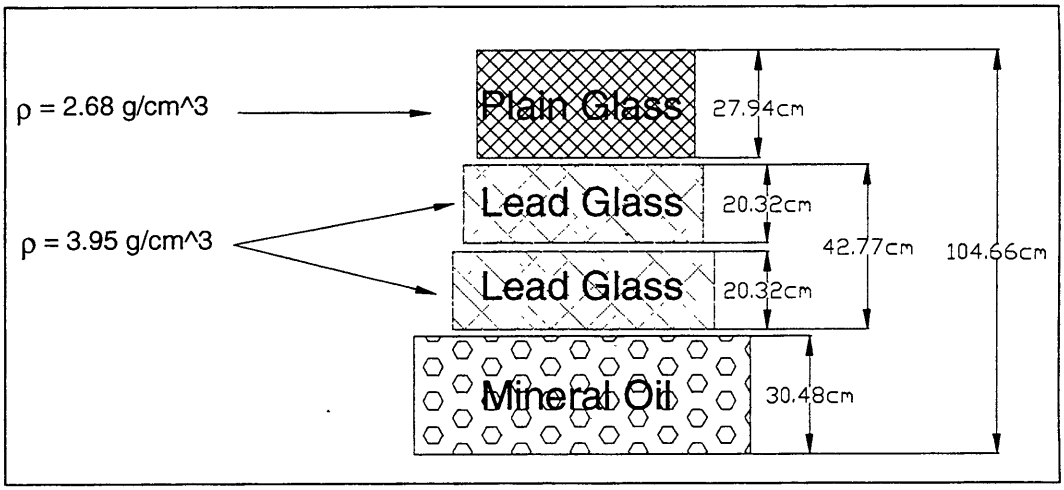

Figure 4.7 Window Combination # 4, two medium density lead glass windows with mineral oil and plain glass.

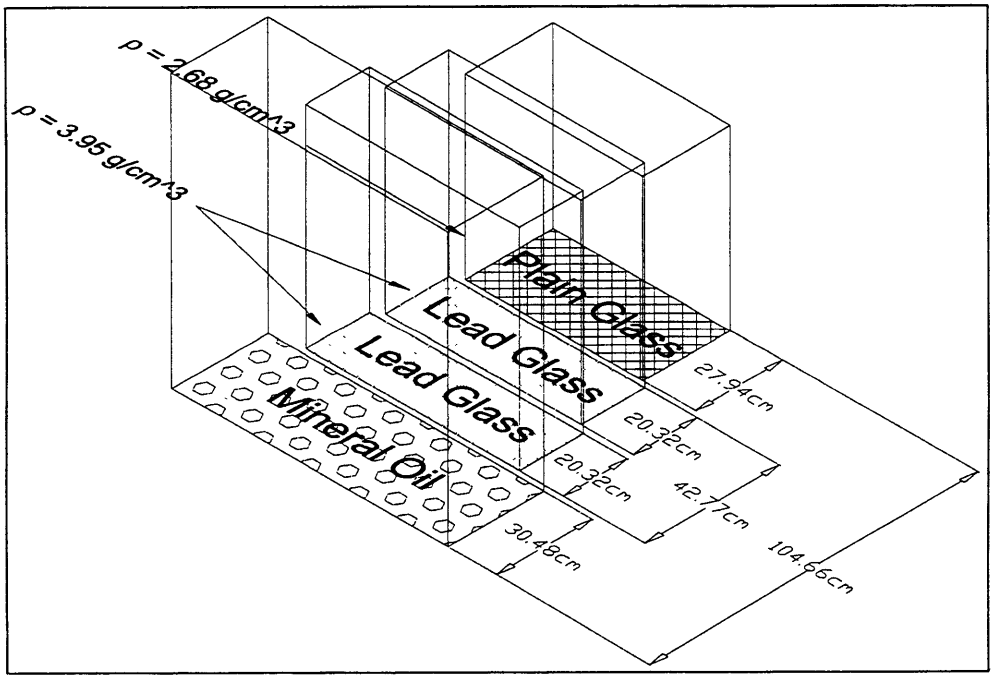

Figure 4.8 Side view of window combination # 4.

4.6 REFERENCES

Etherington, H., *Nuclear Reactor Handbook,* McGraw-Hill, Inc., 1958.

Jaeger, R.G, "Shielding Materials", *Engineering Compendium on Radiation Shielding,* Vol.II, Springer-Verlag, New York Inc, 1975.

Lide, D., *Handbook of Chemistry and Physics, 74th Edition*, CRC Press,1994.

Rockwell, T. , *Reactor Shielding Design Manual,* D. Van Nostrand Company, Inc., 1956.

Schaeffer, N.M., *Reactor Shielding for Nuclear Engineers,* U.S. Atomic Energy Commission, 1973.

CHAPTER 5

SHIELDING DESIGN USING MONTE CARLO SIMULATIONS

5.1 MONTE CARLO METHOD

A computational approach was employed as an alternative to the analytical calculations described in chapters 2 and 3 by using the Monte Carlo N-Particle code (MCNP)[30]. The Monte Carlo radiation transport code is a way of simulating the transport of the neutrons and gamma rays in the new medical room by simulating individual particles using probability distribution functions, rather than solving a transport equation. Information from these simulations can be used to determine the shielding required for the new medical room.

Several problems were associated with this technique. Due to the complexity of a three-dimensional transport model for the medical room model, obtaining statistically accurate results for dose rates at the various locations in the room was difficult. Additionally, the number of particles penetrating through several meters of air and finally through several feet of concrete required a substantial amount of computer run time to obtain an adequate result. Weight windows were used as a variance reduction technique to remedy this problem. However, obtaining results with less than 10 % error still proved

[30] Briesmeister, J., MCNP- A General Monte Carlo N-Particle Transport Code, Version 4B, Report LA-7396-M Revised, Los Alamos National Laboratory.

to be extremely difficult through large depths of concrete. For these reasons, the results obtained were analyzed cautiously and compared to the analytical and experimental shielding calculations.

5.2 MCNP MODELS

Simulations using the Monte Carlo transport code consisted of three different geometric models of the medical room. These models consisted of: 1) a model with incremental planes in the side wall and window, 3) a model with planes exiting the collimator on the beam centerline axis and off centerline, 3) and a model with incremental planes in the back wall and door. The first model was used to measure the neutron and gamma flux at various depths of a concrete side wall. To measure the amount of neutron and gamma radiation reflecting off the lead collimator the second model was used. Additionally, a third model measured the neutron and gamma fluxes at varying depths in the back wall and door.

5.2.1 Side Wall Model

Radiation reaching the side wall is greatest when a target is in the beam, as mentioned in Chapter 2. A geometric model of the medical room with a head phantom located 15 cm from the beam opening was used in the Monte Carlo simulation to determine the amount of concrete required to shield the side wall of the medical room. The origin of the input file for the medical room was W.S Kiger's[31] fission converter model std486

[31] W. Stead Kiger, MIT Ph.D. candidate.

with modifications made to the shutter systems by B. Sutharshan[32], file bs020. Figure 5.1, below, shows the MCNP generated plot of the medical room geometry used for this simulation. The right wall of the medical room was divided into 5 cm increments to measure neutron and gamma fluxes at varying depths in the concrete. These increments were also necessary for improving the accuracy of the simulation via variance reduction. This segmented area is a high density concrete wall 90 cm thick, 140 cm long, and 300 cm in height. Next to the segmented wall is a smaller region, also divided into 5 cm increments. This section of the wall represents the viewing window, composed of water. Capture gamma production from hydrogen was measured using this water-filled window. The neutron attenuation properties of water were comparable to the neutron shielding materials under consideration for the final window design. Hydrogen content in the possible neutron shielding materials was similar to water.

[32] Balendra Sutharshan, Ph.D.

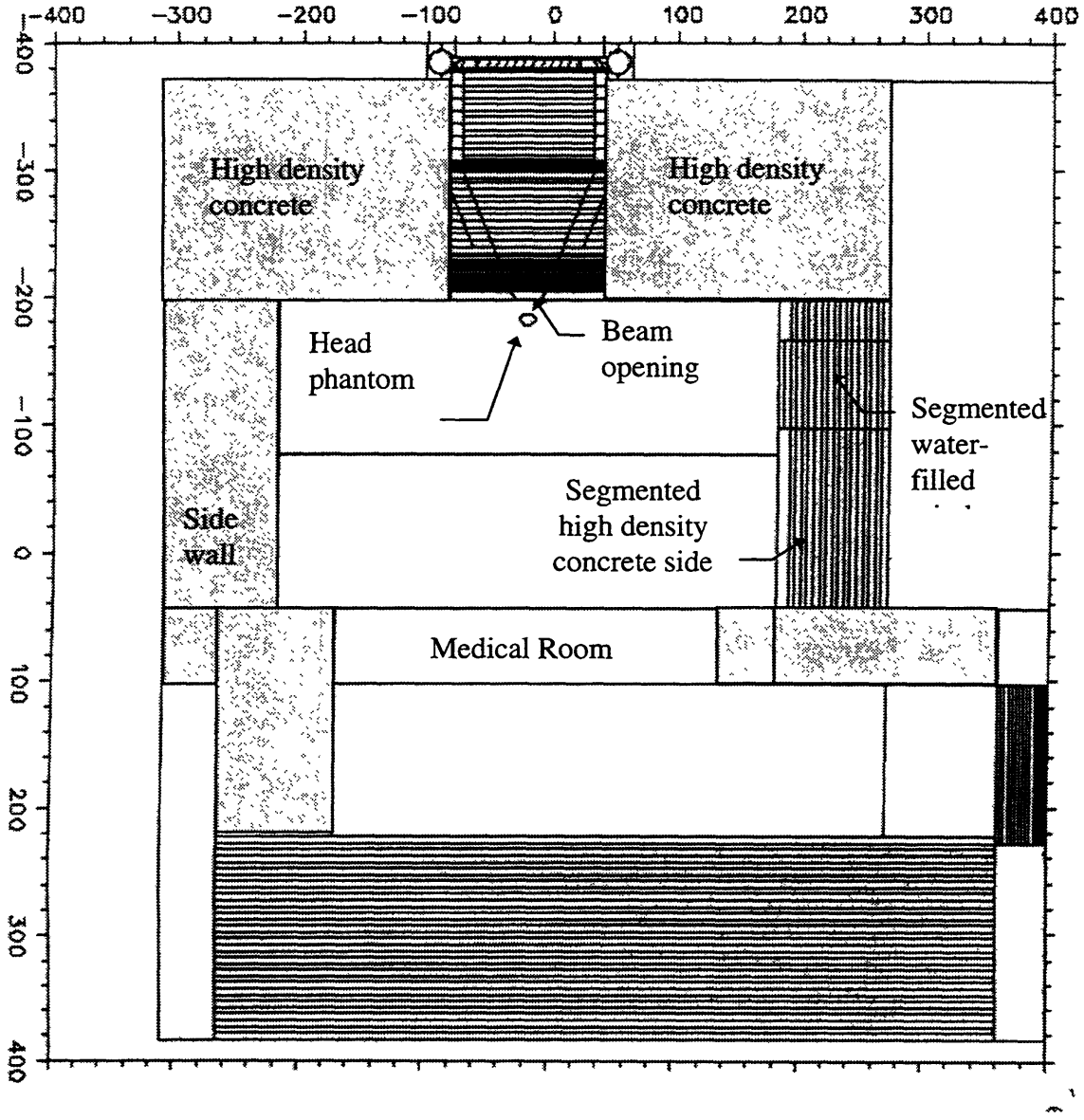

Figure 5.1 MCNP model used to determine side wall thickness.

For a source of radiation a surface source file was written at the beam wall. This source file contained all the neutrons and gammas originating from the fission converter fuel tank and exiting the collimator, into the medical room.

Surface tallies segmented over the specified area measured the neutron and gamma flux through the incremental depths in the material. The tallies were divided into different energy bins of less than 1 ev, 1 ev-10 kev, and 10 kev-20 Mev for thermal, epithermal, and fast neutron flux measurements. The gamma flux tallies were divided into incremental energy bins of 0.05 Mev, from 0.0 Mev up to 1.0 Mev. At energies higher than 1.0 Mev the energy bins increased by 0.2 Mev increments.

5.2.2 Lead Collimator Reflection Model

Analysis of the side wall results, see section 5.3, and analytical calculations performed by Dr. Tarcisio Campos[33] revealed some unusually high fluxes at the side walls. An MCNP simulation was performed to find the source of this radiation. From the work by Tarcisio, it was suspected that neutrons and gammas were reflecting off the lead collimator of the beam. This would explain the unusual flux levels at the side walls. To test this hypothesis, a simulation was done calculating the neutron and gamma fluxes in the beam centerline and off centerline, 48 cm to the side. A clearer description of the model is shown in the figure 5.2 below.

[33] Visiting Professor.

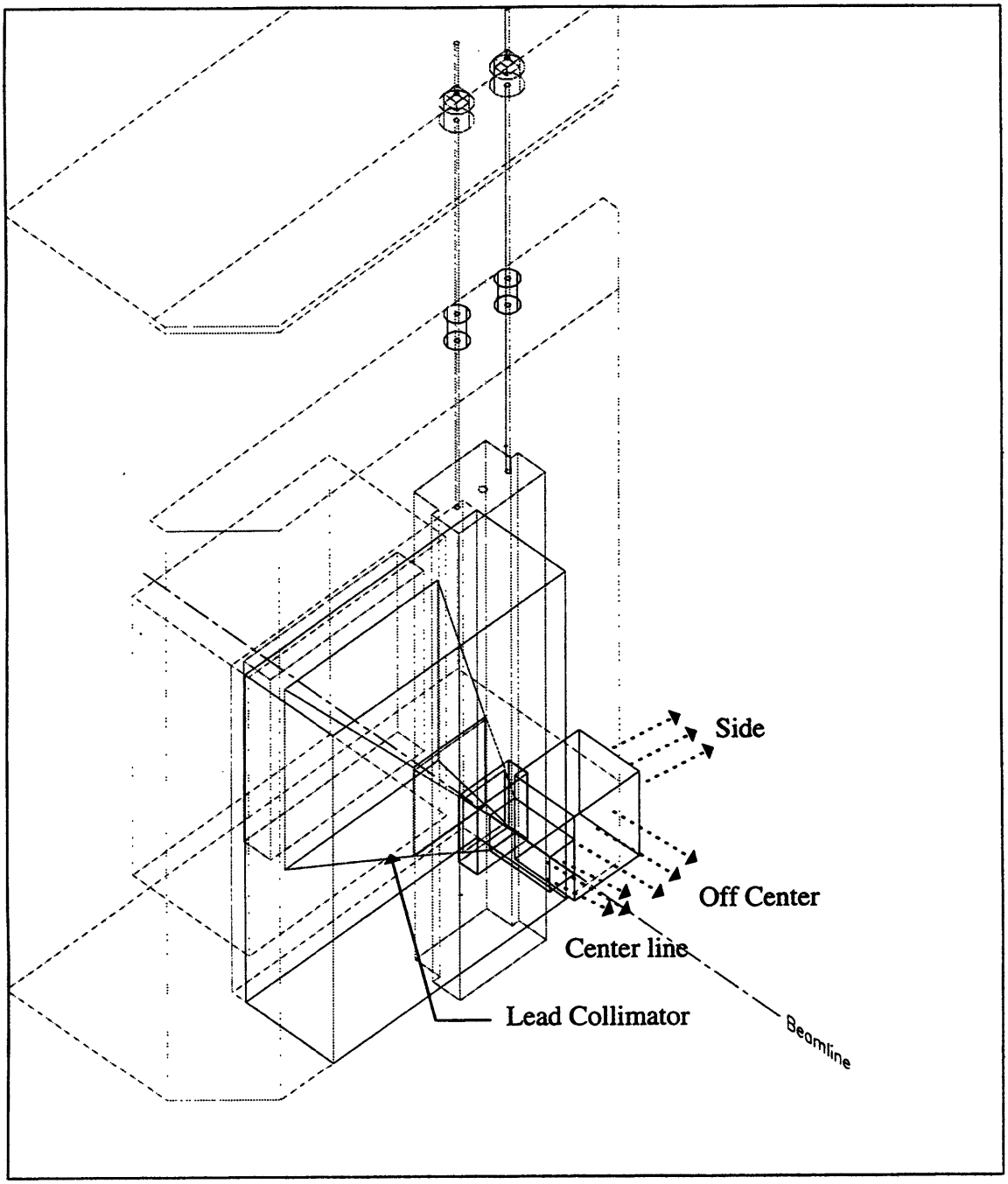

Figure 5.2 Diagram showing the cubes where the flux was measured.

Using one of Kent Riley's[34] MCNP models of the filter/moderator and collimator assembly as a basis for this model, tally planes were added 48 cm in front of the beam, 10 cm and 58 cm to the right of the beam centerline, and 26 cm above and below the beam centerline. This made two cubes. One cube was located on the beam centerline with dimensions 20 cm wide, 20 cm tall, and 48 cm in depth. The other cube, the off center cube, was located next to the beam opening with dimensions of 48 cm wide, 52 cm tall, and 48 cm in depth. The neutron and gamma fluxes were calculated at the front face of each cube and at the right face of the off center cube by using surface tallies.

5.2.3 Door Model

To determine the shielding needed for the door and back wall a model with a direct beam of radiation, without a target, was used. The model was made using B. Sutharshan's[3] MCNP model, bs020, of the medical room back wall as a basis. The back wall was located a distance of 450 cm from the beam opening. A mini-maze was used to model the doorway. This consisted of a 45 cm long and 60 cm wide concrete block located at the corner of the right wall, before the doorway. A 225 cm walkway, 120 cm wide, shielded the door from any direct radiation. The door was composed of high density concrete, segmented into depths of 3 cm increments. Again, weight windows were used for variance reduction throughout the model and were crucial in obtaining statistically significant results in the door region of the model.

[34] MCNP input file kjr306, Kent Riley, MIT Ph.D. student.

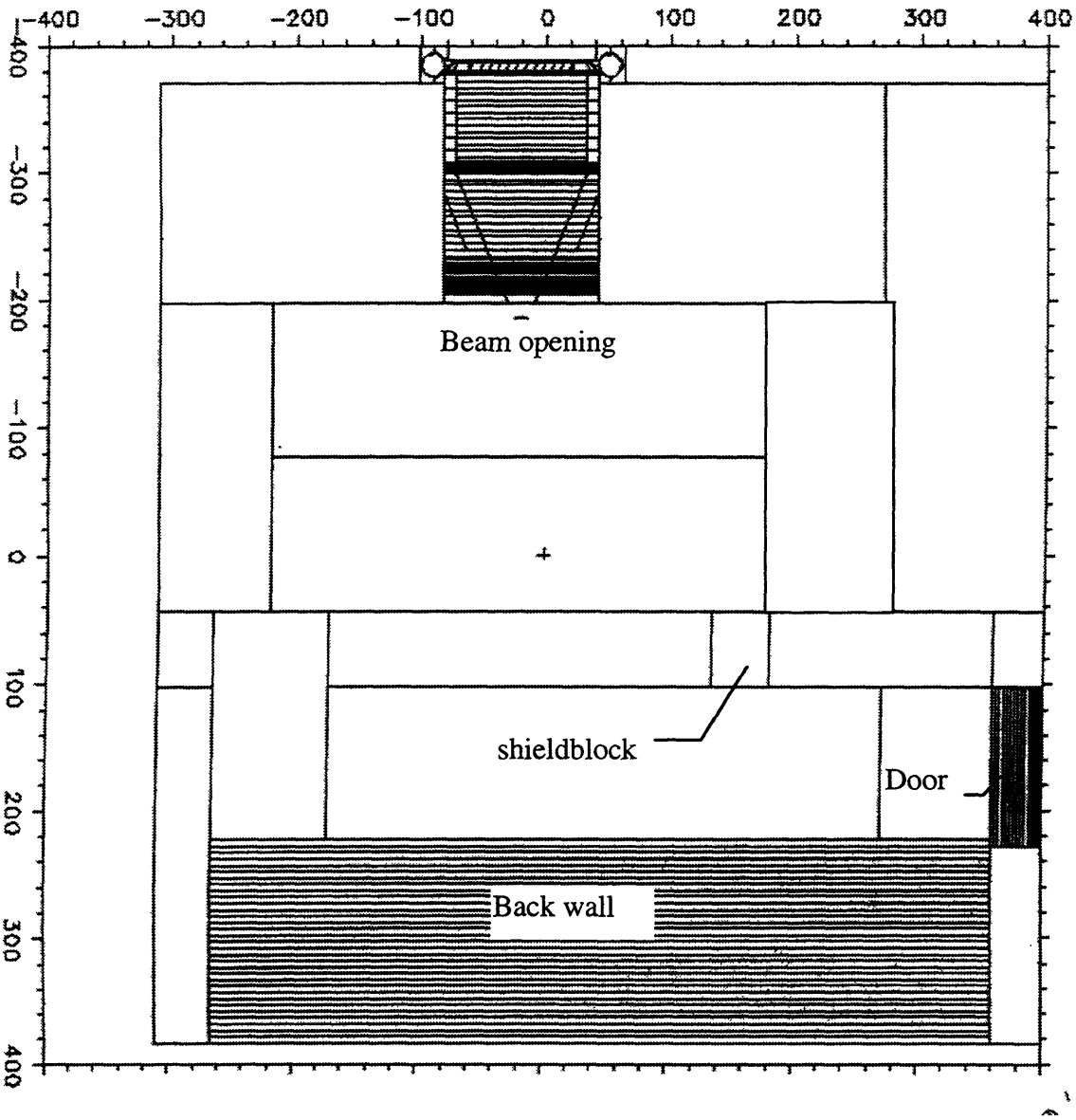

Figure 5.3 MCNP plot of door model.

Like the side wall model, a surface source on the beam wall was used to simulate the radiation coming out the fission converter beam. To calculate the neutron and gamma flux going through the door, surface tallies were used. These tallies were segmented and averaged over the area of the door. The neutron and gamma fluxes were calculated at the inner surface of the door and every 3 cm thereafter. In addition to calculating the fluxes at the door, the neutron and gamma fluxes coming off the shieldblock were also calculated. The thermal neutron flux from this calculation was used to determine the capture gamma dose rate produced from hydrogen neutron capture, as described in section 3.2.1. Also of importance were the neutron and gamma fluxes at the back wall, which was divided into 5 cm increments. Based on previous work by Balendra Sutharshan[35] 90 cm of high density concrete should be sufficient shielding for the back wall. To verify this, surface tallies, segmented and averaged over the area of the back wall, were used at planes 90 cm-115 cm into the back wall to calculate the neutron and gamma fluxes.

5.3 RESULTS

5.3.1 Side Wall Results

Results from the side wall MCNP simulations are displayed in the table below. The table lists the neutron and gamma fluxes for different energy bins. These fluxes were measured over the region of the right side wall between the window and the shieldblock.

[35] Balendra Sutharshan, MIT Ph.d. thesis, Engineering Design of a Fission Converter-Based Epithermal Beam for BNCT.

Table 5.1 Flux at inner surface of right side wall.

Particle Type	Flux (particles/cm2.sec)	Dose Rate (rem/hr)	% Error
Thermal Neutrons	3.75x106	13.78	4.8 %
Epithermal Neutrons	3.08x107	113.24	4.9 %
Fast Neutrons	2.68x105	35.67	10.5%
Gammas	1.27x107	18.31	4.0 %

The dose rates listed in table 5.1 are about a factor of 10 higher than calculated in chapter 2. Also, the fluxes at the side wall are only a few orders of magnitude lower than at the beam opening. These unusual results are explained by the lead collimator reflection simulation, described in section 5.3.2.

The fluxes in table 5.1 were transformed into dose rates using the equations 2.1 and 2.2. The following graphs show the MCNP results for the side shielding determination. It is important to note that the MNCP tallies for both neutron and photon dose rates were not taken at angles 90 degrees from the phantom. The tallies were averaged over a section of the side wall, at angles between 37 and 68 degrees. As mentioned previously in chapter 2, the dose rates scattered to the wall at these angles are higher than at 90 degrees. Therefore the MCNP results for the amount of shielding needed to reduce the dose rates to 1 mrem/hr should be slightly higher than calculated in section 2.4.1.

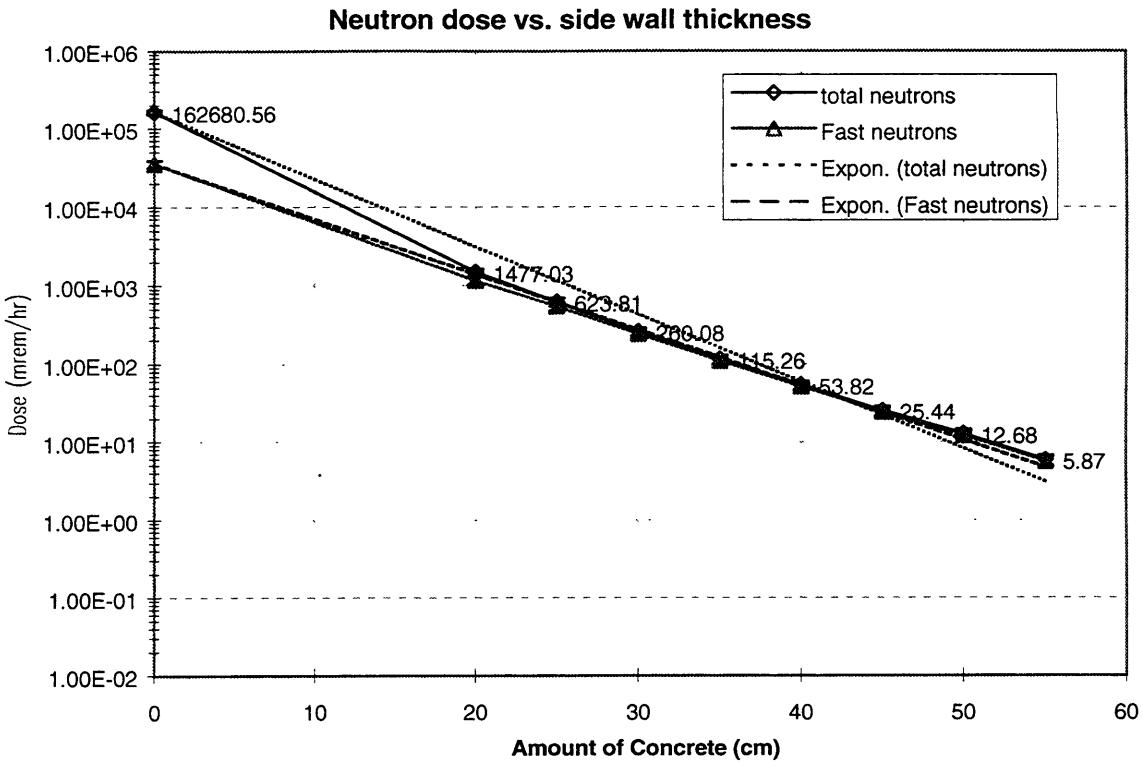

Figure 5.4 MCNP results of neutron dose rates through a high density concrete side wall.

Some important information is contained in Figure 5.4. The figure shows the total neutron dose rate and the fast neutron dose rate. It is interesting to point out that at the inside of the wall the total neutron dose rate is almost five times the fast neutron dose rate. However, after about 25 cm of concrete the fast neutron component dominates the total neutron dose rate. This is an important observation because in the analytical shielding calculations, explained in chapter 2, the thermal and epithermal neutron components were ignored. The MCNP results validate that assumption. Another useful piece of information obtained from data in the figure is a more accurate fast neutron

removal cross section. The dotted lines in the graph are trendlines that were exponentially fit to the dose rates. From these trendlines an exponential attenuation coefficient was found. This was done by finding the removal cross section for each 5 cm increment in the concrete wall.

$$\Sigma r_i = \frac{\ln \frac{D_{i+1}}{D_i}}{x_{i+1} - x_i} \qquad \textbf{(5.1)}$$

From these incremental removal cross sections, an average removal cross section was obtained. For the fast neutrons this removal cross section was determined to be 0.146 cm^{-1}. This is much larger than the reported removal cross section of 0.11 cm^{-1} used in the analytical calculations.[36] The reported cross section was determined with a fission spectrum, so the removal cross section obtained from the MCNP simulation is more representative of the lower energy fast neutrons found in the fission converter beam.

After 55 cm into the concrete, the errors for the surface tallies were too large for the data to be statistically significant. To determine the amount of concrete needed to reduce the dose outside the side wall to 1 mrem/hr, the removal cross section, obtained from MCNP results, and the dose rate at the inside of the wall, from table 5.1, were applied to equation 5.2.

$$Xconcrete = \frac{\ln \frac{D}{Do}}{-\Sigma_r} \qquad \textbf{(5.2)}$$

[36] Jaeger, Engineering Compendium on Radiation Shielding, Vol. II.

A high density concrete wall 71.6 cm thick is required at the side wall to reduce dose rates directly outside the room to 1 mrem/hr.

The gamma dose rates through the concrete side wall are shown in the graph below. Like with the neutron data, an attenuation coefficient was determined. This coefficient of 0.118 cm^{-1} is lower than the reported value of 0.1361 cm^{-1}, but it incorporates the buildup and production of gammas in the material.

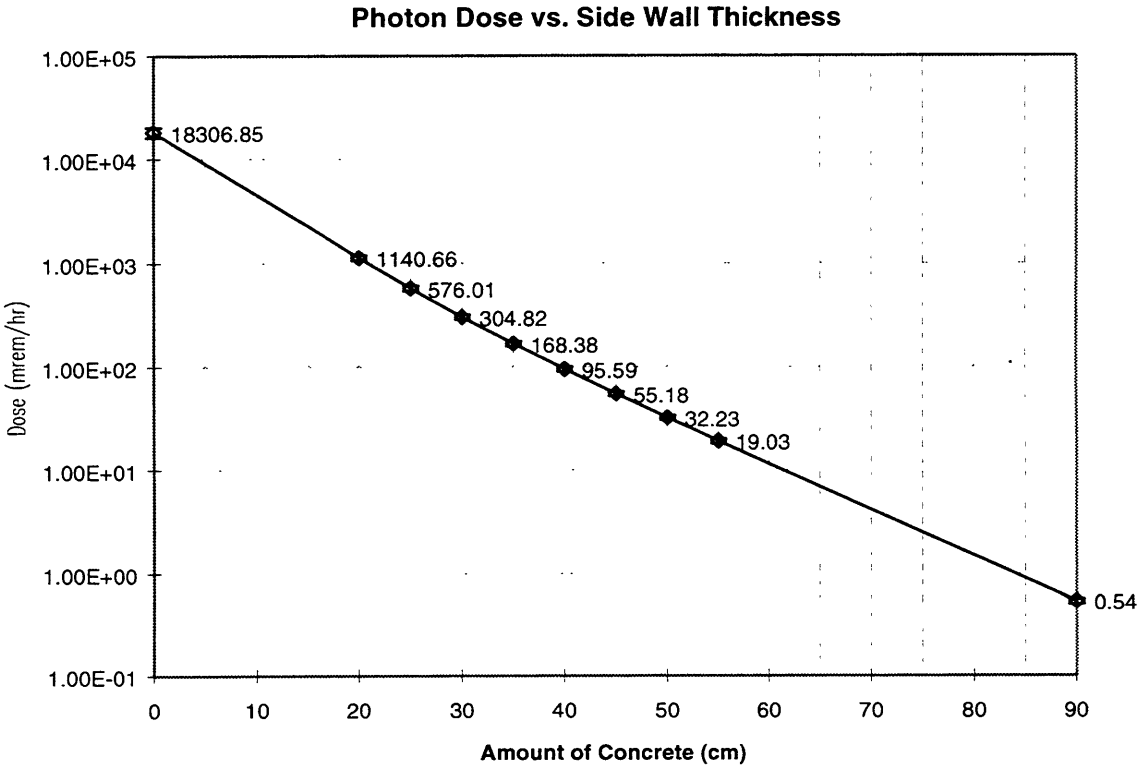

Figure 5.5 MCNP results of gamma dose rates through high density concrete side wall.

The tallies for gamma flux through the side wall had very low errors. After 90 cm through the.concrete, the error in the tally was only 5.6 %. Because of this low error, determining the amount of concrete needed for shielding at the side wall using equation 5.2 was not necessary. But as a check, the attenuation coefficient determined by the MCNP data along with the dose rate at the inner surface of the side wall (from MCNP) were applied to equation 5.2 to find the amount of concrete needed. A side wall of high density concrete 83.4 cm thick is necessary to shield the side wall, based on the MCNP results.

Summary of MCNP Side Wall Results

Table 5.2 Summary of MCNP side wall results.

Material	Amount of material needed to reduce gamma dose rate to 1 mrem/hr (cm)	Amount of material needed to reduce neutron dose rate to 1 mrem/hr (cm)
High Density Concrete $\rho = 3.76$ g/cm^3	83.4	71.6

5.3.2 Window Results

Using the MCNP results for thermal neutron flux to determine the dose rates from capture gamma production, as described in section 2.4.2, was not possible. Obviously, the thermal neutron flux drops dramatically in water. Obtaining statistically accurate information about the thermal neutron flux through the window was extremely difficult. As an alternate method of estimating the gamma production by hydrogen neutron capture

reactions in the water-filled window, the total gamma dose rates through the window were found, shown in the graph below.

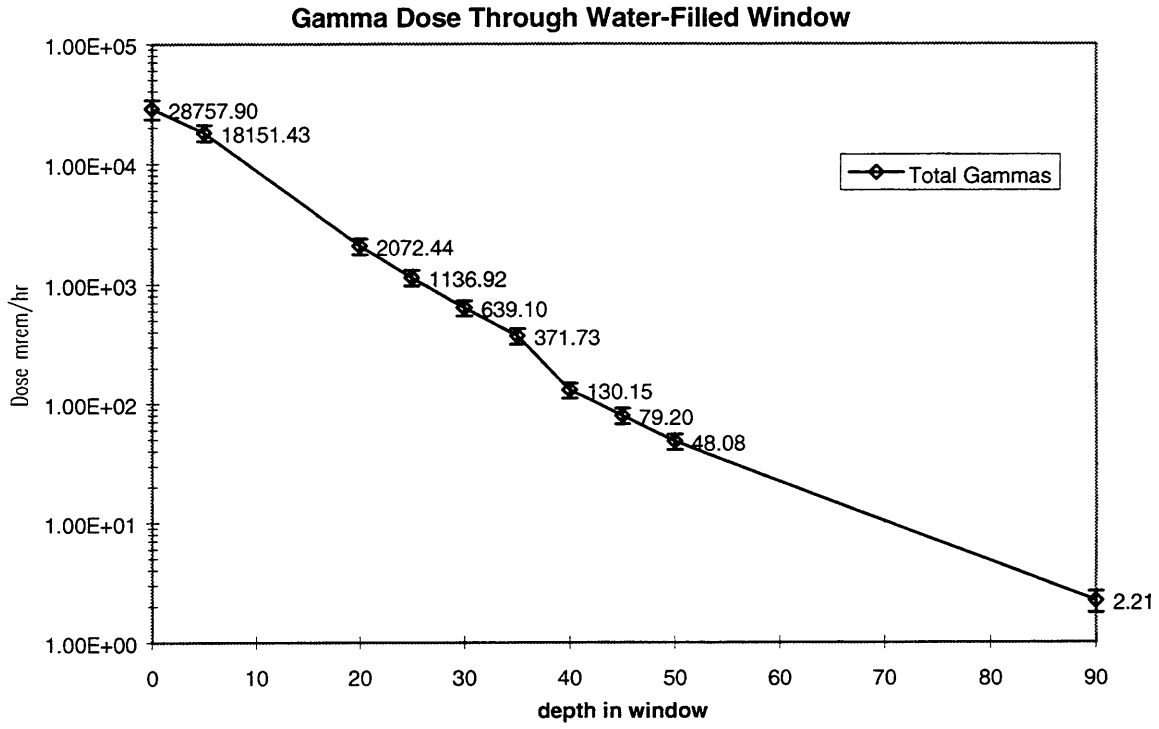

Figure 5.6 Dose rates from capture gamma production at each incremental depth in window.

The neutron and gamma attenuation properties and the hydrogen content of water are comparable to mineral oil. By looking at the dose rate after 30 cm of water, an understanding of the effect the productions of capture gammas have on the total gamma dose rate incident on the lead glass was obtained. Recall in section 4.5 the final window design specifies 30 cm of mineral oil then a lead glass shield. The MCNP determined gamma dose rate incorporates the capture gamma dose rate. This total gamma dose rate of 640 mrem/hr requires shielding by the lead glass. However, this MCNP determined

dose rate is less than the 781 mrem/hr, determined by analytical calculations, incident on the lead glass. Therefore, the shielding specified in chapter 4 for the shielded window is more than adequate for reducing the dose rates outside the side wall to less than 1 mrem/hr.

5.3.3 Lead Collimator Reflection Results

Table 5.3 lists the results of the lead collimator reflection simulation. The results show large flux levels at the "off center" position. At this off center position the flux does not fall off as quickly as in centerline position. The reduction in flux 48 cm from the beam wall is only a factor of two in the off center position whereas this reduction is a factor of 10 in the centerline position.

Table 5.3 MCNP results of flux at different locations.

Position	Distance from beam wall (cm)	ϕthermal (n/cm^2.sec)	ϕepithermal (n/cm^2.sec)	ϕfast (n/cm^2.sec)	ϕgamma (γ/cm^2.sec)
Beam	x = 0	8.07E+08	1.25E+10	5.39E+08	1.31E+08
Centerline	x = 48	8.77E+07	1.35E+09	7.47E+07	1.91E+07
Off	x = 0	1.07E+08	1.58E+09	6.18E+07	1.13E+08
Centerline	x = 48	4.67E+07	7.97E+08	3.76E+07	3.00E+07
Side	y = 58	5.03E+06	6.49E+07	2.07E+06	7.42E+06

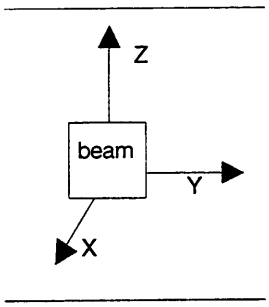

Figure 5.7 Diagram explaining the location of flux measurements. The x-axis is coming out of the beam where the beam center is defined by coordinates 0,0,0.

This interestingly large flux coming off the side of the beam opening supports the idea that neutron and gamma radiation are reflecting off the lead collimator towards the back corners of the side walls. This would explain the unexpectedly high dose rates on the inner surface of the side wall, mentioned above. The figure below shows the radiation scattering off the lead collimator. From the angles at which the radiation can reflect off the collimator and exit through the beam opening it is obvious that the side walls would be the recipients of this reflected radiation.

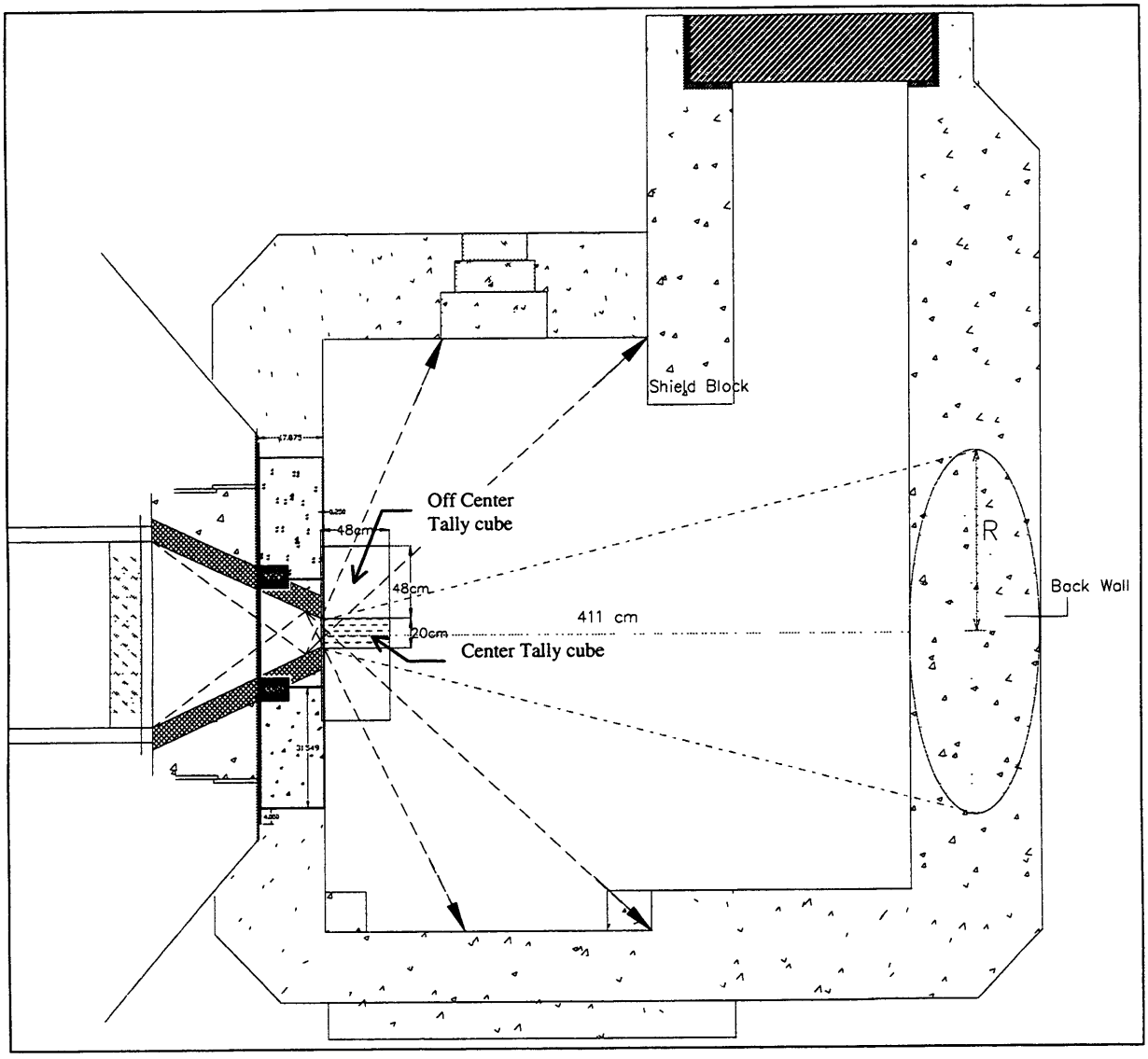

Figure 5.8 Radiation reflection off the lead collimator.

Table 5.4 Comparison of flux levels at the beam wall and side wall of the medical room.

	Flux at beam center x = 48	Flux off center x = 48	Flux at side y = 58 cm	Flux at side wall, mcnp medical room model
thermal	9.32E+07	2.71E+07	3.27E+06	3.75E+06
epithermal	1.37E+09	4.63E+08	4.59E+07	2.08E+07
fast	7.19E+07	3.52E+07	2.00E+06	2.68E+05
gamma	1.91E+07	3.00E+07	7.42E+06	1.27E+07

5.3.4 Door Results

Results from the door simulation provide insight into several key factors. Dose rates at the end of the shield block should confirm that the major portion of the radiation reaching the door comes from reflection off the back wall because of the albedo's dependence on the reflection angle, discussed in section 3.2.2, figure 3.4. Also, dose rates at the door surface should give some idea as to whether the analytical calculations were valid. Dose rates at the inner surface of the door are listed in the following table. The dose rates listed are the dose rates averaged over the surface of the door.

Table 5.5 MCNP results at inner surface of door.

Particle Type	Flux (particles/cm^2.sec)	Dose Rate (rem/hr)	% Error
Thermal Neutrons	1.09×10^5	0.485	5.3 %
Epithermal Neutrons	1.14×10^6	4.06	5.6 %
Fast Neutrons	1.53×10^4	2.04	16.8 %
Gammas	1.42×10^6	1.76	4.6 %

Table 5.6 lists the dose rates at the end surface of the shield block. The end surface is the part of the shield block in the medical room doorway, not in direct sight of the beam. Dose rates at this surface stem from leakage radiation penetrating through the block and from reflection off the back wall.

Table 5.6 Flux levels and dose rates at end of shield block.

Particle Type	Flux (particles/cm^2.sec)	Dose Rate (rem/hr)	% Error
Thermal Neutrons	5.62×10^5	2.5	6.7 %
Epithermal Neutrons	5.71×10^6	20.3	5.6 %
Fast Neutrons	7.58×10^4	10.1	14.6 %
Gammas	4.42×10^6	5.4	11.5 %

Comparing the dose rates at the door to the dose rates at the end of the shield block reveals that the dose rates at the door are on average about 1/5 of the dose rates at the shield block. This confirms that the majority of the dose at the door is coming from the back wall. Figure 3.6 is a graph of the albedo for concrete at different reflection angles. In the graph, the albedo at reflection angles between 25 to 50 degrees (where the shield block is located) is 5 times larger than the albedo at reflection angles larger than 60 degrees (where the door is located).

Table 5.5 shows that the largest portion of the dose rate at the door comes from epithermal neutrons, which were neglected in the analytical calculations. Epithermal neutrons and thermal neutrons were neglected in the analytical calculations because it was assumed that they would attenuate through large shields before fast neutrons would. The graph below shows the total neutron and fast neutron dose rates through 55 cm of a high density concrete door. Like in the side wall case, the epithermal and thermal neutrons attenuate much faster than the fast neutrons. So even though the fast neutron dose rate is only a 1/3 of the total neutron dose rate incident on the door, it dominates the neutron dose rate after about 20 cm into the door.

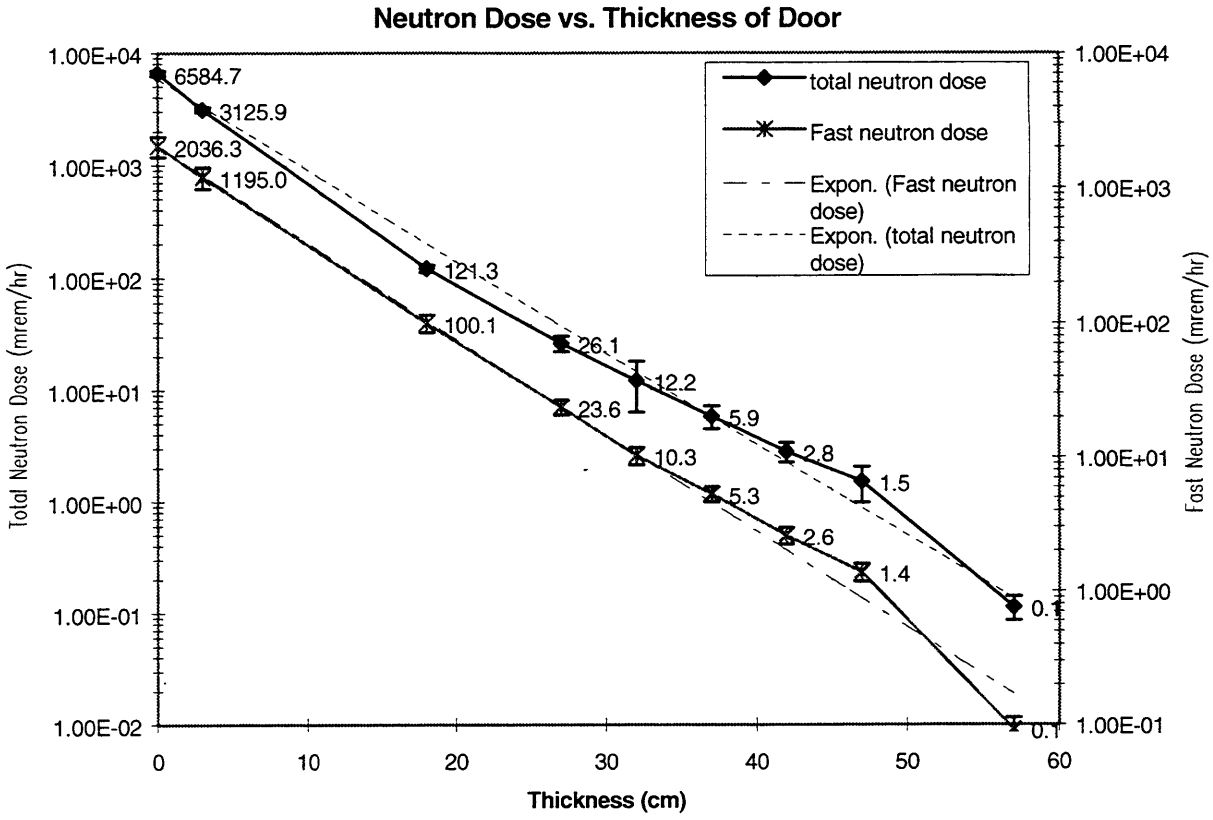

Figure 5.9 MCNP results of neutron dose rates through a high density concrete door.

After 40 cm through the concrete door, the error in the tallies becomes too large to rely on for determining the amount of shielding needed to reduce dose rates outside the door to less than 1 mrem/hr. To make use of the dose rates obtained at depths less than 40 cm, the average macroscopic removal cross section for the high density concrete door was derived using equation 5.1. A macroscopic removal cross section of 0.153 cm^{-1} was calculated for the fast neutrons traveling through the concrete door. This value is larger than the removal cross section derived for the same material at the side wall. The difference in the two cross sections can be explained by the difference in energy

spectrums of the fast neutrons. The neutrons incident on the door have traveled through 4.5 m of air and scattered once or more off concrete before finally reaching the door. Due to these multiple interactions, the energy of the neutrons at the door should be less than at the side wall, and therefore would have a slightly larger removal cross section. Using the removal cross section derived for the door and the fast neutron dose rate obtained from MCNP, the amount of high density concrete needed to reduce the dose rate outside the door to 1 mrem/hr is 57.4 cm.

In the graph below are the gamma dose rates through the concrete door. The dose rates presented in the graph include dose rates from incident gammas and from capture gammas created in the concrete.

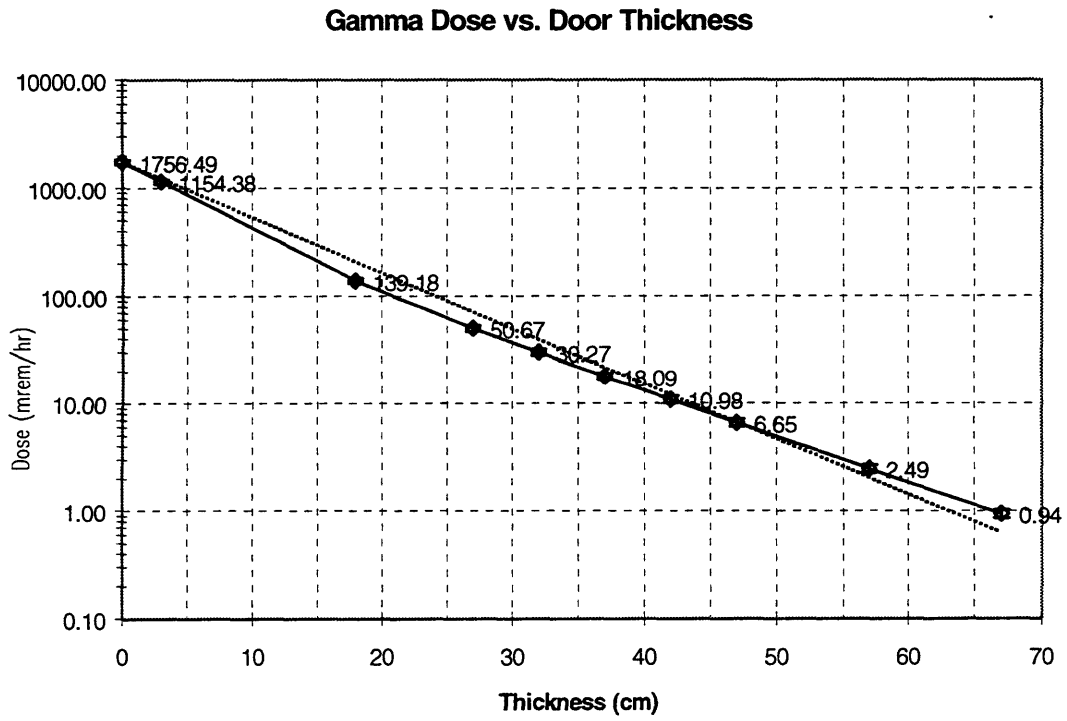

Figure 5.10 Gamma dose rates through a high density concrete door, from MCNP.

Statistics for these results were good throughout the door, with 8.7% error in the dose rate after 67 cm of concrete. But, as a check, an attenuation coefficient was extrapolated from the data. This gamma attenuation coefficient, which includes buildup and production of gammas in the material, was determined as 0.1105 cm^{-1}. Using equation 5.2, the amount of high density concrete needed to reduce the dose rate outside the door to 1 mrem/hr is 67.6 cm.

Summary of MCNP Door Results

Table 5.7 Summary of MCNP door results.

Material	Amount of material needed to reduce gamma dose rate to 1 mrem/hr (cm)	Amount of material needed to reduce neutron dose rate to 1 mrem/hr (cm)
High Density Concrete $\rho = 3.76$ g/cm^3	67.6	57.4

5.3.5 Back wall Results

MCNP results for the neutron dose rates through the back wall are shown in the following graph. The graph only shows four data points measured. Again, tallies were taken at these depths only because previous work indicated that 90 cm of high

density concrete would be sufficient shielding for the back wall. This simulation verified the previous work.

From the data a macroscopic removal cross section for neutrons of 0.112 cm^{-1} was obtained. This value closely matches the 0.11 value cited in literature. Using the extrapolated removal cross section and the fast neutron dose rate at the beginning of the wall, 27.8 rem/hr (11 % error), the amount of concrete needed at the back wall was determined. A high density concrete wall 91.1 cm thick is needed at the back wall to reduce the outside dose rate to 1 mrem/hr.

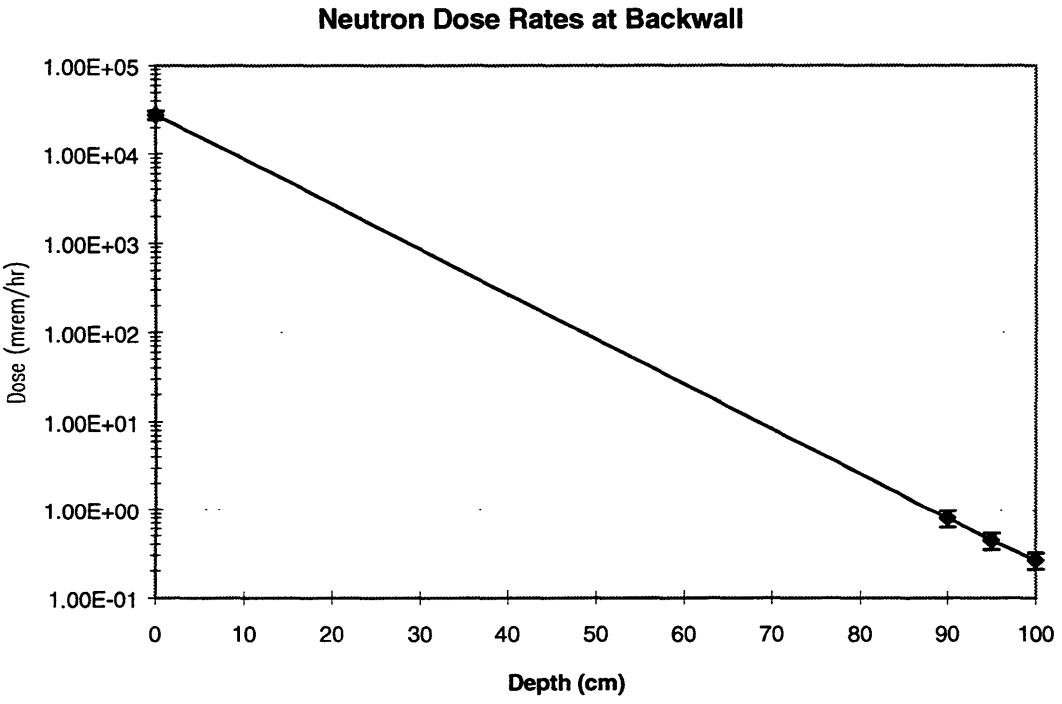

Figure 5.11 MCNP results for neutron dose rates through a high density concrete back wall.

Similarly, results for the gamma dose rates through the back wall were obtained from the MCNP simulations. Extrapolating an attenuation coefficient for gammas in the back wall, an attenuation coefficient of 0.102 cm^{-1} was obtained. This attenuation coefficient incorporates the buildup and production of gammas in the concrete back wall. Applying this coefficient with the gamma dose rate at the inner surface of the back wall, from MCNP, the amount of concrete needed to reduce the dose rate to 1 mrem/hr was found. The gamma dose rate at the inner surface of the back wa11 was 7.97 rem/hr with a 4.8 % error. A back wall made high density concrete 88.4 cm thick is needed for shielding the gamma radiation.

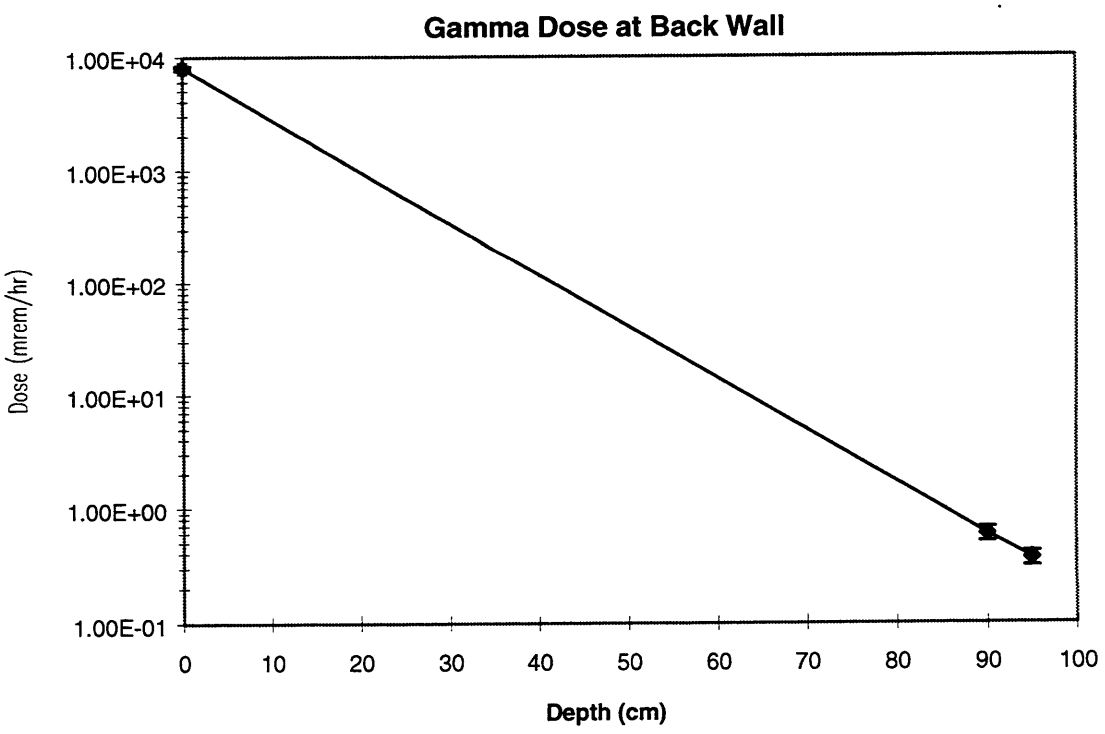

Figure 5.12 Gamma dose rates at various depths in a high density concrete back wall.

Summary of MCNP Back Wall Results

Table 5.8 Summary of MCNP back wall results.

Material	Amount of material needed to reduce gamma dose rate to 1 mrem/hr (cm)	Amount of material needed to reduce neutron dose rate to 1 mrem/hr (cm)
High Density Concrete $\rho = 3.76$ g/cm^3	88.4	91.1

5.4 COMPARISON OF MCNP RESULTS TO ANALYTICAL RESULTS

Before comparing the MCNP results and analytical calculations some differences in the medical room layout that affect the shielding should be pointed out. After the MCNP shielding study, the fission converter fast shutter system was moved 40 cm forward, into the medical room. Due to space considerations, the length of the medical room was not kept at 450 cm. Rather, it was reduced to 411 cm. This moved the back wall closer to the direct beam, relocated the window along the side wall, and brought the shield block and door closer to the beam wall. The effect this move had on the dose rates at the locations mentioned above was dealt with in the analytical calculations, but not in the MCNP calculations. This will cause a discrepancy in the comparison of a few percent, particularly for the door and back wall results.

The following table summarizes the results from both the analytical calculations and the Monte Carlo simulations. In Table 5.9, the material used for determining the amount of shielding needed is high density concrete with a density of 3.76 g/cm^3.

Table 5.9 Comparison of MCNP and analytical results.

Radiation Type	Dose Rate **MNCP** (rem/hr)	Dose Rate **Calculated** (rem/hr)	Amount of shielding needed to reduce dose rate to 1mrem/hr **MCNP** (cm)	Amount of shielding needed to reduce dose rate to 1 mrem/hr **Calculated** (cm)	% Difference in shielding needed
Side Wall					
fast neutrons	35.67	3.23	71.6	73	1.9 %
gammas	18.31	2.45	83.4	73	14.3 %
Back Wall					
fast neutrons	27.8	68.2	91.1	100	9.8 %
gammas	7.97	5.56	88.4	79	11.9 %
Door					
fast neutrons	2.04	1.76	57.4	67	16.7 %
gammas	1.76	1.69	67.6	70	3.6 %

Despite the difficulties in obtaining statistically valid results using MCNP and the

assumptions and simplifications made in the analytical calculations, the results from the two methods agree surprisingly well.

5.5 REFERENCES

Booth, Thomas E, "A Sample Problem for Variance Reduction in MCNP", Report LA-10363-MS, Los Alamos National Laboratory.

Breismeister, J., *MCNP-A General Monte Carlo N-Particle Transport Code, Version 4B*, Report LA-7396-M Revised, Los Alamos National Laboratory, 1997.

Campos, T, Personal communication.

Folkert, M., *Monte Carlo Simulation of Neutron Shielding for Proton Therapy Facilities,* MS thesis, Massachusetts Institute of Technology, 1998.

Holloway, James. "A Minimalist MCNP Manual and Local Guide", A report on using MCNP at the University of Michigan College of Engineering, 1993.

Jaeger, R.G, "Shielding Fundamentals and Methods", *Engineering Compendium on Radiation Shielding*, Vol. I, Springer-Verlag, New York Inc, 1968.

Jaeger, R.G, "Shielding Materials", *Engineering Compendium on Radiation Shielding*, Vol.II, Springer-Verlag, New York Inc, 1975.

Kiger, W.S, *Neutronic Design of a Fission Converter-Based Epithermal Beam for Neutron Capture Therapy,* Nucl. E. Thesis, Massachusetts Institute of Technology, 1996.

Redmond, E.L, Personal communication.

Redmond, E.L, Yanch, J.C, Harling, O.K, "Monte Carlo Simulation of the Massachusetts Institute of Technology Research Reactor", *Nuclear Technology*, Vol. 106, Apr, 1994.

Riley, K., Ph.D. thesis, Massachusetts Institute of Technology (to be published in 2000).

Sutharshan, B, *Engineering Design of a Fission Converter-Based Epithermal Beam for Neutron Capture Therapy,* Ph.D. thesis, Massachusetts Institute of Technology, 1998.

CHAPTER 6

VERIFICATION OF ANALYTICAL METHODS USED FOR SHIELDING CALCULATIONS

6.1 INTRODUCTION

The methods described in Chapters 2 and 3 for determining the shielding required for the new medical room were applied to the current medical room. This served as a means of verifying the shielding calculations performed for the new medical room. The process consisted of analytical calculations and experimental methods. First, dose calculations at critical locations in the current medical room were performed. These analytical calculations were then compared to experimental measurements taken in the current medical room to assess their validity. The attenuation coefficients for ordinary concrete based on reported data were then compared to attenuation coefficients derived from experimental data. The experimental attenuation coefficients were determined by measuring the count rates on the inside of the medical room wall and directly outside the room. The radiation transport calculations through ducts were also verified experimentally by applying the methods described in chapter 3 to the current medical room doorway and measuring the count rates at locations along the doorway.

6.2 DOSE CALCULATIONS AT THE BEAM PORT OF THE CURRENT MEDICAL ROOM

The dose rates at the opening of the beam port in the current medical room are 1.5 cGy/min for fast neutrons and 1.7 cGy/min for gamma rays.[37] Using the same average energies as used in chapter 2, 1 Mev for neutrons and 3 Mev for gammas, the corresponding equivalent dose rates are:

$$D_{fn} = 900 \text{ rem/hr}$$

$$D_{\gamma} = 102 \text{ rem/hr}$$

6.2.1 Dose Rates on the Inside of the Medical Room Side Wall

Dose scattering from the head, when placed in M67 medical beam

Dose rates resulting from radiation scattering off a human head or phantom and from capture gamma rays created by hydrogen neutron capture were calculated using the method described in section 2.4.2. First, the initial neutron and gamma fluxes were attenuated by the tissue in the head after traversing a distance of 8 cm. Using equation 2.3, fast neutron and gamma dose rates at the brain were then determined.

$$D_{fn,brain} = 507 \text{ rem/hr}$$

$$D_{\gamma,brain} = 73.5 \text{ rem/hr} + D_{capture_{\gamma}}$$

The dose rate from secondary gamma rays created by (n,γ) reactions with the hydrogen in the brain tissue was determined using equations 2.4 and 2.5. The average

[37] Dose rates from Kent Riley's Beam Characterization Measurements.

thermal neutron flux in the brain is lower in the current medical beam, M67, than the value reported in Chapter 2 for the fission converter beam. The average thermal neutron flux was approximated to be one half the maximum thermal neutron flux in the brain. This maximum flux was obtained from Figure 5.43, in W.S Kiger's thesis[38], which showed the MCNP calculated flux in a phantom using the M67 beam. Using this value of 2.28×10^8 n/cm^{2}sec, as the average thermal neutron flux in the brain, ϕth_{avg}, the dose rate from capture gammas at the surface of the brain was determined to be:

$$D_{capture_{\gamma},brain} = 50.68 \text{ rem/hr.}$$

Dose directly inside the medical room side wall

As in Chapter 2, calculations for the dose rate outside the medical room wall assume that the radiation is scattered off the head or phantom at 90 degrees. Using equations 2.7-2.9 to account for the energy loss in the radiation that is scattered off the head at 90 degrees, the dose rates incident on the side wall at 90 degrees to the incoming beam direction were calculated to be:

$$D_{fn,scatter} = 340 \text{ rem/hr}$$

$$D_{\gamma,scatter} = 7.03 \text{ rem/hr.}$$

Again, the gamma dose rate, $D_{\gamma,scatter}$, is specific to a scattering angle of 90 degrees, and does not include the dose rate from capture gammas generated by (n,γ) reactions with

[38] William S. Kiger, MIT Engineer's Thesis. Neutronic Design of a Fission-Converter Based Epithermal Neutron Beam for Neutron Capture Therapy, figure 5.43, p.383.

hydrogen in the brain. The capture gammas emitted scatter isotropically off the brain's surface.

In contrast to Chapter 2, where the dose rates directly outside the medical room side wall were calculated, here the dose rates inside the side wall are of interest. Determining the dose rates inside the room is necessary in order to compare the analytical method to the experimental measurements. The distance between the phantom and the side wall is 183 cm. Equations 2.6 and 2.10 were used to find the neutron and gamma dose rates at the inner surface of the side wall.

$$D_{fn,inside\ wall} = 0.65 \text{ rem/hr}$$

$$D_{capture_{\gamma},\ inside\ wall} = 0.0967 \text{ rem/hr}$$

$$D_{\gamma,total,inside\ wall} = 0.101 \text{ rem/hr}$$

6.2.2 Dose at Doorway Entrance (direct beam)

The current medical beam has a large angle of spread, as determined in section 3.3.3. Due to this spread in the beam, a significant amount of radiation is scattered from the medical room floor. Of particular interest is the radiation scattering in the direction of the doorway. Without a patient or phantom in the beam, no direct radiation reaches the door. The dose at the door must then come from radiation scattering off the floor of the medical room towards the doorway. Determining the fraction of radiation that reaches the door is important in the verification of the door design for the new medical room. The dose rate at the door was calculated by determining the amount of radiation incident upon the floor

that scatters to the door way. Using equation 2.14, with a total beam spread of 38°, the dose rates at the floor are

$$D_{fn,floor} = 7.2 \text{ rem/hr}$$

$$D_{\gamma,\,floor} = 0.813 \text{ rem/hr}.$$

A significant portion of the radiation that is incident upon the floor is scattered towards the doorway. Figure 6.1 shows the irradiated surface of the floor and the radiation scattering towards the door.

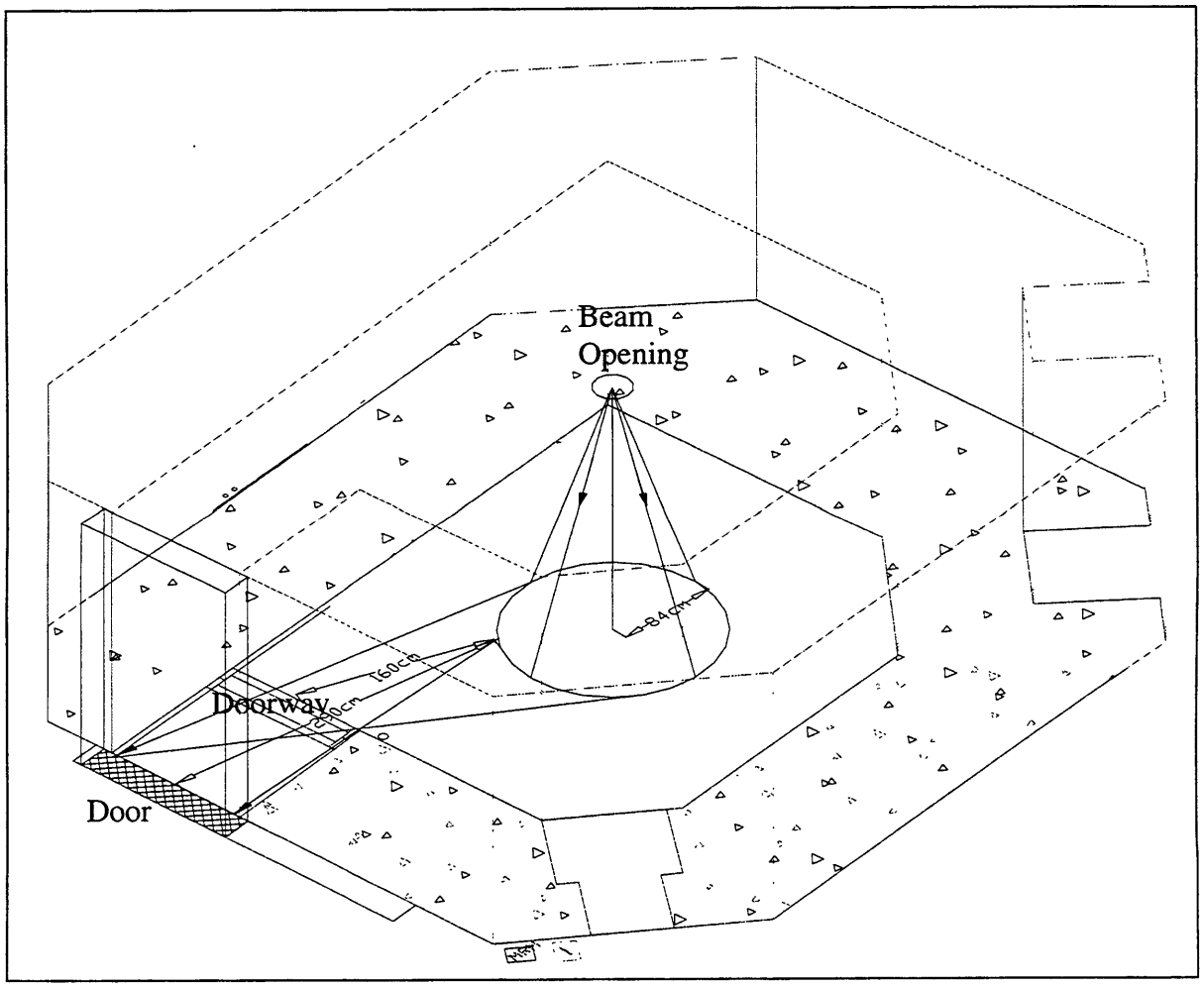

Figure 6.1 Radiation scattering off floor towards medical room door.

Using the dose rates at the floor, the dose rates at the inside of the doorway (where the masonite doors are located) and at the inner surface of the door were determined. To calculate these dose rates the albedo methods described in chapter 3 were used. For neutrons the values for concrete albedos, listed in Figure 3.7, were used. To determine the gamma dose rate at the inside of the door the calculated albedos for concrete displayed in Figure 3.13 were used. A 90 degree angle was used for the azimuthal angle. Unlike the calculations described in chapter 3, 53 and 67 degree reflection angles were chosen to determine the dose rate at the doorway and door, respectively. These angles were chosen rather than a 90 degree reflection angle because it allowed for comparison with the measured dose rates at the door. The dose rates were measured with a detector at a height of 119 cm from the floor, which makes a 53 degree angle with respect to the normal on the floor when the detector is placed at the doorway. The doorway is located 160 cm away from the irradiated portion of the floor. When the detector is at the inner door surface, 290 cm away from the irradiated area on the floor, it makes a 67 degree angle with the normal to the floor. An incident angle of 19 degrees was used for dose rate calculations. Applying these angles with the corresponding distance to equation 3.4, the dose rates at the doorway and door were obtained.

$D_{fn,\ doorway} = 0.49$ rem/hr

$D_{\gamma,\ door\ way} = 0.002$ rem/hr

$D_{fn,\ door} = 0.1$ rem/hr

$D_{\gamma,\ door} = 5.3e\text{-}4$ rem/hr

6.3 SHIELDING CALCULATIONS FOR CURRENT MEDICAL ROOM

The shielding thickness required to attenuate the calculated dose rates at the medical room wall and door to 1 mrem/hr was determined using equations 2.16-2.18. The medical room walls are made of 4' thick (122 cm) ordinary concrete. Attenuation properties for ordinary concrete are 0.0851 cm^{-1} for the gamma attenuation coefficient and 0.074 cm^{-1} for fast neutron removal cross section.[36] The current medical room door is made of 10" of steel (25.4 cm). The thickness of these materials required to attenuate the radiation at the door to 1 mrem/hr was determined and compared to the existing shield thickness in the current room.

Table 6.1 Amount of ordinary concrete needed to reduce dose at side wall to 1 mrem/hr.

$D\gamma$ = 100 mrem/hr, Dfn = 650 mrem/hr incident on wall

Material	Thickness needed to shield gamma dose rate to 1 mrem/hr (cm)	Buildup factor for gamma rays	Thickness needed to shield fast neutrons dose rate to 1 mrem/hr (cm)
ordinary concrete $\rho = 2.33$ g/cm^3	74	5.56	88

Table 6.2 Amount of material needed to reduce dose rate outside door to 1 mrem/hr.

$D\gamma$ = 0.53 mrem/hr , Dfn = 100 mrem/hr incident on door

Material	Thickness needed to shield gamma dose to 1 mrem/hr (cm)	Buildup factor for gamma rays	Thickness needed to shield fast neutrons to 1 mrem/hr (cm)
ordinary concrete $\rho = 2.33$ g/cm^3	none, dose rate is 0.53 mrem/hr	1	62
steel $\rho = 7.8$	none, dose rate is 0.53 mrem/hr	1	28

Based on analytical calculations, the current medical room door, excluding the separate masonite door, should attenuate the radiation outside the medical room to a total dose rate of 1.4 mrem/hr. However, as discussed in the next section, the neutron dose rates outside the medical room door with the masonite door open are higher than anticipated by this estimate.

6.4 EXPERIMENTAL MEASUREMENTS OF CURRENT MEDICAL ROOM SHIELDING

The M67 beam and existing medical room were used to validate the analytical methods used in the design of the new medical room. Measurements of the neutron and gamma count rates were taken at various locations of importance in the existing medical room. From these measurements, ratios of attenuation were obtained and compared to the ratios of the calculated dose rates from section 6.2. Also, by measuring the transmission through the concrete and steel shields, experimental attenuation coefficients for the two materials were obtained and compared to the available data on attenuation coefficients. Additionally, the fraction of radiation that scatters off concrete was found, as shown in section 3.3.

6.4.1 Method

Three separate experiments were performed to obtain the necessary dose rates required to verify the shielding calculations. The first sets of measurements were performed with the reactor power at 4.5 MW. For these measurements a layer of 8 ½ " thick concrete blocks covering an area of 31 ½" x 69 ½" was placed on the floor

directly beneath the beam opening. Three detectors were used to measure the fast neutron, thermal neutron, and gamma dose rates at the locations shown in the figure below. The detector used for the neutron count rate measurements was a Europium-doped LiI detector with 10" bonner sphere for the fast neutron measurements. A GM detector was used to measure the gamma dose rates. A third detector, Rem 500 2 inch TE proportional counter, determined the total neutron dose rates directly outside the room. Before the experiment, these detectors were calibrated using Co-60 and PuBe sources. The measurements were taken with the detector placed on top of a stand. The height from the centerline of the detector to the floor was 47 ".

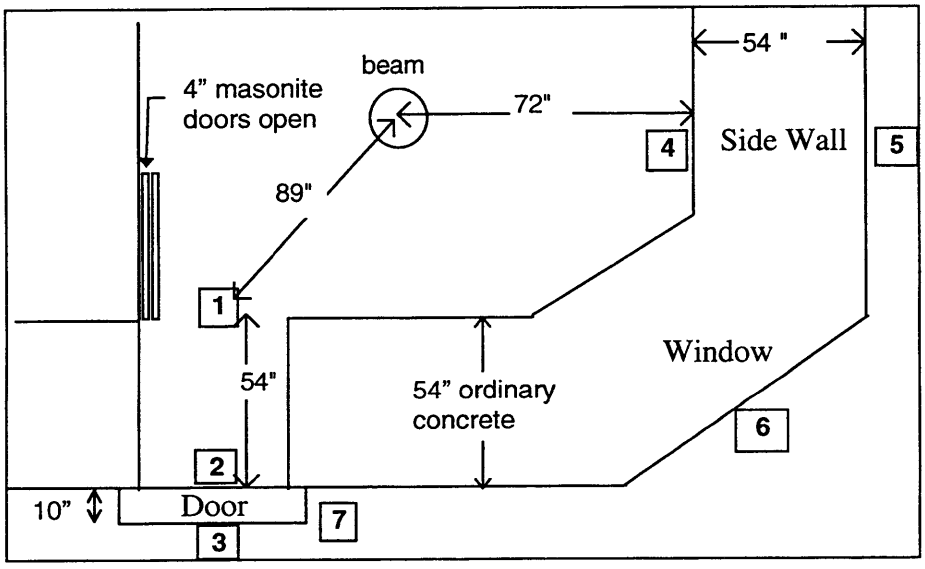

Figure 6.2 Experimental setup of medical room irradiation, top view.

The second set of measurements determined the dose rates at the beam centerline. This experiment was performed with the reactor power at 10 kW. The experimental

method for the second set of measurements was described in section 3.3.2. The data obtained from those measurements was adjusted to correct for the low power.

The purpose of the third experiment was to measure the amount of radiation that scatters off a patient's head and reaches the side wall during an irradiation. This was done by placing two sets of personnel dosimetry on the side wall, 90 degrees from the patient's head. The dosimetry consisted of a Landauer TLD and NeutrakER. The sets were placed at distance of 4.5" and 29" from the ceiling. The figure below shows the experimental setup.

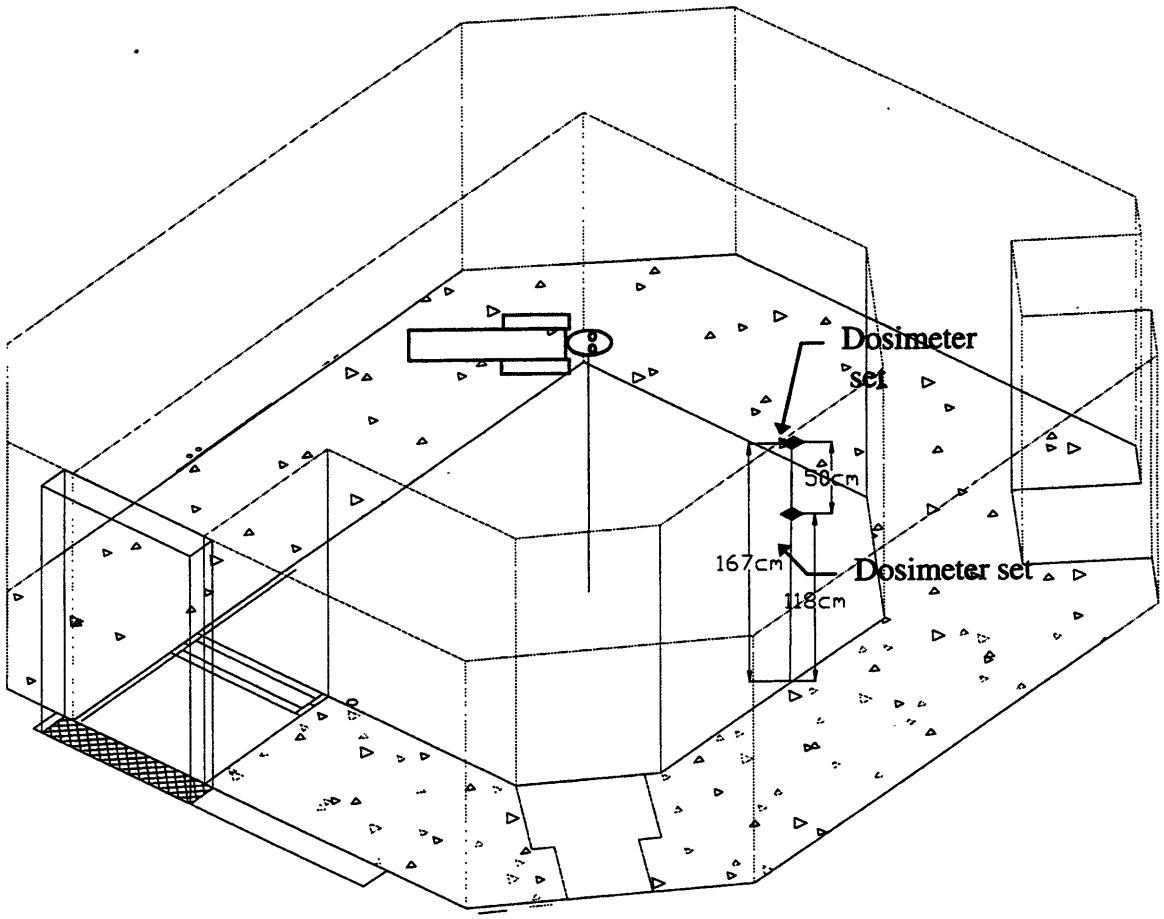

Figure 6.3 Experimental setup with patient in beam.

6.4.2 Results of Experiment

Tables 6.3-6.6 list the results of the measurements taken at the locations specified in figure 6.3.

Table 6.3 Summary of measurements taken from experiment 1. Reactor power at 4.5 MW.

Location of Measurement	Fast Neutrons		Thermal Neutrons		Photons
	average count rate per min	deviation from mean (cpm)	average count rate per min	deviation from mean (cpm)	dose rate per hour (mR/hr)
1	26269	161.2	50418.8	168.64	550
2	7435.4	70.24	18223.6	85.76	300
3	2100	NA	1850	NA	14
4	63562.6	1012.5	187832	255.2	588.5
5	NA	NA	9.3	0.3	0.4
6	25		130		1.2
7	1700		5000		26

Table 6.4 Dose measurements outside of the medical room door at position 3 in Figure 6.2. Reactor Power at 4.5 MW.

Neutron Dose Rate* Outside Steel Door (masonite door open)		Neutron Dose* at Right Crack Outside Door (masonite door open)	
mrem/hr	mrad/hr	mrem/hr	mrad/hr
84.35 $\pm$ 6.35	6.90 $\pm$ 0.256	20.62 $\pm$ 4.78	2.07 $\pm$ 0.259

*Total neutron dose rate is reported. This includes the dose rates from thermal, epithermal and fast neutrons.

Table 6.5 Measurements in beam centerline from experiment 2. Reactor Power at 10 KW, measurement values listed below have been converted to 4.5 MW.

Measurements in Beam Center line			
Distance from Beam	Average Fast Neutron counts (counts/min)	Average Fast Neutron Dose rem/hr	Gamma Dose rem/hr
17 cm	$1.09 \times 10^6 \pm 5.44 \times 10^4$	180.29 $\pm$ 3.65	103.82
87 cm	$1.53 \times 10^5 \pm 4.71 \times 10^3$	30.89 $\pm$ 1.5	15.8
193 cm	$9.24 \times 10^4 \pm 2.46 \times 10^3$	11.36 $\pm$ 0.74	7.22

Table 6.6 Results of dose rates at wall from scatter off patient's head.

Patient	Neutron Dose Rate 4.5" from ceiling (rem/hr)	Neutron Dose Rate 29" from ceiling (rem/hr)	Gamma Dose Rate 4.5" from ceiling (rem/hr)	Gamma Dose Rate 29" from ceiling (rem/hr)
M.W.	5.967	3.658	0.7032	0.4387
E.L.	8.35	7.44	0.8198	0.713

The measurements listed in table 6.5 were adjusted to account for the lowered reactor power using the channel 7 current readings. The values for current obtained from reactor operations were 79.9 μA for 4.5 MW and 0.177 μA for 10 kW.

Using the data listed in table 6.3, fast neutron and gamma attenuation coefficients for ordinary concrete and steel were derived. The attenuation coefficients in concrete were determined by taking the natural log of the ratio of counts at locations 5 and 4 and dividing by the thickness of the concrete. In determining the gamma attenuation coefficient, an initial guess of the buildup factor was made. After an initial gamma attenuation coefficient was found, an iterative process was used to correct for the actual buildup and find the actual attenuation coefficient. This process was repeated to determine the attenuation coefficients for steel, using measurements at locations 2 and 3.

Table 6.7 Calculated attenuation coefficients using the results from measurements taken in current medical room.

Material	Fast neutron removal cross section cm^{-1}	Gamma attenuation coefficient cm^{-1}
ordinary concrete $\rho = 2.33$	0.0645	0.0684
steel $\rho = 7.8$	0.0498	0.173

These experimental values were compared to the values listed in Volume II of the Engineering Compendium on Radiation Shielding, by Jaeger, which were used for the attenuation coefficients in the new medical room calculations. The values listed in the compendium for ordinary concrete are 0.0740 cm^{-1} for fast neutron removal cross section and 0.0851 cm^{-1} for the gamma attenuation coefficient, assuming 3 Mev gamma rays. For steel these values are 0.168 cm^{-1} for neutrons and 0.279 cm^{-1} for gamma rays. It is important to note the large discrepancy between the measured values and reported values for the attenuation coefficients of steel. Unlike the coefficients for ordinary concrete, the values for steel are drastically different. This may explain why the 25.4 cm steel door in the medical room that should theoretically shield the doorway to 1.4 mrem/hr still leaves a dose rate outside the room of about 85 mrem/hr. The discrepancy in reported and measured gamma attenuation coefficients could result from the capture gammas created by (n,γ) reactions in the steel door. These gamma rays, with energies as high as 10 Mev, would contribute a significant dose outside the door. However, this does not explain the large discrepancy in neutron attenuation values. This will be discussed further in section 6.5.

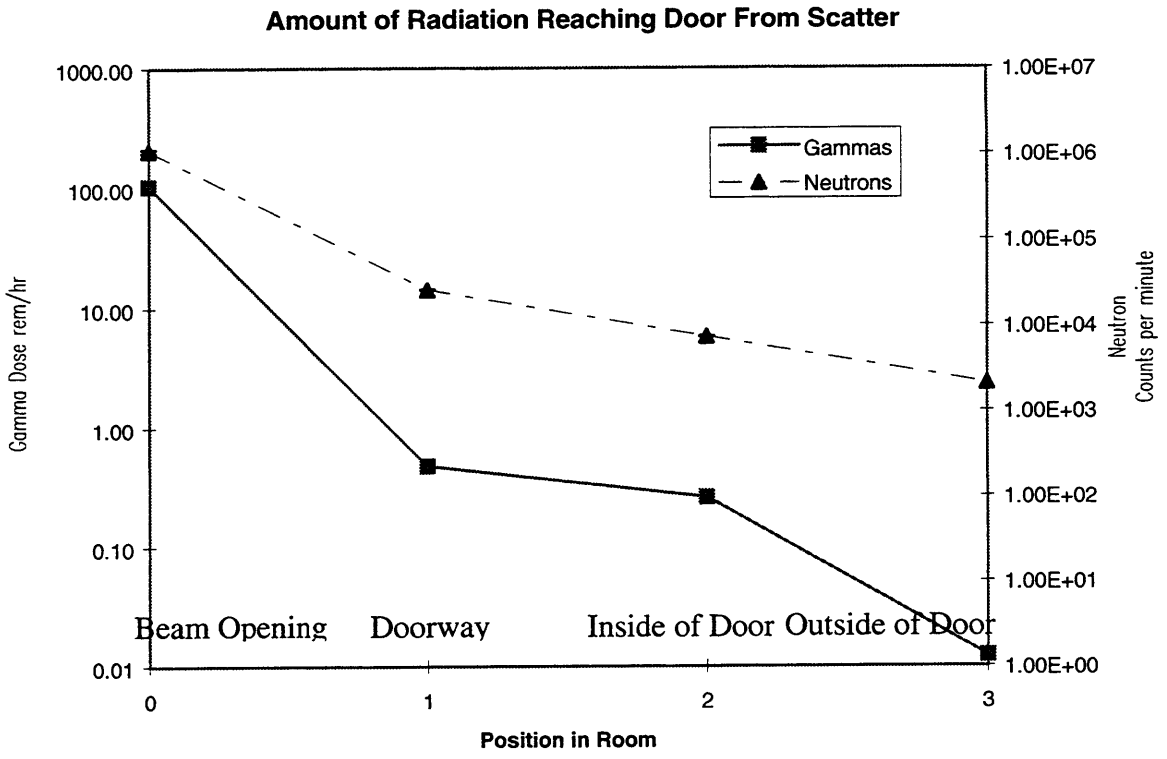

Figure 6.4 Results of radiation transport measurement from beam opening (0), to doorway (1), to door (2), and finally to outside of the door (3).

Figure 6.4 shows the measurements for the neutron count rates and gamma dose rates taken at the beam opening, the doorway, directly before the door, and outside the door. Using these values, the fraction of radiation scattered towards the doorway that finally reaches the door was determined by calculating the ratio of counts from the beam centerline measurements to the counts from measurements taken at locations 1 and 2. The ratios used the beam centerline measurement taken with the detector 17 cm from the beam opening. These ratios are shown in the following graph and listed in table 6.8.

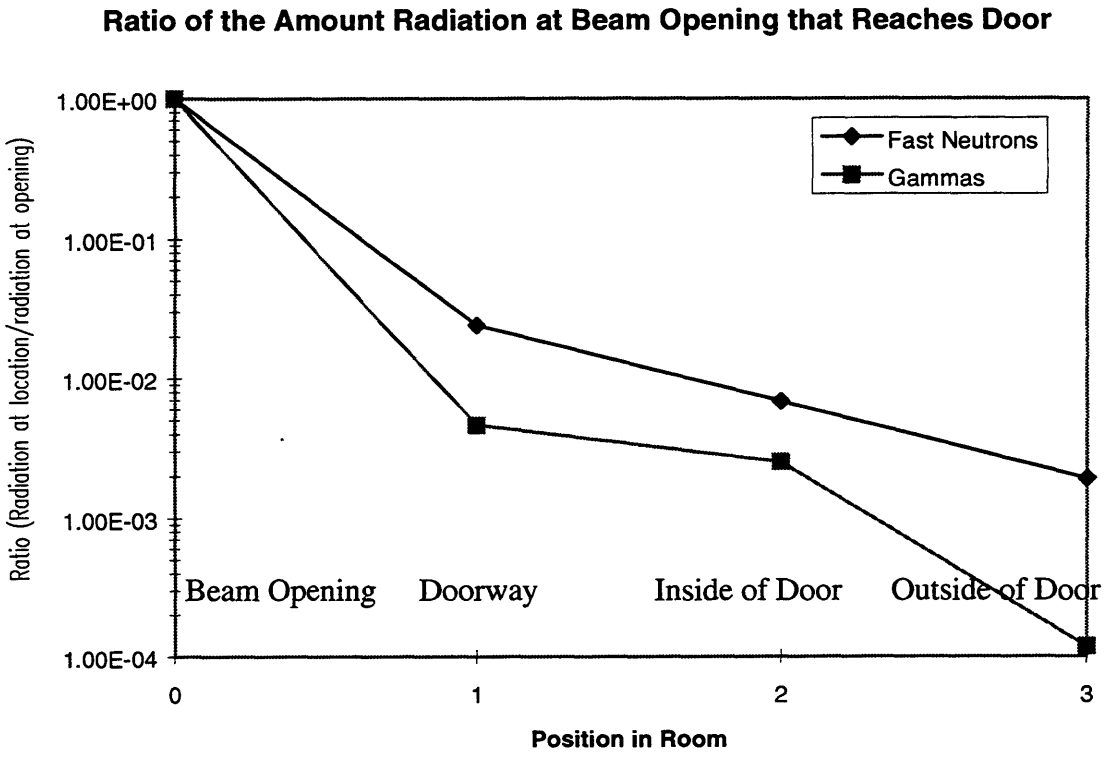

Figure 6.5 Measured ratios of the amount of radiation that is transported to the doorway (1), inner surface of the door (2), and outside the door (3) from beam opening (0).

Table 6.8 Fraction of initial radiation transported to different locations, measured values.

Fraction of Radiation at Beam Opening Reaching Door		
	neutrons	gammas
beam to doorway	2.41e-2	4.6e-2
doorway to door	2.83e-1	5.4e-1
beam to inside of door	6.8e-3	2.5e-3
beam to outside of door	1.9e-3	2.0e-4

6.5 COMPARISON OF EXPERIMENTAL MEASUREMENTS AND CALCULATED VALUES

The ratios of the calculated dose rates at the entrance to the doorway and the door inner surface to the dose rate at the beam opening are shown in Figure 6.6 below. From the figure it is obvious that a larger percentage of initial neutrons are transported to the door than initial gammas. Based on this method, the small portion of gamma radiation reaching the door, shown in table 6.9, should be negligible. However, the experimental measurements reveal a dose rate of 14 mR/hr incident on the inner surface of the door. This discrepancy can be explained by several factors. First, the analytical calculations did not take into account possible capture gammas production in the medical room walls. In the shielding calculations for the new room, the capture gamma component from the medical room walls was considered to be the greatest source of gammas at the door. Additionally, when measuring the dose rate with detectors located next to the walls, a significant amount of radiation will scatter off the door (as described in chapter 3), back into the detector. This will skew the detector measurements, producing a larger dose rate.

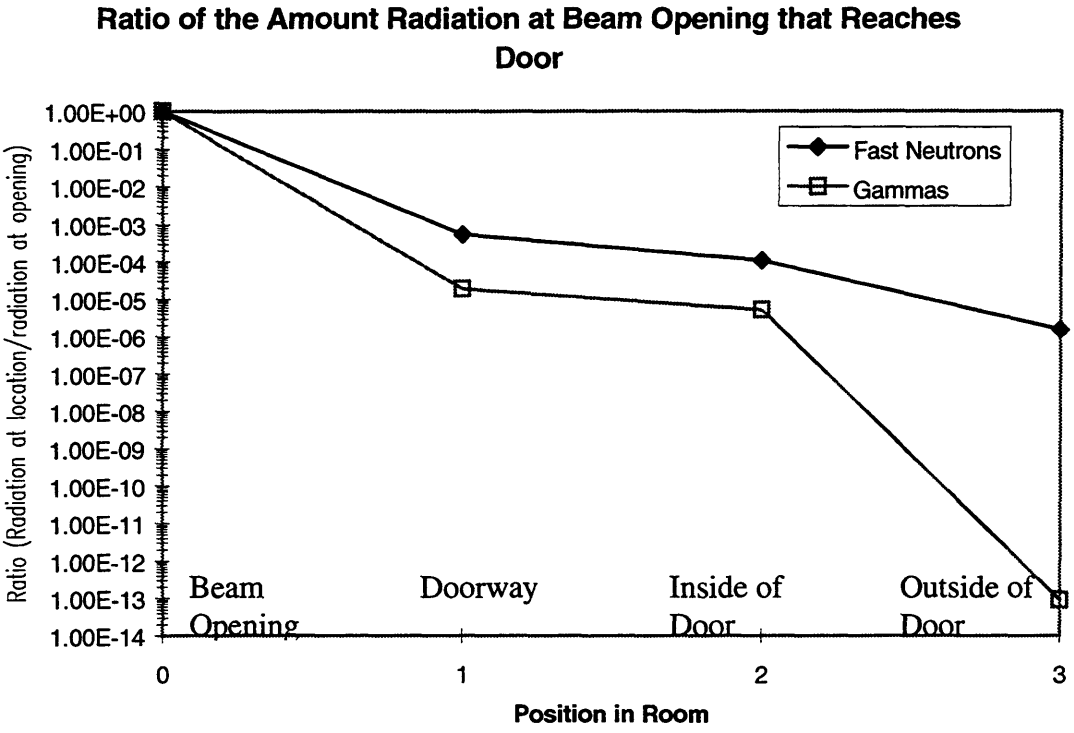

Figure 6.6 Calculated ratios of the amount of radiation that is transported to doorway (1), inner surface of door (2), and outside of door (3) from beam opening (0).

Table 6.9 Amount of initial radiation reaching door, calculated values.

Fraction of Radiation Reaching Door		
	neutrons	gammas
beam to doorway	2.7e-3	2e-5
doorway to door	2.04e-1	2.65e-1
beam to inside of door	5.6e-4	5e-6
beam to outside of door	7.8e-6	9e-14

Comparing Table 6.9, which lists the calculated ratios, to the measured ratios of the radiation at the beam opening to the radiation at the doorway and door, Table 6.8, a difference of a factor of 10 is noticed. However, the calculated ratios and the measured ratios for the amount of radiation at the doorway compared to the amount of radiation

at the door are very similar. The ratio of the radiation at the inside of the door to the radiation at the doorway was measured as 28.3 % and calculated as 20.4%. This would mean that the factor of ten difference (2.41 % measured, 0.27 % calculated) in the measured and calculated beam opening to door ratios must stem from the calculation of the dose rate at the doorway. The calculation of dose rate in the doorway assumed scatter from only one surface, the floor. As mentioned in chapter 5, radiation scattering may occur from any of the various surfaces that were not analyzed in the current room shielding calculations.

Results from the patient scattering experiment also suggest that modeling the attenuation in the beam as geometric attenuation only may not be accurate. The experimental dose rates from scatter off the head were a about a factor of 10 higher for neutrons and a factor of 7 higher for gammas. It is interesting to note that these are the same orders of difference between the MCNP results and the calculated results for dose rates at the side wall of the new medical room. In that case it was decided that the excess radiation at the side wall was due to radiation scattering off the collimator. A more in depth study of the characteristics of the current beam would need to be done before the same statement can be made. However, this would explain the large difference in the calculated and measured dose rates at the side wall and doorway.

Another discrepancy in the calculated and measured values occurs in the attenuation by a 25.4 cm thick steel door. The measured attenuation coefficient for steel results in a neutron dose rate outside the steel door 20 times higher than the dose rate calculated

with the reported attenuation coefficient. One important fact to note is that only one fast neutron count rate was measured outside the door, unlike the other measurements. However, this does not explain why the average neutron dose rate measured outside the room was 85 mrem/hr. A more in depth analysis of the experimental data is needed before a the difference in calculated and experimental results can be correctly explained. The following are several factors could have contributed to this larger than anticipated neutron dose rate. One is that the detector used to measure the neutron dose rate measures the total neutron dose rate, including thermal, epithermal, and fast neutrons. This would give a much larger than anticipated dose rate outside the door. Nonetheless, the LiI detector, used to measure the fast neutron count rate, still gave a larger rate outside the door than expected. Additionally, in the analytical calculations for the current room an energy of 1 Mev was assumed for fast neutrons. The actual energy spectrum of the beam is unknown. If the energy is higher than the 1 Mev the attenuation coefficient used in the analytical calculation could underestimate the amount of shielding needed. On the other hand, at energies lower than 1 Mev, the neutron cross section for iron exhibits different behavior. The graph below, Figure 6.7shows the scattering cross section for iron. At the 1 Mev energy range the resonances in the cross section are oscillatory with small overall variance. In the lower region of the fast neutron energy range however, there are large resonances in the scattering cross section. Information about the energy of fast neutrons in the M67 beam might help in explaining the large dose rates outside the door. Another explanation for the discrepancy in calculated and measured dose rates outside the steel door is that the calculated value was obtained using a removal cross section for

the attenuation coefficient of steel. This removal cross section is based upon information obtained with fission energy neutrons and is treated as energy independent. However, as shown in figure 6.7, the cross section of steel is energy dependent. The removal cross section method is only valid if the shield thickness is greater than 3 relaxation lengths.[39] The 10" steel door in the current medical room is less than 3 relaxation lengths, so the analytical method should underestimate the dose rate outside the steel door. This offers an explanation for the discrepancy in the two results. Transmission factors for steel would be a better alternative to analytical shielding calculations with thin shields. Transmission factors for ~30 cm give results comparable to the measured results obtained from this experiment.[40] However, the thickness of the door for the new medical room will be much greater than 3 relaxation lengths.

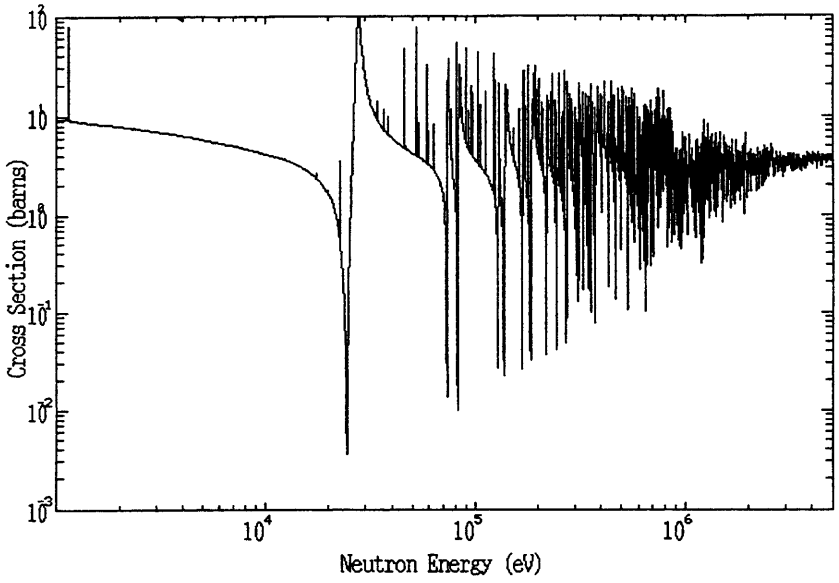

Figure 6.7 Neutron scattering cross sections for iron.

[39] Jaeger, Engineering Compendium on Radiation Shielding, Vol. II, 9.1.12.26, p.177.
[40] Jiang, S., Sheu, R., A Practical Neutron Shielding Code, Appendix A, Health Physics Vol. 73, No.6, 1997.

6.6 CONCLUSIONS

Further analysis of the beam characteristics in the current medical room is needed before determining whether or not the analytical methods are valid. Discrepancies in the dose rates obtained from both methods were narrowed down to one possible source of error. In the current room the beam seems to display more than a geometric attenuation at locations far from the beam. If this can be verified, then the study would confirm that the analytical method used to calculate the shielding is valid. Additionally, it is important to obtain more information on the energy spectrum of fast neutrons in the M67 beam. This information may effect the decision in what material choices to use for the new medical room door.

6.7 REFERENCES

Campos, T., Personal communication.

Jaeger, R.G, "Shielding Fundamentals and Methods", *Engineering Compendium on Radiation Shielding*, Vol. I, Springer-Verlag, New York Inc, 1968.

Jaeger, R.G, "Shielding Materials", *Engineering Compendium on Radiation Shielding*, Vol.II, Springer-Verlag, New York Inc, 1975.

Jiang, S.H., Sheu, R.J., "A Practical Neutron Shielding Code", *Health Physics*, Vol. 73, No. 6, 1997.

Kiger, W.S, *Neutronic Design of a Fission Converter-Based Epithermal Beam for Neutron Capture Therapy,* Nucl. E. Thesis, Massachusetts Institute of Technology, 1996.

McWilliams, F., Personal comunication.

CHAPTER 7

PATIENT POSITIONING SYSTEM

7.1 INTRODUCTION

The fission converter BNCT facility will have a horizontal beam port, unlike the current facility which utilizes a vertical port. This will require some modifications to the current treatment planning process, particularly patient positioning. A system for positioning the patient in the proper beam orientation is needed for the new facility. This system must allow positioning so that the horizontal beam may treat all types of cancer. Optimally, a method for determining where, in 3D space, the patient's head corresponds to the prescribed treatment plan would be incorporated into the positioning system. This will be crucial when the irradiation times are shortened to a few minutes. At shorter irradiation times, correct prediction of patient orientation will be a key factor in effective treatment as well as allowing for a larger number of irradiations in a given time period.

7.2 SPECIFICATIONS

7.2.1 Movement

Several criteria were important in analyzing what type of positioning system would be best suited for the new facility. One of these is movement. It is important that the positioning system be versatile to allow for the treatment of a cancer at any location of the body. The following degrees of freedom are necessary to ensure that all types of cancers

may be treated:

- 2 horizontal movements,
- 2 vertical movements,
- translational movement,
- rotational movement.

7.2.2 Size

Another important factor in deciding upon a positioning system is the size of the system. The system needs to accommodate most patients. This requires the positioning system to be large enough to hold a person 6'2" tall. It must also have a 500 pound weight capacity. This leads to an additional factor to consider, mass of the system.

7.2.3 Material

The mass of the system must be reasonable to allow for manual movement by medical staff and personnel. Therefore the positioning system should be made out of a lightweight material. However, the positioning system must still be durable enough to meet the weight requirements mentioned above. Additionally, a non-activating material is essential to minimize dose to the medical and reactor personnel who handle the positioning system after irradiations.

7.2.4 Control

A sophisticated computerized control system for positioning is not necessary at this time. Instead, a more simple manually operated system will be used. This system

will consist of hydraulics and mechanical levers for manual operation and adjustment of the patient position.

7.3 MODIFICATIONS TO MEDICAL ROOM FOR POSITIONING

In section 2.3, possible medical room designs were presented. Both of these designs impose severe limitations on the positioning of a patient in all possible beam configurations. The width of the inner dimensions of the medical room only allow for a 5'6" patient to be treated in the stretched-out supine position, perpendicular to the beam, as shown in the figure below. While it may be possible to simply arrange the patient in a different configuration, limiting the positioning range within the room is undesirable.

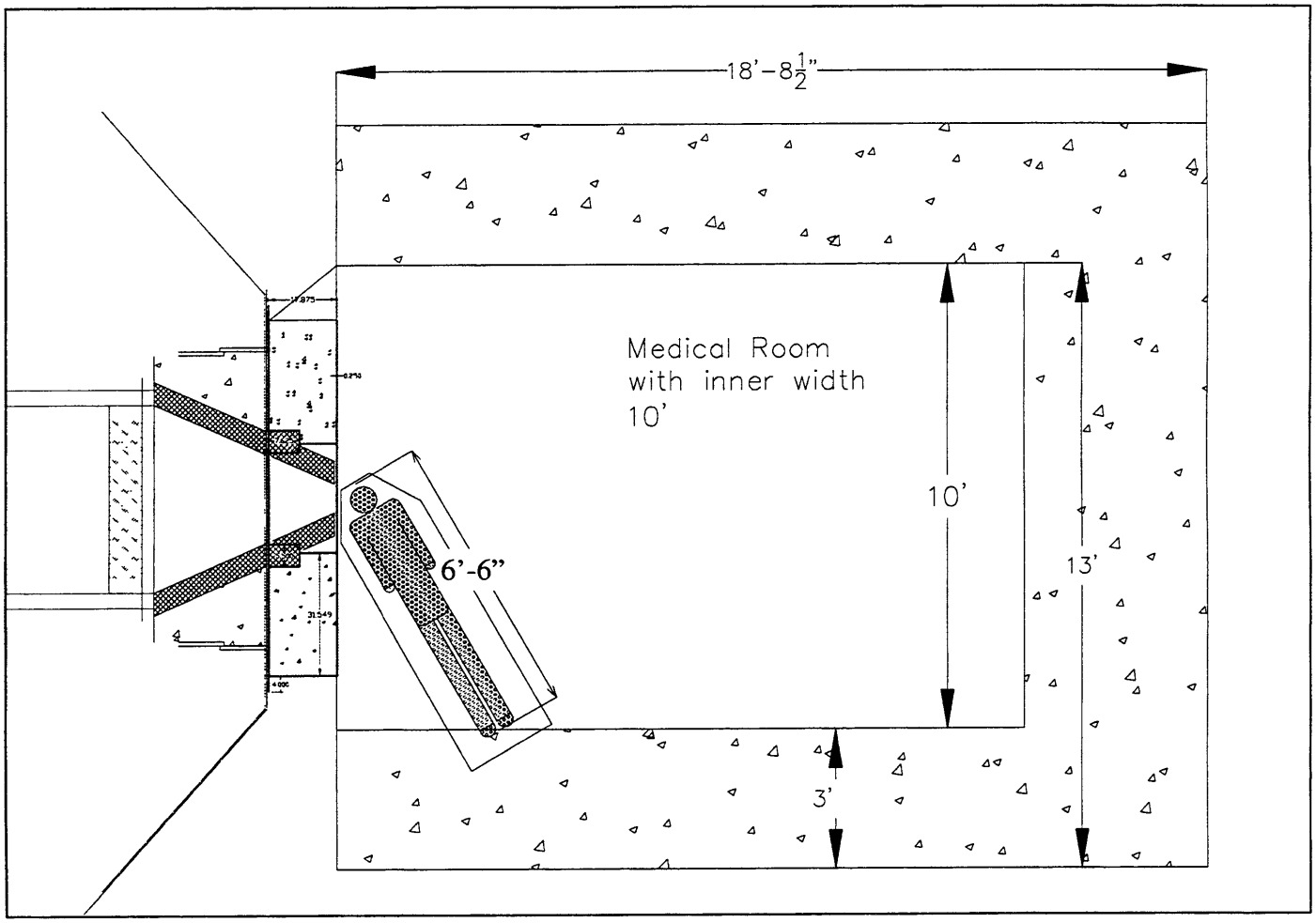

Figure 7.1 Medical room with dimensions as specified in Safety Evaluation Report. A patient over 5 feet could not fit into the room without contorting.

Additionally, the beam height is only 3 feet high. This greatly impacts the flexibility of positioning a patient in all directions. This beam height eliminates the use of only one positioning system because the same system cannot be used to treat patients oriented in a supine position and a seated positions. This is demonstrated in the following figure.

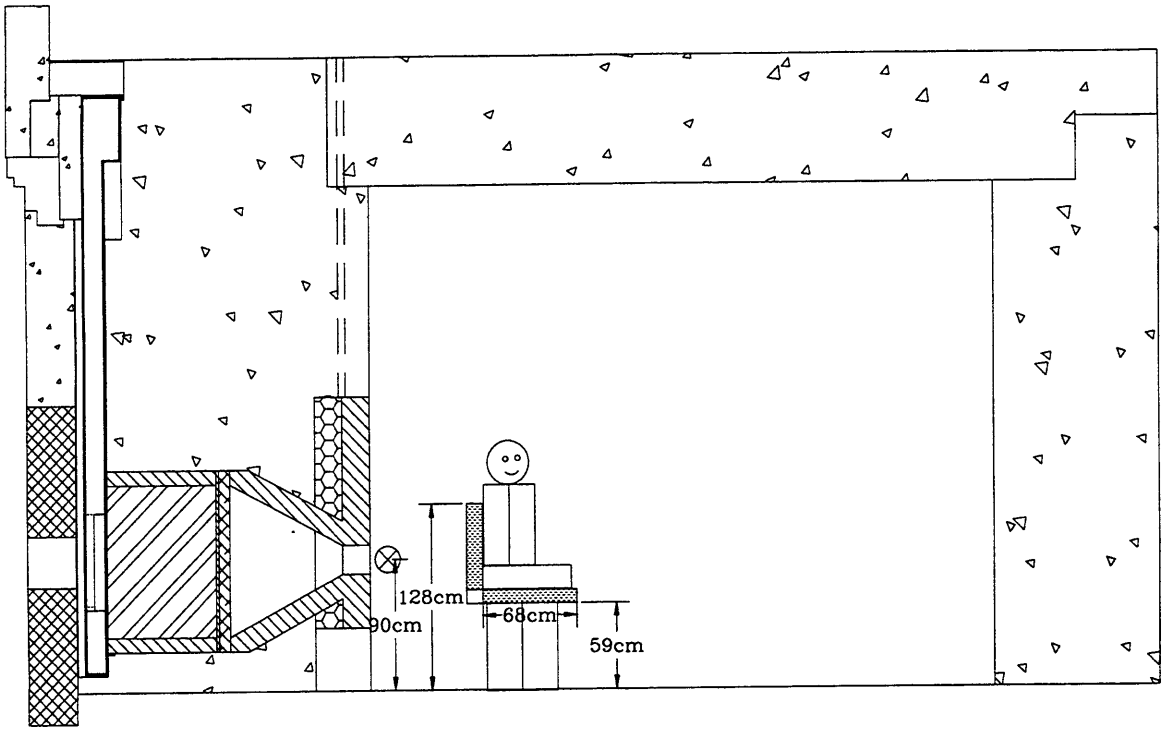

Figure 7.2 Drawing showing a 6-foot patient in a seated position.

After viewing several positioning systems that could transform from a bed into a chair position, it was noticed that the minimum height these systems could obtain was about two feet. With a beam height of three feet, using one positioning system for treating patients in a supine and a chair configuration is not possible, as demonstrated in the figure below.

To remedy the problems mentioned above, the medical room and beam designs were modified. The medical room was expanded to a width of 13' to allow for a 6'6" patient to fit comfortably in the supine position, perpendicular to the beam. This imposed some problems with interference between the medical room and structures in the reactor. These interference will be discussed in chapter 8. Additionally, the beam height was

modified to allow greater flexibility in positioning. The beam was raised 6" to a height 3'6".

7.4 RANGE OF MOTIONS FOR POSITIONING SYSTEMS

As a test to determine what motions were necessary for a horizontal beam a mock-up of the medical room was used. The mock up modeled the inner dimensions of the room and beam. Several different positioning setups were evaluated to determine what range of motion will be needed in the new facility. For the different positioning systems a standard chair, a lounger, an upright chair back, and a typical operating table were evaluated. Each system had its advantages, however for a head irradiation the simplest position was a reclined or seated position. This position can be achieved using a simple lounge chair or an operating table. The reclining position resembles the seated chair position, but it allows for a single positioning system to be used.

7.5 SUGGESTIONS

Ideally, multiple positioning systems should be used to achieve the different types of motion desired for the treatments. However, most of the positioning needs can be achieved by the used of a typical operating table, which has all the required range of motions. The only drawback is that with a horizontal beam an operating table cannot be used in a seated position due to the height limitations. Overall, the best option for a positioning system is a typical operating table and a chair resembling a beach chair for irradiations of the head in the seated position.

7.6 REFERENCES

Flanz, J., Gall, K., Goitein, M. Rosenthal, S., "Design of a Highly Accurate Patient Positioning System for NPTC", *PTCOG XXV and Hadrontherapy Symposium,* 1997.

Rosenthal, S., Personal communication.

Yam, S., *Design of Patient Positioning System, Body Phantom, and Patient Shielding for the Boron Neutron Capture Therapy Project at MITRII*, S.M. thesis, Massachusetts Institute of Technology, 1993.

CHAPTER 8

ENGINEERING DESIGN OF MEDICAL ROOM SHIELDING

8.1 INTRODUCTION

A layout for the medical room was chosen to best accommodate the shielding requirements described in the preceding chapters and to fit in the available space on the reactor floor. The layout needed to allow space for the medical room door and provide adequate passage for both the medical room doorway and the space between the medical room and containment building. Another important factor in the design of the medical room layout was the available space inside the room for patient positioning. Ideally the room should accommodate a wide range of patients. A patient height of 6'6" was chosen as the height for the design. Additionally, the layout must provide space for the window, ventilation and electrical ducts, as well as adequate space outside the room for the control panel and medical preparation area. After analyzing many different designs an optimal layout of the room was found, as shown in the figure below.

After a layout for the room was chosen, the actual blocks needed to construct the medical room were designed. The design incorporated the use of existing shield blocks, new shield blocks, a window, a door, a ceiling, and ducts for a ventilation system.

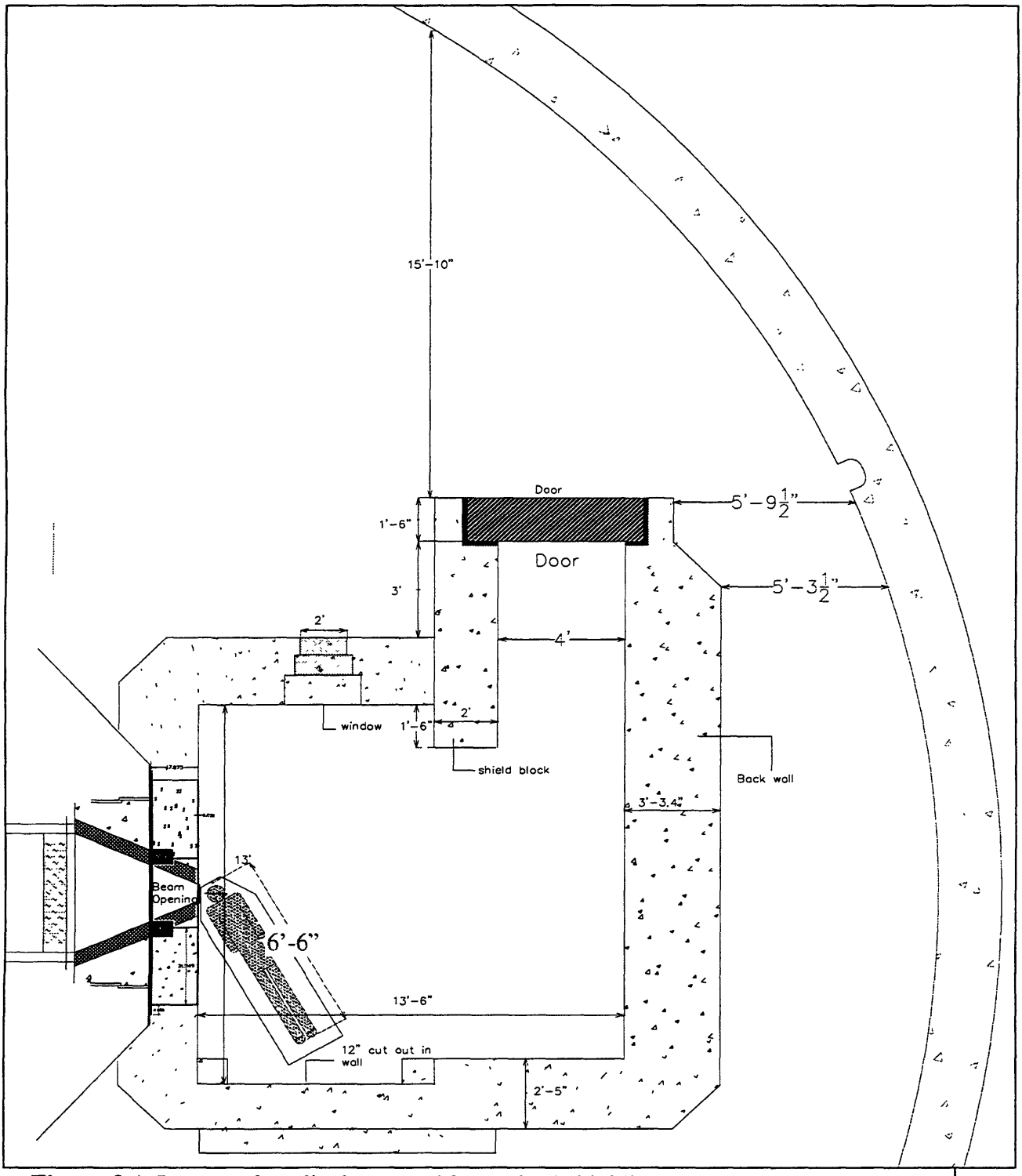

Figure 8.1 Layout of medical room with required shielding.

8.2 PROPERTIES OF EXISTING SHIELD BLOCKS

The area where the medical room will be located is currently occupied the Hohlraum, that is composed of high density concrete blocks. Ideally, these blocks should be incorporated into the shielding design of the new medical room to reduce waste and cost.

In considering the type of material to use for shielding, the following factors were analyzed: cost, gamma and neutron shielding properties, ease of use, and bulk. A surplus of high density concrete blocks is currently available after the dismantling of the Hohlraum. Specifically, the high density concrete in the Hohlraum is Swedish Ore I-2a concrete. If well suited for shielding, the reuse of these concrete blocks for the medical room would prove to be very cost effective.

8.2.1 Verification of Concrete Type

Further analysis was necessary to measure the shielding capabilities of these blocks. First, the density of the concrete was measured to verify the type. The type of concrete used for the blocks is presumably Ilmenite Swedish I-2a concrete. As a confirmation of concrete type core samples were drilled from three separate concrete blocks. Samples were taken from blocks SO-4, NO-1, and SI-2. The density of the concrete was measured by weighing the samples and measuring the volume of water each sample displaced. The density of the concrete was determined to be 3.94 ± 0.01 g/cm^3, which is larger than the reported 3.76 g/cm^3 density of I-2a concrete. The elemental composition of I-2a concrete is listed in the table 8.

Table 8.1 Elemental composition of I-2a concrete.

Element	grams of element/cm3 concrete
H	0.0219
O	1.34
Mg	0.021
Al	0.0218
Si	0.0560
Ca	0.234
Ti	0.959
Mn	0.0302
Fe	1.064
total	3.76

8.2.2 Shielding Properties of Existing Concrete

After verification of the concrete type, transmission curves were generated with the use of MCNP to determine the attenuation properties of the concrete. This entailed calculating neutron and photon fluence at various depths in a 100 cm slab of I-2a concrete using a monoenergetic neutron point source. Three runs were performed with a neutron source ranging in energies of 10 Kev, 0.4 Mev, and 1 Mev. The results from this study are displayed in the graphs below. The study revealed that I-2a concrete is excellent to shield the fission converter BNCT facility.

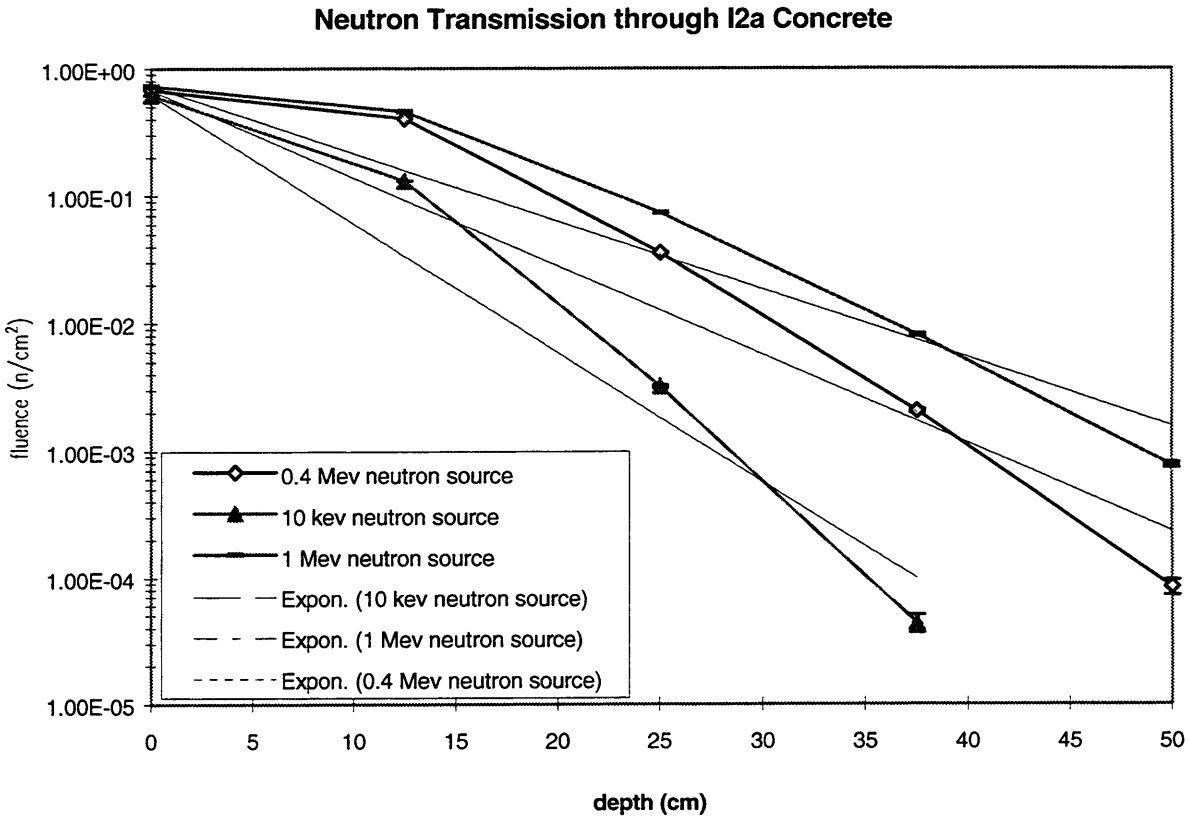

Figure 8.2 MCNP results of neutron transmission through I-2a concrete.

Using the data presented in figure 8.2 and equation 5.1, removal cross sections were derived for I-2a concrete. This included cross sections for epithermal neutrons, with energy of 10 kev, for fast neutrons, with an energy of 0.4 Mev (the average energy found in fission converter[41]), and for fast neutrons with an energy of 1 Mev (the energy used in the analytical shielding calculations). These values are 0.255 cm^{-1} for 10 kev neutrons, 0.18 cm^{-1} for 0.4 Mev neutrons, and 0.137 cm^{-1} for 1 Mev neutrons . The removal cross sections reveal that this type of concrete is an excellent neutron shield.

[41] Average energy of fast neutrons comes from W.S. Kiger's thesis, Table 5.20.

A further look at the elemental neutrons cross sections of I-2a concrete reiterates this concrete's suitability for shielding this particular facility. Below are graphs showing the individual elemental cross sections for a broad range of neutron energies. Each cross section is weighted by the element's weight fraction in the concrete. Note the significant resonances in the epithermal range. These resonances are important in that they help to quickly attenuate the large flux of epithermal neutrons that comprise the majority of the beam. This is helpful in reducing the capture gamma dose component. The total cross section in the fast neutron range, while smaller than at lower energies, is still significantly larger than ordinary concrete and better than the cross section for water.

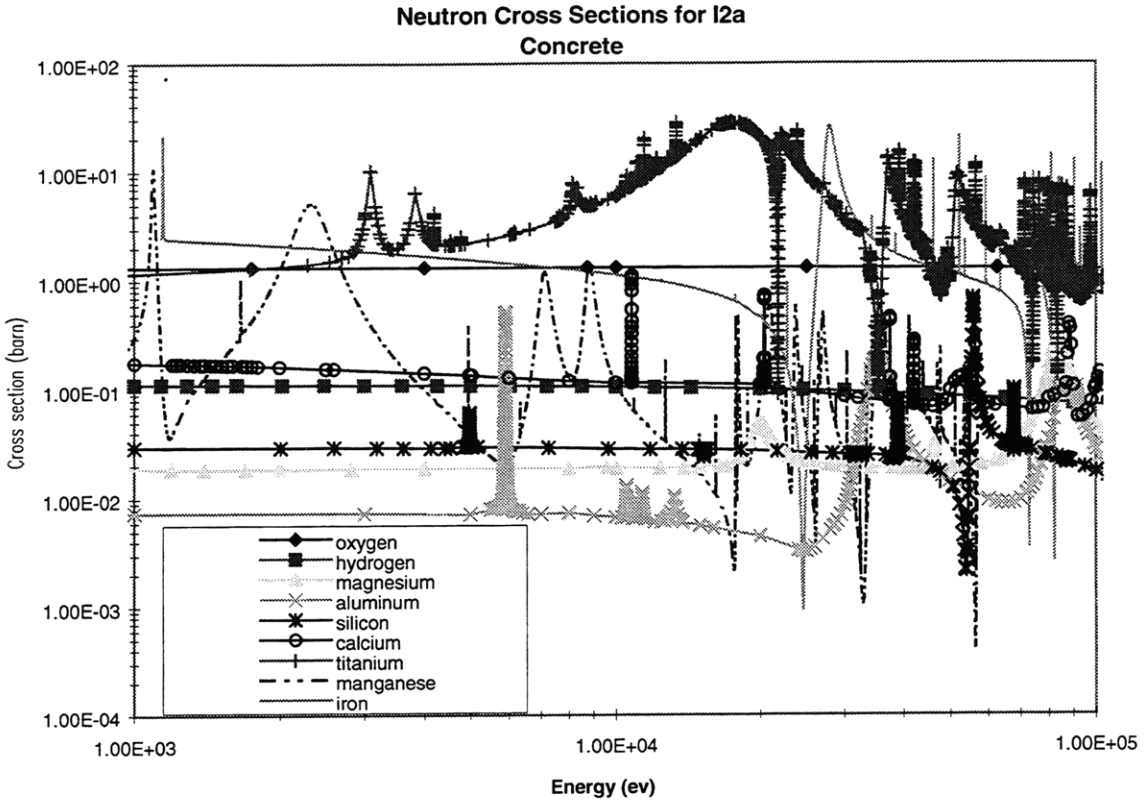

Figure 8.3 Weighted elemental neutron cross section for I-2a concrete, epithermal range.

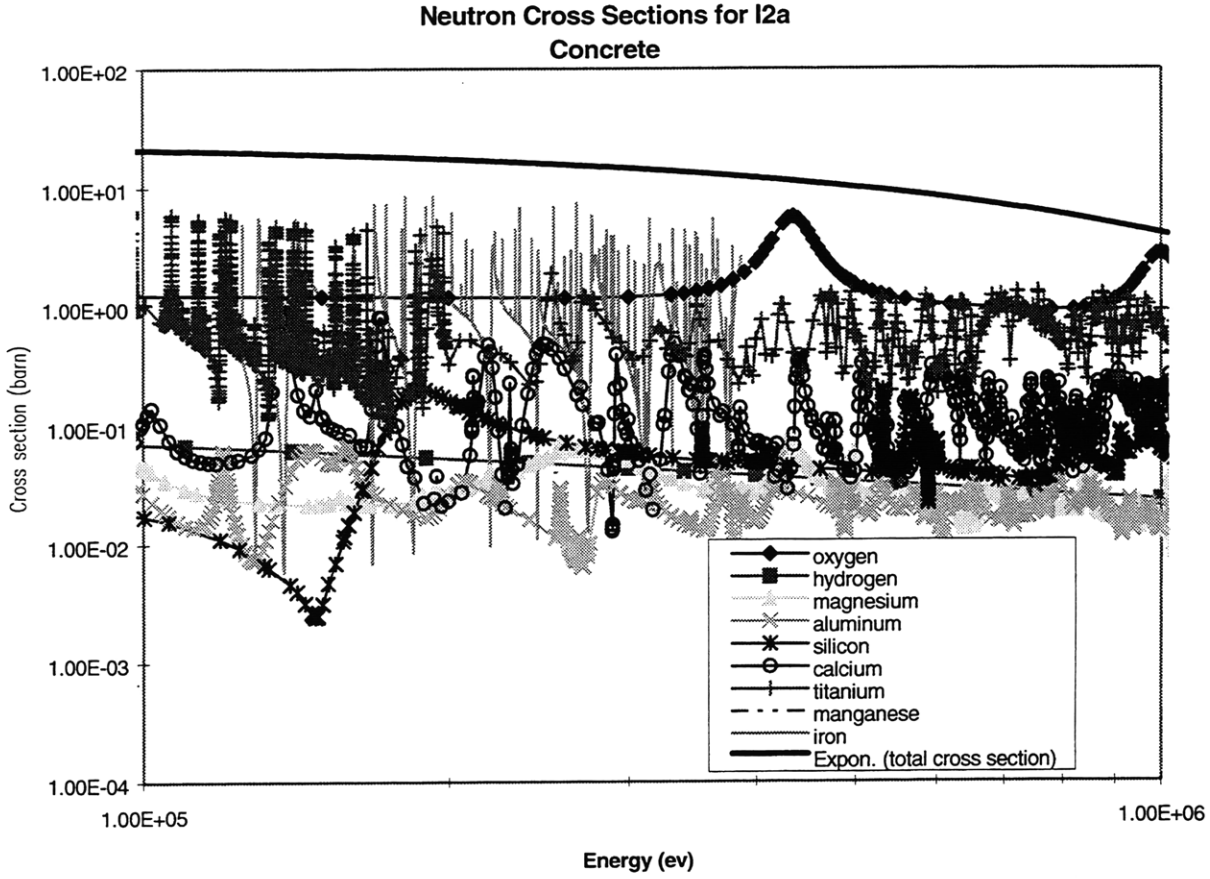

Figure 8.4 Weighted elemental neutron cross sections for I-2a concrete, fast neutron range.

In addition to information about the neutron shielding properties of I-2a concrete, information about the production of capture gammas from neutron capture by elements in I-2a concrete was obtained. The following graph shows the gamma fluence at various depths in the concrete. Since the source used in the MCNP model was a neutron source only, the fluence of gammas comes from capture gammas produced in the concrete. The average energy of the capture gammas was 1.1 Mev. Figure 8.3, shows that most of the capture gamma production occurs in the first 15 cm of the concrete, many are

produced when the neutrons first hit the concrete. This means most of the capture gamma production occurring at the inner surface of the wall can be eliminated by using a neutron absorbing paint on the inner wall surface. To prevent capture gamma production at depths of 10 -20 cm in the concrete wall, ^{10}B or ^{6}Li would need to be added in the concrete walls at those depths.

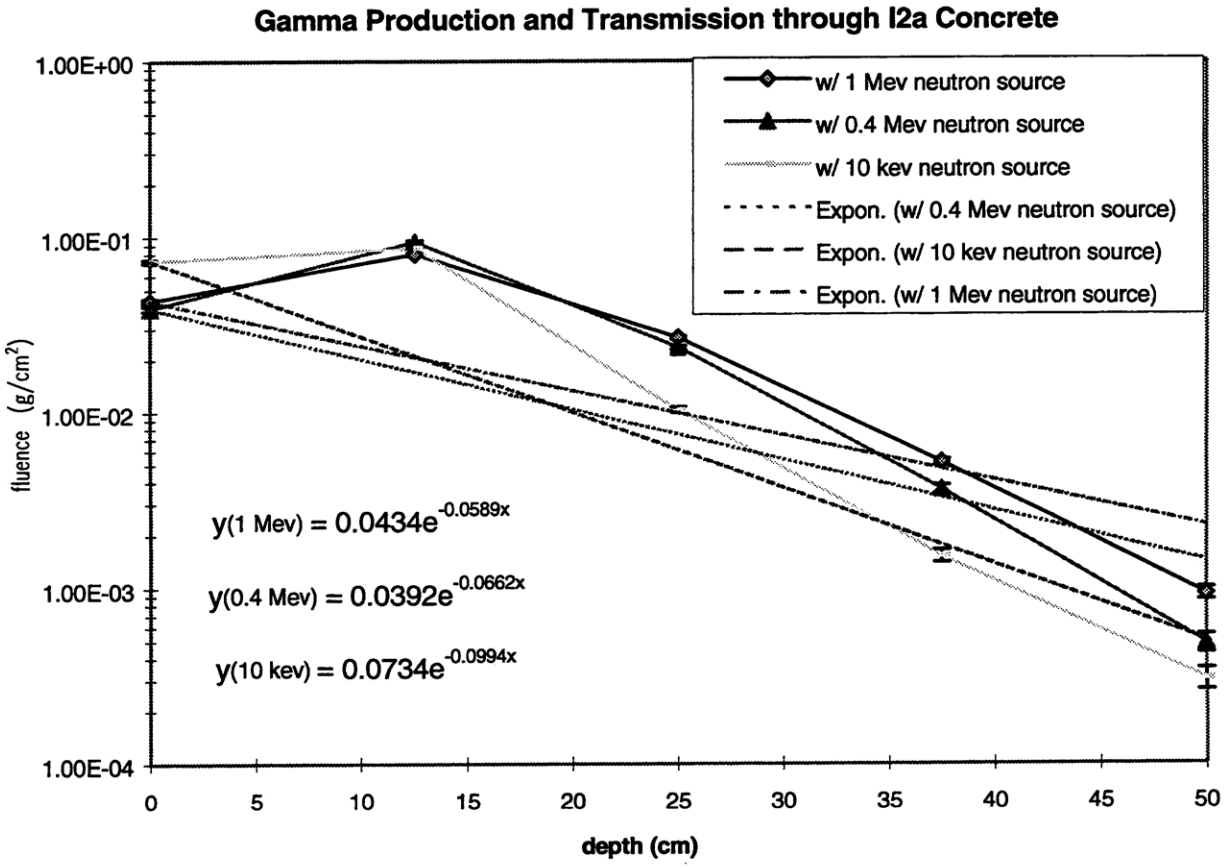

Figure 8.5 MCNP results of capture gamma production and transmission through I-2a concrete.

8.2.3 Physical Properties of Existing Concrete Blocks

The following table lists existing blocks with their dimensions and weight.

Table 8.2 Properties of existing concrete blocks.

Block	Thickness	Height	Length	Volume (cm^3)	Weight with holes filled (tons)	Weight after corners removed* (tons)
NO-1	21"	8"	14'-1.5"	4.67E+05	2.03	1.78
NO-2	21"	7'-4"	14'-1.5"	5.13E+06	22.38	19.61
NO-3	21"	7'-4"	14'-1.5"	5.13E+06	22.38	19.61
NI-1	21"	7'-4"	7'-11"	2.88E+06	12.54	
NI-2	21"	7'-4"	10'-7.5"	3.86E+06	16.83	15.45
NI-4	21"	7'-4"	21.25"	6.44E+05	2.81	1.42
SO-1	21"	8"	14'-1.5"	4.67E+05	2.03	1.78
SO-2	21"	7'-4"	14'-1.5"	5.13E+06	22.38	19.61
SO-3	21"	7'-4"	14'-1.5"	5.13E+06	22.38	19.61
SI-1	21"	7'-4"	7'-11"	2.88E+06	12.54	
SI-2	21"	7'-4"	10'-7.5"	3.86E+06	16.83	15.45
SI-4	21"	7'-4"	21.25"	6.44E+05	2.81	1.42
WO-1	21"	6'-5"	3'-0.5"	9.67E+05	4.22	
WO-2	21"	6'-5"	3'-0.5"	9.67E+05	4.22	
WO-3	21"	10"	12'-6"	5.20E+05	2.27	
WO-4	21"	7'-4"	12'-6"	4.58E+06	19.96	
WI-1	21"	6'-6"	2'-11.5"	9.53E+05	4.15	
WI-2	21"	6'-6"	2'-11.5"	9.53E+05	4.15	
WI-3	21"	19"	12'-6"	9.89E+05	4.31	
WI-4	21"	7'-4"	12'-6"	4.58E+06	19.96	
FO-1	36"	9'-6"	4'	3.23E+06	14.07	
FO-2	24"	9'-6"	6'	3.23E+06	14.07	
FO-3	36"	9'-6"	4'	3.23E+06	14.07	
FI-2	24"	9'-6"	6'	3.23E+06	14.07	
T-1	24"	NA	NA			
T-2	24"	NA	NA			
T-3	24"	NA	NA			
T-4	24"	NA	NA			
T-5	24"	NA	NA			
T-6	24"	NA	NA			
T-7	24"	NA	NA			

* Some existing blocks have 45 degree angled corners, making them trapezoidal rather than rectangular. This weight does not include the cuts made to the existing blocks for final shaping, as described in section 8.4.5.

The following pictures are drawings of the actual blocks, showing dimensions of the blocks and other details, such as holes. Not all the existing blocks are shown here. The drawings only include the blocks that will be incorporated into the new medical room.

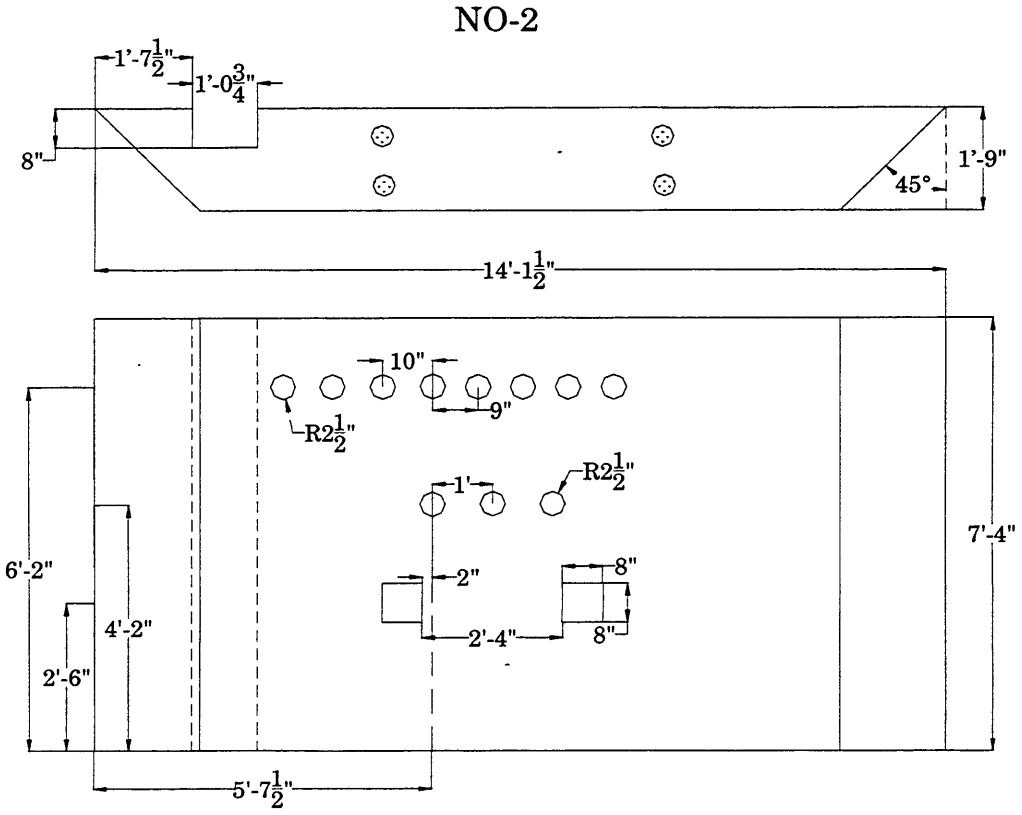

Figure 8.6 Block NO-2 will make up part of the right wall and left wall.

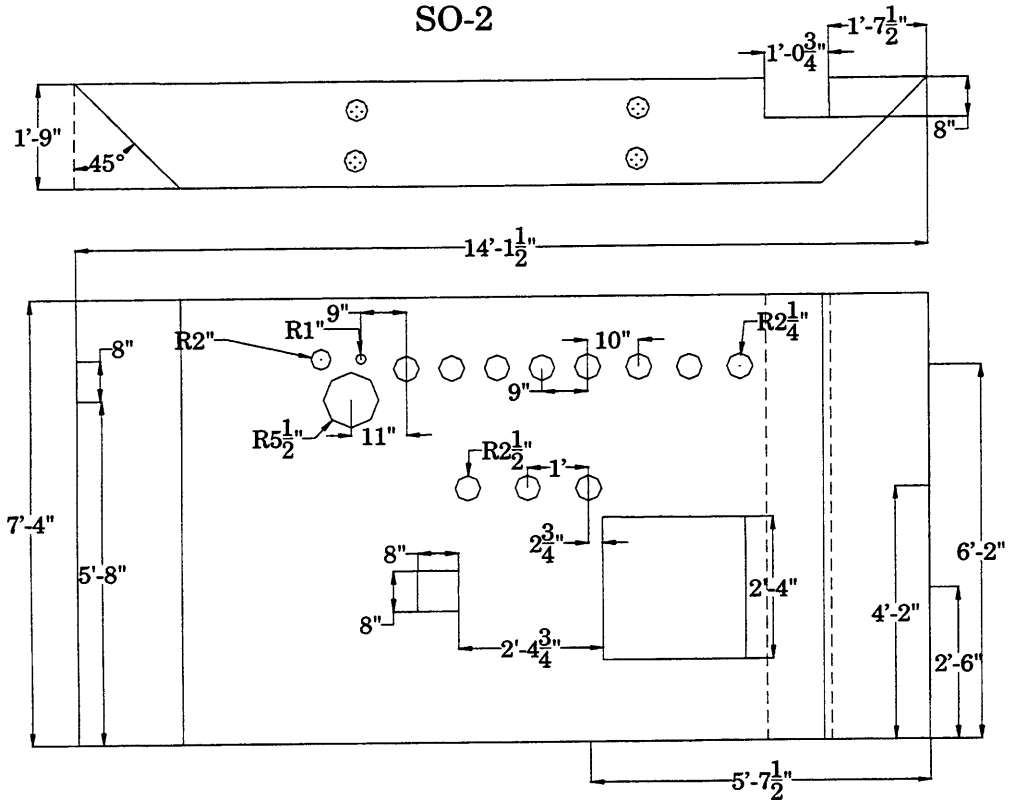

Figure 8.7 SO-2 will be cut and placed at the outer perimeter of the left wall.

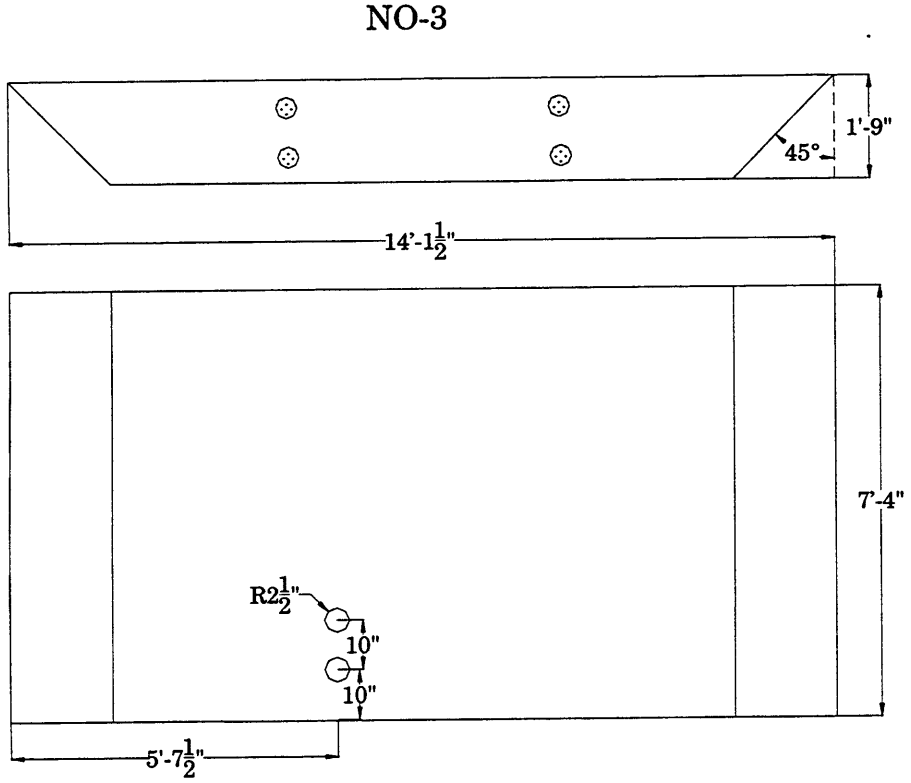

Figure 8.8 NO-3 will comprise part of the right wall.

SO-3

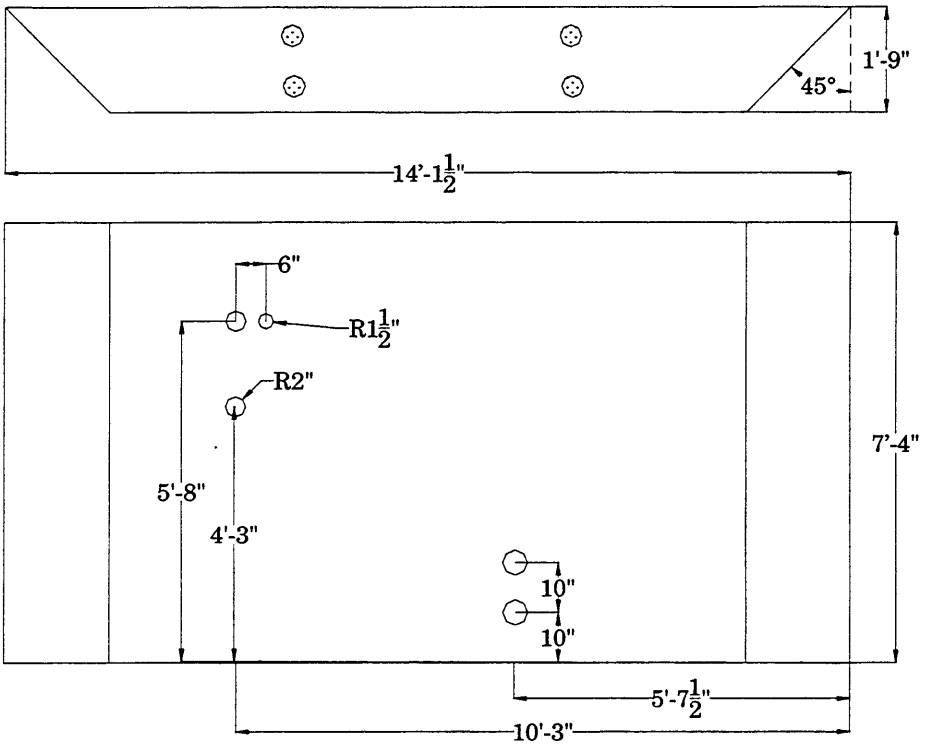

Figure 8.10 Block SO-3 will be used to shield the ceiling.

NI-1

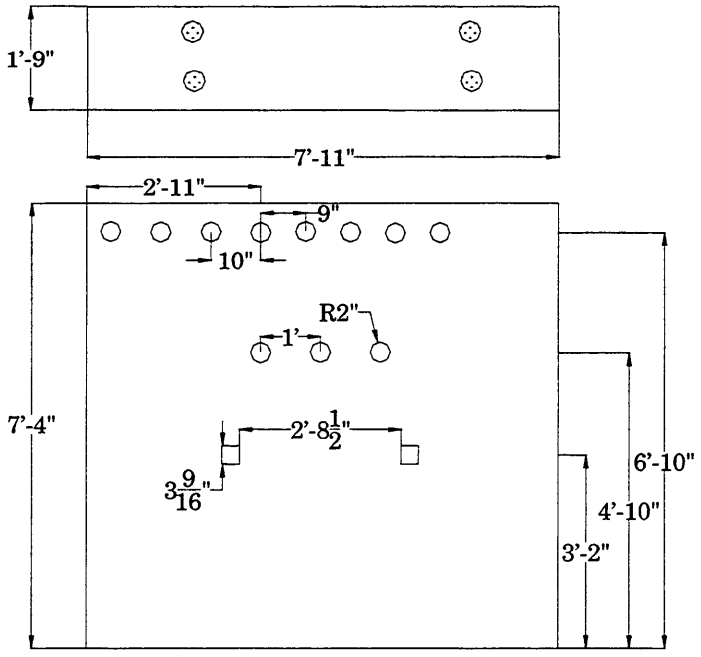

Figure 8.9 NI-1 will be used for the inner portion of the wall.

SI-1

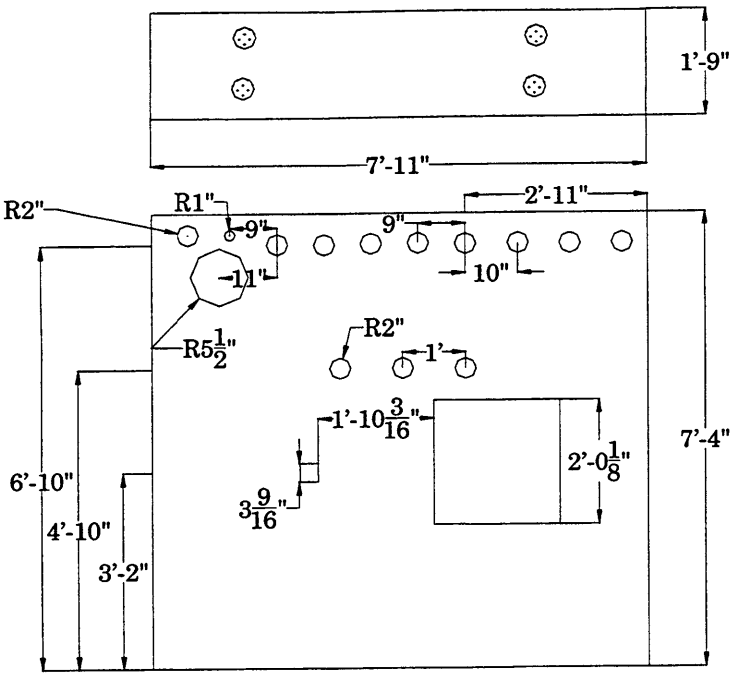

Figure 8.11 SI-1 will be used for the doorway.

NI-2

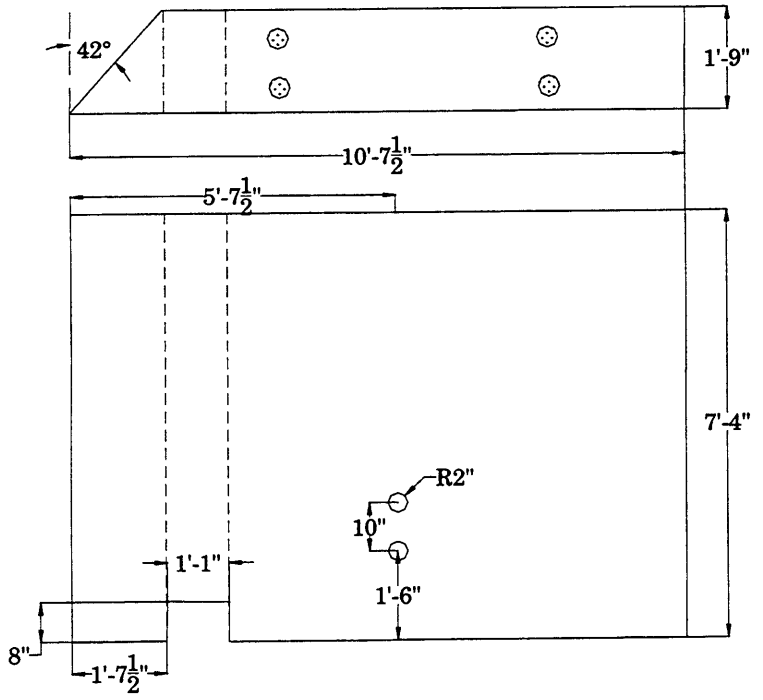

Figure 8.12 NI-2 will make up an inner part of the back wall and the doorway.

Figure 8.14 NI-4 will sit between the reactor face and medical room

Figure 8.13 SI-4 will also sit between the re face and medical room, on the right side.

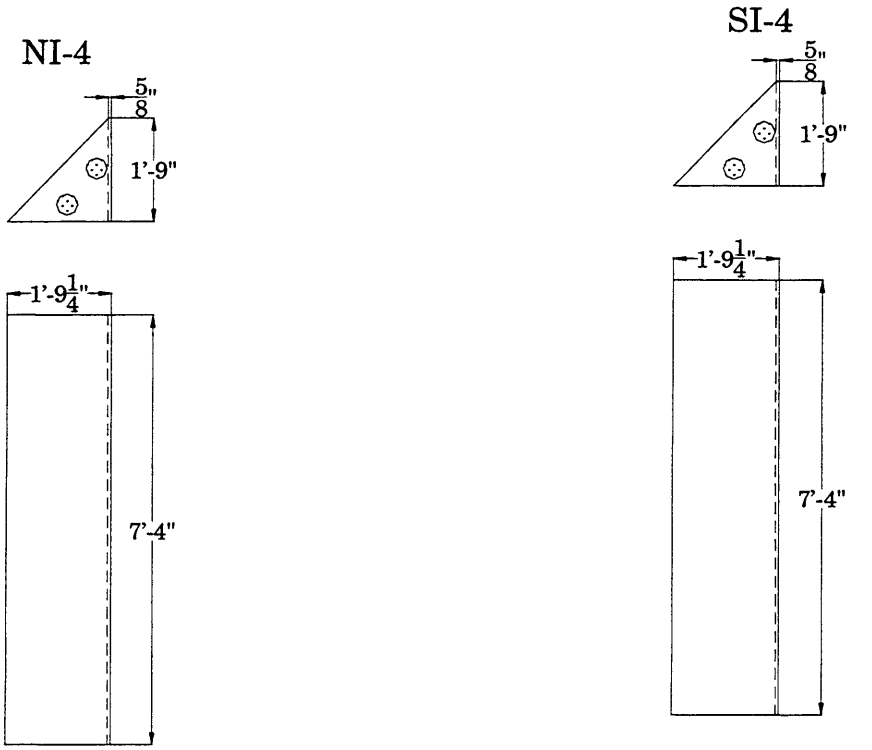

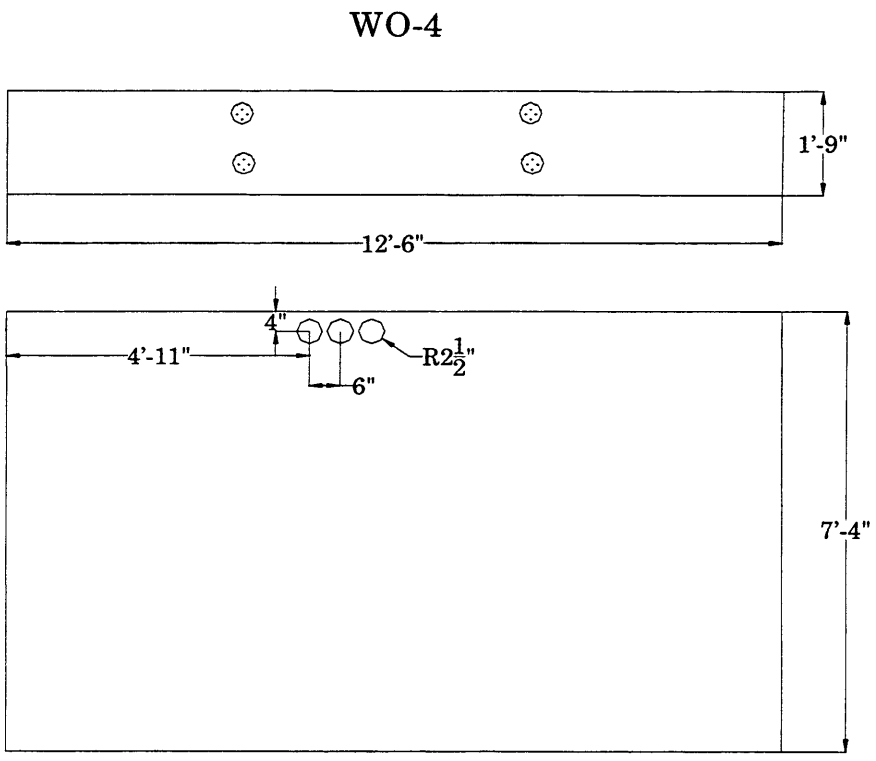

Figure 8.15 The outer portion of the back wall is made up partly by

WO-2

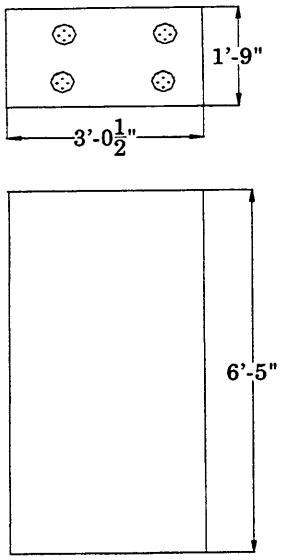

Figure8.16 WO-2 will be used for the shieldblock near the doorway.

WI-1

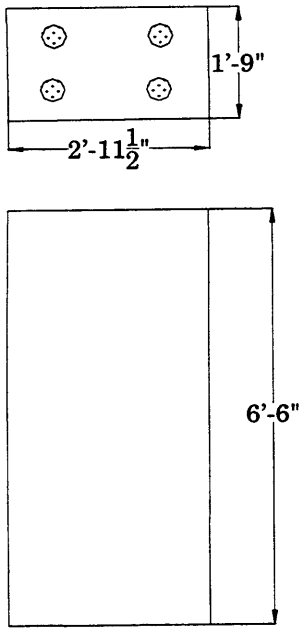

WI-2

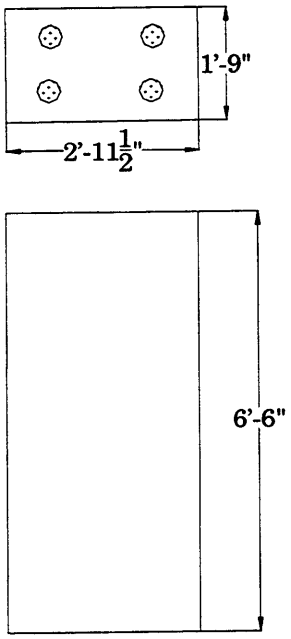

Figure 8.17 WI-1 and WI-2 will rest on either side of the shutter shield bl

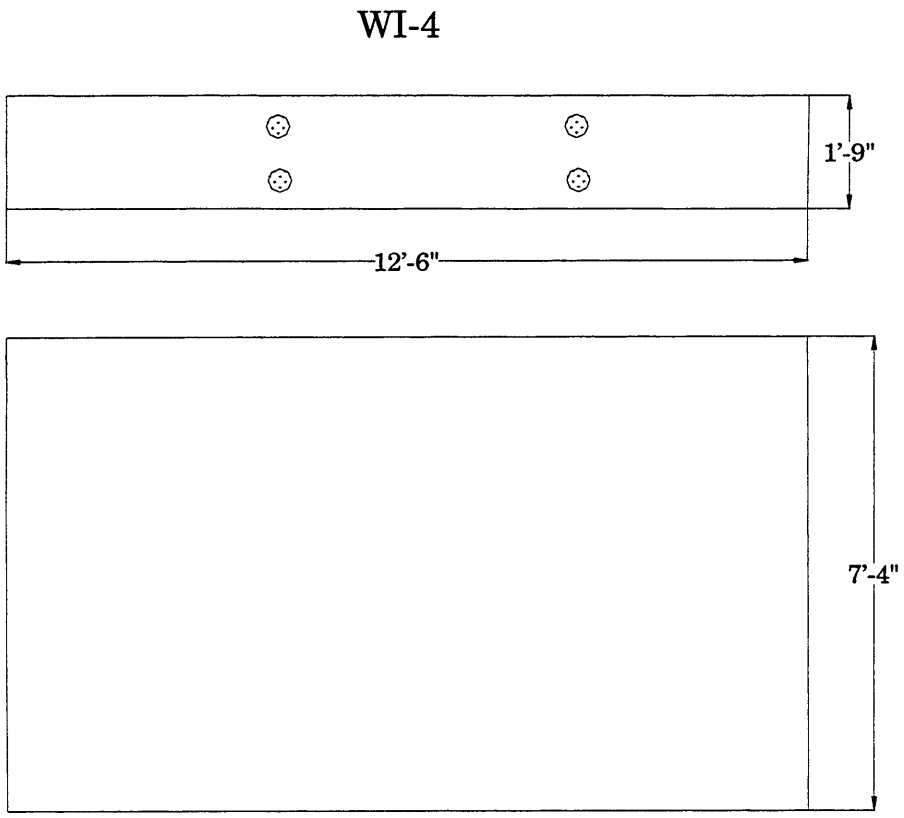

Figure 8.18 Another part of the ceiling will be shielded by WI-4.

FO-2

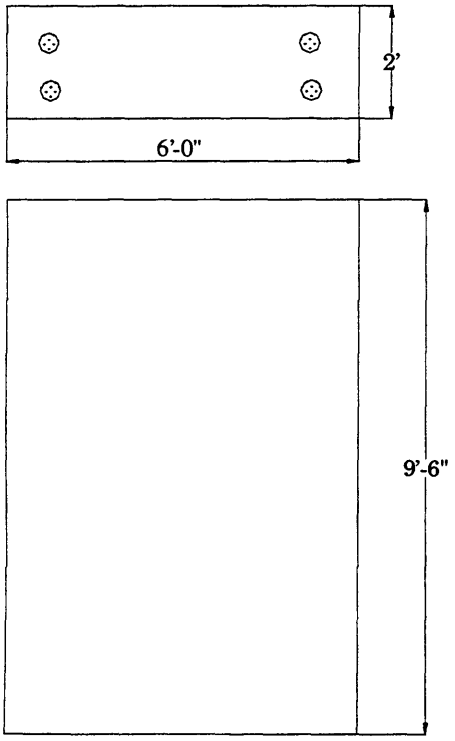

Figure 8.19 FO-2 will be flipped on its side and used for the inner right wall.

FI-2

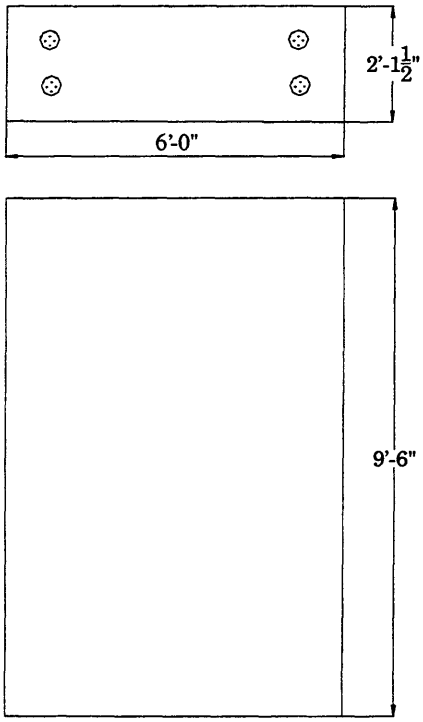

Figure 8.20 FI-2 will be used for the back wall.

8.3 INCORPORATION OF EXISTING SHIELD BLOCKS INTO MEDICAL ROOM DESIGN

After analyzing the shielding and physical properties of the existing blocks, an optimal arrangement to configure the existing blocks into the layout of the new medical room was found. The following picture shows the plan view using the existing blocks in the medical room configuration shown in figure 8.1. Dotted lines indicate cuts needed.

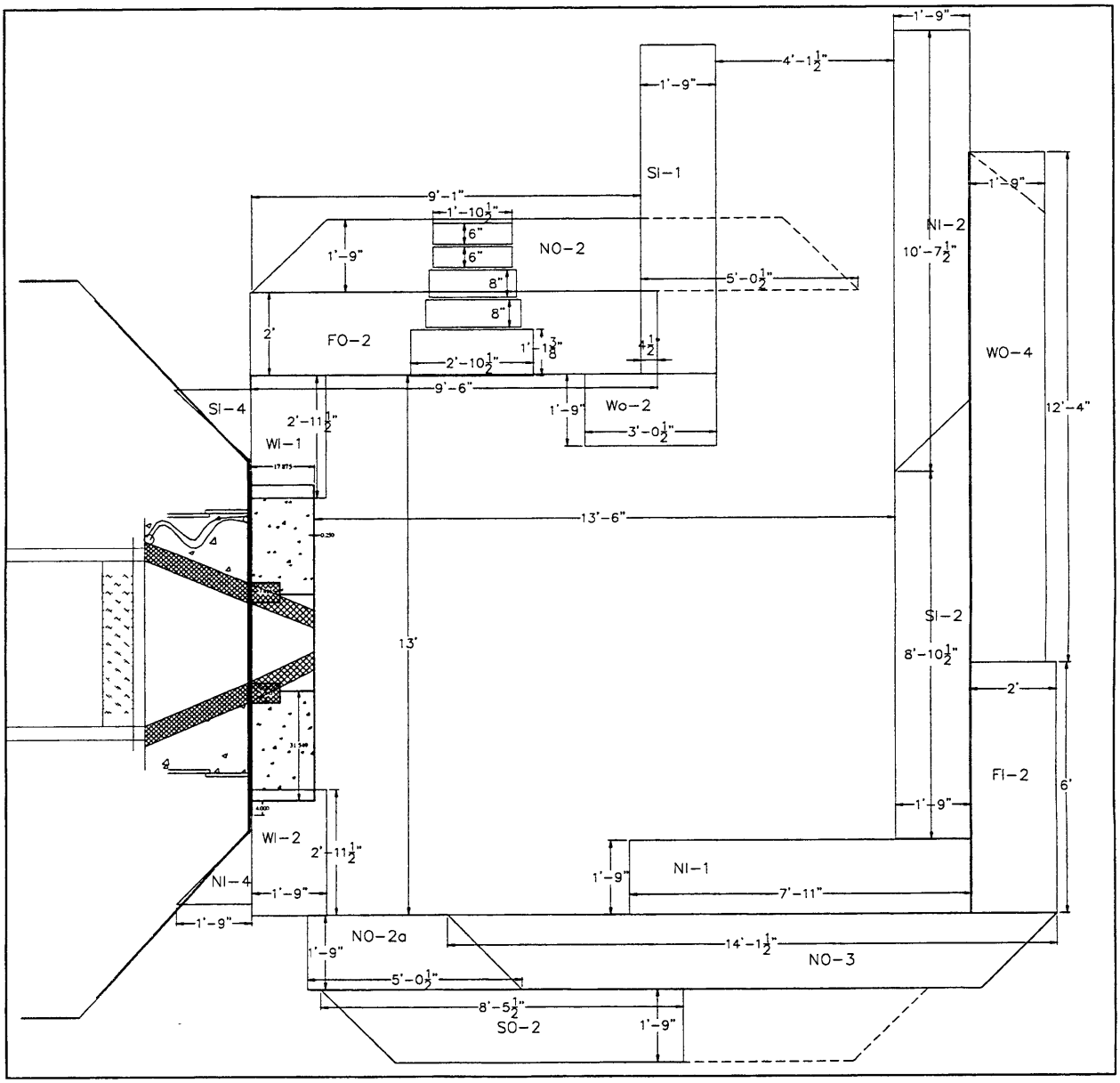

Figure 8.21 Medical room design with existing blocks.

8.4 DESIGN OF ADDITIONAL SHIELDING

8.4.1 Medical Room Ceiling

Using the existing blocks, most of the medical room walls can be made. However, the height of the existing blocks and the desired height of the medical room are different. It is desired to have a ceiling of 8.5 feet inside the new medical room. Most of the blocks are 7'-4" (see block drawings). A method of elevating the side and back walls to eliminate streaming cracks is necessary for the this design.

Besides using existing blocks for the side and back walls, two existing blocks will be used for the ceiling shield blocks. The figure below shows these two blocks in the three-dimensional space. It is not structurally feasible to use these two blocks alone for the ceiling. The weight of each block is about 20 tons, and the blocks do not contain rebars. Additionally, these two blocks are only 53 cm thick. A ceiling 73 cm thick is needed for adequate shielding. To remedy the problem, a structurally sound ceiling base will be designed. This base will contain necessary I-beams or rebars to support its weight as well as the weight of the two existing blocks and equipment placed on the medical room ceiling. In addition to providing the structural support for the ceiling, the ceiling base will also incorporate spacer blocks which will eliminate the height differential of the side and back walls. T. Campos[42], will be designing the ceiling base. Figure 8.22 shows the distance across the top of the medical room that the ceiling will span.

[42] Visiting Professor.

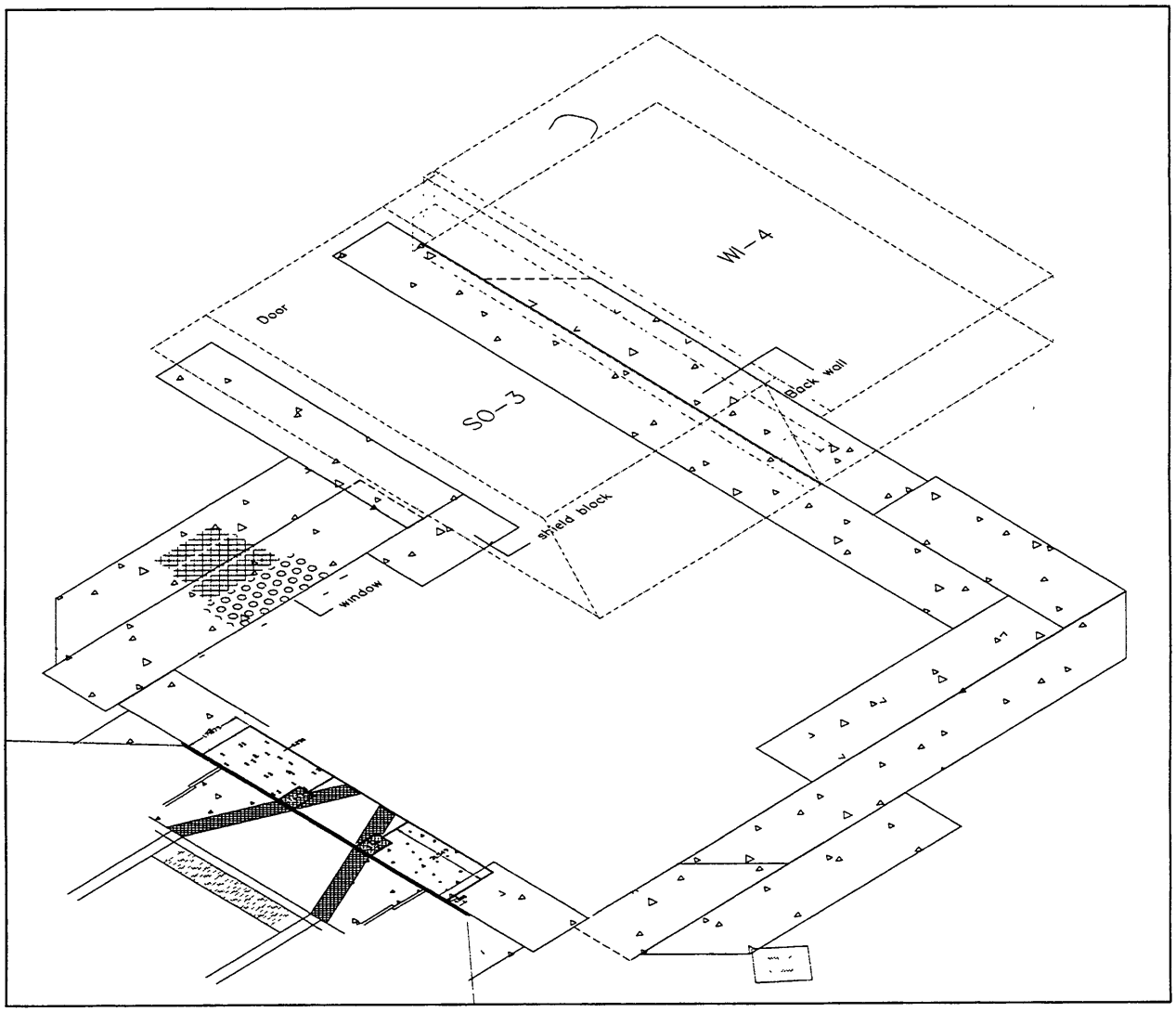

Figure 8.22 Existing blocks in ceiling position.

8.4.2 Spacer Blocks

In the following drawings, the height difference in the walls is noticeable. In the space available between the height of the existing blocks and the desired height for the ceiling base, concrete spacer blocks will be made. Some of these blocks will be candidates for housing necessary electrical conduits and ventilation ducts.

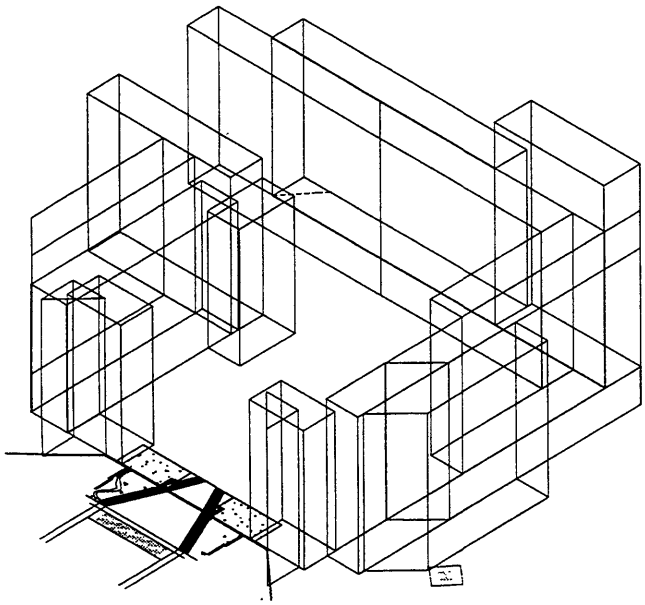

Figure 8.23 Northwest view of room, showing height difference in blocks.

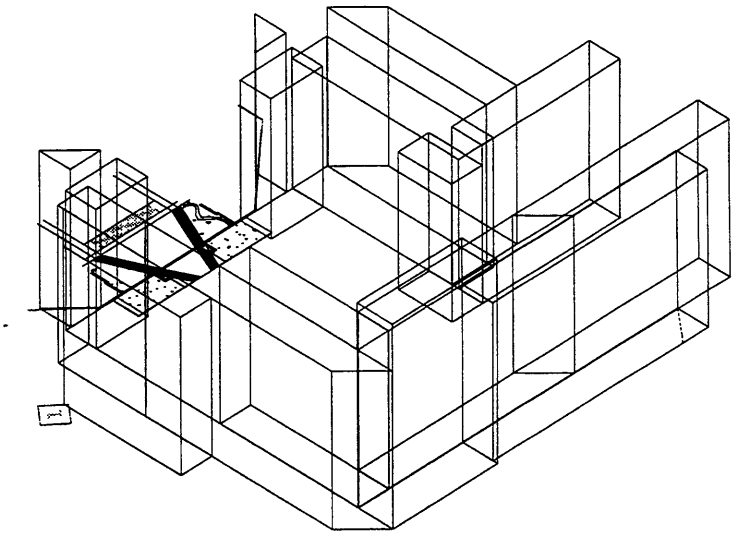

Figure 8.24 Northeast view of room.

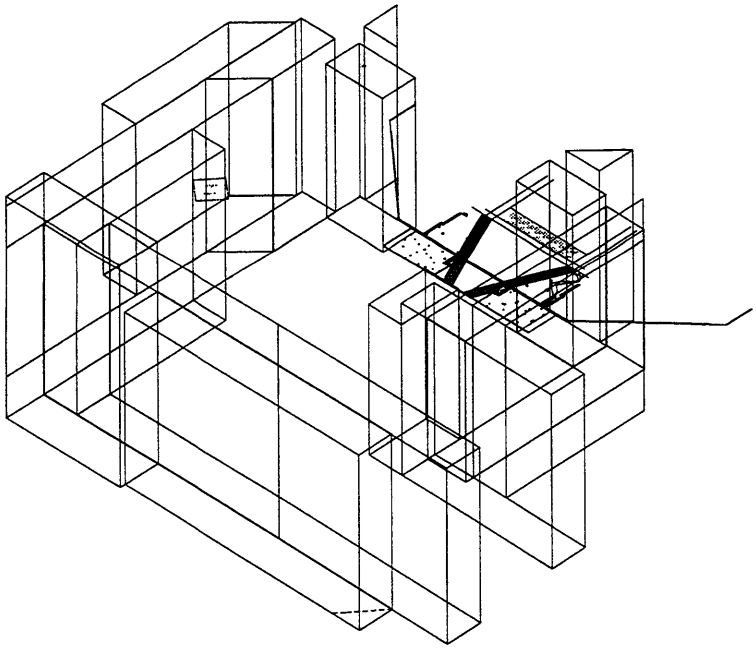

Figure 8.25 Southeast view of room.

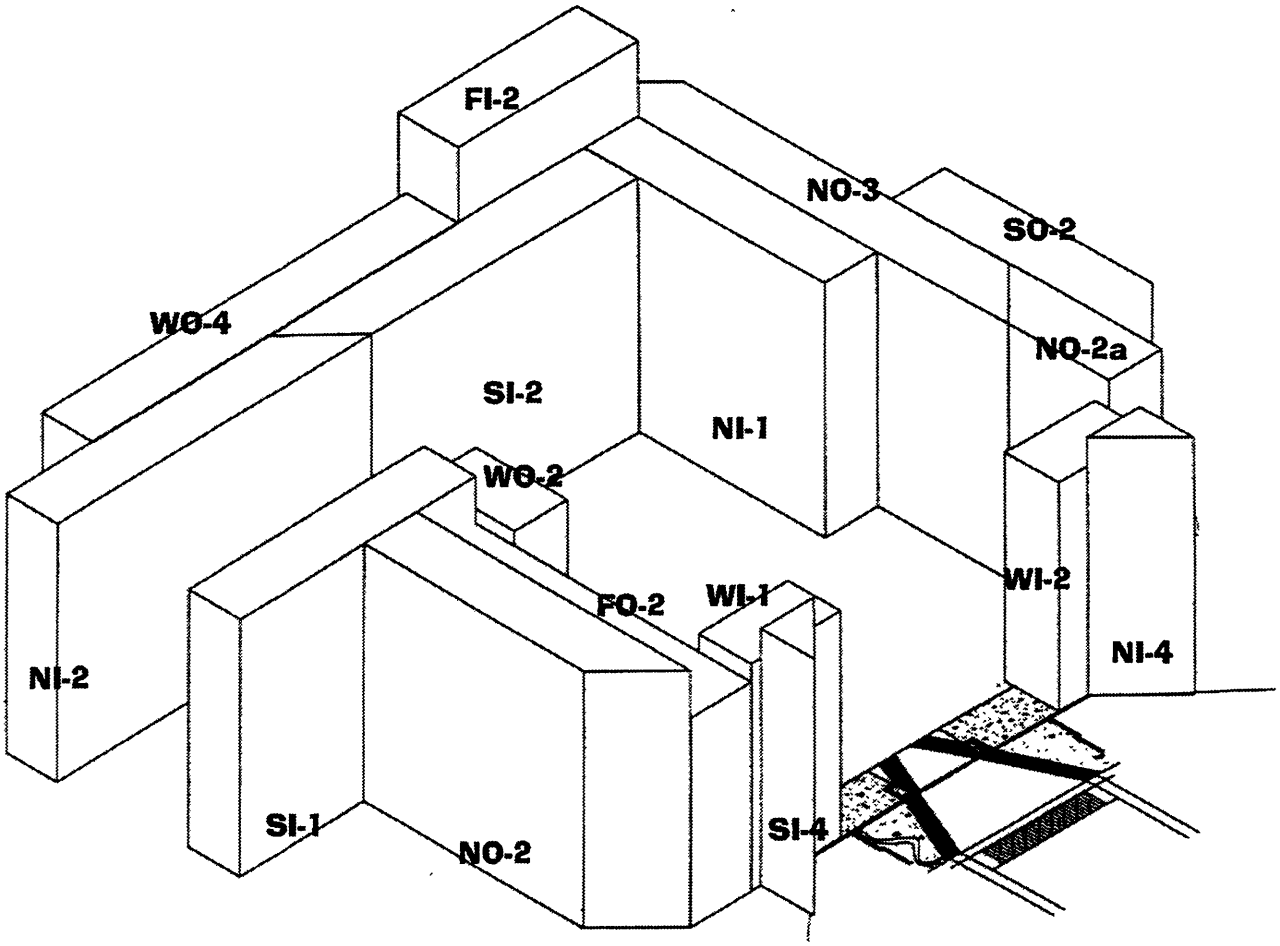

Figure 8.26 Three dimensional view of medical room with existing blocks for side and back walls. Drawing shows the different height in the walls.

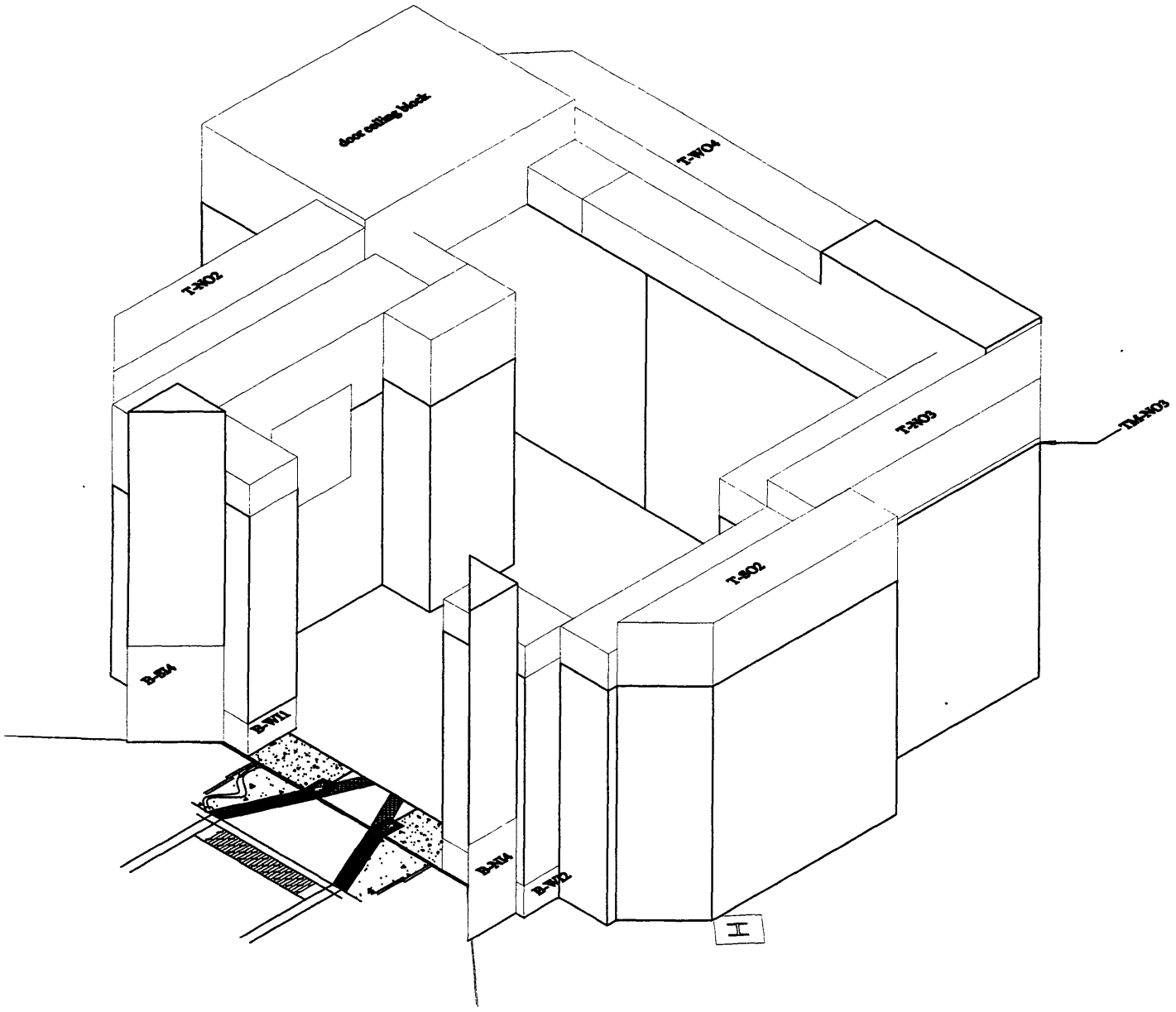

Figure 8.27 Three dimensional view of medical room with spacer blocks for unifying height. Spacer blocks are drawn in lighter lines and labeled. The inner, unlabeled, spacer blocks will be incorporated into the medical room ceiling base.

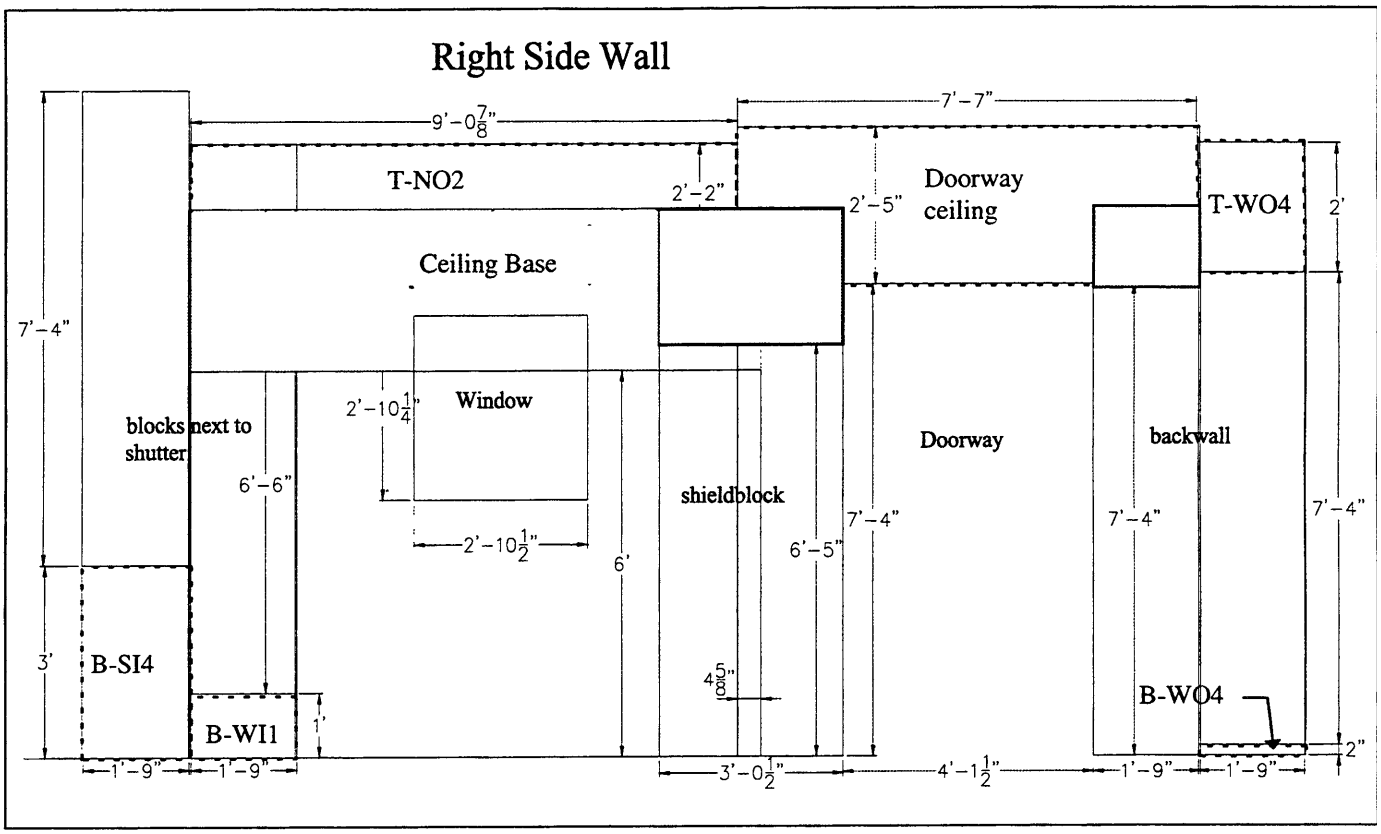

Figure 8.28 View of right side wall, showing spacer blocks(dotted lines) that house a portion of the shielded window, the ventilation entrance duct and possible exit duct.

The drawing above is the inside view of the right wall. Spacer blocks are drawn in, varying in heights, to adjust the wall height to a level that will allow the ceiling to lie on top of the inner blocks. All the inner spacer blocks will be incorporated into the ceiling base, shown in Figure 8.28 shaded in gray. The side wall is layered in two rows. The height of the inner row is set at 8'-6", with the use of spacer blocks. A possible location for one of the ventilation exit ducts is in the spacer blocks beneath the blocks labeled "blocks next to shutter". The spacer block has an available size of 1' height by 21 " thick and 2'-11.5" long in which to incorporate a serpentine shaped conduit. Also notice

that the shielded window does not sit entirely into the bottom block. Instead it runs up into the spacer block. This will make the cut in the existing block simpler.

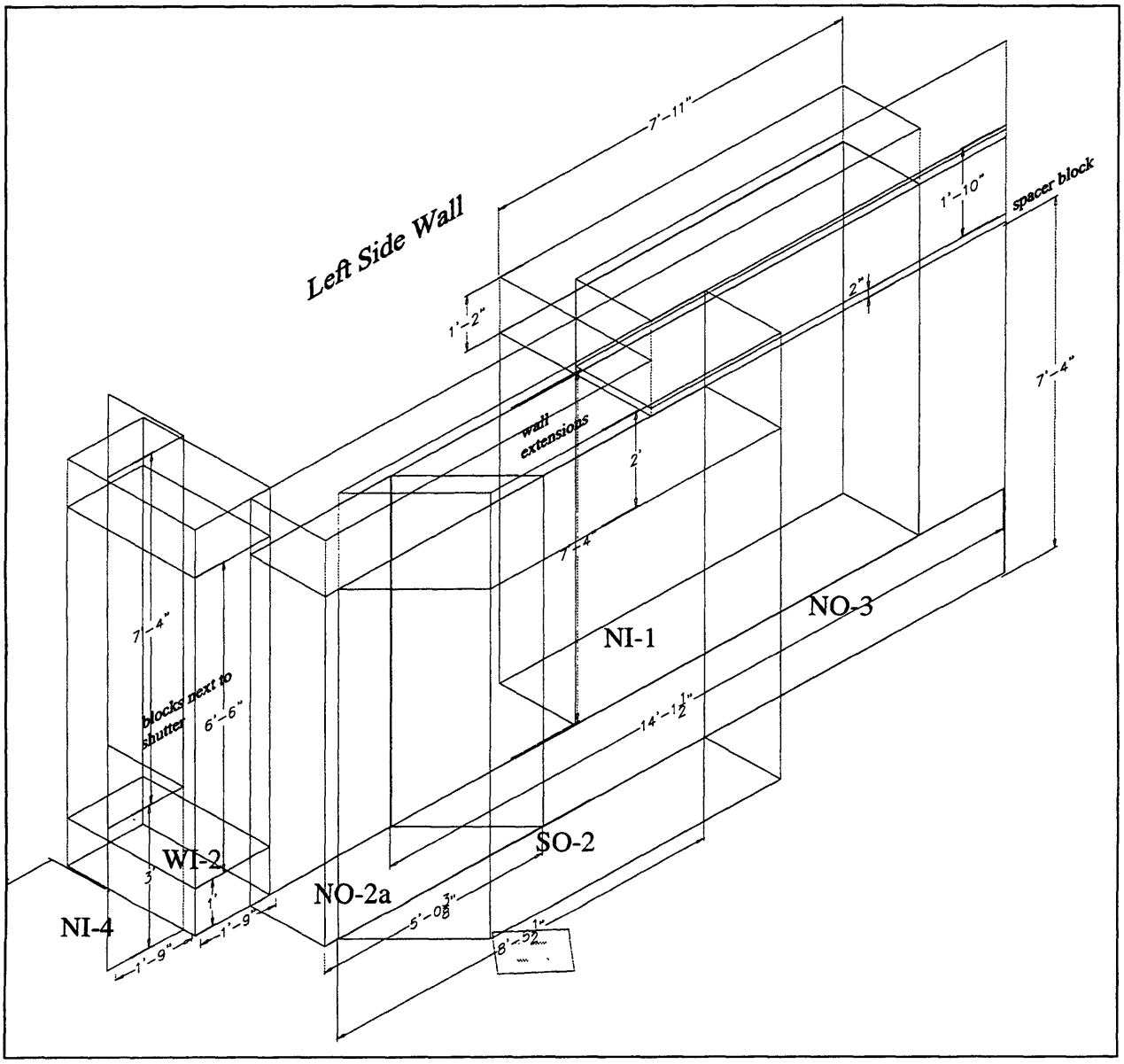

Figure 8.29 Left side wall showing spacer blocks and streaming prevention blocks. Drawing also shows one possible location for ventilation exit duct.

The left side wall has a similar arrangement to the right wall, with the exception that the two rows of shield blocks are the same height, 7'-4". This is a concern because of streaming through the crack between the ceiling base and the side wall tops. To solve this problem, the middle block, NO-3, and outer block, SO-2, are extended 2" in height. Above the extension on NO-3, a separate spacer block is placed to eliminate the diagonal streaming crack between NI-1 and SO-2. This block is separate to keep the total weight under 20 tons, which is the limit of the crane used to move the blocks.

Like the right wall, the "blocks next to shutter" have spacer blocks placed on the floor so that a ventilation exit duct can be incorporated in to them. The gap between NO-2a, WI-4, and NI-4 will be occupied by a new block that will also house a leg of the ventilation duct.

Figure 8.30 is a drawing of the back wall of the medical room. It incorporates some of the same features as the left wall. The walls WO-4, SI-2, and NI-2 are all the same height. This leaves a straight path for streaming to occur. Like the left wall, the outer wall was extended by adding 2" on the floor, beneath block WO-4. The total weight of WO-4 is just under 20 tons with the extension. The drawing also shows the lower ceiling height of the doorway. The ceiling is lower in that area to try to minimize interference with the back platform (explained in section 8.5.1). This ceiling block is the prime candidate for the entrance ventilation duct.

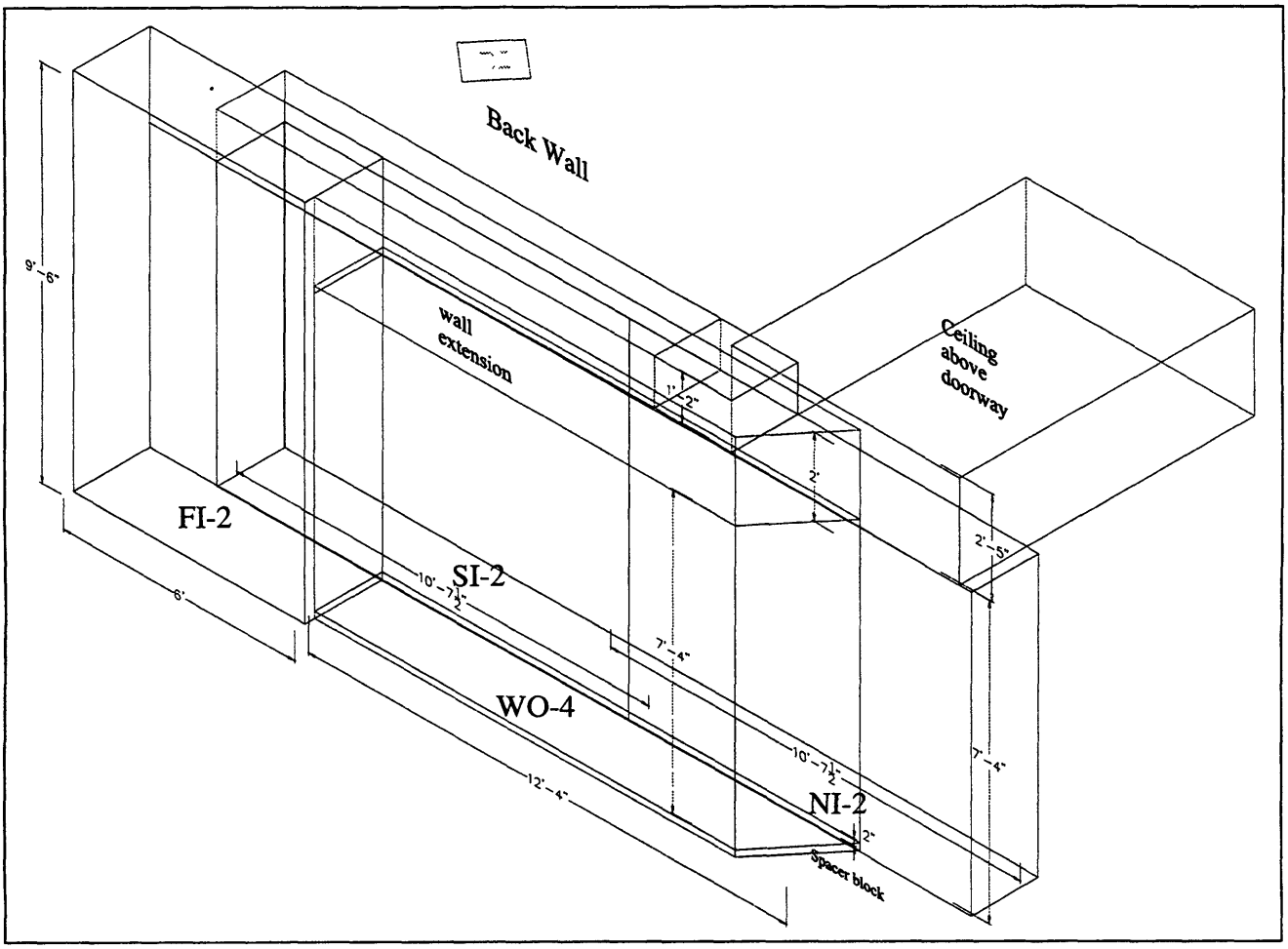

Figure 8.30 Back wall with spacer blocks. Possible entrance duct for ventilation system will be placed into the upper wall extensions.

With the spacer blocks described above, the ceiling base can sit flat on top of the medical room. The spacer blocks found on the inner perimeter of blocks in the medical room will be part of the actual ceiling base. The following drawing, Figure 8.31, shows how the spacer blocks will be used as a foundation for the ceiling base. The dark blocks represent the spacer blocks and the medium dark blocks represent the high strength ceiling base.

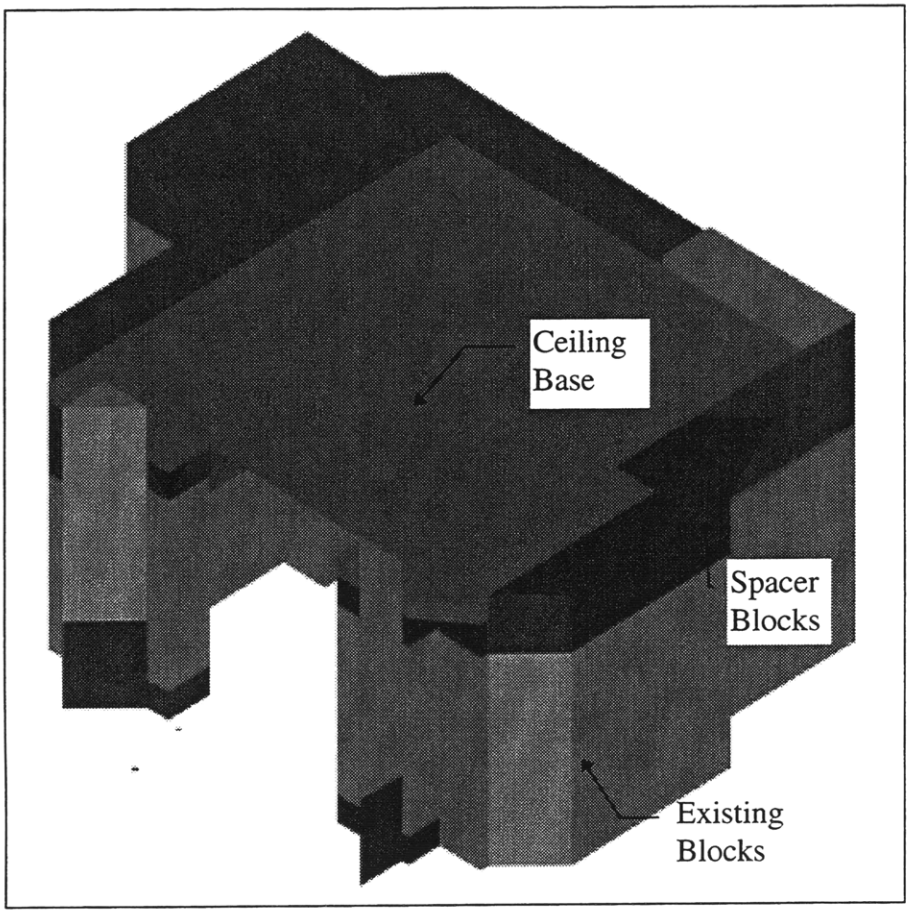

Figure 8.31 Isometric Picture of medical room with ceiling base with incorporated spacer blocks at its base. Refer to Figure 8.27.

8.4.3 Ventilation Ducts

During an irradiation neutrons interact with argon in the air. The result is ^{41}Ar, an isotope that decays by emitting a gamma with energy of 1.29 Mev.

$$(Air)^{40}_{18}Ar + {}^{1}_{0}n \rightarrow {}^{41}_{18}Ar_{T1/2(1.83h)} \rightarrow {}^{0}_{-1}\beta(1.2\,Mev) + {}^{0}_{0}\gamma(1.29\,Mev) + {}^{41}_{19}K$$

The occupational limit on the derived air concentration (DAC) of ^{41}Ar in the air is $3x10^{-3}$μCi/L.[43] An estimate of the ^{41}Ar level in the room after a three hour irradiation was performed by Kent Riley[44]. His calculations give a concentration of $9.4x10^{-2}$ μCi/L. To reduce the level of ^{41}Ar in the air after an irradiation, a ventilation system is required. An estimated flow rate of 900ft^3/min is needed to reduce the concentration in the room to 1 DAC in 1 min.[45] A preliminary design of the ducts needed for the ventilation system is shown below. The design is basically a shielding design of the duct system. A further analysis will be performed by Tarcisio Campos to optimize this shielding design with the required flow rates. Entrance to the reactor ventilation system is located in the containment shell, beneath the catwalk, directly in front of the back wall. Tie-ins to the exhaust system are located on the floor next the "blocks next to shutter". The exhaust ports are rated at 600 ft^3/min.

---

[43] 10CFR Part 20, Appendix B.
[44] Ph.D. student.
[45] Fred McWilliams, RPO, MITRII.

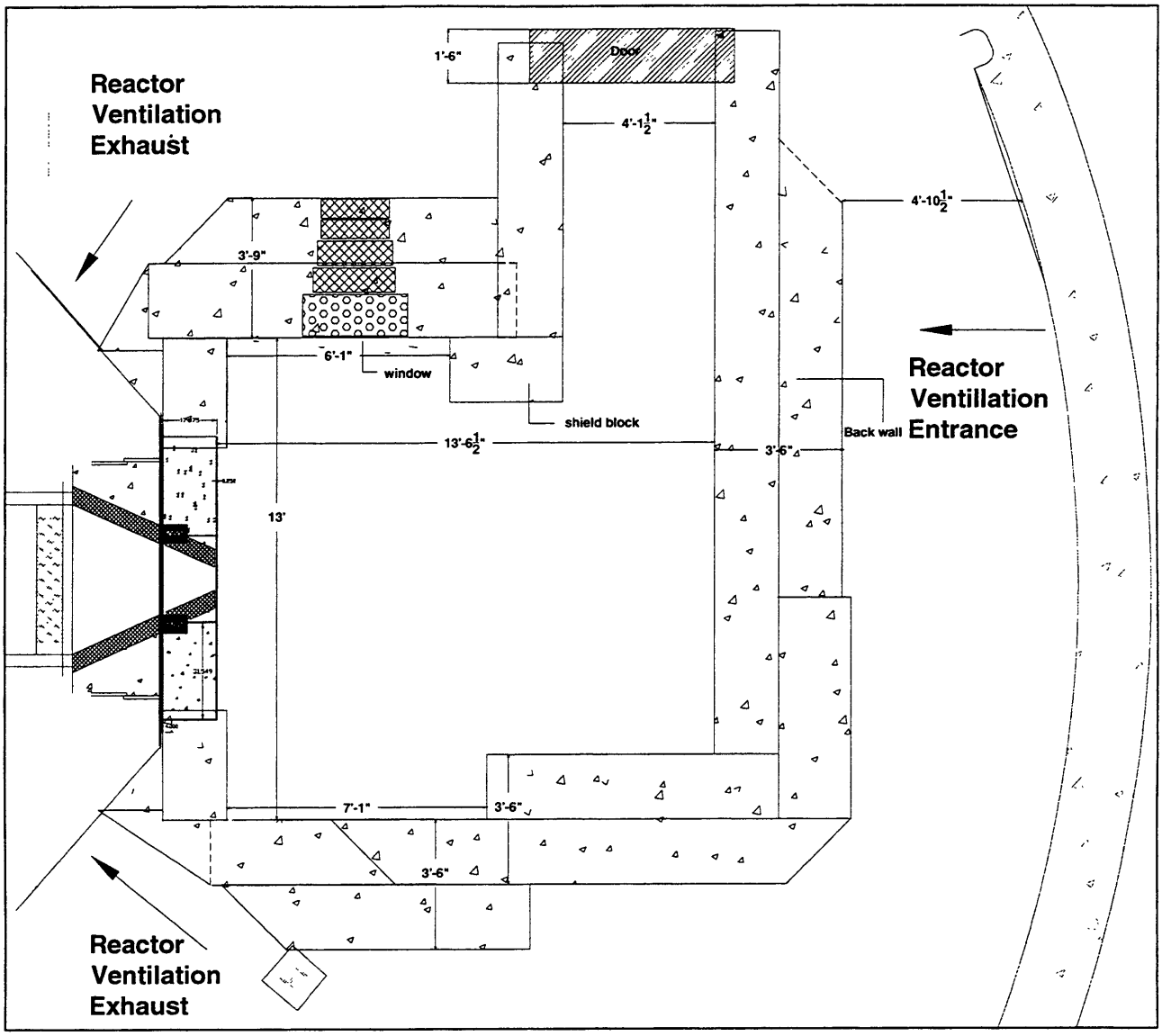

Figure 8.32 Drawing showing location of entrance and exit port to reactor ventilation system.

Dose rates outside the inlet ventilation duct were calculated using the Simon-Clifford[46] equation for ducts.

[46] Rockwell, Reactor Shielding Design Manual, p. 278.

$$\frac{\Phi}{\Phi_o} = 10e^{-\Sigma_r \cdot L} \frac{1}{8}\left(\frac{d}{L_1}\right)^2 \frac{1}{8}\left(\frac{d}{L_2}\right)^2 \cdots \frac{1}{8}\left(\frac{d}{L_i}\right)^2 \qquad \textbf{(8.1)}$$

Φ is the dose rate outside the inlet opening, and Φ_0 is the dose rate at the exit opening, in this case the inside of the room. Σr is the removal cross section of the material inside duct. In this case the material is air, which is assumed to have a removal cross section of zero.[5] The total length the of duct is represented as L, where L_1, L_2, ...L_i represents the length of one leg of the duct. The diameter of the duct is d. The dose rate at the inside of the duct opening was assumed to be equal to the twice dose rate at the door, which assumes no target in the beam. This assumption is very conservative because while the duct is located closer to the scattering surfaces than the door, the albedo at that angle of reflection is much smaller. Using the dimensions shown in Figure 8.33 for equation 8.1, the attenuation through the duct, Φ/Φ_0, is 1.22×10^{-3}. These give a dose rate outside the duct inlet of 1.12 mrem/hr, using the conservative estimate of the dose rate on the inside of the duct. The duct total height is 2'-6", whereas the ceiling height is 2'-5". The extra inch is in the square opening.

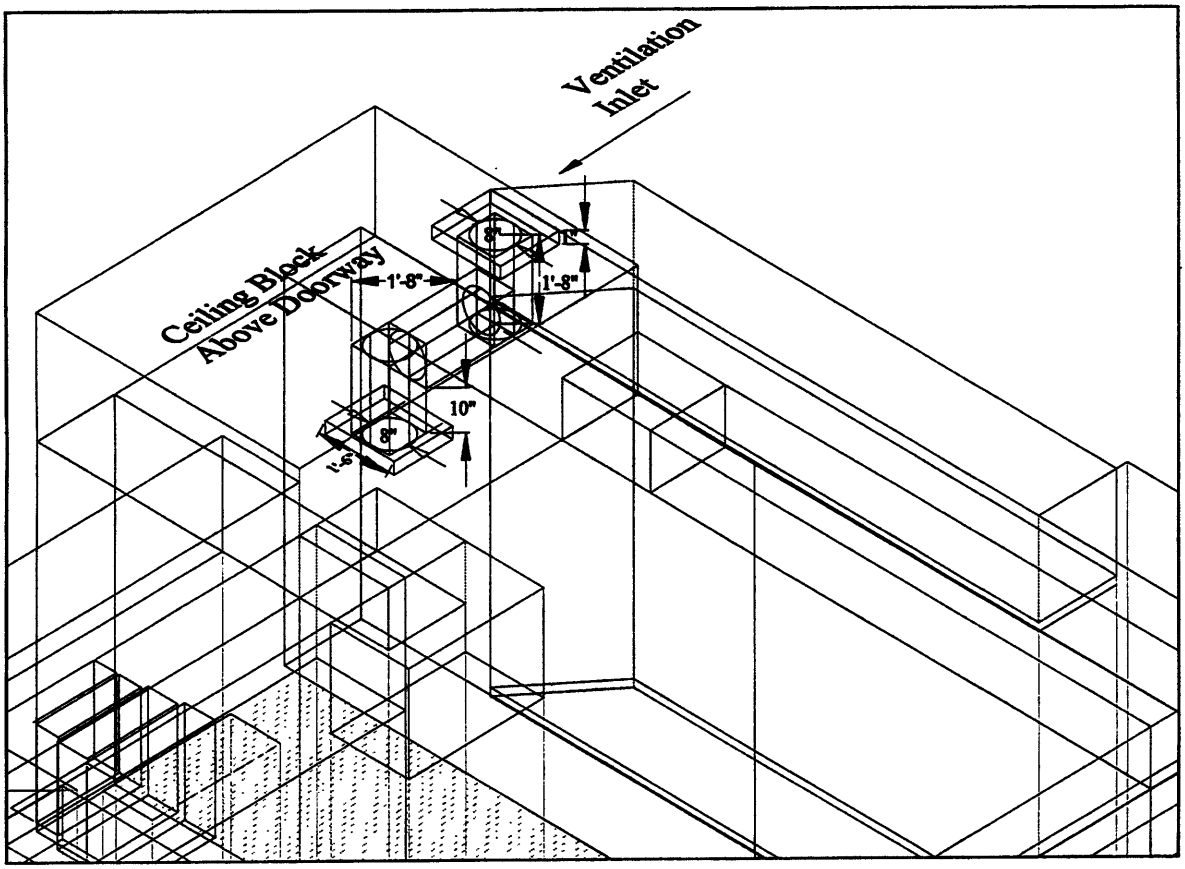

Figure 8.33 Ventilation inlet duct.

Similar to the inlet duct, a duct was designed at the bottom corner of the medical room for the ventilation exhaust. Figure 8.34 shows this exhaust duct that has four legs and a pipe diameter of 8"[47]. The attenuation through this duct was calculated using equation 8.1 and assuming the dose rates at the duct are same as the dose rates at the floor with a target in the beam, as calculated in section 2.4.4. The attenuation through the duct was calculated as Φ/Φ_o equals 5.06×10^{-6}. This gives a dose rate outside the duct of 0.032 mrem/hr.

[47] 8 inches was chosen as the diameter of the duct for this preliminary design based on personal communication with Fred McWilliams, radiation protection officer.

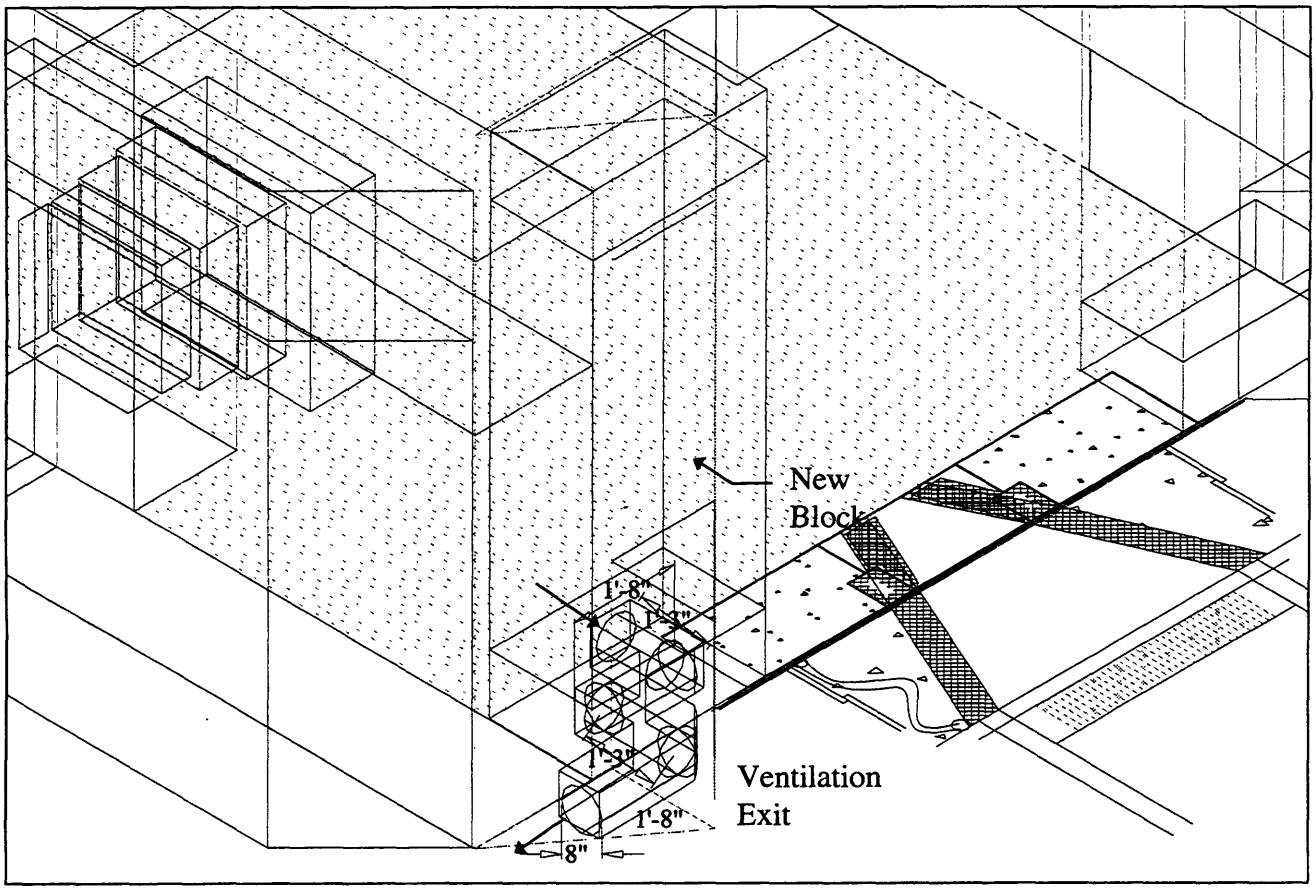

Figure 8.34 Ventilation exhaust duct.

The outermost block in the ventilation exit duct shown in Figure 8.34 is a new shield block that needs to be constructed. A drawing of the block is shown in section 8.4.4.

In addition to the exit duct on the right side of the medical room, the use of another exit duct is possible. The location of the other exit duct is on the left side of the shutter. The following figure shows the design of this additional ventilation exhaust duct. The attenuation by this duct is 2.24×10^{-4}. This gives a total dose rate outside the duct of 2.25 mrem/hr, using the dose rates at the floor from section 2.4.4. The dose rate outside the duct is a little higher than desired. However, this calculation overestimates the dose

because when a patient is in the beam the dose rate at the floor is higher than the dose rate at the corner where the duct is located. Even though the dose rate exiting the left exhaust duct is larger than desired, it still meets the federal regulations. To reduce the dose rate exiting the duct, a fourth bend could be added so that the left duct is identical to the right side duct.

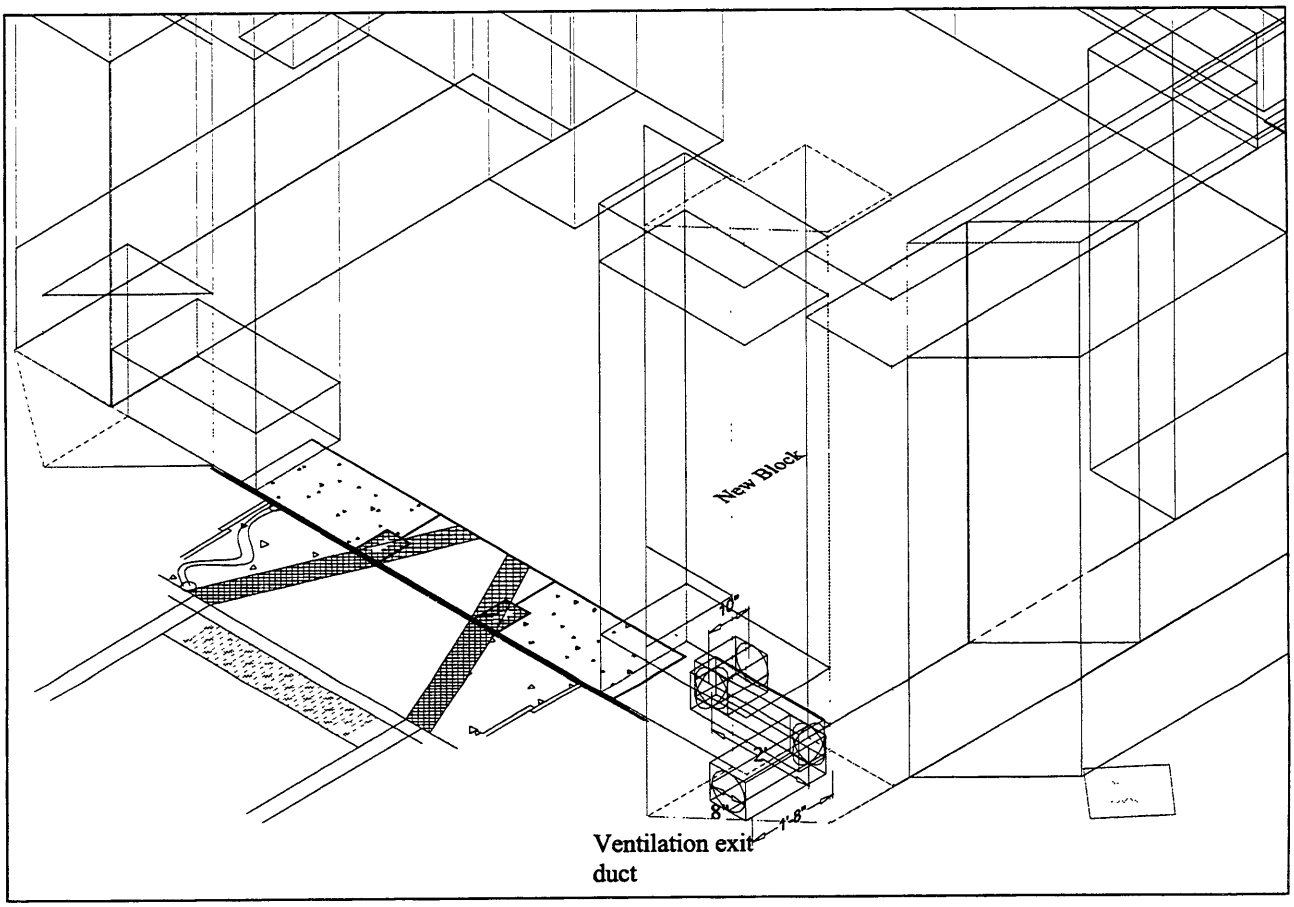

Figure 8.35 Left side ventilation exhaust duct.

Figure 8.35 shows another new block. The height of the block is 10'-4", like the block on its left. This block will meet up with the ceiling, making a flat surface across

the medical room top. A drawing of this new block with dimensions is shown in section 8.4.4.

8.4.4 Specifications for Additional Shield Blocks

As mentioned throughout the previous section, some new blocks will need to be constructed. The following drawings are descriptions of the blocks that need to be constructed. These drawings show all the new blocks, except for the ceiling base and the ceiling above the doorway. The block in Figure 8.37 and Figure 8.36 is the block located at the left corner of the room near the reactor. This is one of the blocks that will hold one of the ventilation exhaust ducts.

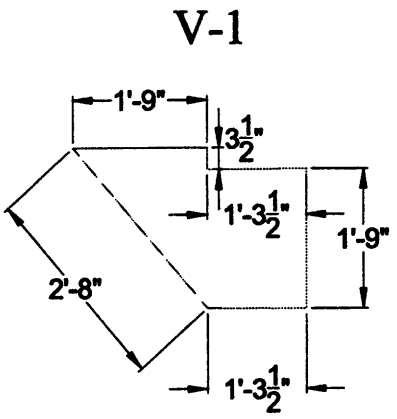

Figure 8.37 Left corner block to fill gap between reactor face and medical room. Top view.

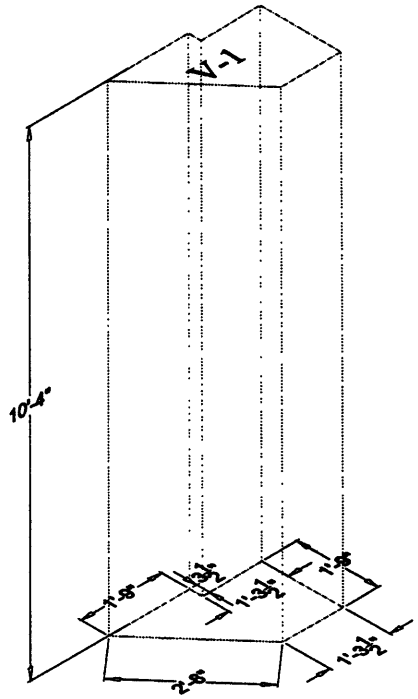

Figure 8.36 Side view of left corner block.

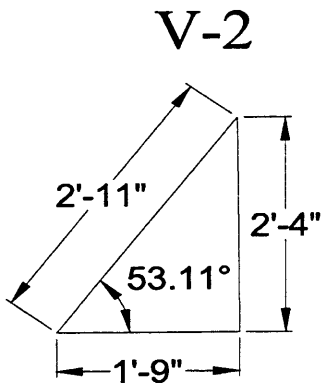

Figure 8.39 Right corner block between reactor and medical room.

On the other corner of the room, another new block needs construction. This block closes the crack between FO-2 and WI-1 and is the location for the other ventilation exhaust duct.

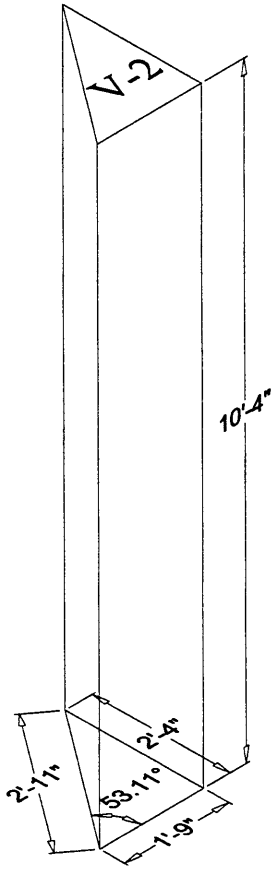

Figure 8.38 Side view of right corner block.

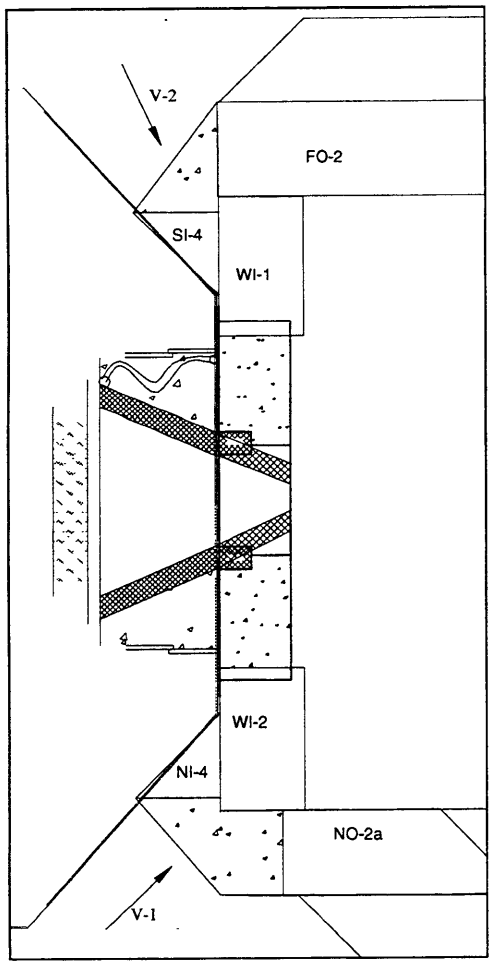

Figure 8.40 Location of blocks V-1 and V-2.

Drawings for the spacer blocks are shown below. Blocks labeled with T designate blocks

that sit on top of existing blocks. Likewise, blocks labeled with B designate spacer blocks which rest on the floor, beneath the existing shield blocks.

Figure 8.41 Top view of spacer blocks T-NO2 and T-SO2. T-NO2 is located on top of the outer right side wall. T-SO2 is located on top of the outer left side wall.

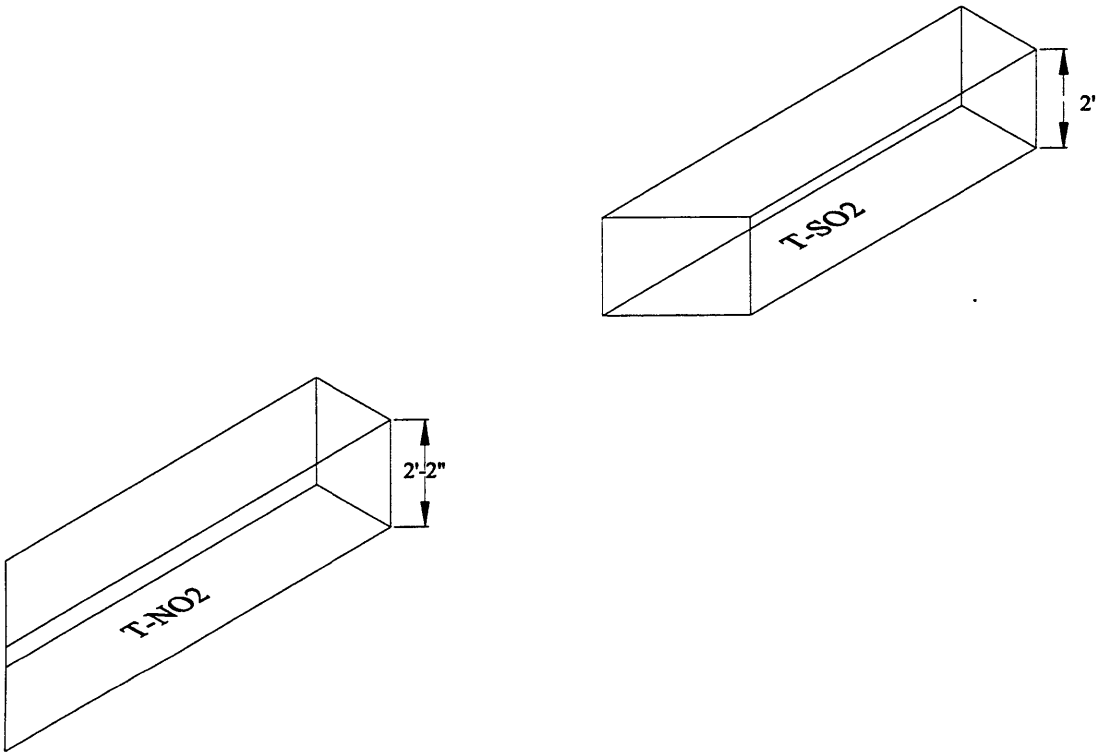

Figure 8.42 Side views of spacer blocks T-NO2 and T-SO2. T-SO2 will be attached to SO-2 to extend the existing block and prevent streaming.

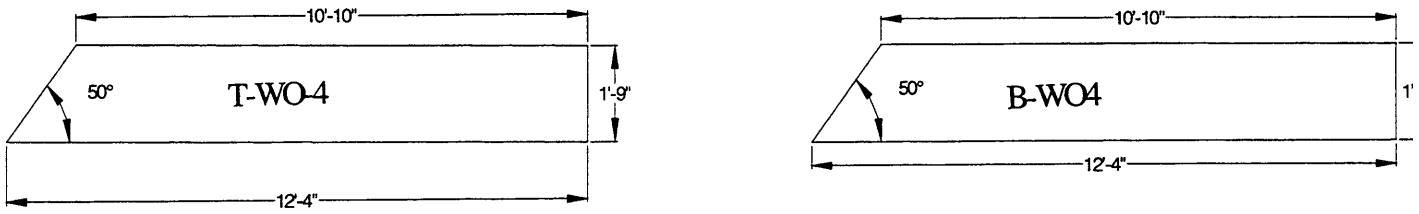

Figure 8.43 Top view of spacer blocks located at the top (T-WO4) and bottom (B-WO4) of the back wall.

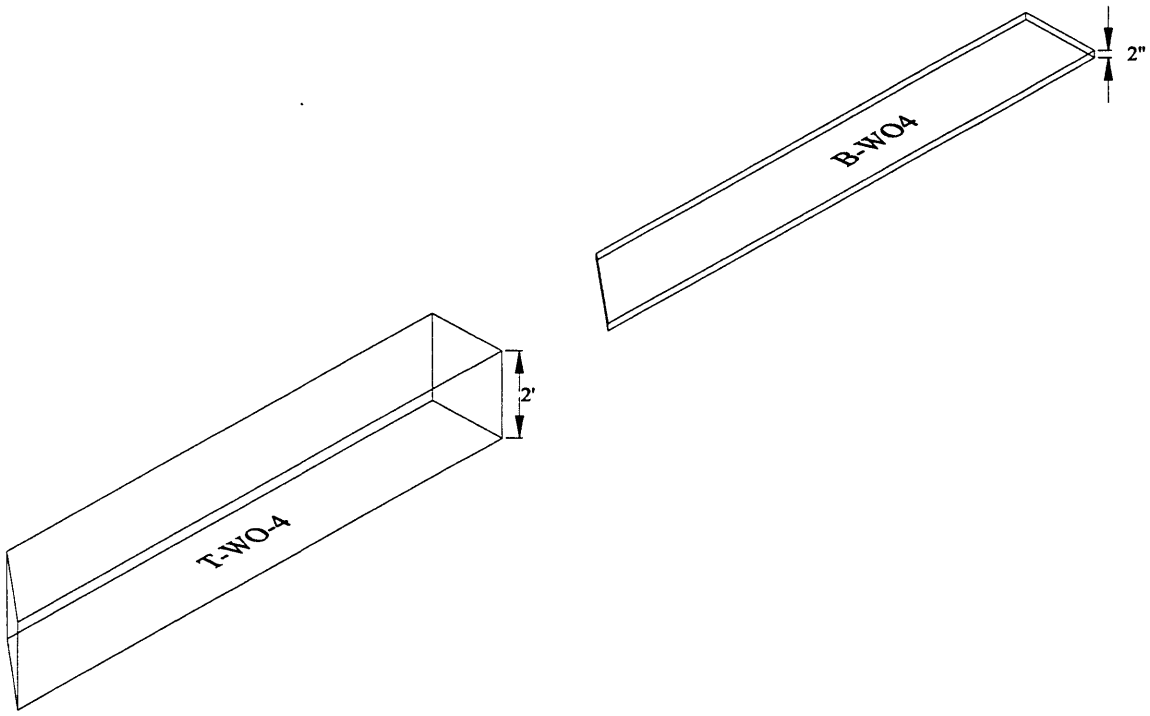

Figure 8.44 Side view of spacer blocks at back wall. B-WO4 will be attached to the base of WO-4 to prevent streaming.

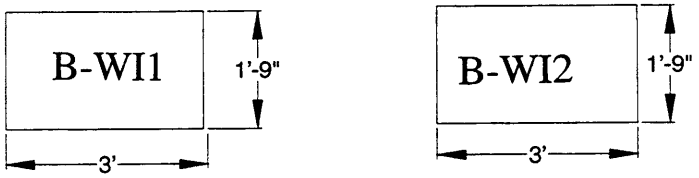

Figure 8.45 Spacer blocks at the bottom of the blocks directly next to the shutter.

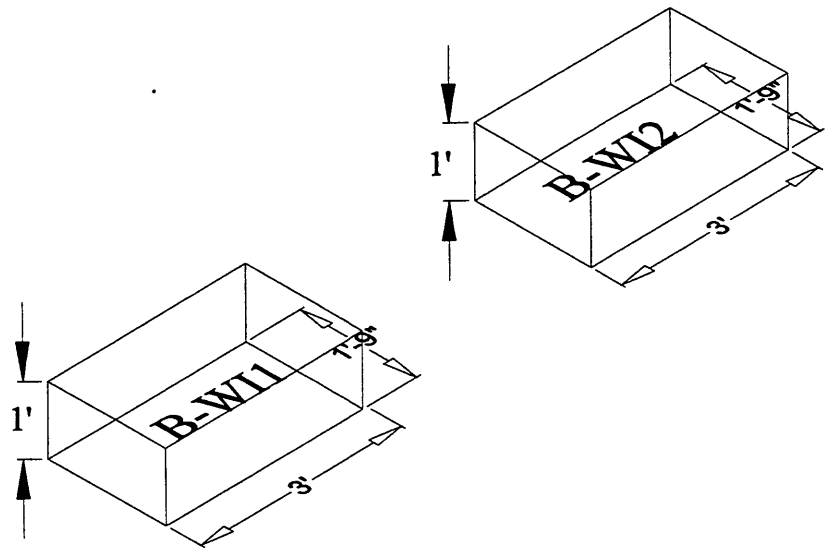

Figure 8.46 Side view of spacer blocks beneath the "blocks next to shutter". These blocks will hold the inlet into the exhaust ventilation ducts.

Figure 8.47 Top views of the spacer blocks located above NO-3, the middle left block.

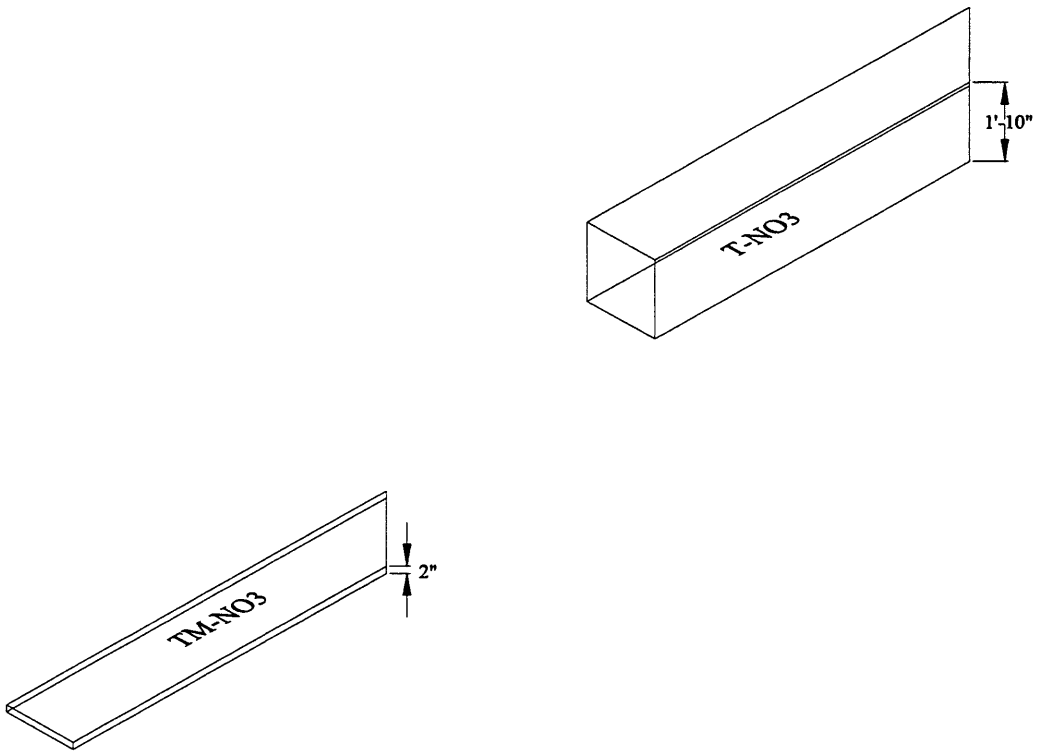

Figure.8.48 Side view of spacer blocks on NO-3 (left wall). TM-NO3 will be attached to NO-3 to prevent streaming. It will sit between NO-3 and T-NO3.

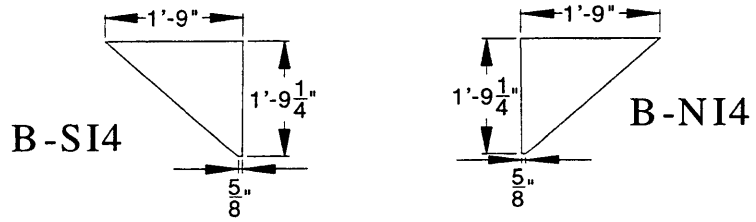

Figure 8.49 Top view of the inner bottom corners of the medical room. These sit between the reactor face and WI-1 and WI-2, respectively.

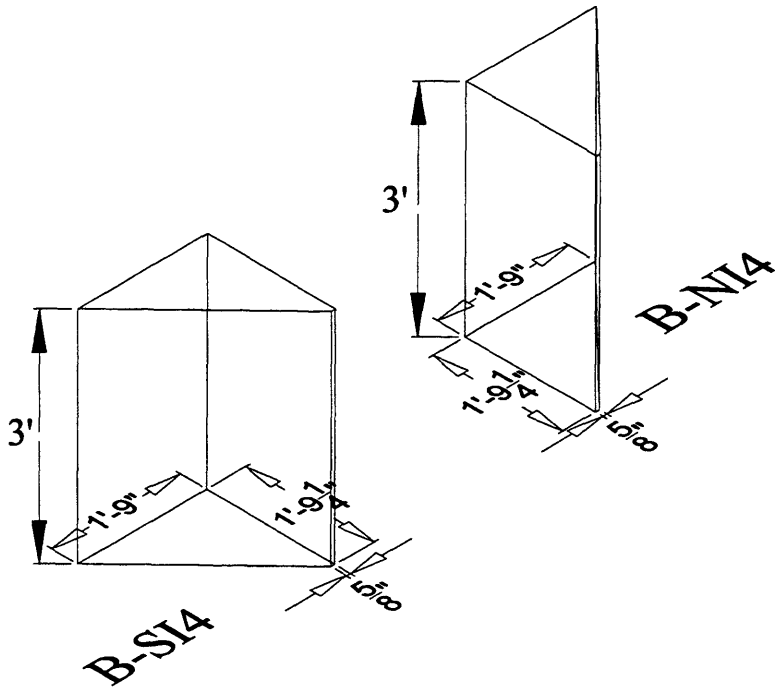

Figure 8.50 Side view of spacer blocks at inner corners of medical room. These blocks will be used as part of the ventilation exhaust duct.

8.4.5 Modifications to Existing Blocks

A few of the existing blocks will have to be modified to fit into the final design. All the holes in the blocks will have to be filled with I-2a concrete. The following drawings show the four existing blocks that need cuts in various locations. The cuts in the blocks are represented by dotted lines.

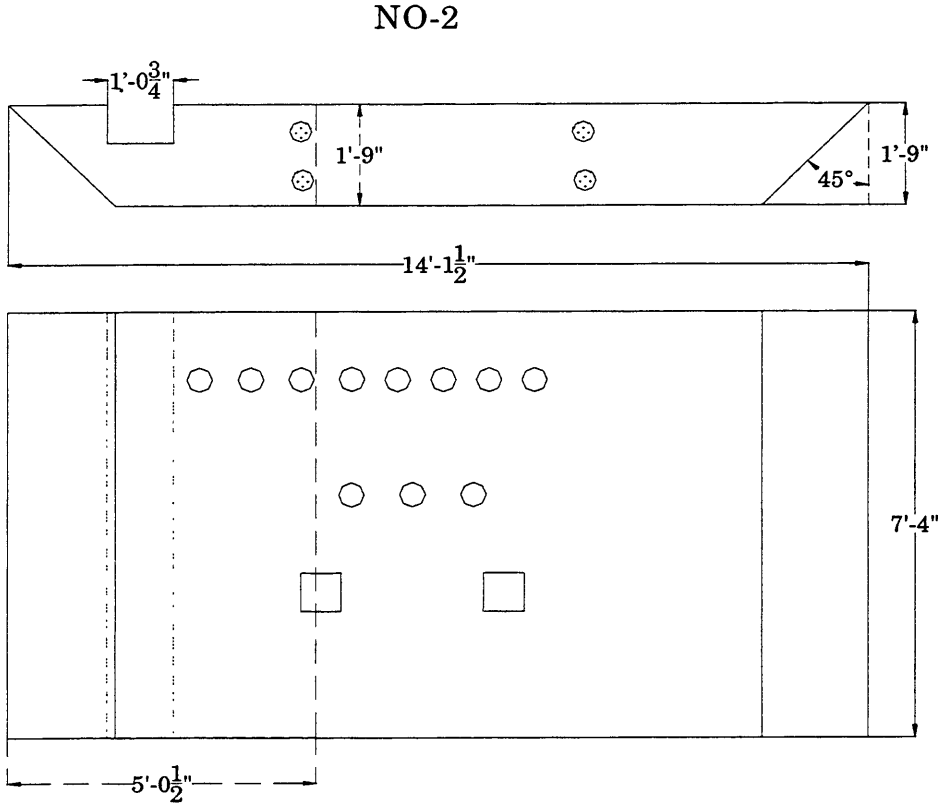

Figure 8.51 Block NO-2 has a straight 5'-1/2" from the left side, all the way through the block. The cut off piece will be used as another shielding block, NO-2a.

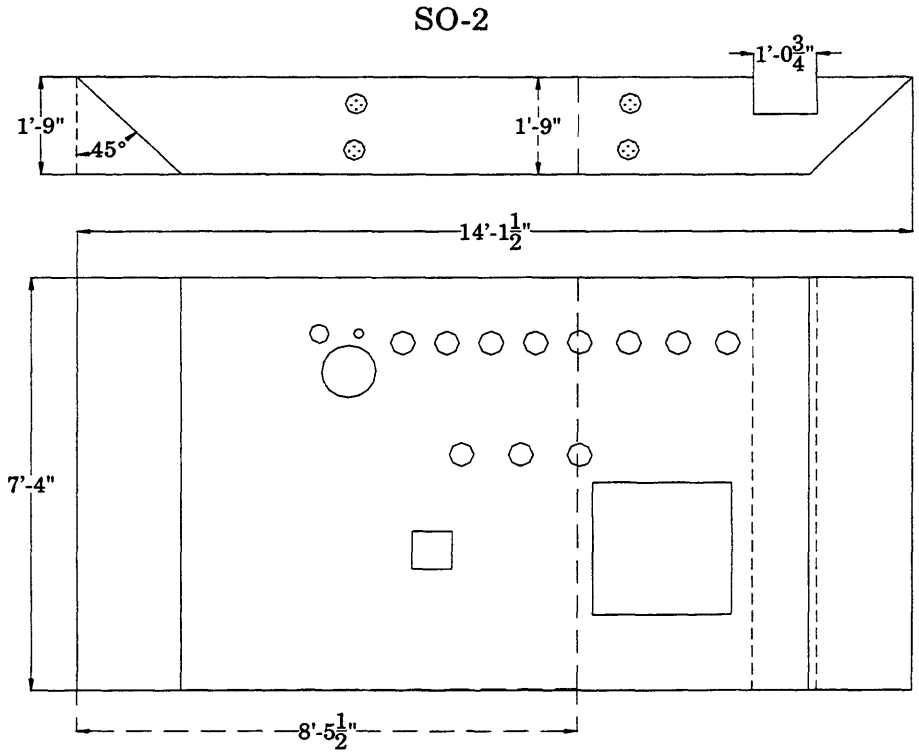

Figure 8.53 The above block has a cut straight through. The cut occurs 8'-5 ½" from the left side. The remaining portion may be discarded.

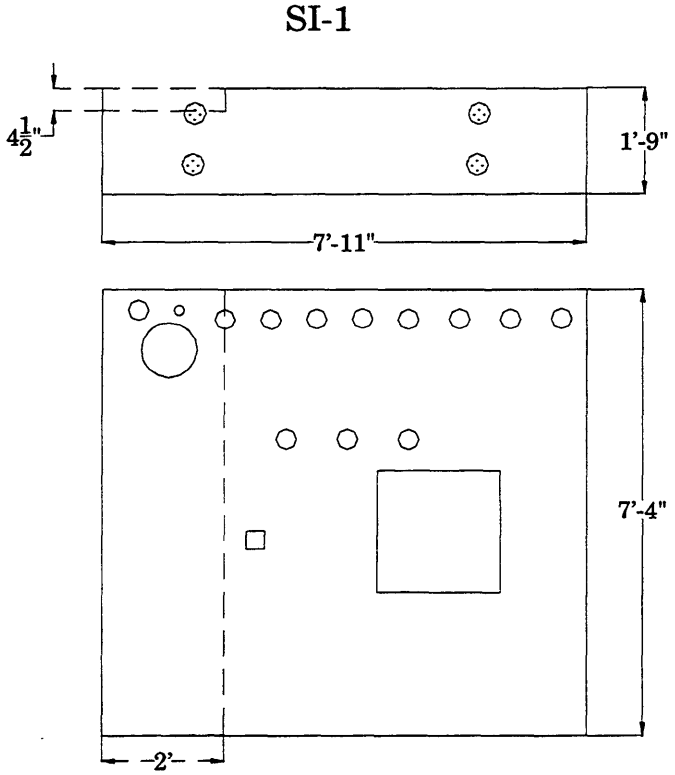

Figure 8.52 SI-1 has a notch in the back left corner. The notch is 4 ½" thick and 2' deep.

WO-4

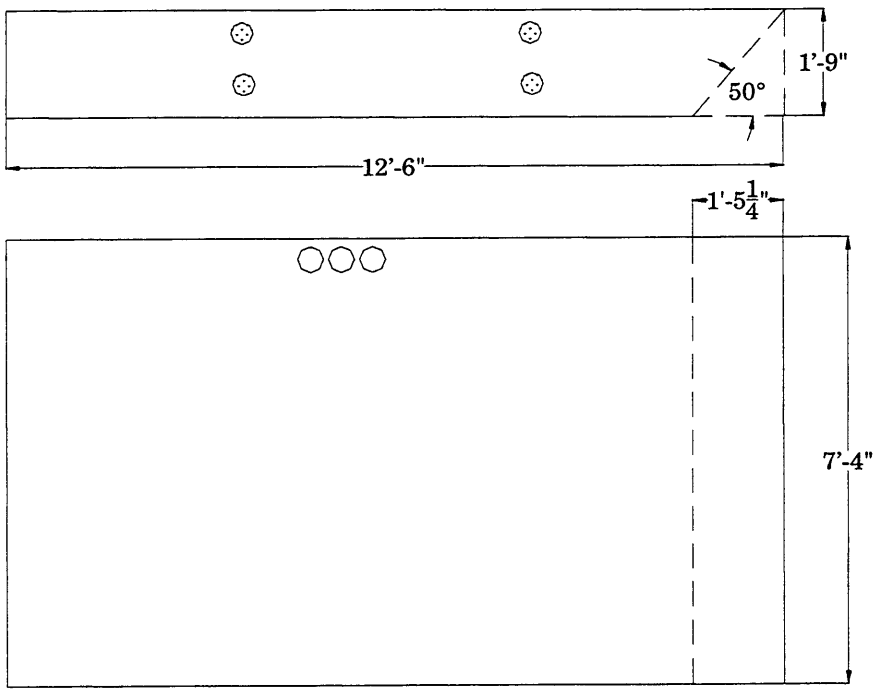

Figure 8.54 WO-4 has a 50 degree angle cut at the right corner. This is to open up space between the reactor containment building and the doorway.

8.5 INTERFERENCE WITH OTHER STRUCTURES

In designing the medical room interference with several structures on the reactor floor was avoided when possible. However, total avoidance was not possible. The critical items of interference are the back platform and part of the front platform.

Interference with the back platform occurs in several locations. First, the support beam for the platform runs directly through the location of FO-2, the right wall that will house part of the window. Second, another support beam sits directly inside the

doorway of the medical room. Although these support beams interfere with the right side of the room, the interference is resolvable. The platform will need to be redesigned in such a way that these support beam can be located elsewhere. A bigger problem is the platform's interference with the medical room ceiling. With the use of existing blocks, the side wall extends outward farther than anticipated. Once the ceiling is applied to the room, it will run directly into the main supporting base of the back platform. Additionally, attached to this side support base are important reactor piping systems. Figure 8.55 displays the interference between the medical room and the back platform.

The interference with the front platform can be alleviated by removing one of the support beams and using an alternative location. However, solving the back platform interference is not as simple. The back platform interferes with the medical room ceiling, the installation of the shielding door, the ceiling above the doorway, and the inlet for the ventilation system. Two possibilities for remedying this interference are 1.) Restructure the platform: raise in height, decrease in area, and provide alternative locations for the support beam, and 2.) Remove the platform altogether. There are opposing views to the two solutions. Both will require much work and planning.

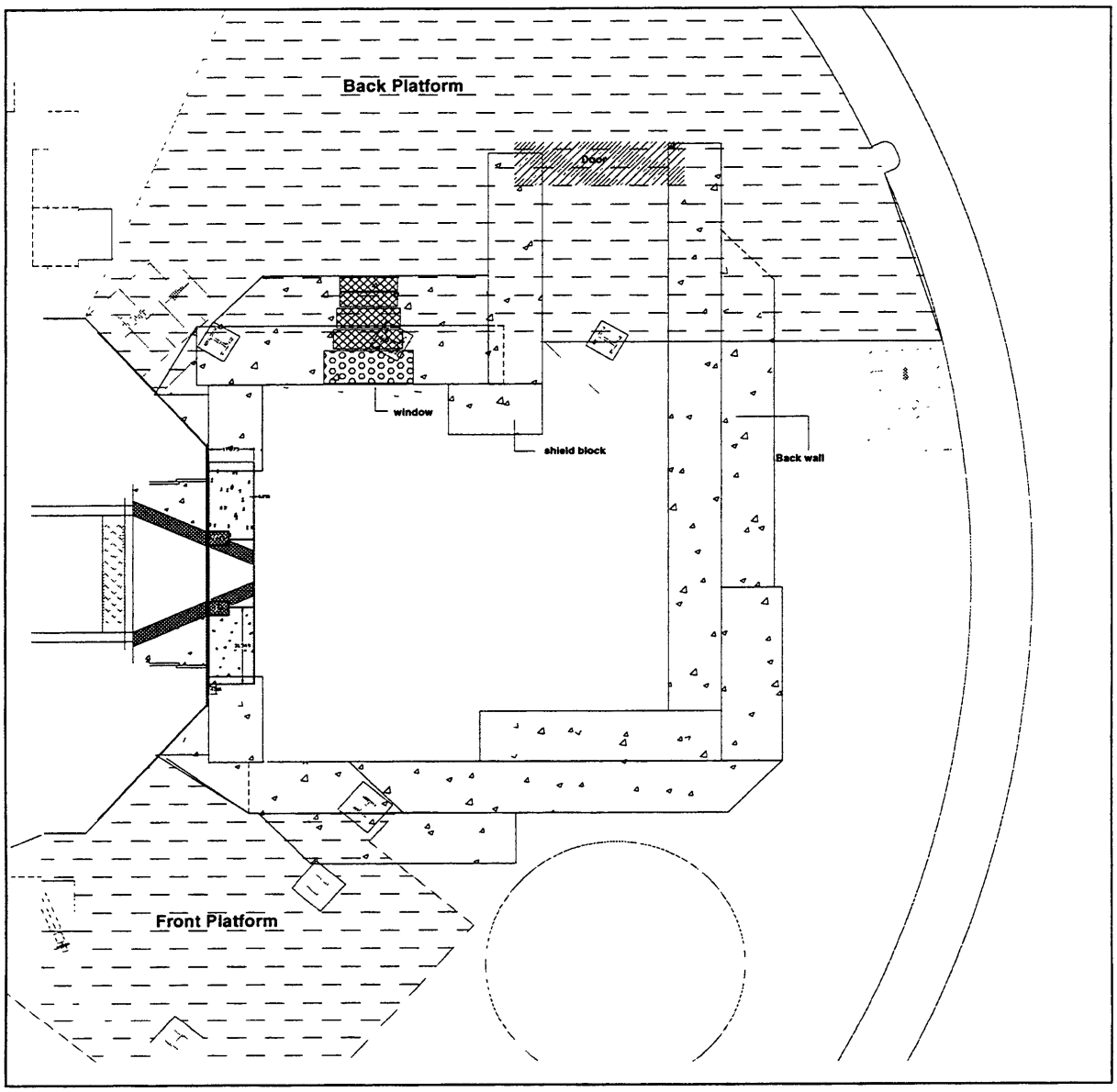

Figure 8.55 Drawing showing interference between medical room and platforms.

8.6 PRELIMINARY DOOR DESIGN

In chapter 3 several options for a shielding were specified. One of these options must eventually be constructed in to structurally sound door with a durable opening and closing mechanism. The mechanical design of the door will be done by Jerry White[48]. Below is preliminary design of a swing door using the all steel option. The door is inset into the wall to prevent radiation streaming through the cracks. The door is made of nine 2" steel plates. On the left side of the door, the plates are stepped with a ½" inset. On the right the first four plates are inset 1". The remaining plates are inset 2", forming a stepped edge on the right side. A hinge is drawn in as an example of an opening and closing mechanism.

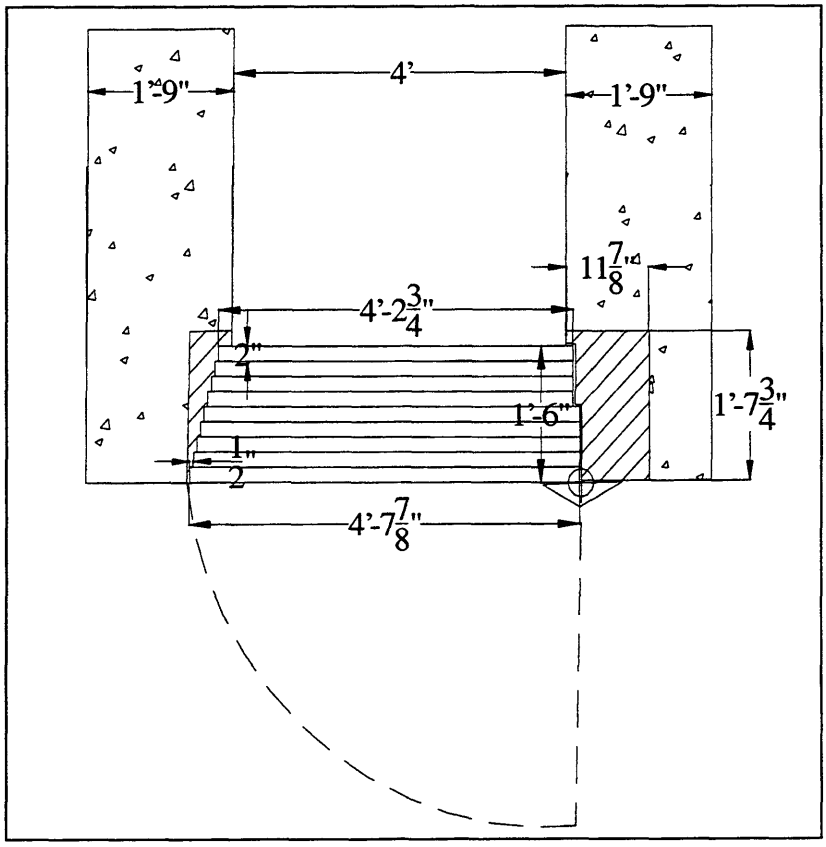

Figure 8.56 Top view of door.

[48] Master's Student.

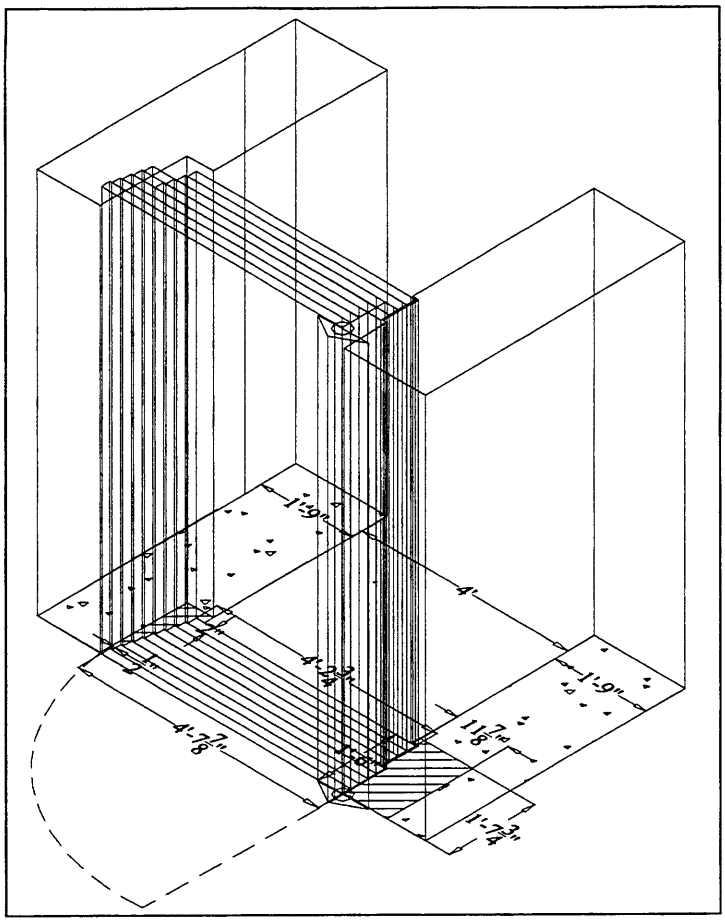

Figure 8.57 Isometric view of door

8.7 FINAL MEDICAL ROOM DESIGN

The design of the medical room presented in this chapter, shown below, incorporates shielded walls, a shielded viewing window, a shielded door, and initial designs of a ventilation system. This design provides more than the necessary shielding at the right wall, left wall and back wall due to the use of existing shield blocks. Anticipated dose rates outside the room are listed in the table below.

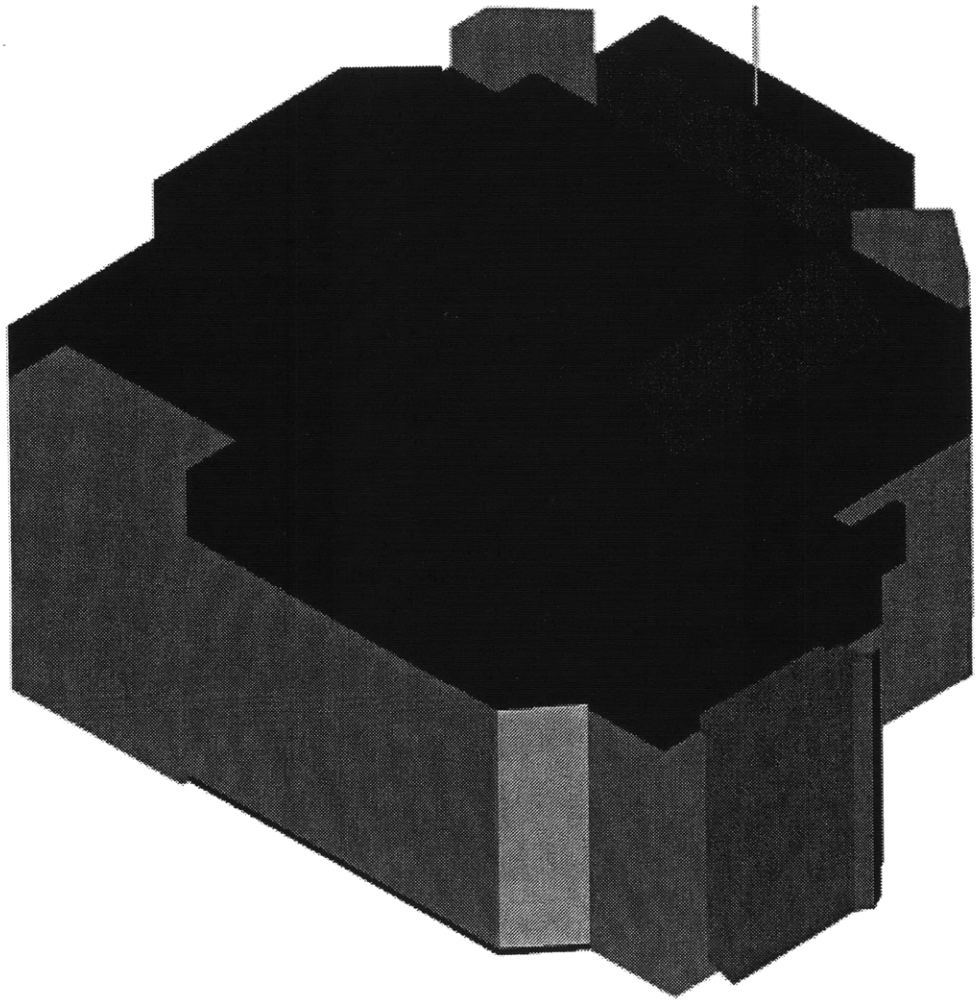

Figure 8.58 Rendered drawing of final design of medical room.

Table 8.3 Anticipated dose rates outside medical room.

Location	Total Dose Rate Outside Wall (mrem/hr)
Right Wall	0.016
Left Wall	0.0373
Back Wall	0.485
Ceiling	1.0
Door	1.0
Window	1.0

8.9 REFERENCES

Block, E., Personal communication.

Campos, T., Personal communication.

Harling, O.K., Personal communication.

Jaeger, R.G, "Shielding Materials", *Engineering Compendium on Radiation Shielding*, Vol.II, Springer-Verlag, New York Inc, 1975.

Jaeger, R.G, "Shield Design and Engineering", *Engineering Compendium on Radiation Shielding*, Vol.III, Springer-Verlag, New York Inc, 1970.

Kiger, W.S, *Neutronic Design of a Fission Converter-Based Epithermal Beam for Neutron Capture Therapy,* Nucl. E. Thesis, Massachusetts Institute of Technology, 1996.

McWilliams, F., Personal communication.

Menadier, P, Personal communication.

NRC, "Title 10, Chapter 1, Part 20" *Code of Federal Regulations-Energy*, United States Nuclear Regulatory Commission, 1995.

Riley, K., Personal communication.

Rockwell, T. , *Reactor Shielding Design Manual,* D. Van Nostrand Company, Inc., 1956.

Stahle, P., Personal communication.

White, J., Personal communication.

CHAPTER 9

SUMMARY AND SUGGESTIONS FOR FUTURE WORK

9.1 SUMMARY

A shielding design was performed for the medical room of the fission converter neutron beam. For the design, an analysis was done to determine the dose rate at various locations in the room that will require shielding. These include: the side walls, ceiling, back wall, door, and window. The dose rates calculated for the side walls were 2.45 rem/hr for gammas and 3.23 rem/hr for fast neutrons. These are the dose rates outside the room, without shielding. For the back wall, the dose rates at the inside surface of the wall were calculated as 5.56 rem/hr for gammas and 68.2 rem/hr for fast neutrons. The dose rates at the door were calculated as 1.69 rem/hr for gammas and 1.76 rem/hr (using the experimental albedo for concrete) for fast neutrons.

Once the dose rates were obtained, the shielding needed to reduce the dose rate outside the medical room to 1 mrem/hr was calculated. This shielding analysis included examination of the properties of several types of shielding materials as described in chapters 3 and 4. Results of the shielding analysis reveal that 73 cm of I-2a concrete is needed for the thickness of side walls and ceiling, and 100 cm of I-2a concrete is needed for the back wall shielding thickness. Several combinations of shielding materials for the window and door were calculated, see Table 3.12 and Table 3.13 for door combinations

and Table 4.9 for the window options.

From the shielding analysis a design of the medical room was performed, as described in chapter 8. The design included the walls of the room using existing concrete blocks, a shielding door for entrance into the medical room, a shielded viewing window, and specifications for additional shielding blocks.

In addition to the medical room design, an analysis of the type of positioning system best suited for the new BNCT facility was performed. From this analysis it was determined that two separate positioning systems would adequately meet positioning needs. These are a standard operating table and a lounge (beach) chair.

9.2 SUGGESTIONS FOR FUTURE WORK

Suggestions for future work include:

- a detailed design of a high strength ceiling that incorporates the ceiling base blocks located on top of the inside of the side and back walls, see Figure 8.27 and Figure 8.31,

- a design of the window frame for the shielded viewing window and specifications for cutting the existing concrete blocks for window insertion. A detailed analysis of the shielding around the window steps should also be performed to prevent radiation streaming around the window frame.

- an in depth analysis of the experimental data described in chapter 6 to explain the difference in experimental and calculated dose rates outside the 10" steel door in the current medical room. Once this is done a decision on which door material, listed in Table 3.12 and Table 3.13, can be made, and specifications for fabrication of the shielding door can be performed. Additionally, the design of an opening and closing mechanism is needed for the door.

- a design of electrical conduits and a ventilation system for the medical room, as well as a lighting system,

- modifications to the front and back platforms, see Figure 8.55, are needed prior the installation of the right medical room wall, ceiling, and door,

- plans for the actual fabrication and installation of the medical room and its components including the details of cutting existing blocks, disposal of unused concrete blocks, installation of the medical room door, window, new concrete spacer blocks, and the ceiling.